BIODEGRADABLE POLYMERS FOR BIOMEDICAL APPLICATIONS

EDITED BY: Liqun Yang, Jianshe Hu, Shuai Jiang, Hongli Mao and Himansu Sekhar Nanda

PUBLISHED IN: Frontiers in Bioengineering and Biotechnology and Frontiers in Materials

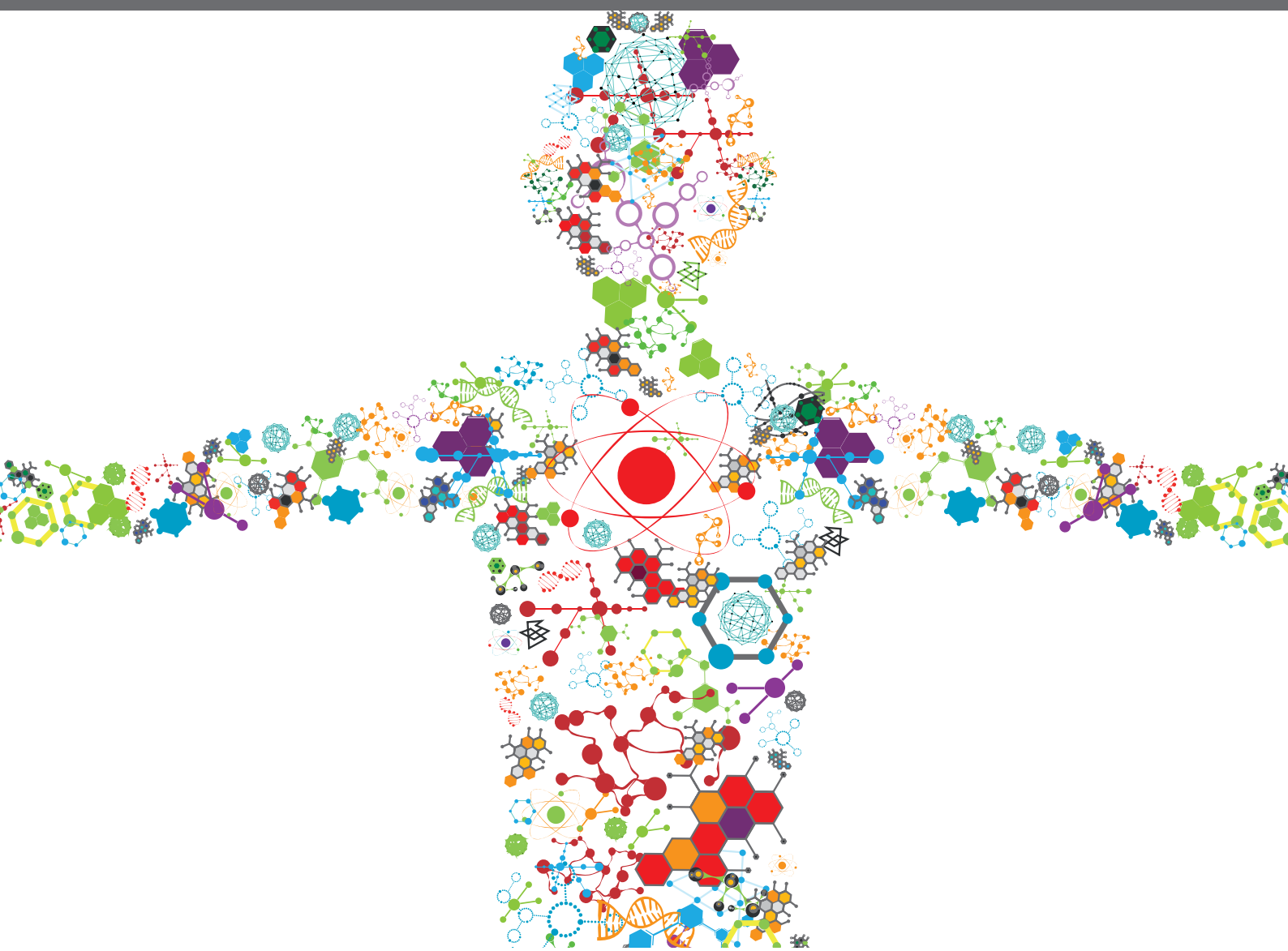

frontiers Research Topics

frontiers

ISSN 1664-8714
ISBN 978-2-88976-571-3
DOI 10.3389/978-2-88976-571-3

About Frontiers

Frontiers is more than just an open-access publisher of scholarly articles: it is a pioneering approach to the world of academia, radically improving the way scholarly research is managed. The grand vision of Frontiers is a world where all people have an equal opportunity to seek, share and generate knowledge. Frontiers provides immediate and permanent online open access to all its publications, but this alone is not enough to realize our grand goals.

Frontiers Journal Series

The Frontiers Journal Series is a multi-tier and interdisciplinary set of open-access, online journals, promising a paradigm shift from the current review, selection and dissemination processes in academic publishing. All Frontiers journals are driven by researchers for researchers; therefore, they constitute a service to the scholarly community. At the same time, the Frontiers Journal Series operates on a revolutionary invention, the tiered publishing system, initially addressing specific communities of scholars, and gradually climbing up to broader public understanding, thus serving the interests of the lay society, too.

Dedication to Quality

Each Frontiers article is a landmark of the highest quality, thanks to genuinely collaborative interactions between authors and review editors, who include some of the world's best academicians. Research must be certified by peers before entering a stream of knowledge that may eventually reach the public - and shape society; therefore, Frontiers only applies the most rigorous and unbiased reviews.
Frontiers revolutionizes research publishing by freely delivering the most outstanding research, evaluated with no bias from both the academic and social point of view. By applying the most advanced information technologies, Frontiers is catapulting scholarly publishing into a new generation.

What are Frontiers Research Topics?

Frontiers Research Topics are very popular trademarks of the Frontiers Journals Series: they are collections of at least ten articles, all centered on a particular subject. With their unique mix of varied contributions from Original Research to Review Articles, Frontiers Research Topics unify the most influential researchers, the latest key findings and historical advances in a hot research area! Find out more on how to host your own Frontiers Research Topic or contribute to one as an author by contacting the Frontiers Editorial Office: frontiersin.org/about/contact

BIODEGRADABLE POLYMERS FOR BIOMEDICAL APPLICATIONS

Topic Editors:
Liqun Yang, China Medical University, China
Jianshe Hu, Northeastern University, China
Shuai Jiang, Max Planck Institute for Polymer Research, Germany
Hongli Mao, Nanjing Tech University, China
Himansu Sekhar Nanda, PDPM Indian Institute of Information Technology, Design and Manufacturing, India

Citation: Yang, L., Hu, J., Jiang, S., Mao, H., Nanda, H. S., eds. (2022). Biodegradable Polymers for Biomedical Applications. Lausanne: Frontiers Media SA. doi: 10.3389/978-2-88976-571-3

Table of Contents

frontiers | Frontiers in Materials

EDITORIAL
published: 21 June 2022
doi: 10.3389/fmats.2022.944755

Editorial: Biodegradable Polymers for Biomedical Applications

Himansu S. Nanda[1,2]*, *Liqun Yang*[3]*, *Jianshe Hu*[4], *Hongli Mao*[5] *and Shuai Jiang*[6]

[1]Biomedical Engineering and Technology Laboratory, PDPM Indian Institute of Information Technology, Design and Manufacturing, Jabalpur, India, [2]International Centre for Sustainable and Net Zero Technologies, PDPM-Indian Institute of Information Technology Design and Manufacturing, Jabalpur, India, [3]NHC Key Laboratory of Reproductive Health and Medical Genetics (China Medical University), Liaoning Research Institute of Family Planning (The Reproductive Hospital of China Medical University), Shenyang, China, [4]Center for Molecular Science and Engineering, College of Science, Northeastern University, Shenyang, China, [5]School of Materials Science and Engineering, Nanjing Tech University, Nanjing, China, [6]Max Planck Institute for Polymer Research, Mainz, Germany

Keywords: biodegradable polymers, chemical synthesis, degradation behavior, drug delivery system, tissue engineering

Editorial on the Research Topic

Biodegradable Polymers for Biomedical Applications

The introduction of biodegradable polymers has redefined medical treatment in an innovative manner due to their high biocompatibility and biodegradability (Toh et al., 2021). Designing biodegradable polymers for biomedical applications involve numerous essential factors such as mechanical properties, chemical properties, and degradation mechanisms (Song et al., 2018). Enzymatic and non-enzymatic breakdown of biodegradable polymers *in vivo*, leaving no foreign material inside the human body post-treatment (Fonseca et al., 2014). The articles in this special issue highlight the most recent and promising biomaterial discoveries in controlled drug delivery, tissue engineering, and biomedical applications.

Polymers such as poly (trimethylene carbonate) (PTMC) have gained significant attention in drug delivery systems (Sanower Hossain et al., 2020). Liu et al. featured an article in which ciprofloxacin hydrochloride was used as a drug model whereas PTMC was a drug carrier for treating chronic osteomyelitis. Ciprofloxacin-PTMC implants were studied *in vitro* and *in vivo* for their release and antibacterial effects. The efficacy of ciprofloxacin-loaded PTMC inserts in treating severe osteomyelitis was validated in that investigation. When used as the biodegradable long-term contraceptive implant carrier, the incompatibility between morphological stability and degradation rate of PTMC prevents this application. To solve this problem, Cai et al. discussed an article in which ternary self-blending films were produced by applying ternary self-blending films to high, medium, and low molecular weight PTMC. The *in vitro* influence of ternary self-blending films on the degradation rate of PTMC was also investigated. The study concluded that ternary self-blending film is an effective approach to more accurately manage the degradation behaviour of PTMC.

The Poly(3-hydroxybutyrate-co-3-hydroxyvalerate) (PHBV) scaffold is a potential three-dimensional biodegradable scaffold for cartilage progenitor cell growth and proliferation (Salomez et al., 2019). Xue et al. investigated the effect of incorporating bioglass within PHBV 3-dimensional porous scaffolds. The study concluded that the bioglass added to PHBV three-dimensional porous scaffolds improves the properties of cartilage progenitor cell-based produced cartilage *in vivo*. Replacing fossil-fuel-derived polymers with biodegradable biobased polymers is essential to the circular bioeconomy method to slow down the dreadful current climate change.

Cyanophycin is a polymer made up of amino acids produced by cyanobacteria and has a wide range of biomedical applications (Kwiatos and Steinbüchel). Kwiatos et al. outlined all *in vitro* and *in vivo* studies related to cyanophycin and described their potential applications.

OPEN ACCESS

Edited and reviewed by:
Hasan Uludag,
University of Alberta, Canada

***Correspondence:**
Himansu S. Nanda
himansu@iiitdmj.ac.in
Liqun Yang
yanglq@lnszjk.com.cn

Specialty section:
This article was submitted to Biomaterials, a section of the journal Frontiers in Materials

Received: *15 May 2022*
Accepted: *03 June 2022*
Published: *21 June 2022*

Citation:
Nanda HS, Yang L, Hu J, Mao H and Jiang S (2022) Editorial: Biodegradable Polymers for Biomedical Applications. Front. Mater. 9:944755. doi: 10.3389/fmats.2022.944755

The blending of biodegradable polymers and biodegradable metals can effectively improve or enhance the properties of the parent materials (Martins et al., 2018). It has been reported that the disintegration of PLGA might result in an acidic medium in local tissues, which impairs bone tissue regeneration and delays the material's degradation rate (Zhao et al., 2021). Metals such as Mg and its alloys have been used in orthopaedic equipment in patients with bone abnormalities. But Mg dissolves rapidly *in vivo*, and the uncontrolled degradation raises the pH of the local environment, affecting the mechanism of osteogenesis (Jana et al., 2022). Based on the complementary physicochemical properties of PLGA and Mg, Wang et al. prepared biodegradable composite material of PLGA and magnesium for treating the bone defects. The study recommended that the PLGA with 10% Mg had efficient osteogenic characteristics and cytocompatibility, it could be used in a variety of therapeutic applications such as bone graft healing and scaffold-based tissue engineering. Besides Mg, zinc and its alloys are essential in tissue engineering. However, the high proportion of zinc ions collected around zinc-based implants becomes a significant challenge in promoting the transfer of zinc and its alloys to clinical applications, which would decrease implant biocompatibility. Surface treatment is an effective method for improving implant biocompatibility by modulating the rate of zinc ion release (Pezzato et al., 2020). Su et al. developed Ca. P conversion coatings on pure zinc to promote biocompatibility. The study concluded that adding PLA/Li-OCP coatings was a promising coating for improving degradation rate and cytocompatibility.

Hydrogels have acquired a lot of attention in drug delivery studies because of their high biocompatibility, degradation rate, and processability (Ahmad et al., 2019). Huang et al. investigated the safety and feasibility of hydrogel-encapsulated multipotent stem cells (MSCs), as well as the improvement of survival, retention, and targeting along with the augmentation of their therapeutic impact. The state of the stem cells encased in the hydrogel was also discussed. For example, the Achilles tendon is frequently injured during athletic training (Chan et al., 2020). Biomedical materials such as polyglycolic acid (PGA), polylactic acid (PLA), etc., are the potential solution in the treatment and healing of soft tissues, tendons, muscles, etc., Zhang et al. summarized the usage of biodegradable materials in the repair of Achilles tendon injuries. The investigated biodegradable polymers were PLA, PLGA, PTMC, and polydioxanone (PDS). The review concluded that Biodegradable polymers containing stem cells or medicines could significantly enhance the healing effect of Achilles tendon injuries. Gelatin-methacryloyl (GelMA) hydrogel is a photopolymer created by attaching photosensitive groups to the side groups of gelatin (Bhattacharya et al., 2020). The effect of concentration of photo-initiator or GelMA, cooling rates, and temperature gradients on pore size have been demonstrated, but the effect of freezing temperatures and time in GelMA hydrogel solution, which could have a significant impact on pore sizes in hydrogels, appears to be overlooked (Celikkin et al., 2018). Liu et al. (gelatin).pdf. investigated the effects of freezing temperatures and times on pore sizes in GelMA hydrogel. The changes in swelling and mechanical properties due to different pore size was also studied. The study concluded that the GelMA hydrogels could have a tunable microstructure by adjusting the freezing conditions, opening many possibilities for tissue engineering applications. Tissue vascularization has long been a significant concern in tissue engineering, as it is crucial for the application and durability of tissue constructions *in vivo*.

Biodegradable polymers have been extensively utilized in 3D printing technology. Ze et al. featured a review article in which basic properties of biodegradable materials typically utilized in indirect 3D bioprinting for vascularization, as well as current advancements in using this technology to vascularize various tissues, were highlighted. The study concluded that with the advancement of biodegradable materials in the future, indirect 3D bioprinting could contribute even more to the advancement in the field of tissue engineering.

Esophageal cancer is a malignant tumour that develops in the oesophagus (Xu et al., 2020). Endoscopic submucosal dissection (ESD) has been recognized as a medical therapy in clinics for early esophageal cancer due to the obvious minimally invasive tumour excision and reduced risk of deterioration Cai et al. A common and significant post-ESD consequence is an esophageal stricture. However, there is currently no clear consensus on managing it successfully. Bao et al. reviewed various oesophagal structure strategies in which biomedical polymers and biomedical derived materials were employed. Initially, the mechanism of the esophageal structure was outlined then-novel biomedical materials prevention strategies were elaborated. The review concluded that biomedical materials have the potential to play a critical role in safely and effectively preventing esophageal stricture after ESD. In addition to the biomedical materials mentioned by Bao et al., Janus particles also have great potential in cancer prevention. Janus particles are non-centrosymmetric colloidal materials with non-centrosymmetric shape, composition, and behavior (Tripathy et al., 2022). Because of the changeable dimension, biocompatibility, and low toxicity of Janus particles, these are widely employed in biomedical disciplines, notably in tumour prevention (Zhao et al., 2009). Feng et al. created Janus particles with the phase transition materials (1-tetradecanol, 1-hexadecanol, and lauric acid) along with polymers in a microfluidic system for sequential and planned drug release at a target location such as tumor tissue. The article concluded that such types of heterologous Janus microparticles with each compartment having different degrading properties, can be used for programmed and sequential drug release.

This special issue covers some recent research on biodegradable polymers for biomedical applications. We believe that the current collection of publications will provide thought-provoking ideas to professionals interested in the topic of biomaterials, as well as serve as a foundational lecture for students and researchers just starting in the field of biomaterials.

AUTHOR CONTRIBUTIONS

All authors listed have made a substantial, direct, and intellectual contribution to the work and approved it for publication.

ACKNOWLEDGMENTS

All authors' contributions, and those of the editorial staff of Frontiers, are appreciated to make this special issue possible.

REFERENCES

Ahmad, S., Ahmad, M., Manzoor, K., Purwar, R., and Ikram, S. (2019). A Review on Latest Innovations in Natural Gums Based Hydrogels: Preparations & Applications. *Int. J. Biol. Macromol.* 136, 870–890. doi:10.1016/J.IJBIOMAC.2019.06.113

Bhattacharya, S. A., Alam, M., Dhungana, K., Yadav, S., Chaudhary, K. R., Chaturvedi, K. K., et al. (2020). Preparation and Evaluation of Diclofenac Gelatin Microspheres Using Coacervation Technique Dual Functional Cationic Solid Lipid Nano Particles of Anticancer Drug View Project Preparation and Evaluation of Diclofenac Gelatin Microspheres Using Coacervation Technique. *Int. J. Pharm. Res. Innov.* 13, 14–21. [Online]. Available: https://www.researchgate.net/publication/339570083.

Celikkin, N., Mastrogiacomo, S., Jaroszewicz, J., Walboomers, X. F., and Swieszkowski, W. (2018). Gelatin Methacrylate Scaffold for Bone Tissue Engineering: The Influence of Polymer Concentration. *J. Biomed. Mat. Res.* 106 (1), 201–209. doi:10.1002/jbm.a.36226

Chan, J. J., Chen, K. K., Sarker, S., Hasija, R., Huang, H.-H., Guzman, J. Z., et al. (2020). Epidemiology of Achilles Tendon Injuries in Collegiate Level Athletes in the United States. *Int. Orthop. (SICOT)* 44 (3), 585–594. doi:10.1007/s00264-019-04471-2

Fonseca, A. C., Gil, M. H., and Simões, P. N. (2014). Biodegradable Poly(ester Amide)s - A Remarkable Opportunity for the Biomedical Area: Review on the Synthesis, Characterization and Applications. *Prog. Polym. Sci.* 39 (7), 1291–1311. doi:10.1016/J.PROGPOLYMSCI.2013.11.007

Jana, A., Das, M., and Balla, V. K. (2022). *In Vitro* and *In Vivo* Degradation Assessment and Preventive Measures of Biodegradable Mg Alloys for Biomedical Applications. *J. Biomed. Mater. Res.* 110 (2), 462–487. doi:10.1002/jbm.a.37297

Martins, C., Sousa, F., Araújo, F., and Sarmento, B. (2018). Functionalizing PLGA and PLGA Derivatives for Drug Delivery and Tissue Regeneration Applications. *Adv. Healthc. Mat.* 7 (1), 1701035. doi:10.1002/adhm.201701035

Pezzato, L., Settimi, A. G., Cerchier, P., Gennari, C., Dabalà, M., and Brunelli, K. (2020). Microstructural and Corrosion Properties of PEO Coated Zinc-Aluminized (ZA) Steel. *Coatings* 10 (5), 448. doi:10.3390/coatings10050448

Salomez, M., George, M., Fabre, P., Touchaleaume, F., Cesar, G., Lajarrige, A., et al. (2019). A Comparative Study of Degradation Mechanisms of PHBV and PBSA under Laboratory-Scale Composting Conditions. *Polym. Degrad. Stab.* 167, 102–113. doi:10.1016/J.POLYMDEGRADSTAB.2019.06.025

Sanower Hossain, M., Mohamed, F., and Affendi Mohd Shafri, M. (2020). Poly(trimethylene Carbonate-Co-Caprolactone): An Emerging Drug Delivery Nanosystem in Pharmaceutics Salinity Stress in Plants View Project Synergistic Effect of Gentamicin and Nigella Sativa Oil View Project Poly(trimethylene Carbonate-Co-Caprolactone): An Emerging Drug Delivery Nanosystem in Pharmaceutics. *Artic. Biomater. Biomech. Bioeng.* 5 (1), 65–86. doi:10.12989/bme.2020.5.1.065

Song, R., Murphy, M., Li, C., Ting, K., Soo, C., and Zheng, Z. (2018). Current Development of Biodegradable Polymeric Materials for Biomedical Applications. *Dddt* Vol. 12, 3117–3145. doi:10.2147/DDDT.S165440

Toh, H. W., Toong, D. W. Y., Ng, J. C. K., Ow, V., Lu, S., Tan, L. P., et al. (2021). Polymer Blends and Polymer Composites for Cardiovascular Implants. *Eur. Polym. J.* 146, 1102492021. doi:10.1016/J.EURPOLYMJ.2020.110249

Tripathy, S. P., Subudhi, S., Ray, A., Behera, P., and Parida, K. (2022). Metal Organic Framework-Based Janus Nanomaterials: Rational Design, Strategic Fabrication and Emerging Applications. *Dalton Trans.* 51 (14), 5352–5366. doi:10.1039/D1DT04380C

Xu, Q.-L., Li, H., Zhu, Y.-J., and Xu, G. (2020). The Treatments and Postoperative Complications of Esophageal Cancer: a Review. *J. Cardiothorac. Surg.* 15 (1), 163. doi:10.1186/s13019-020-01202-2

Zhao, D., Zhu, T., Li, J., Cui, L., Zhang, Z., Zhuang, X., et al. (2021). Poly(lactic-co-glycolic Acid)-Based Composite Bone-Substitute Materials. *Bioact. Mater.* 6 (2), 346–360. doi:10.1016/j.bioactmat.2020.08.016

Zhao, L. B., Pan, L., Zhang, K., Guo, S. S., Liu, W., Wang, Y., et al. (2009). Generation of Janus Alginate Hydrogel Particles with Magnetic Anisotropy for Cell Encapsulation. *Lab. Chip* 9 (20), 2981. doi:10.1039/b907478c

Conflict of Interest: The authors declare that the research was conducted in the absence of any commercial or financial relationships that could be construed as a potential conflict of interest.

Publisher's Note: All claims expressed in this article are solely those of the authors and do not necessarily represent those of their affiliated organizations, or those of the publisher, the editors and the reviewers. Any product that may be evaluated in this article, or claim that may be made by its manufacturer, is not guaranteed or endorsed by the publisher.

frontiers in Bioengineering and Biotechnology

ORIGINAL RESEARCH
published: 09 September 2021
doi: 10.3389/fbioe.2021.756758

Microfluidic Preparation of Janus Microparticles With Temperature and pH Triggered Degradation Properties

*Zi-Yi Feng[1], Tao-Tao Liu[2], Zhen-Tao Sang[2], Zhen-Sheng Lin[2], Xin Su[1], Xiao-Ting Sun[3], Hua-Zhe Yang[2], Ting Wang[1] and Shu Guo[1]**

[1]Department of Plastic Surgery, The First Affiliated Hospital of China Medical University, Shenyang, China, [2]School of Intelligent Medicine, China Medical University, Shenyang, China, [3]School of Forensic Medicine, China Medical University, Shenyang, China

Based on the phase separation phenomenon in micro-droplets, polymer-lipid Janus particles were prepared on a microfluidic flow focusing chip. Phase separation of droplets was caused by solvent volatilization and Janus morphology was formed under the action of interfacial tension. Because phase change from solid to liquid of the lipid hemisphere could be triggered by physiological temperature, the lipid hemisphere could be used for rapid release of drugs. While the polymer we selected was pH sensitive that the polymer hemisphere could degrade under acidic conditions, making it possible to release drugs in a specific pH environment, such as tumor tissues. Janus particles with different structures were obtained by changing the experimental conditions. To widen the application range of the particles, fatty alcohol and fatty acid-based phase change materials were also employed to prepare the particles, such as 1-tetradecanol, 1-hexadecanol and lauric acid. The melting points of these substances are higher than the physiological temperature, which can be applied in fever triggered drug release or in thermotherapy. The introduction of poly (lactic-co-glycolic acid) enabled the formation of multicompartment particles with three distinct materials. With different degradation properties of each compartment, the particles generated in this work may find applications in programmed and sequential drug release triggered by multiple stimuli.

Keywords: microfluidics, phase separation, Janus particle, phase change material, degradation

OPEN ACCESS

Edited by:
Liqun Yang,
China Medical University, China

Reviewed by:
Yun-Yun Wei,
Shandong First Medical University, China
Chiyu Sun,
Shenyang Medical College, China

****Correspondence:***
Shu Guo
sguo@cmu.edu.cn

Specialty section:
This article was submitted to Biomaterials, a section of the journal Frontiers in Bioengineering and Biotechnology

Received: *11 August 2021*
Accepted: *30 August 2021*
Published: *09 September 2021*

Citation:
Feng Z-Y, Liu T-T, Sang Z-T, Lin Z-S, Su X, Sun X-T, Yang H-Z, Wang T and Guo S (2021) Microfluidic Preparation of Janus Microparticles With Temperature and pH Triggered Degradation Properties. Front. Bioeng. Biotechnol. 9:756758. doi: 10.3389/fbioe.2021.756758

INTRODUCTION

Janus particles are a kind of colloidal materials with non-centrosymmetric characteristics in morphology, composition and properties. It was first proposed by De Gennes, a French scientist, when he won the Nobel Prize in 1991 (de Gennes, 1992). The word "Janus" originated from the ancient Roman double-faced God, a reflection of its asymmetry. In recent years, as typical multifunctional materials, Janus particles have emerged in the fields of chemistry, physics, life sciences and so on (Hu et al., 2012; Kaewsaneha et al., 2013). The morphology of Janus particles is diverse including dumbbell, rod, snowman or any of a variety of other shapes, in addition, Janus particles assembled from block polymers or small molecules can also be divided into dendritic, vesicular, and other structures. According to the composition of particles, Janus particles can be divided into polymer type, inorganic type and polymer inorganic hybrid type (Su et al., 2019). Janus particles with nano/micron size have not only complex morphology, but also possess the inherent optical, magnetic and electronic properties in each part (Jin and Gao, 2009). It is well recognized that

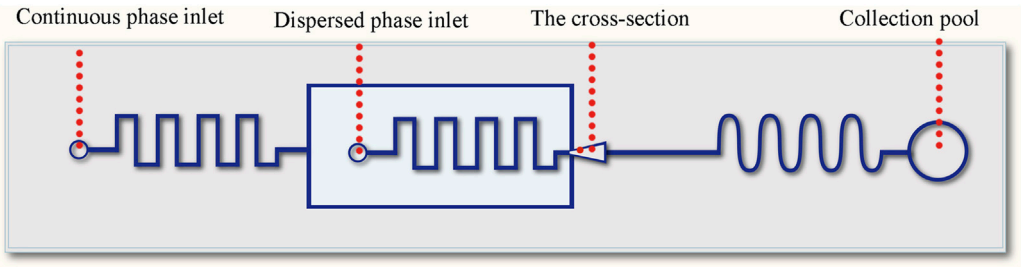

FIGURE 1 | Schematic diagram of the microfluidic chip.

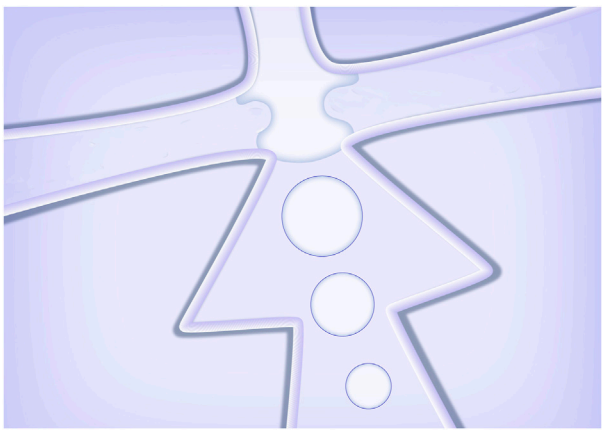

FIGURE 2 | Schematic diagram of the droplets formed in the cross-section.

properties and applications of Janus particles are highly dependent on their morphology and chemical composition. Janus particles with adjustable size, biocompatibility, and low toxicity are widely used in biomedical fields, especially in the fields related to living cell research and tumor inhibition, such as cell encapsulation (Zhao et al., 2009; Maeda et al., 2012), cell imaging (Yi et al., 2016; Li et al., 2019), drug delivery (Xuan et al., 2014; M. El-Sherbiny and Abbas, 2016; Feng et al., 2019; Severino et al., 2019) and so on. At present, Janus particles have covered the whole range from nano scale to micron scale. Micron or submicron Janus particles can be prepared by a series of methods, the conventional preparation methods of Janus particles mainly include emulsion method, interface protection method, phase separation method, surface nucleation method and self-assembly method (Du and O'Reilly, 2011). These methods usually have high preparation throughput, and can realize the preparation of nano-sized Janus particles, some of these technologies have successfully prepared small-size Janus particles (Walther and Müller, 2013). However, the inherent limitations of conventional preparation methods are that it is difficult to achieve accurate control of particle morphology and to prepare particles with complex structure. In addition, the monodispersity and reproducibility of the particle production are relatively poor (Ali et al., 2021).

In recent years, microfluidic technology has gradually become a research hotspot, it is reported to have substantial applications in biology and medical research, for it can integrate a variety of complex biological and chemical reactions on a tiny chip, which greatly saves resources and costs (Hansen and Quake, 2003). Microfluidic platform is robust in producing polymer-based Janus particles. The main methods include droplet-based method and flow-lithography method. Among them, the droplet based method uses the micro-droplets with asymmetric morphology formed by shear force, electric field and centrifugal force in microfluidic system as the templates of Janus particles, combined with appropriate curing methods (Yu et al., 2021). While the flow-lithography method is a micro projection technology based on photo-polymerization of multiphase laminar flow. The fluid in the microfluidic chip is exposed to an ultraviolet beam with preset shape, causing the irradiated fluid to partially polymerize according to the beam shape to obtain Janus particles. The whole preparation process can be completed with the help of a commercial fluorescence microscope (Chizari et al., 2020; Sun et al., 2014). Microfluidic method can endow Janus particles with complex structure (such as three-dimensional asymmetric structure) or sophisticated morphology (such as graphic coding morphology) and the control of particle size, which greatly expands the design and application scope of Janus particles (Shepherd et al., 2006). However, the materials used in Janus particle preparation by microfluidic method are limited to polymers, which greatly restricts their application (Shakeri et al., 2021). Especially in drug delivery, the integration of a variety of materials is desired to achieve different degradation characteristics in a single carrier, so as to realize programmed, sequential or triggered release of different drugs.

In the present work, we fabricated Janus particles with temperature and pH triggered degradation characteristics by integration of pH sensitive polymers and phase change lipids in a microfluidic device. In addition, fatty alcohols, and fatty acids were also employed to produce the particles in order to achieve more controllable temperature triggered degradation. The triple-phase structure was also explored by adding a third material in order to realize a more programmed degradation mode. These particles are expected to have application potential in personalized and programmed drug delivery.

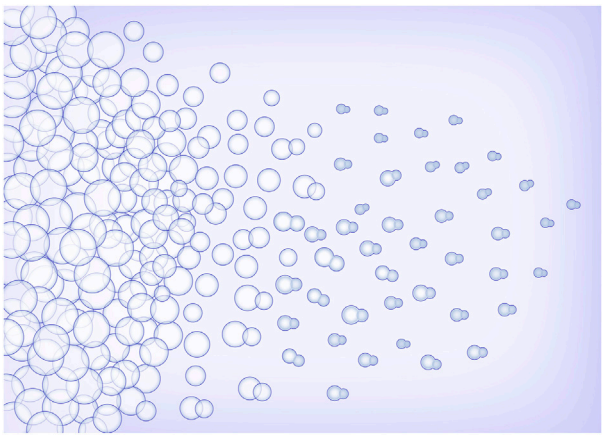

FIGURE 3 | Schematic diagram of droplets phase separation.

MATERIAL AND METHODS

Reagents

Poly (butyl methacrylate-co-(2-dimethylaminoethyl) methacrylate-co-methyl methacrylate) (p (BMA-co-DAMA-co-MMA), Eudragit E100) was perchased from Shanghai Dexiang Medicine Tech. Co., Ltd. Poly (lactic-co-glycolic acid) (PLGA) (50:50, Mw 10,000) was purchased from Jinan Daigang Biomaterial Co., Ltd., China. Hydrogenated coconut glyceride lipid (HCG lipid, Softisan 100) was purchased from Sasol (China) Co., Ltd., Nanjing, China. Dimethyl carbonate (DMC, >98%) was purchased from TCI (Shanghai) Development Co., Ltd., China. Polyvinyl alcohol (PVA, Mw 1750 ± 50), 1-tetradecanol, 1-hexadecanol, lauric acid, sodium dodecyl sulfate (SDS), Span 80 and dichloromethane (>99.5%) were purchased from Sinopharm Chemical Reagent Corporation, Shanghai, China. EM 90 was purchased from Evonik Industries, Shanghai, China. All of the above reagents were used as received without further purification, and deionized water was used throughout the experiment.

Preparation of Microfluidic Chip

A flow-focusing sheath and winding channels were designed on a chip to fabricate the templet droplets, the schematic diagram is shown in **Figure 1**.

The whole device was made from polydimethylsiloxane (PDMS), consisting a channel layer and a substrate layer. The microfluidic channel was designed with flow focusing and winding structures. The flow focusing structure was used for the formation of oil-in-water droplets (**Figure 2**), and the downstream winding structure was used for the on-line solvent volatilization. The channel structure consists of a dispersed phase inlet, a continuous phase inlet and an outlet collection pool, and the phase separation process of droplets happened in the collection pool. The width of the winding channel for introducing the continuous and dispersed phase is 50 μm. The width of the main winding channel is 100 μm. The cross section of all channels is rectangular with a depth of 75 μm. The microfluidic chip was fabricated with the method of SoftLithography. Hydrophilic modification was carried out to produce oil-in-water droplets. 0.3 wt% PVA solution was applied to wash the channel for 0.5 h (flow rate 0.5 μl/min) to form a hydrophilic coating on the channel wall.

Preparation of Solutions and Microparticles

A mixed solution of polymer and lipid (both concentrations were 5 mg/ml) in DMC with 0.5% (v/v) Span 80 was used as the dispersed phase. 0.3 wt% PVA solution with 0.1 wt% SDS was employed as the continuous phase. To prepare the particles, the solutions were injected into the microchip by syringe pumps (pump11 Elite, Harvard, United States) with glass syringes (Hamilton, Switzerland). The flow rates of dispersed phase and continuous phase were set at 1 μl/min and 2 μl/min, respectively. And the resulted particles were collected into a sample cell using a pipettor. The collected particles were afterwards placed in a refrigerator at 4°C for 5 min to cure the lipid, and then stirred under room temperature (around 25°C) for 2 h for complete removal of the solvent. The droplets and particles were observed by using a stereomicroscope with digital camera (MC-D500U, Phenix, China).

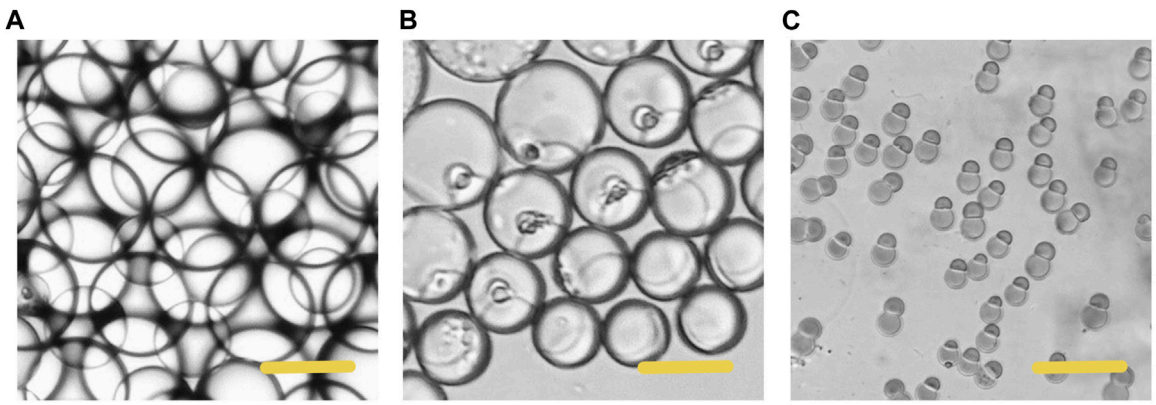

FIGURE 4 | Microscopic images of the phase separation process of droplets **(A)** The initially formed droplet **(B)** The droplet size decreased with size decreased with solvent volatilization **(C)** The formation of the Janus particles. Scale bars represent 100 μm in all images.

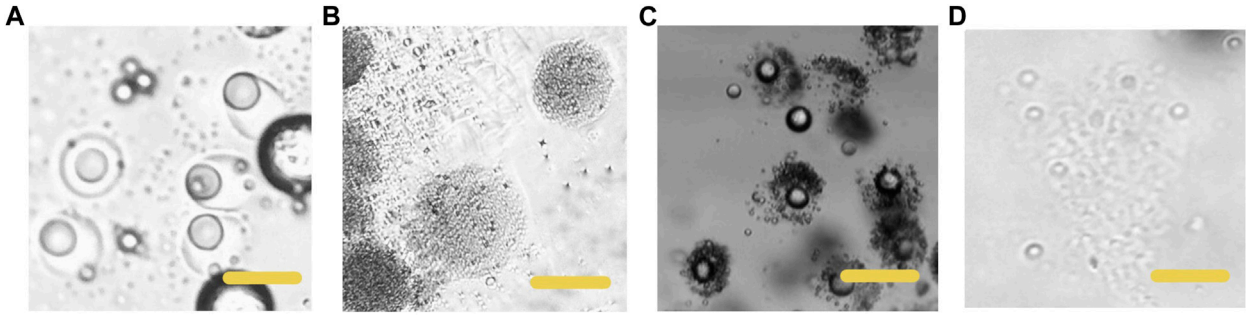

FIGURE 5 | Microscopic images of the particles dissolving at different conditions **(A)** The HCG lipid melted in 37°C, PH 7.4 **(B)** The p (BMA-co-DAMA-co-MMA) dissolved when the environment pH was adjusted to 4,37°C **(C)** the p (BMA-co-DAMA-co-MMA) dissolved when the environment pH was 4,25°C **(D)** the HCG lipid melted when the temperature was raised to 37°C. Scale bars represent 100 μm in all images.

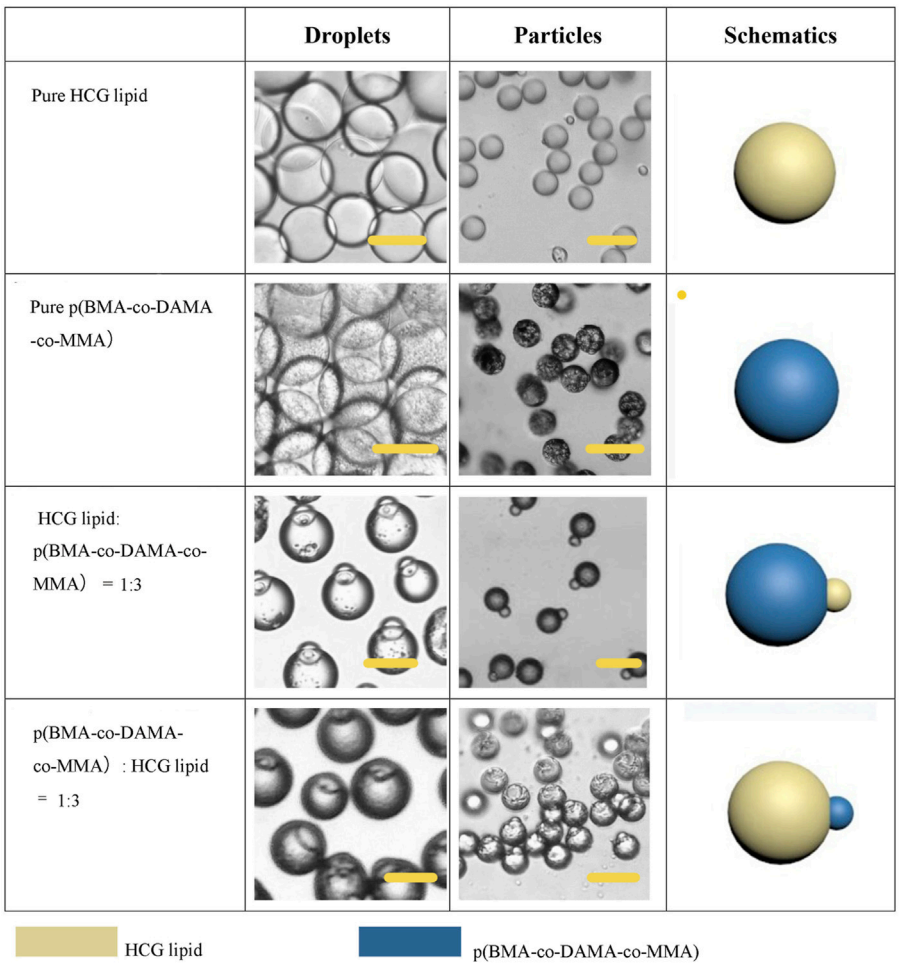

FIGURE 6 | Schematic diagrams and microscopic images of droplets and particles with different phase ration. Scale bars represent 100 μm in all images.

RESULTS

Formation of Janus Droplets and Particles

Janus particles composed of materials with different physicochemical properties, have advantages when used as drug carriers in two main aspects: firstly, it is conducive to realize the segmented release control of drug loaded by particles, secondly, it is beneficial to realize the loading of different drugs. In this work, we focus on the p (BMA-co-DAMA-co-MMA) and HCG lipid which are approved by the

U.S. Food and Drug Administration (FDA) to be used as drug additive (Mullard, 2020). p (BMA-co-DAMA-co-MMA) is widely used in gastric coating, enteric coating, sustained and controlled release coating, protective and isolation coating, sustained release matrix material and matrix adhesive material for transdermal drug delivery. p (BMA-co-DAMA-co-MMA) is formed by emulsion polymerization, it does not dissolve in neutral condition, but dissolves rapidly in the environment where the pH is lower than 5. HCG lipid has a melting point of 35 ± 1°C, and when it is used as a drug carrier, physiological temperature triggered phase transition and drug release will occur, thus it is often used in ointments, skin care product and drug microcarriers. Therefore, when the properties of these two materials are given to one Janus particle simultaneously, not only the segmented release control according to different temperatures and pH values can be realized, but also the sequential release when loading different drugs may be achieved.

However, it is difficult to prepare heterologous Janus particles by conventional methods, for the size and structure of the prepared particles are difficult to control. Microfluidic droplet technology can meet the demand of controllable preparation of heterologous Janus particles. Due to the difference in properties, the phase separation phenomenon in the droplet can be used to construct the Janus morphology. The typical process is that under the conditions of solvent volatilization, different components in droplets are separated spontaneously and gathered in different areas of the droplets respectively. We used the continuous phase to shear the dispersed phase to form the oil in water type droplets, and in the downstream a continuous winding channel was designed to allow for sufficient flow time for solvent evaporation. The permeability of PDMS allowed the solvent to evaporate into gas to avoid a large number or volume of bubbles. In general, the shape and aspect ratio of the channel had no significant effect on the droplet formation and phase separation. At the same time, due to the decrease of the flow rate (the flow rate of the dispersed phase would slow down when entering a wider channel from a narrow one), the droplets were easier to accumulate in the channel. However, if the flow time of the droplets in the chip was too short, the solvent evaporation of the droplet would be insufficient. Therefore, it is a necessity to maintain a reasonable width of the winding channel. After optimization, 100 μm was selected as the width of the winding channel. And after continuous test, 1 μl/min and 2 μl/min were chosen as the flow rates of the dispersed phase and the continuous phase, respectively. The process of droplet phase separation is shown in **Figure 3**.

In the process of droplet phase separation, the droplet size decreased with solvent volatilization, 100 μm (long diameter) at the beginning, while after 30 s in the pool, it dropped to 50 μm. After collecting the droplets and volatilizing the solvent, the short diameter of Janus particles was 20 μm and the long diameter was 40 μm. The droplet size decreased by 20% after another 2 h of the solvent evaporation. The results indicated that the efficiency of solvent evaporation was higher in the first 30 s in the collection pool. The rapid evaporation and phase separation can be attributed to the following aspects: firstly, the droplets formed in the microfluidic system are small in volume, usually in the order of pL or nL. Secondly, the design of the winding channel intensified the disturbance of the components in the droplet, thirdly, the selected solvent has good volatility. **Figure 4** exhibits the whole process of the Janus particle formation. The droplets were formed at the flow focusing structure under the action of shear force. With solvent evaporating, the droplets shrunk and the concentrated contents started to separate from each other to minimize the Gibbs free energy (Min et al., 2016). When the droplet size decreased, the internal components of the droplet were stratified. This phenomenon was caused by the difference of affinity between polymer and lipid. With the solvent volatilizing, the two components in the droplet were gradually exposed to the water phase, and they had different solubility in the water phase, thus forming different solidification regions. In the final form of the Janus droplet, the interface between polymer and lipid was clear. What is more, the following off-chip quick-freezing and stirring were necessary to maintain the regular shape of the lipid compartments and to minimize the solvent residual.

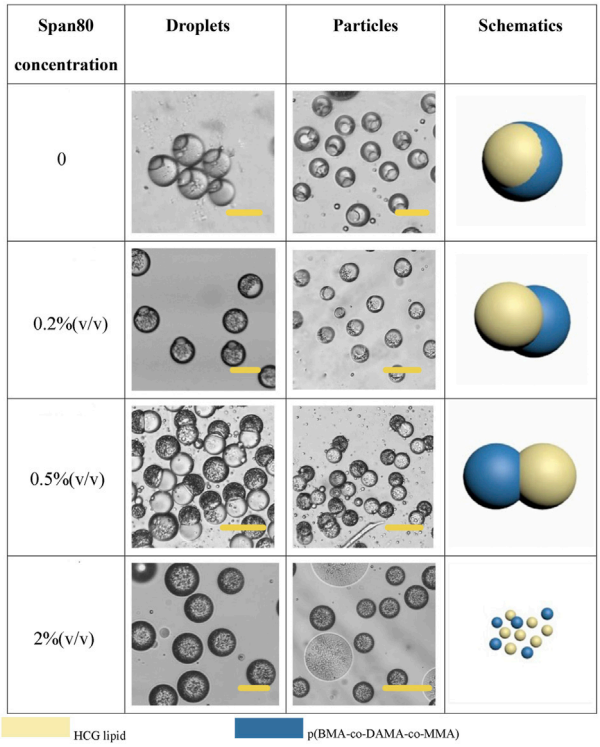

FIGURE 7 | Schematic diagrams and microscopic images of droplets and particles with different Span 80 concentration Scale bars represent 100 μm in all images.

Degradation of the Lipid and Polymer Compartments

The lipid we selected would experience phase transition from solid to liquid under human body temperature. Therefore, we simulated the degradation process of particles at body

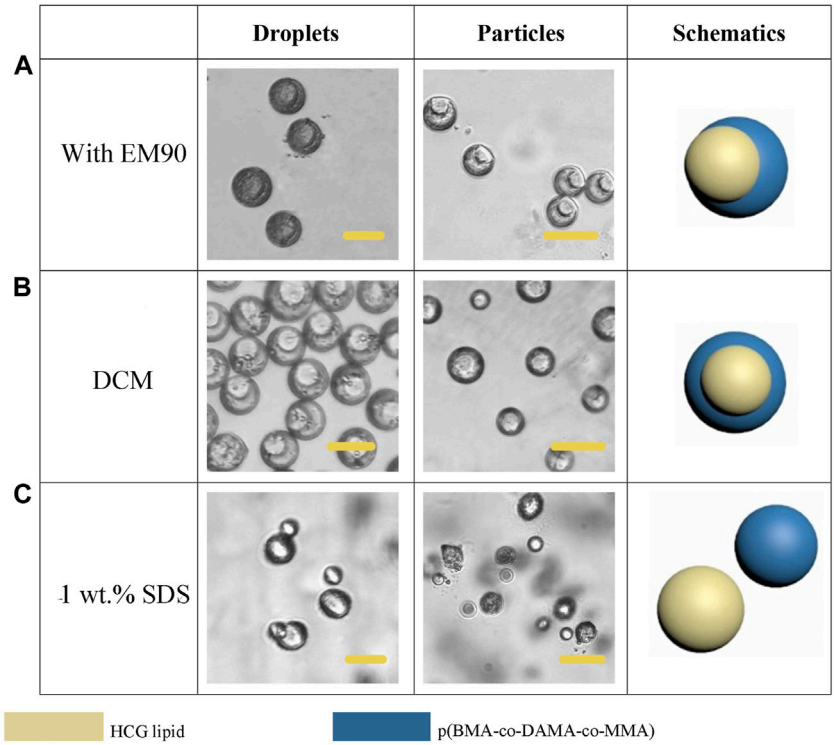

FIGURE 8 | Schematic diagrams and microscopic images of droplets and particles prepared with EM90 as surfactant **(A)**, DCM as solvent **(B)** and increased SDS concentration **(C)**. Scale bars represent 100 μm in all images.

temperature (37°C). Phase transition from solid to liquid of the lipid hemisphere is shown in **Figure 5**. The particles were heated at 37°C for 60 s, the lipid hemisphere began to melt and deform (**Figure 5A**). After incubation for 120 s, the lipid fraction was completely melted and adhered around the polymer hemisphere. However, from the aspect of appearance, the polymer hemisphere did not degrade. For the polymer hemisphere was able to dissolve in acid environment, we subsequently adjusted the environmental pH to 4, and observed that the remaining polymer dissolved completely (**Figure 5B**). On the contrary, when the pH was adjusted to 4, the appearance of lipid did not change significantly at room temperature (**Figure 5C**, **Supplementary Video S1**). After complete dissolution of the polymer, the left particles were heated to 37°C and maintained for a period of time, and the lipid then melted (**Figure 5D**, **Supplementary Video S2**).

This degradation mode plays an important role in many drugs delivery schemes. For example, in the therapy of some gastric diseases or tumor (Wang et al., 2021), local high-dose administration is a necessity to maintain the efficacy under acidic conditions. The release mode triggered by physiological temperature and environmental pH does not need the usage of photo-thermal materials. What is more, the whole preparation process of the particles is simple and fast. For all the materials we used are safe and non-toxic, which can be excreted from the body fluid circulation after administration. Due to the small mass and volume of particles, the effect of lipid on cardiovascular and cerebrovascular system can be ignored (Pardridge, 2012). Moreover, the dosage of drug carrier can be reduced by reasonably increasing the drug loading, so as to reduce the possible impact of drug carrier on human body. Although the lipid selected in our research has a low melting point, it can remain solid at normal room temperature. After being made into drug loaded particles, it can also be stored at a lower temperature. The time required for complete melting is enough to complete the delivery of particles to the therapeutic target by injection. Because the pH of tumor or some organs of the body is different from that of the surrounding (Ramsay and Carr, 2011), targeted drug delivery can be achieved in this mode.

Control of Particle Phase Ratio

Firstly, we explored the Janus particles and droplets formed by different proportions of lipid and polymer. **Figure 6** shows the structure diagram and micrographs of droplets and particles with different compositions. When the particles were dispersed in water, they tended to be vertically arranged due to the low density of lipid, thus some of the particles in some photos do not show biphasic morphology. After phase separation, the proportion of two phases in the droplet was basically the same as that in the dispersed phase solution, and the particles could also maintain the present proportion of the two phases. Single phase polymer or lipid particles can be obtained by volatilization of solvent in droplets containing a single material. These particles also have high uniformity. Multiphase laminar flow can achieve the same goal, the volume ratio of different phases in the droplet is usually

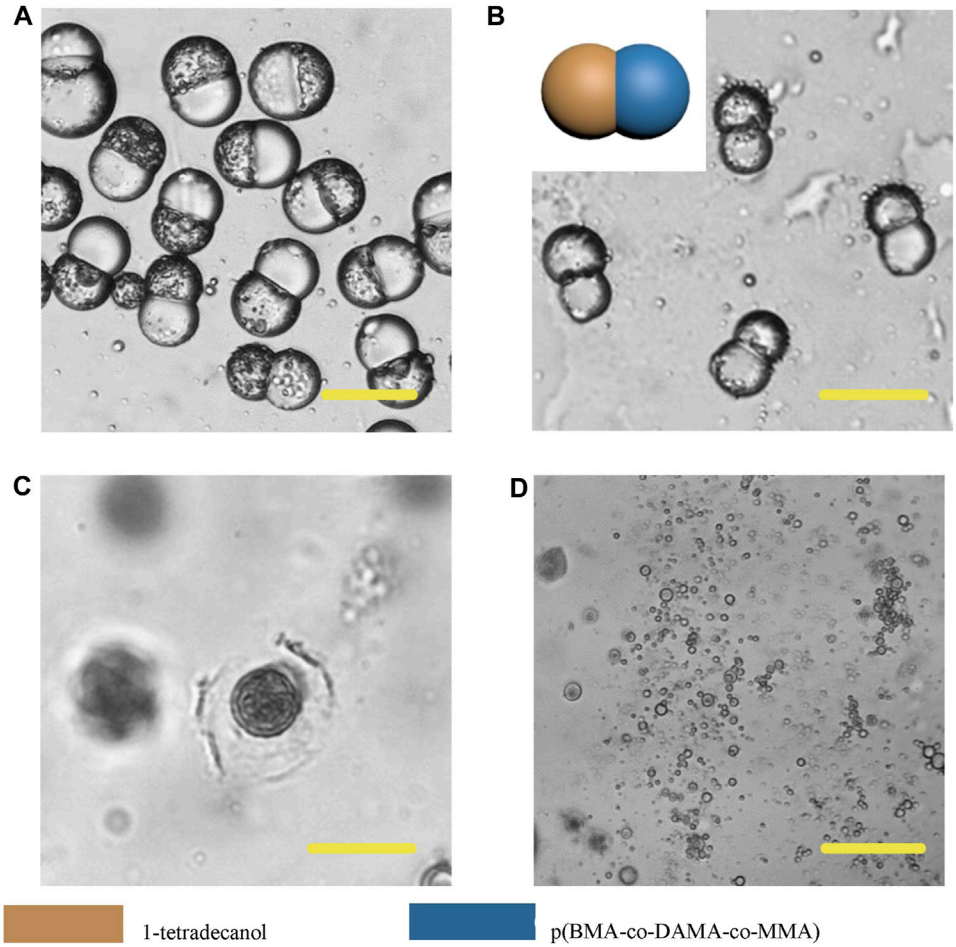

FIGURE 9 | Microscopic images of droplets **(A)**, particles **(B)** composed of 1-tetradecanol and p (BMA-co-DAMA-co-MMA) **(C)** 1-tetradecanol region melted at 39°C **(D)** The p (BMA-co-DAMA-co-MMA) degraded in pH 4 environment Scale bars represent 100 μm in all images.

controlled by adjusting the flow rate ratio of different phases in laminar flow (Gao and Chen, 2008). However, it is difficult to accurately control the volume ratio of two phases and the mass ratio of two phases in solidified particles. Moreover, when the velocity difference between two phases is large, the phase with low velocity may not flow into the channel and form multiphase laminar flow with the other phase. In the method proposed here, the phase separation based preparation method does not need the formation of laminar flow. Only by fixing the component ratio of the solution, the volume ratio of the two phases in a droplet and a particle can be accurately controlled without adjusting the flow rate. Flexible control of phase ratio of Janus particles is quite essential when used as drug carriers and therapeutic factors. For example, when this kind of particle is used as a drug carrier, the phase ratio can be adjusted according to the actual application to regulate the release amount at different release stages or the loading ratio of two drugs.

Structure Control

In addition to the phase ratio, the effect of other factors on the morphology of Janus particles were also explored. In fact, the final morphology of the droplet is determined by the interfacial tension between different phases, and the wettability between different phases is reflected by the spreading coefficient (*Si*) (Sun et al., 2019). Under our experimental conditions, when the concentration of Span 80 is 0.5% (v/v), the Janus (dumbbell) shape formed. As is well accepted that surfactant is pivotal to regulate the interfacial tension, we further investigated the role of Span 80 in this system. The concentration of Span 80 affected the degree of particle separation, as is shown in **Figure 7**. When the concentration of Span 80 was varied from 0 to 0.5% (v/v), the lipid and polymer hemispheres became apart from each other gradually. But when we increased the concentration to 2% (v/v), the law was broken. Janus particles were no longer formed. Lipids and polymers had no independent solidification areas. Instead, a whole droplet was wrapped with many small particles. With the evaporation of the solvent, the particles became unstable and broke up spontaneously. This phenomenon may attribute to the fact that high concentration of Span 80 surfactant led to tardy separation of the two phases, as

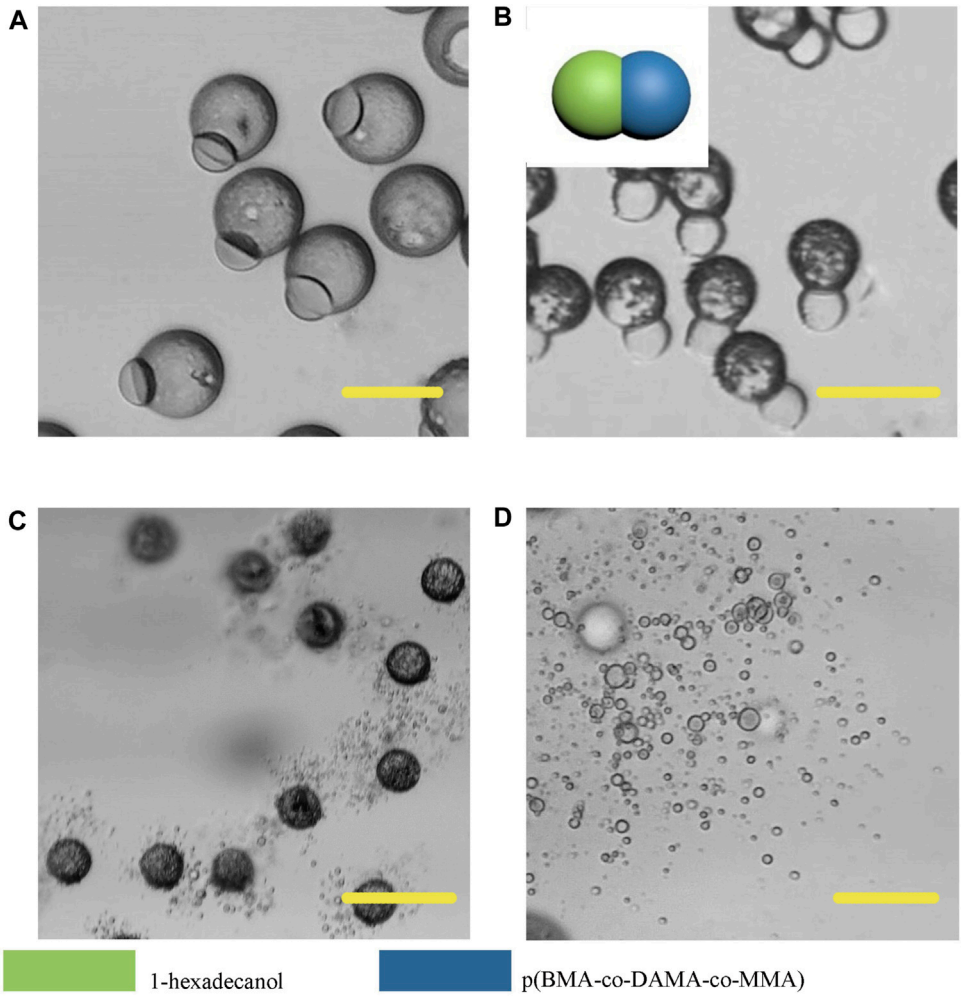

FIGURE 10 | Microscopic images of droplets **(A)**, particles **(B)** composed 1-hexadecanol and p (BMA-co-DAMA-co-MMA) **(C)** 1-hexadecanol region melted at 49°C **(D)** The p (BMA-co-DAMA-co-MMA) degraded in pH 4 environment Scale bars represent 100 μm in all images.

well as a low interfacial tension between the organic phase and the aqueous phase, which resulted in an increased *Si* of the aqueous phase and therefore completely separated lipid and polymer.

EM 90 was also tested as the surfactant in the organic phase, when 0.5% (v/v) EM 90 was applied, the particles turned into an eccentrically encapsulated core-shell structure with the lipid compartment as an inner core (**Figure 8A**). Solvent also has a significant impact on the particle morphology. When we used DCM as the solvent for dispersed phase, most of the lipid formed a complete sphere and gathered in the center of the polymer shell (**Figure 8B**). SDS was employed as an aqueous anionic surfactant, and increasing of the concentration of SDS in the aqueous phase to 1 wt.% would allow for the total separation of two compartments, for a higher SDS concentration led to restraint of the interfacial tension between the aqueous phase and the polymer/lipid phase, the *Si* of the aqueous phase turned to be more positive, leading to complete dewetting of the organic phases (**Figure 8C**). And the size and shape of particles may be further broadened by optimizing the experimental conditions.

Exploration of Fatty Alcohol-and Fatty Acid-Based Phase Change Materials

In order to further broaden the application scenarios of Janus particles, we tested more phase change materials to combine with the polymer. The phase change material is a kind of thermosensitive material which can transform into a liquid phase when heated to melting points (Choi et al., 2010). And some fatty alcohols and fatty acids are typical phase change materials. Here, 1-tetradecanol (melting range 38 and 39°C), 1-hexadecanol (melting range 47–49°C) and lauric acid (melting point 49°C) were selected to serve as the temperature sensitive hemisphere in Janus particles. In the case of an elevated body temperature due to fever, inflammation, some other diseases or during thermal-therapies, the lipid compartments would melt and rapidly release the loaded drugs (Hyun et al., 2014). We

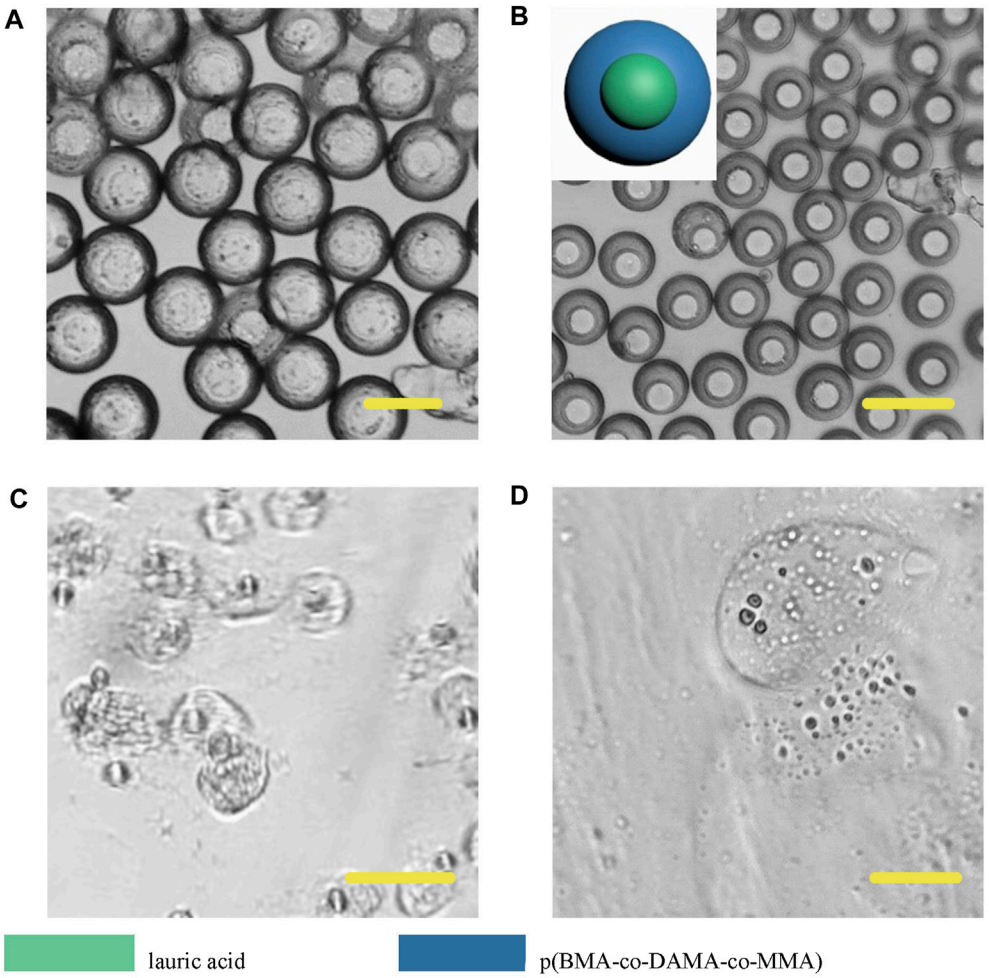

FIGURE 11 | Microscopic images of droplets **(A)**, particles **(B)** composed of lauric acid and p (BMA-co-DAMA-co-MMA) **(C)** Lauric acid region melted at 49°C **(D)** The p (BMA-co-DAMA-co-MMA) degraded in pH 4 environment Scale bars represent 100 μm in all images.

adopted the same experimental conditions except for changing the phase change materials. The results showed that the 1-tetradecanol (**Figure 9**) and 1-hexadecanol (**Figure 10**) exhibited similar Janus (dumbbell) structure with the HCG lipid. The interface of the two phases is clear, where the dark rough hemisphere is polymer, and the white smooth hemisphere is lipid. The degradation of lipid and polymer hemispheres were further investigated, we heated the particles to 39 and 49°C, respectively. The lipid phase melted at the corresponding melting point, while the polymer phase did not show a significant change. Then we adjusted the environment pH of the particles to 4, Similarly, the polymer degraded rapidly and the entire hemisphere collapsed.

However, different from the previous results, Janus particles made from lauric acid and polymer formed core-shell structure (**Figure 11**). When we heated the particle dispersing solution to 49°C, the particle surface did not appear any change, but when we adjusted the pH to 4, the particle shell degraded, thus we could infer that the outer layer was the p (BMA-co-DAMA-co-MMA) and the inner layer was the lauric acid. After the outer polymer was completely dissolved, we raised the temperature to 49°C, and the inner layer melted instantaneously. This result confirmed our hypothesis. The exploration of fatty alcohols and fatty acids has expanded the scope of materials that can be introduced to fabricate Janus particles in a microfluidic device, and has also increased more possibilities for further application.

Preliminary Study on Multicompartment Microparticle Generation by Phase Separation

In recent years, the fabrication of double-phasic particle by phase separation method has been gradually improved, but study on multicompartment particle fabrication by this method is rare. Based on the previous study of biphasic Janus particles, we tried to construct multicompartment particles to enrich the function of particles. We applied a third polymer, PLGA, due to its well acknowledged capability in providing sustained drug release. Some studies have indicated that PLGA took 35 days to completely degrade in phosphate buffered saline *in vitro* (Ding and Zhu, 2018). Therefore, the addition of PLGA in the whole system can achieve sustained release, temperature triggered

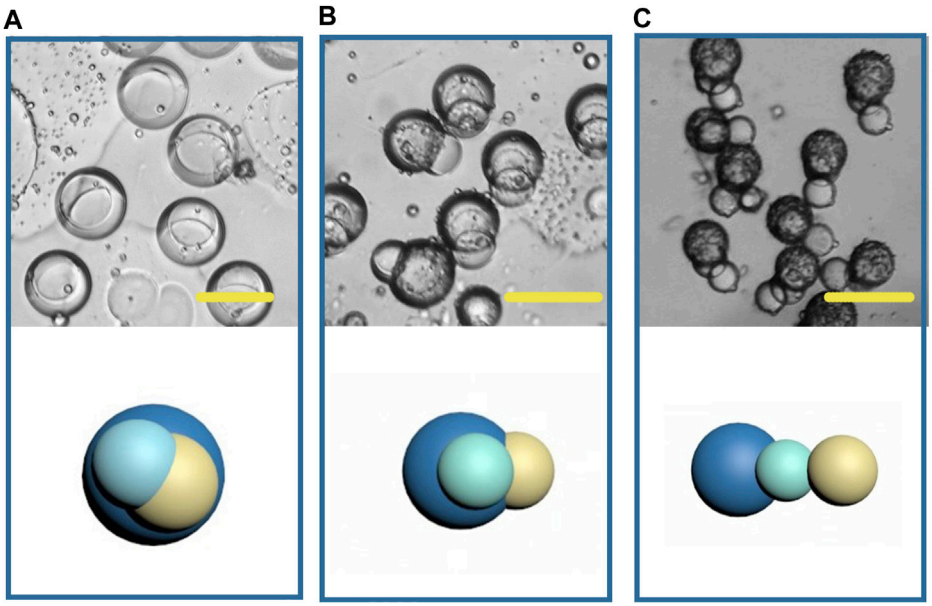

FIGURE 12 | Microscopic images and the schematic diagrams of multicompartment droplets **(A)**, particles **(B, C)**. Scale bars represent 100 μm in all images.

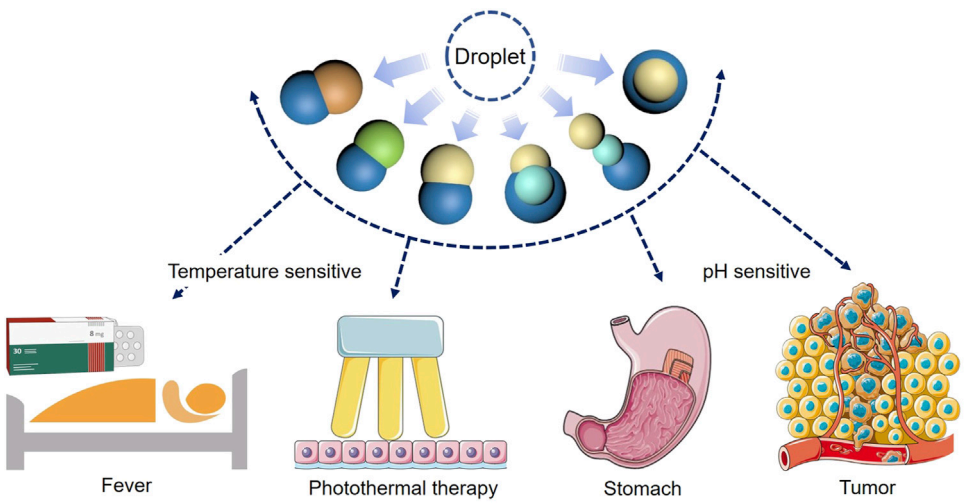

FIGURE 13 | Schematic diagrams of the function of the Janus particles.

release and pH triggered release with a same particle. The size of the newly formed droplets containing three components was 150 μm (long diameter), larger than that of the Janus droplets, and the structure of the triple droplets is shown in **Figure 12A**. As the solvent volatilized, the components in the droplet were gradually exposed to the water phase and because of their different solubility, different solidification regions formed, and then gradually formed multicompartment particles. In the newly formed particles, lipid located on one side, and the core-shell structure formed by the two polymers was on the other side (**Figure 12B**). When the phase separation process was complete, a final structure with three compartments linking together was observed (**Figure 12C**). This structure may be desired in programmed drug release, coding, self-assembly, and so on. And a series of triple structure may be fabricated through interfacial tension regulation in the future work.

DISCUSSION

Firstly, we prepared polymer-lipid Janus microparticles based on phase separation of micro-droplets. The microparticles have

dumbbell like structure and clear two-phase interface. The lipid hemisphere made from HCG lipid can degrade at physiological temperature, while the polymer hemisphere made from p (BMA-co-DAMA-co-MMA) can degrade in acidic environment, which can meet the demand of drug release at a target site, such as tumor tissue. Moreover, the particles prepared in microfluidic system have high homogeneity and tunability of size and morphology, which makes it easier to achieve effective control of drug release when the particles are used as drug carriers. 1-tetradecanol, 1-hexadecanol and lauric acid were employed to mix with the polymer to produce Janus particles, with an aim to adjust the trigger temperature for degradation of the lipid hemispheres. The development of multicompartment structure by phase separation was also explored. PLGA was added on the basis of HCG lipid and p (BMA-co-DAMA-co-MMA) to achieve sustained drug release property. The triple particles possessed a linear structure with three compartments.

The microfluidic preparation method established in this work is simple and mild, and has universality in a variety of polymer and lipid materials, which provides a path for the preparation of functional heterologous Janus particles. In addition, due to the unique structure of Janus particles, different drugs or other cargoes can be simultaneously loaded in the particles. According to the practical or personalized demands, various types of drug loading particles can be prepared by regulating the particle structure to form a controlled release system with different combinations of synergistic drugs. Compared with using polymers to manufacture Janus particles, the most significant innovation of this work is that phase change materials (1-tetradecanol, 1-hexadecanol and lauric acid) were introduced to phase separation systems, which had different physical and chemical properties from polymers. Integration of polymer and phase change materials had given rise to one Janus particle with different degradation properties. And the two materials were sensitive to different stimuli, enabling triggered degradation of each compartment. The future work can be devoted to the achievement of more advanced phase separation systems and more complex structures, so as to realize programed degradation and drug release in many scenarios (**Figure 13**).

DATA AVAILABILITY STATEMENT

The original contributions presented in the study are included in the article/**Supplementary Material**, further inquiries can be directed to the corresponding author.

AUTHOR CONTRIBUTIONS

Conceptualization: Z-YF, T-TL, and Z-TS; original article preparation: Z-SL, XS, and TW; draft correction, supervision and editing: X-TS, H-ZY, and SG. All authors listed have made substantial contribution to the article, which is acknowledged and confirmed by themselves. All authors have read and agreed on the final version of the article.

FUNDING

This research was funded by the project from the Natural Science Foundation of Liaoning Province of China (No. 2020-MS-166), Foundation of the Education Department of Liaoning Province in China (No. QN2019035), and the National Natural Science Foundation of China (No. 81500897).

ACKNOWLEDGMENTS

We would like to thank all the colleagues who have made contributions to this manuscript.

SUPPLEMENTARY MATERIAL

The Supplementary Material for this article can be found online at: https://www.frontiersin.org/articles/10.3389/fbioe.2021.756758/full#supplementary-material

REFERENCES

Ali, A., Zaman, A., Sayed, E., Evans, D., Morgan, S., Samwell, C., et al. (2021). Electrohydrodynamic Atomisation Driven Design and Engineering of Opportunistic Particulate Systems for Applications in Drug Delivery, Therapeutics and Pharmaceutics. Advanced Drug Delivery Reviews. *Adv. Drug Deliv. Rev.* 176, 113788. doi:10.1016/j.addr.2021.04.026

Chizari, S., Udani, S., Farzaneh, A., Stoecklein, D., Carlo, D. D., and Hopkins, J. B. (2020). Scanning Two-Photon Continuous Flow Lithography for the Fabrication of Multi-Functional Microparticles. *Opt. Express* 28 (26), 40088–40098. doi:10.1364/oe.410090

Choi, S.-W., Zhang, Y., and Xia, Y. (2010). A Temperature-Sensitive Drug Release System Based on Phase-Change Materials. *Angew. Chem. Int. Edition* 49 (43), 7904–7908. doi:10.1002/anie.201004057

de Gennes, P. G. (1992). Soft Matter. *Science* 256 (5056), 495–497. doi:10.1126/science.256.5056.495

Ding, D., and Zhu, Q. (2018). Recent Advances of PLGA Micro/nanoparticles for the Delivery of Biomacromolecular Therapeutics. *Mater. Sci. Eng. C* 92, 1041–1060. doi:10.1016/j.msec.2017.12.036

Du, J., and O'Reilly, R. K. (2011). Anisotropic Particles with Patchy, Multicompartment and Janus Architectures: Preparation and Application. *Chem. Soc. Rev.* 40 (5), 2402–2416. doi:10.1039/c0cs00216j

Feng, Z.-Q., Yan, K., Li, J., Xu, X., Yuan, T., Wang, T., et al. (2019). Magnetic Janus Particles as a Multifunctional Drug Delivery System for Paclitaxel in Efficient Cancer Treatment. *Mater. Sci. Eng. C* 104, 110001. doi:10.1016/j.msec.2019.110001

Gao, Y., and Chen, L. (2008). Versatile Control of Multiphase Laminar Flow for In-Channel Microfabrication. *Lab. Chip* 8 (10), 1695–1699. doi:10.1039/b807468b

Hansen, C., and Quake, S. R. (2003). Microfluidics in Structural Biology: Smaller, Faster... Better. *Curr. Opin. Struct. Biol.* 13 (5), 538–544. doi:10.1016/j.sbi.2003.09.010

Hu, J., Zhou, S., Sun, Y., Fang, X., and Wu, L. (2012). Fabrication, Properties and Applications of Janus Particles. *Chem. Soc. Rev.* 41 (11), 4356–4378. doi:10.1039/c2cs35032g

Hyun, D. C., Levinson, N. S., Jeong, U., and Xia, Y. (2014). Emerging Applications of Phase-Change Materials (PCMs): Teaching an Old Dog New Tricks. *Angew. Chem. Int. Ed.* 53 (15), 3780–3795. doi:10.1002/anie.201305201

Jin, Y., and Gao, X. (2009). Plasmonic Fluorescent Quantum Dots. *Nat. Nanotech* 4 (9), 571–576. doi:10.1038/nnano.2009.193

Kaewsaneha, C., Tangboriboonrat, P., Polpanich, D., Eissa, M., and Elaissari, A. (2013). Janus Colloidal Particles: Preparation, Properties, and Biomedical Applications. *ACS Appl. Mater. Inter.* 5 (6), 1857–1869. doi:10.1021/am302528g

Li, Y., Hao, L., Liu, F., Yin, L., Yan, S., Zhao, H., et al. (2019). Cell Penetrating Peptide-Modified Nanoparticles for Tumor Targeted Imaging and Synergistic Effect of Sonodynamic/HIFU Therapy. *Ijn* 14, 5875–5894. doi:10.2147/ijn.s212184

Maeda, K., Onoe, H., Takinoue, M., and Takeuchi, S. (2012). Controlled Synthesis of 3D Multi-Compartmental Particles with Centrifuge-Based Microdroplet Formation from a Multi-Barrelled Capillary. *Adv. Mater.* 24 (10), 1340–1346. doi:10.1002/adma.201102560

M. El-Sherbiny, I., and Abbas, Y. (2016). Janus Nano- and Microparticles as Smart Drug Delivery Systems. *Cpb* 17 (8), 673–682. doi:10.2174/1389201017666160401145438

Min, N. G., Ku, M., Yang, J., and Kim, S.-H. (2016). Microfluidic Production of Uniform Microcarriers with Multicompartments through Phase Separation in Emulsion Drops. *Chem. Mater.* 28 (5), 1430–1438. doi:10.1021/acs.chemmater.5b04798

Mullard, A. (2020). FDA Drug Approvals. *Nat. Rev. Drug Discov.* 20 (2), 85–90. doi:10.1038/d41573-019-00070-3

Pardridge, W. M. (2012). Drug Transport across the Blood-Brain Barrier. *J. Cereb. Blood Flow Metab.* 32 (11), 1959–1972. doi:10.1038/jcbfm.2012.126

Ramsay, P. T., and Carr, A. (2011). Gastric Acid and Digestive Physiology. *Surg. Clin. North America* 91 (5), 977–982. doi:10.1016/j.suc.2011.06.010

Severino, P., da Silva, C. F., Andrade, L. N., de Lima Oliveira, D., Campos, J., and Souto, E. B. (2019). Alginate Nanoparticles for Drug Delivery and Targeting. *Cpd* 25 (11), 1312–1334. doi:10.2174/1381612825666190425163424

Shakeri, A., Khan, S., and Didar, T. F. (2021). Conventional and Emerging Strategies for the Fabrication and Functionalization of PDMS-Based Microfluidic Devices. *Lab. Chip* 21 (16), 3053–3075. doi:10.1039/d1lc00288k

Shepherd, R. F., Conrad, J. C., Rhodes, S. K., Link, D. R., Marquez, M., Weitz, D. A., et al. (2006). Microfluidic Assembly of Homogeneous and Janus Colloid-Filled Hydrogel Granules. *Langmuir* 22 (21), 8618–8622. doi:10.1021/la060759+

Su, H., Hurd Price, C.-A., Jing, L., Tian, Q., Liu, J., and Qian, K. (2019). Janus Particles: Design, Preparation, and Biomedical Applications. *Mater. Today Bio* 4, 100033. doi:10.1016/j.mtbio.2019.100033

Sun, X.-T., Guo, R., Wang, D.-N., Wei, Y.-Y., Yang, C.-G., and Xu, Z.-R. (2019). Microfluidic Preparation of Polymer-Lipid Janus Microparticles with Staged Drug Release Property. *J. Colloid Interf. Sci.* 553, 631–638. doi:10.1016/j.jcis.2019.06.069

Sun, X.-T., Liu, M., and Xu, Z.-R. (2014). Microfluidic Fabrication of Multifunctional Particles and Their Analytical Applications. *Talanta* 121, 163–177. doi:10.1016/j.talanta.2013.12.060

Walther, A., and Müller, A. H. E. (2013). Janus Particles: Synthesis, Self-Assembly, Physical Properties, and Applications. *Chem. Rev.* 113 (7), 5194–5261. doi:10.1021/cr300089t

Wang, Q., Tian, Y., Liu, L., Chen, C., Zhang, W., Wang, L., et al. (2021). Precise Targeting Therapy of Orthotopic Gastric Carcinoma by siRNA and Chemotherapeutic Drug Codelivered in pH-Sensitive Nano Platform. *Adv. Healthc. Mater.* 7, e2100966. doi:10.1002/adhm.202100966

Xuan, M., Shao, J., Lin, X., Dai, L., and He, Q. (2014). Self-propelled Janus Mesoporous Silica Nanomotors with Sub-100 Nm Diameters for Drug Encapsulation and Delivery. *Chemphyschem* 15 (11), 2255–2260. doi:10.1002/cphc.201402111

Yi, Y., Sanchez, L., Gao, Y., and Yu, Y. (2016). Janus Particles for Biological Imaging and Sensing. *Analyst* 141 (12), 3526–3539. doi:10.1039/c6an00325g

Yu, Z., Geisler, K., Leontidou, T., Young, R. E. B., Vonlanthen, S. E., Purton, S., et al. (2021). Droplet-based Microfluidic Screening and Sorting of Microalgal Populations for Strain Engineering Applications. *Algal Res.*, 56. 102293. doi:10.1016/j.algal.2021.102293

Zhao, L. B., Pan, L., Zhang, K., Guo, S. S., Liu, W., Wang, Y., et al. (2009). Generation of Janus Alginate Hydrogel Particles with Magnetic Anisotropy for Cell Encapsulation. *Lab. Chip* 9 (20), 2981–2986. doi:10.1039/b907478c

Conflict of Interest: The authors declare that the research was conducted in the absence of any commercial or financial relationships that could be construed as a potential conflict of interest.

The handling editor declared a shared affiliation with the authors at time of review.

Publisher's Note: All claims expressed in this article are solely those of the authors and do not necessarily represent those of their affiliated organizations, or those of the publisher, the editors and the reviewers. Any product that may be evaluated in this article, or claim that may be made by its manufacturer, is not guaranteed or endorsed by the publisher.

frontiers in Materials

ORIGINAL RESEARCH
published: 15 September 2021
doi: 10.3389/fmats.2021.733535

More Precise Control of the *In Vitro* Enzymatic Degradation *via* Ternary Self-Blending of High/Medium/Low Molecular Weight Poly(trimethylene carbonate)

Guiyang Cai[1], Zhipeng Hou[2,3], Peng Li[3], Wei Sun[4], Jing Guo[3], Liqun Yang[3] and Qing Yang[1]**

[1]Department of Obstetrics and Gynecology, Shengjing Hospital of China Medical University, Shenyang, China, [2]Center for Molecular Science and Engineering, College of Science, Northeastern University, Shenyang, China, [3]NHC Key Laboratory of Reproductive Health and Medical Genetics (Liaoning Research Institute of Family Planning), China Medical University, Shenyang, China, [4]Department of Cell Biology, Key Laboratory of Cell Biology, Ministry of Public Health, and Key Laboratory of Medical Cell Biology, Ministry of Education, China Medical University, Shenyang, China*

OPEN ACCESS

Edited by:
Yilong Cheng,
Xi'an Jiaotong University, China

Reviewed by:
Lesan Yan,
Wuhan University of Technology, China
Jun Yue,
Sun Yat-sen University, China

***Correspondence:**
Liqun Yang
yanglq@lnszjk.com.cn
Qing Yang
yangqing_sj@126.com

Specialty section:
This article was submitted to Biomaterials, a section of the journal Frontiers in Materials

Received: *30 June 2021*
Accepted: *18 August 2021*
Published: *15 September 2021*

Citation:
Cai G, Hou Z, Li P, Sun W, Guo J, Yang L and Yang Q (2021) More Precise Control of the In Vitro Enzymatic Degradation via Ternary Self-Blending of High/Medium/Low Molecular Weight Poly(trimethylene carbonate). Front. Mater. 8:733535. doi: 10.3389/fmats.2021.733535

To more precisely control the degradation rate of poly(trimethylene carbonate) (PTMC), self-blending films were prepared *via* the ternary self-blending of pure PTMC with a molecular weight of 334, 152, and 57 kg/mol. The *in vitro* enzymolysis degradation of the ternary self-blending films was performed in lipase solutions. The results showed that ternary self-blending could control the degradation of PTMC by adjusting the mass ratio of high/medium/low molecular weight PTMC in the composition, and the $PTMC_{334}$/$PTMC_{152}$/$PTMC_{57}$ films with a mass ratio of 1/4/16 showed mass loss of 85.96% after seven weeks of degradation, while that of $PTMC_{334}$/$PTMC_{152}$/$PTMC_{57}$ films with a mass ratio of 1/1/1 was 96.39%. The former and latter's degradation rate constant was 13.263 and 23.981%/w, respectively, and the former presented better morphology stability than the latter. The strategy of ternary self-blending could simultaneously bestow PTMC with a lower degradation rate and good morphology stability, indicating that ternary self-blending is an efficient way to control the degradation performance of PTMC more precisely.

Keywords: poly(trimethylene carbonate), ternary self-blending, *In vitro* enzymatic degradation, lipase, degradation rate, form-stability

INTRODUCTION

Biomaterials play a critical role in tissue engineering and drug delivery systems (Woodruff and Hutmacher, 2010; Danhier et al., 2012; Raquez et al., 2013). As one of the essential biomaterials, poly(trimethylene carbonate) (PTMC) has also fascinated the extensive attention of researchers given its excellent biocompatibility and well biodegradation behavior, showing great potential applications in biomedical fields (Li et al., 2020; Mohajeri et al., 2020). Owing to its advantage of no acidic degradation products, PTMC is particularly suitable as a carrier for biodegradable contraceptive implants (Yang et al., 2012; Yang et al., 2013). However, the incompatibility between the morphology stability and degradation rate of PTMC hinders its application in biodegradable long-term contraceptive implants. Specifically, PTMC of low molecular weight presents a slower degradation rate while it deforms easily at room temperature (Zhang et al., 2006), usually causing an explosive release, which is undesirable in the implant systems. The increase in molecular weight can strengthen the morphology stability of PTMC, which also could result in a faster

degradation rate (Yang et al., 2015a), leading to a failure in the achievement of long-term applications. Hence, it is necessary to simultaneously endow PTMC with a lower degradation rate and good morphology stability, making it the most promising carrier for biodegradable long-term contraceptive implants.

Significant efforts have been devoted to this aim. Copolymerization is one of the most efficient strategies to improve polymer properties. It has been reported that poly(ε-caprolactone) (PCL) has a slow degradation rate and good mechanical properties *in vivo* due to its semicrystalline nature. Therefore, it will reduce the degradation rate and heighten the morphology stability of PTMC when introducing PCL segments into the structure of PTMC (Yang et al., 2014a). Similar observations also have been found for the copolymers of trimethylene carbonate (TMC) and 5,5-dimethyl-trimethylene carbonate (DTC) (Hou et al., 2019; Hou et al., 2020). In addition, cross-linking could form a three-dimensional network structure between cross-linking points, which has been demonstrated as an effective strategy to improve the morphology stability and decrease the degradation rate of PTMC (Yang et al., 2014b; Yang et al., 2016; Hou et al., 2017).

Although the strategies mentioned above could tailor the degradation rate and morphology stability, they also influence the comprehensive properties of PTMC. For instance, an undesired late inflammatory response might be evoked by the crystalline fragments formed during the degradation of PTMC copolymers (Bos et al., 1991). Hence, it is necessary to develop a more effective and appropriate method to tailor the degradation rate and morphology stability of PTMC. Blending is another common strategy to improve the performance of polymers (Han et al., 2010; Joy et al., 2020), and the more significant advantage of self-blending is that it does not introduce other components while improving polymer properties, totally remaining the performance advantages of polymer without adverse effects. In our previous work, binary self-blending of PTMC was performed with high molecular weight PTMC and low molecular weight PTMC. The results of *in vitro* enzymatic degradation showed that the degradation rate and morphology stability of the binary self-blending films could be regulated d by the mass ratio of high molecular weight PTMC to low molecular weight PTMC (Hou et al., 2021), indicating that binary self-blending is an efficient strategy to handle the degradation properties of PTMC.

Ternary self-blending was performed to the high/medium/low molecular weight PTMC in this study to obtain the ternary self-blending films. The *in vitro* enzymatic degradation of the obtained ternary self-blending films was performed in lipase solutions to investigate the role of ternary self-blending in the degradation rate and morphology stability of PTMC, with the aim of more precisely controlling the degradation behaviors of PTMC to meet the requirements of being a carrier for the biodegradable long-term contraceptive implants.

EXPERIMENTAL SECTION

Materials

TMC monomer was purchased from Daigang Biomaterial Co., Ltd. (Jinan, Shandong, China), recrystallized twice with ethyl acetate before use, and dried under vacuum at 37°C to remove the solvent. $Sn(Oct)_2$ (95%) and lipase solutions (from *Thermomyces lanuginosus*, ≥100,000 U/g) were purchased from Sigma-Aldrich and used as received without any treatment. All other solvents and reagents were of analytical grade and used as provided except where noted.

Methods

Synthesis of PTMC

PTMC of different molecular weights were prepared as described previously (Yang et al., 2015a). The bulk ring-opening polymerization (ROP) of TMC was carried out in a heat-sealed glass tube under a high vacuum at 130 ± 2°C for 24 h using $Sn(Oct)_2$ as a catalyst. After polymerization, all simple polymers were removed from the glass tube and dissolved in chloroform, precipitated and purified in cold methanol, and dried at 37°C under vacuum. The synthesized homopolymer and TMC monomer conversion were characterized from ^{1}H NMR spectra obtained in $CDCl_3$ on a Bruker ARX 300 (Bruker, Zurich, Switzerland) using tetramethylsilane (TMS) as an internal standard. Number-average (Mn) and polydispersity indices (PDI) of PTMC homopolymers were determined by GPC (Waters, Milford, MA, United States), and the sample was eluted at 35°C with THF at a rate of 1 ml/min. Values are calculated using polystyrene as a standard.

Preparation of PTMC Films and the Ternary Self-Blending Films

PTMC films and the ternary self-blending films were fabricated by solvent casting. In short, PTMC homopolymers of different molecular weights were dissolved separately in chloroform or self-blended according to the preset mass ratios in chloroform and then were transferred to Teflon® dishes. After vacuum drying to constant weight, the films were obtained using a puncher. The thermal properties of the homopolymer and self-blending films were evaluated using Netzsch DSC 200 F3 (Netzsch, Selb, Germany). The test temperature was −100–100°C, with a 10°C/min heating rate under a nitrogen flow.

In Vitro Enzymatic Degradation Study

The enzymolysis degradation of PTMC films and the ternary self-blending films (10 mm diameter; approximately 2 mm thickness) was performed in lipase (from *Thermomyces lanuginosus*, ≥100,000 U/g). The films were put into glass tubes containing 500 μL lipase solutions and conditioned at 37°C with gentle shaking for 8 h per day. The degradation medium was refreshed twice a week. Two parallel samples were removed at one-week intervals, washed with distilled water, and blotted dry. Subsequently, the related measurements were carried out after drying the films to constant weight under vacuum. The mass loss of the samples was obtained according to the following equations:

$$Mass\,loss\,(\%) = \frac{w_i - w_d}{w_i} \times 100. \quad (1)$$

w_i represents the initial weight of the sample before degradation, and w_d represents the dry weight of the piece after degradation.

TABLE 1 | The characteristics of PTMC homopolymers.

No.	Conversion (%)[a]	Mn[b] (kg/mol)	PDI[c]
$PTMC_{57}$	99	57	1.70
$PTMC_{152}$	98	152	2.20
$PTMC_{334}$	98	334	1.39

[a]*Calculated from ^{1}H NMR spectra.*
[b]*Determined by GPC analysis.*
[c]*Determined by GPC analysis.*

The microscopic morphologies of film surface were analyzed by SEM (HITACHI SU8010, Chiyoda-ku, Tokyo, Japan) after sputter coating the samples with gold using an ion sputtering apparatus. The pH of the degradation medium was measured using a Toledo-Mettler InLabMicro™ pH meter with a microelectrode (Toledo-Mettler, Zurich, Switzerland).

RESULTS AND DISCUSSION

PTMC Synthesis

As shown in **Table 1,** PTMC homopolymers of different molecular weights and broad polydispersity indices were prepared by ROP of TMC in this study, and the high/medium/low molecular weight was 334, 152, and 57 kg/mol, respectively. ^{1}H NMR test results indicated nearly complete monomer conversion during polymerization.

Preparation of PTMC Films and the Ternary Self-Blending Films

PTMC films and the ternary self-blending films were fabricated by solvent casting. After drying, the obtained PTMC films were transparent, which was led by the amorphous nature of PTMC, as shown by the DSC curve without melting peak. The glass transition temperature (T_g) increased from −17.8 to −14.4°C as the molecular weight raised from 57 to 334 kDa (**Table 2**). The ternary self-blending films were also amorphous and transparent, and the T_g values were in the range of −16.0~−16.8°C and decreased slightly as the mass ratio of low molecular weight PTMC increased in the composition. The low *Tg* value makes the ternary self-blending films flexible at physiological temperature and more suitable for subcutaneous tissues.

In Vitro Enzymatic Degradation

Enzymes such as lipase are capable of degrading polycarbonate polymers. In this study, the degradation behaviors of the ternary self-blending films were investigated in lipase solutions (from *Thermomyces lanuginosus*, ≥100,000 U/g), with high/medium/low molecular weight PTMC films as a straightforward comparison. **Figure 1** shows the changes in mass loss of the ternary self-blending films and PTMC films with degradation time.

As shown in **Figure 1**, the mass loss of the ternary self-blending films and PTMC films presented an excellent linear relationship with the degradation time. The high molecular weight $PTMC_{334}$ films gave the fastest degradation with a mass loss of 97.95% after four weeks of degradation, and the medium molecular weight $PTMC_{152}$ films showed relatively slower degradation than $PTMC_{334}$ films and lost their initial mass of 85.36% after four weeks of degradation. The low molecular weight $PTMC_{57}$ films degraded slowest, displaying a mass loss of 26.46% in eight weeks. Obviously, the higher the molecular weight, the more significant degradation of PTMC films. The result was in coincidence with that of our previous work (Yang et al., 2015a). As for the ternary self-blending films, the mass loss was related to the mass ratio of high/medium/low molecular weight PTMC in the composition. The $PTMC_{334}$/$PTMC_{152}$/$PTMC_{57}$ films with a mass ratio of 1/1/1 showed a mass loss of 96.39% after four weeks of degradation, while those with a mass ratio of 1/4/16 displayed much slower degradation with a mass loss of 85.96% after seven weeks of degradation (**Figure 1**).

The degradation rate constant *k* was calculated from the slope of the linear fitting curve of mass loss (Yang et al., 2015b). The *k* values of PTMC films and the ternary self-blending films were listed in **Table 3**, as the mass fraction of high molecular weight $PTMC_{334}$ raised in the composition from 4.76 and 33.3 to 100%, the *k* value increased obviously from 13.263 and 23.981 to 26.085%/w, respectively, for the $PTMC_{334}$/$PTMC_{152}$/$PTMC_{57}$ films with a mass ratio of 1/4/16, 1/1/1, and 1/0/0, while the *k* value significantly decreased from 23.981 and 13.263 to 3.664%/w (**Table 3**) as the proportion of low molecular weight $PTMC_{57}$ in the ternary self-blending films increased from 33.3 and 76.19 to 100% for the $PTMC_{334}$/$PTMC_{152}$/$PTMC_{57}$ films with a mass ratio of 1/1/1, 1/4/16, and 0/0/1. The degradation rate constant *k* of the ternary self-blending films enlarged obviously with the fraction increase of high molecular weight $PTMC_{334}$ and reduced with that of low molecular weight $PTMC_{57}$ in the composition, confirming again that the molecular weight has an important

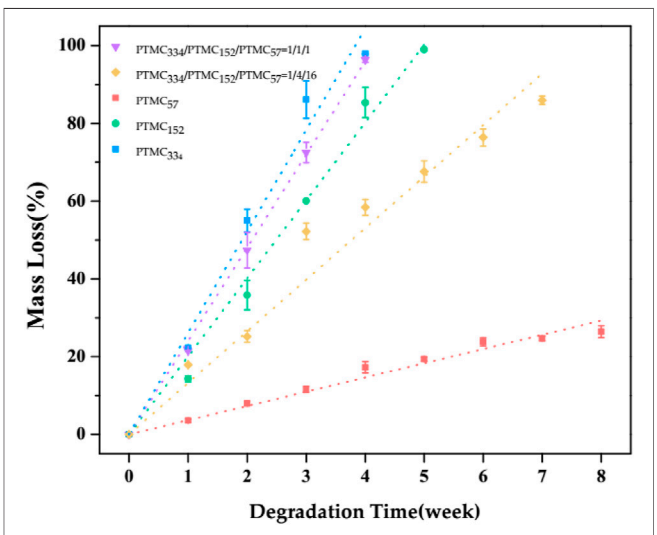

FIGURE 1 | The mass loss of PTMC films and the ternary self-blending films as a function of degradation time.

TABLE 2 | Preparation of PTMC films and the ternary self-blending films.

No.	$PTMC_{334}/PTMC_{152}/PTMC_{57}$[a]	T_g (°C)[b]
1	0/0/1	−17.8
2	1/4/16	−16.8
3	0/1/0	−15.4
4	1/1/1	−16.0
5	1/0/0	−14.4

[a]*Mass ratio of $PTMC_{334}$, $PTMC_{152}$, and $PTMC_{57}$.*
[b]*Obtained from the second run of heating.*

impact on the degradation rate of PTMC. The results showed that the degradation rate of PTMC could be controlled by ternary self-blending *via* the regulation of the composition. In our previous work (Hou et al., 2021), the binary self-blending films were prepared using high molecular weight $PTMC_{334}$ and low molecular weight $PTMC_{57}$, and the $PTMC_{334}/PTMC_{57}$ self-blending films with a mass ratio of 1/1 showed a k value of 19.4645%/w, which was similar to that of $PTMC_{152}$ films (k = 20.052%/w) in this study. Interestingly, the k value of $PTMC_{334}/PTMC_{152}/PTMC_{57}$ films with a mass ratio of 1/1/1 was increased to 23.981%/w after introducing $PTMC_{152}$ into the $PTMC_{334}/PTMC_{57}$ binary self-blending films. Furthermore, the k value of $PTMC_{334}/PTMC_{57}$ self-blending films with a mass ratio of 1/16 was 5.219%/w (Hou et al., 2021), which significantly increased to 13.263%/w for $PTMC_{334}/PTMC_{152}/PTMC_{57}$ films with a mass ratio of 1/4/16. It was attributed to the decrease in the content of low molecular weight $PTMC_{57}$ in the composition caused by the introduction of $PTMC_{152}$ into the $PTMC_{334}/PTMC_{57}$ self-blending films because the molecular weight plays a vital role in the degradation of PTMC; the lower the molecular weight, the much slower the degradation of PTMC (Yang et al., 2015a). The results indicated that the degradation rate of PTMC films could be tailored more precisely *via* ternary self-blending as compared with binary self-blending.

In addition to the controllable degradation rate, good morphology stability is also a desired property for PTMC to be applied as the carrier of biodegradable implants. The macroscopic morphology of PTMC films and the ternary self-blending films with degradation time was recorded to observe the morphology stability during degradation, displayed in **Figure 2**. As shown in **Figure 2**, the film of low molecular weight $PTMC_{57}$ had poor morphology stability and changed the initial shape to spherical at week 1, while the $PTMC_{152}$ film could retain its initial appearance in two weeks and became irregular after four weeks of degradation. High molecular weight $PTMC_{334}$ film presented better morphology stability, and it can still maintain the film shape after three weeks of degradation, although there were visible holes on the surface. The higher the molecular weight, the much better the morphology stability. As for the ternary self-blending films, the $PTMC_{334}/PTMC_{152}/PTMC_{57}$ films with a mass ratio of 1/4/16 showed better morphology stability than those with a mass ratio of 1/1/1, which remained the initial shape with no deformation last for four weeks and could keep the film-like form after six weeks of degradation. The morphology stability and degradation rate results indicated that ternary self-blending of high/medium/low molecular weight PTMC could make PTMC have a slower degradation rate and better morphology stability simultaneously during the degradation periods. More specifically, the degradation cycle of the $PTMC_{334}/PTMC_{152}/PTMC_{57}$ films with a mass ratio of 1/4/16 was long enough, and it could retain good morphology stability during the degradation process, making it a promising candidate for long-term implants *in vivo*.

It has been reported that the enzymes can play a role as a surfactant to disperse the degradation products into the surrounding media (Yang et al., 2015a). The surface of PTMC samples would be changed accordingly with holes and pits during the degradation periods. **Figure 3** shows the morphology changes of PTMC films and the ternary self-blending films before and after degradation in lipase solutions. As a representative, the surface morphology changes of $PTMC_{334}/PTMC_{152}/PTMC_{57}$ films with a mass ratio of 1/4/16 were described in detail. The film surface was flat and smooth before the degradation, and it became rough with cracks as the degradation occurred after one week, and then small holes and pits emerged on the sample surface after three weeks of degradation, indicating the loss of degradation products. As the degradation prolonged to week 5, the erosion became prominent, and the sample surface became much rough, as noted in the number increase of holes. The results indicated that more degradation products were dispersed to the medium with the aid of lipase.

Figure 3 also shows the surface morphology of the PTMC films and the ternary self-blending films with different compositions after three weeks of degradation. The surface morphology changed with the design of the resulting films. After three weeks of degradation, more prominent and bottomless pits were observed on the surface of $PTMC_{334}$ and $PTMC_{334}/PTMC_{152}/PTMC_{57}$ films with a mass ratio of 1/1/1, indicating that more severe degradation occurred. The size of pits

TABLE 3 | The degradation rate constant k of PTMC films and the ternary self-blending films.

No.	$PTMC_{334}/PTMC_{152}/PTMC_{57}$[a]	Degradation rate constant k	Correlation coefficient
		%/w[b]	R
1	0/0/1	3.664	0.996
2	1/4/16	13.263	0.995
3	0/1/0	20.052	0.998
4	1/1/1	23.981	0.999
5	1/0/0	26.085	0.997

[a]*Mass ratio of $PTMC_{334}$, $PTMC_{152}$, and $PTMC_{57}$.*
[b]*Percentage of mass loss per week.*

FIGURE 2 | The macroscopic observation of the PTMC films PTMC films and ternary self-blending films at different times in 37°C lipase.

on the surface of $PTMC_{152}$ and $PTMC_{334}/PTMC_{152}/PTMC_{57}$ films with a mass ratio of 1/4/16 became much smaller, resulting in minor roughness. The $PTMC_{57}$ presented a relatively smooth surface with cracks rather than pits or holes. The SEM results were coincidental with that of mass loss.

It has been reported that PTMC does not produce acidic products during degradation (Yang et al., 2015a). For the ternary self-blending films, the degradation products also should be nonacidic due to their polycarbonate structure. In **Figure 4**, the pH of the lipase solution as a function of the degradation time was displayed. As expected, no acidification was observed when the degradation of ternary self-blending films occurred, powerfully demonstrating that the ternary self-blending films degraded without acidic products. It is beneficial to eliminate the inflammatory evoked by the acidic degradation products (Zhu et al., 1991; Karp et al., 2003; Sachlos et al., 2003). In addition, the accelerated degradation caused by the autocatalysis (Bergsma et al., 1995) will not occur during the degradation of the ternary self-blending films, promoting the more widespread application of the ternary self-blending films in the biomedical fields.

CONCLUSION

In this study, PTMC with high/medium/low molecular weight of 334, 152, and 57 kg/mol, respectively, was prepared, and ternary self-blending of high/medium/low molecular weight PTMC was performed to obtain the self-blending PTMC films. The *in vitro*

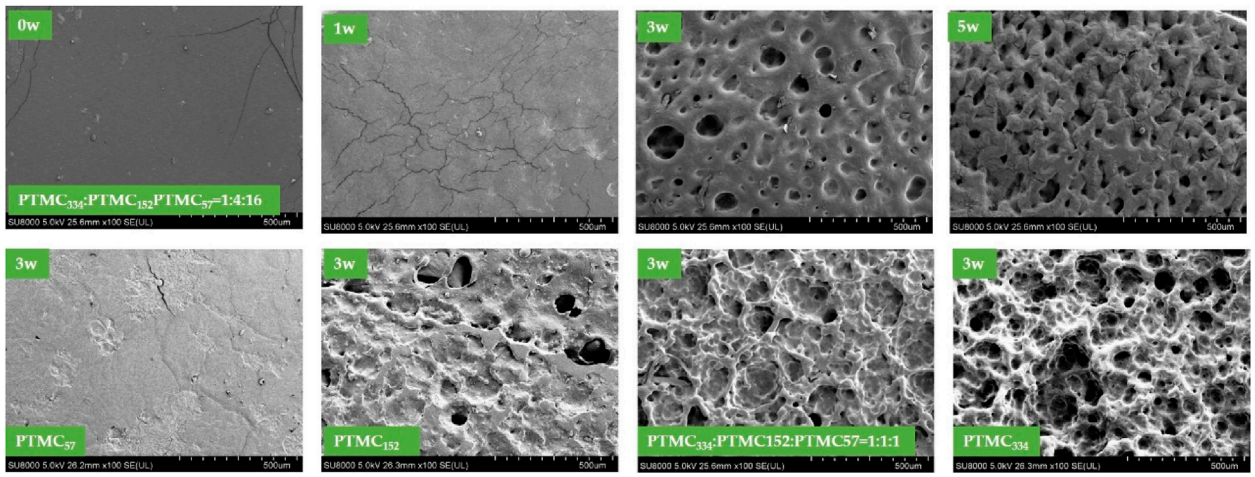

FIGURE 3 | The surface morphology of PTMC films and the ternary self-blending films after degradation in lipase solutions.

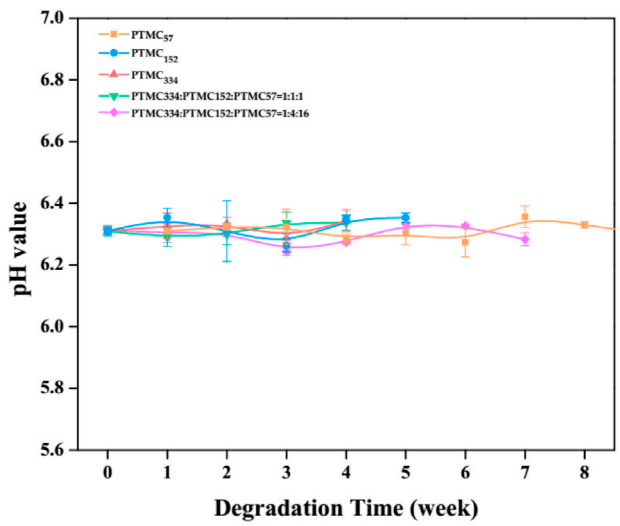

FIGURE 4 | The pH of lipase solutions of PTMC films and the ternary self-blending films during enzymatic degradation.

enzymatic degradation behavior of the ternary self-blending films was carried out in lipase solutions compared to that of the pure high/medium/low molecular weight PTMC films to investigate the effect of ternary self-blending on the degradation behaviors of PTMC. The results showed that the ternary self-blending films presented glass transition temperature lower than physiological temperature, making them more suitable for application *in vivo*. The results of mass loss and degradation rate constant indicated that ternary self-blending could lower the degradation rate of high molecular weight PTMC and enhance that of low molecular weight PTMC. The composition also influenced the degradation of the ternary self-blending films. The higher the content of the low molecular weight PTMC in the composition, the lower the degradation rate of the ternary self-blending films, as shown by the results of degradation rate constant and SEM. The $PTMC_{334}/PTMC_{152}/PTMC_{57}$ film with a mass ratio of 1/4/16 showed a lower degradation rate constant of 13.263%/w, which also displayed better morphology stability to make the initial shape last for six weeks, with no acidic degradation products formed during degradation periods. The results indicated that ternary self-blending of high/medium/low molecular weight PTMC could more precisely control the *in vitro* enzymatic degradation of PTMC to meet the requirement as carriers for the biodegradable long-term contraceptive implants.

DATA AVAILABILITY STATEMENT

The original contributions presented in the study are included in the article/Supplementary Material; further inquiries can be directed to the corresponding authors.

AUTHOR CONTRIBUTIONS

GC and ZH performed the experiments, GC collected and analyzed the data and wrote the initial draft; LY and QY conceived and designed the experiments; WS and PL reviewed and edited the draft; JG performed the tests.

FUNDING

This work was supported by the National Key Research & Development Program of China (2016YFC1000902), the National Natural Science Foundation of China (No. 81872125), the Liaoning Revitalization Talents Program (XLYC1807142), the Department of Science & Technology of Liaoning Province (2018225079), the Educational Department of Liaoning Province (ZF2019040), the Shenyang Science and Technology Bureau (RC190426), and the Outstanding Scientific Fund of Shengjing Hospital (No. 201704).

REFERENCES

Bergsma, J., De Bruijn, W. C., Rozema, F. R., Bos, R. R., and Boering, G. (1995). Late Degradation Tissue Response to Poly(?-Lactide) Bone Plates and Screws. *Biomaterials* 16 (1), 25–31. doi:10.1016/0142-9612(95)91092-d

Bos, R. R. M., Rozema, F. B., Boering, G., Nijenhius, A. J., Pennings, A. J., Verwey, A. B., et al. (1991). Degradation of and Tissue Reaction to Biodegradable poly(L-Lactide) for Use as Internal Fixation of Fractures: A Study in Rats. *Biomaterials* 12 (1), 32–36. doi:10.1016/0142-9612(91)90128-w

Danhier, F., Ansorena, E., Silva, J. M., Coco, R., Le Breton, A., and Préat, V. (2012). PLGA-Based Nanoparticles: An Overview of Biomedical Applications. *J. controlled release* 161 (2), 505–522. doi:10.1016/j.jconrel.2012.01.043

Han, J., Branford-White, C. J., and Zhu, L.-M. (2010). Preparation of Poly(ε-Caprolactone)/poly(trimethylene Carbonate) Blend Nanofibers by Electrospinning. *Carbohydr. Polym.* 79 (1), 214–218. doi:10.1016/j.carbpol.2009.07.052

Hou, Z., Hu, J., Li, J., Zhang, W., Li, M., Guo, J., et al. (2017). The *In Vitro* Enzymatic Degradation of Cross-Linked Poly(trimethylene Carbonate) Networks. *Polymers* 9 (11), 605. doi:10.3390/polym9110605

Hou, Z., Zhang, W., Guo, J., Chen, Z., Hu, J., and Yang, L. (2019). The *In Vitro* Enzymatic Degradation of Poly(trimethylene Carbonate-Co-2, 2′-dimethyltrimethylene Carbonate). *Eur. Polym. J.* 112, 51–59. doi:10.1016/j.eurpolymj.2018.12.027

Hou, Z., Li, P., Guo, J., Wang, J., Hu, J., and Yang, L. (2020). The Effect of Molecular Weight on thermal Properties and Degradation Behavior of Copolymers Based on TMC and DTC. *Polym. Degrad. Stab.* 175, 109128. doi:10.1016/j.polymdegradstab.2020.109128

Hou, Z., Chen, S., Li, Z., Chen, Z., Hu, J., Guo, J., et al. (2021). Controllable Degradation of Poly (Trimethylene Carbonate) *via* Self-Blending with Different Molecular Weights. *Polym. Degrad. Stab.* 189, 109596. doi:10.1016/j.polymdegradstab.2021.109596

Joy, J., Aid-Launais, R., Pereira, J., Pavon-Djavid, G., Ray, A. R., Letourneur, D., et al. (2020). Gelatin-Polytrimethylene Carbonate Blend Based Electrospun Tubular Construct as a Potential Vascular Biomaterial. *Mater. Sci. Eng. C* 106, 110178. doi:10.1016/j.msec.2019.110178

Karp, J. M., Shoichet, M. S., and Davies, J. E. (2003). Bone Formation on Two-Dimensional poly(DL-Lactide-Co-Glycolide) (PLGA) Films and Three-Dimensional PLGA Tissue Engineering Scaffoldsin Vitro. *J. Biomed. Mater. Res.* 64A (2), 388–396. doi:10.1002/jbm.a.10420

Li, X., Chen, H., Xie, S., Wang, N., Wu, S., Duan, Y., et al. (2020). Fabrication of Photo-Crosslinkable Poly(Trimethylene Carbonate)/Polycaprolactone Nanofibrous Scaffolds for Tendon Regeneration. *Int. J. Nanomedicine* 15, 6373–6383. doi:10.2147/IJN.S246966

Mohajeri, S., Chen, F., de Prinse, M., Phung, T., Burke-Kleinman, J., Maurice, D. H., et al. (2020). Liquid Degradable Poly(trimethylene-Carbonate-Co-5-Hydroxy-Trimethylene Carbonate): An Injectable Drug Delivery Vehicle for Acid-Sensitive Drugs. *Mol. Pharmaceutics* 17 (4), 1363–1376. doi:10.1021/acs.molpharmaceut.0c00064

Raquez, J. M., Habibi, Y., Murariu, M., and Dubois, P. (2013). Polylactide (PLA)-Based Nanocomposites. *Prog. Polym. Sci.* 38 (10-11), 1504–1542. doi:10.1016/j.progpolymsci.2013.05.014

Sachlos, E., Czernuszka, J. T., and Czernuszka, J. (2003). Making Tissue Engineering Scaffolds Work. Review: The Application of Solid Freeform Fabrication Technology to the Production of Tissue Engineering Scaffolds. *Eur. Cel Mater* 5 (1), 29–40. doi:10.22203/ecm.v005a03

Woodruff, M. A., and Hutmacher, D. W. (2010). The Return of a Forgotten Polymer-Polycaprolactone in the 21st century. *Prog. Polym. Sci.* 35 (10), 1217–1256. doi:10.1016/j.progpolymsci.2010.04.002

Yang, L.-Q., Yang, D., Guan, Y.-M., Li, J.-X., and Li, M. (2012). Random Copolymers Based on Trimethylene Carbonate and ε-Caprolactone for Implant Applications: Synthesis and Properties. *J. Appl. Polym. Sci.* 124 (5), 3714–3720. doi:10.1002/app.35355

Yang, L.-Q., He, B., Meng, S., Zhang, J.-Z., Li, M., Guo, J., et al. (2013). Biodegradable Cross-Linked Poly(trimethylene Carbonate) Networks for Implant Applications: Synthesis and Properties. *Polymer* 54 (11), 2668–2675. doi:10.1016/j.polymer.2013.03.059

Yang, L., Li, J., Meng, S., Jin, Y., Zhang, J., Li, M., et al. (2014). The *In Vitro* and *In Vivo* Degradation Behavior of Poly (Trimethylene Carbonate-Co-ε-Caprolactone) Implants. *Polymer* 55 (20), 5111–5124. doi:10.1016/j.polymer.2014.08.027

Yang, L., Li, J., Jin, Y., Zhang, J., Li, M., and Gu, Z. (2014). Highly Efficient Cross-Linking of Poly(trimethylene Carbonate) *via* Bis(trimethylene Carbonate) or Bis(ε-Caprolactone). *Polymer* 55 (26), 6686–6695. doi:10.1016/j.polymer.2014.10.072

Yang, L., Li, J., Zhang, W., Jin, Y., Zhang, J., Liu, Y., et al. (2015). The Degradation of Poly(trimethylene Carbonate) Implants: The Role of Molecular Weight and Enzymes. *Polym. Degrad. Stab.* 122, 77–87. doi:10.1016/j.polymdegradstab.2015.10.016

Yang, L., Li, J., Jin, Y., Li, M., and Gu, Z. (2015). *In Vitro* enzymatic Degradation of the Cross-Linked Poly(ε-Caprolactone) Implants. *Polym. Degrad. Stab.* 112, 10–19. doi:10.1016/j.polymdegradstab.2014.12.008

Yang, L., Li, J., Li, M., and Gu, Z. (2016). The *In Vitro* and *In Vivo* Degradation of Cross-Linked Poly(trimethylene Carbonate)-Based Networks. *Polymers* 8 (4), 151. doi:10.3390/polym8040151

Zhang, Z., Kuijer, R., Bulstra, S. K., Grijpma, D. W., and Feijen, J. (2006). The *In Vivo* and *In Vitro* Degradation Behavior of Poly(trimethylene Carbonate). *Biomaterials* 27 (9), 1741–1748. doi:10.1016/j.biomaterials.2005.09.017

Zhu, K. J., Hendren, R. W., Jensen, K., and Pitt, C. G. (1991). Synthesis, Properties, and Biodegradation of Poly(1,3-Trimethylene Carbonate). *Macromolecules* 24 (8), 1736–1740. doi:10.1021/ma00008a008

Conflict of Interest: The authors declare that the research was conducted in the absence of any commercial or financial relationships that could be construed as a potential conflict of interest.

frontiers in Bioengineering and Biotechnology

MINI REVIEW
published: 19 October 2021
doi: 10.3389/fbioe.2021.763804

Cyanophycin Modifications—Widening the Application Potential

Natalia Kwiatos and Alexander Steinbüchel*

International Center for Research on Innovative Biobased Materials (ICRI-BioM)—International Research Agenda, Lodz University of Technology, Lodz, Poland

A circular bioeconomy approach is essential to slowing down the fearsome ongoing climate change. Replacing polymers derived from fossil fuels with biodegradable biobased polymers is one crucial part of this strategy. Cyanophycin is a polymer consisting of amino acids produced by cyanobacteria with many potential applications. It consists mainly of aspartic acid and arginine, however, its composition may be changed at the production stage depending on the conditions of the polymerization reaction, as well as the characteristics of the enzyme cyanophycin synthetase, which is the key enzyme of catalysis. Cyanophycin synthetases from many sources were expressed heterologously in bacteria, yeast and plants aiming at high yields of the polymer or at introducing different amino acids into the structure. Furthermore, cyanophycin can be modified at the post-production level by chemical and enzymatic methods. In addition, cyanophycin can be combined with other compounds to yield hybrid materials. Although cyanophycin is an attractive polymer for industry, its usage as a sole material remains so far limited. Finding new variants of cyanophycin may bring this polymer closer to real-world applications. This short review summarizes all modifications of cyanophycin and its variants that have been reported within the literature until now, additionally addressing their potential applications.

Keywords: cyanophycin, multi-L-arginyl-poly-L-aspartate, polyaminoacid, biopolymer, chemical and enzymatic modifications

OPEN ACCESS

Edited by:
Liqun Yang,
China Medical University, China

Reviewed by:
Li Li,
Guangdong Medical University, China
Stephan Klähn,
Helmholtz Centre for Environmental Research (UFZ), Germany

****Correspondence:***
Natalia Kwiatos
natalia.kwiatos@p.lodz.pl

Specialty section:
This article was submitted to Biomaterials, a section of the journal Frontiers in Bioengineering and Biotechnology

Received: *24 August 2021*
Accepted: *05 October 2021*
Published: *19 October 2021*

Citation:
Kwiatos N and Steinbüchel A (2021) Cyanophycin Modifications—Widening the Application Potential. Front. Bioeng. Biotechnol. 9:763804. doi: 10.3389/fbioe.2021.763804

INTRODUCTION

Cyanophycin, also referred to as cyanophycin granule polypeptide or multi-L-arginyl-poly-L-aspartate, is a non-ribosomally synthesized amino acid polymer found in cyanobacteria and some heterotrophic bacteria. It serves microorganisms as a temporary storage compound primarily for nitrogen, but also for energy and carbon (Merritt et al., 1994; Li et al., 2001; Frommeyer et al., 2016). It is composed of aspartic acid in the backbone and arginine residues as the side chains (**Figure 1 Figure 1A**). Typically, these amino acids are present in equimolar amounts. Cyanophycin is synthesized by the enzyme cyanophycin synthetase (CphA), which requires a primer, Mg^{2+}, K^{+}, ATP and two amino acids for its catalytic action (Simon, 1976). CphA uses a short peptide as a primer and then extends it to produce cyanophycin (Berg et al., 2000; Sharon et al., 2021). The α-carboxylic group of aspartic acid in the backbone is activated by phosphorylation, whereby ATP is converted to ADP. Then, the next aspartic acid is bound by peptide bond to the C-terminus of the backbone. Next, the γ-carboxylic acid is activated by phosphorylation and arginine is attached at this position by an isopeptide bond (Forchhammer and Watzer, 2016; Frommeyer et al., 2016; Du et al., 2019).

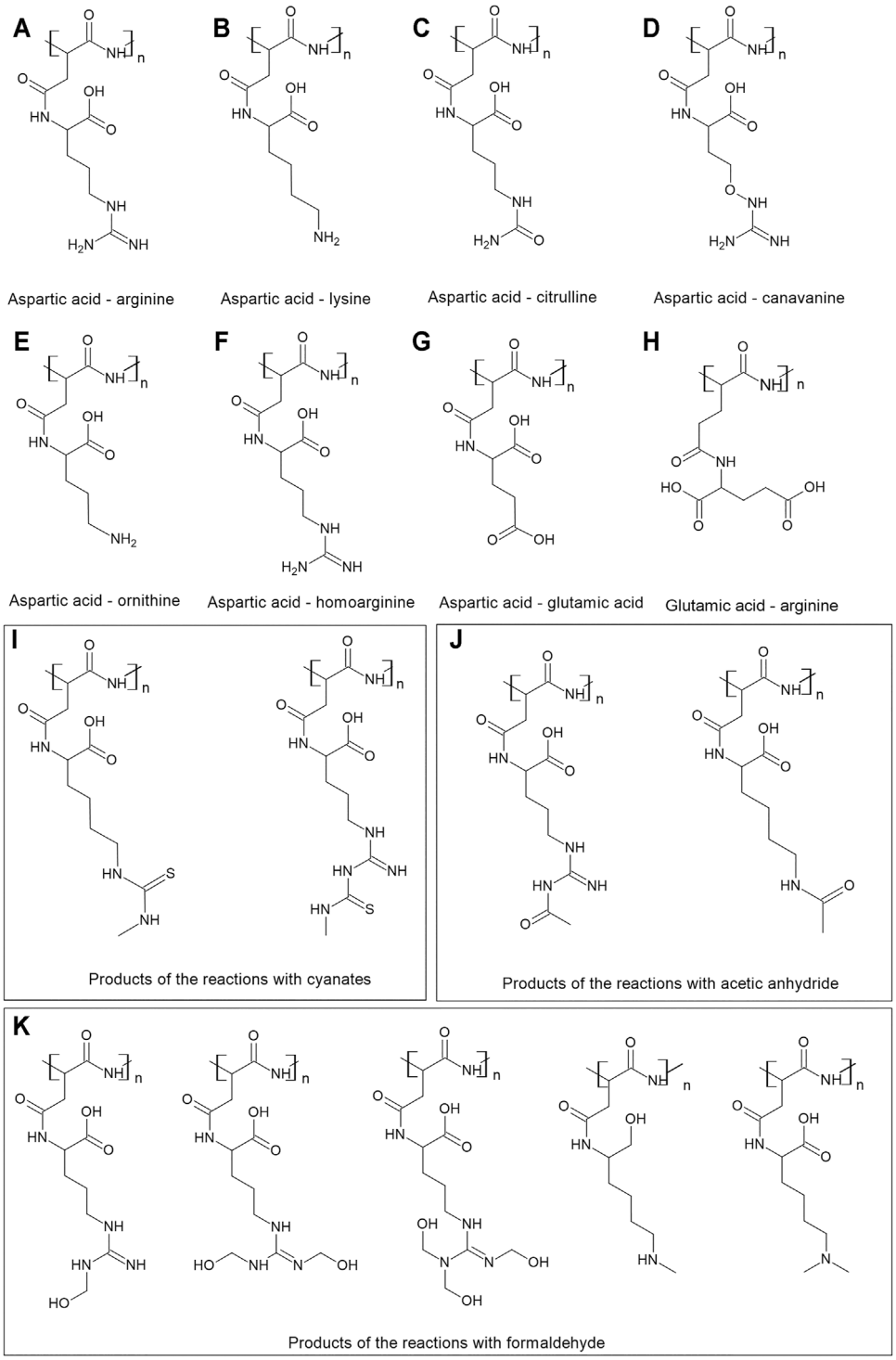

FIGURE 1 | Cyanophycin and its modifications. **(A)** The basic structure of cyanophycin–aspartic acid in the backbone and arginine in the side chain; the next drawings present cyanophycin with aspartic acid in the backbone and different side chains: **(B)** lysine, **(C)** citrulline, **(D)** canavanine, **(E)** ornithine, **(F)** homoarginine, **(G)** glutamic acid. **(H)** glutamic acid in the backbone and arginine in the side chain. The drawings I-K presents the structures of the products of the reactions of cyanophycin with **(H)** cyanates, **(I)** acetic anhydride **(J)** formaldehyde.

Cyanophycin occurs mainly as an insoluble inclusion in the cytoplasm, but is also soluble under certain conditions. Cyanophycin is a polydisperse polymer with molecular masses between 25 and 100 kDa (Frommeyer et al., 2016; Du et al., 2019). The molecular mass range for insoluble cyanophycin is approximately between 20 and 25 kDa, while for soluble

cyanophycin this value lies between 8 and 20 kDa. Regular cyanophycin is regarded as insoluble at pH values between 6 and 8, and its solubility decreases with increasing molar mass. Detailed studies revealed that soluble cyanophycin fractions possess a higher lysine to arginine ratio relative to the insoluble form (Khlystov et al., 2017). The 3D structure of cyanophycin is not known, however, circular dichroism studies showed that under acidic conditions it exhibited a defined secondary structure containing β-sheets (Simon et al., 1980). Cyanophycin possesses negatively charged α-hydroxyl groups and positively charged arginine and lysine side chains, therefore, it is a zwitterion. Cyanophycin binds with other cyanophycin chains by charged interactions and hydrogen bonds. In addition, intra-chain interactions also occur.

Purified soluble cyanophycin is a white amorphous powder, while the purified insoluble fraction is a mixture of white and brownish solids. The reason for the occurrence of the brownish solids is unknown. Its mechanical properties are similar to other unplasticized polypeptides–it is rigid and brittle. According to previous studies (Khlystov et al., 2017) its Young's modulus is 560 MPa, while the ultimate compressive strength is around 78 MPa and strain-at-break is 17 ± 4%. Cyanophycin is thermally stable up to 200°C, being pyrolyzed at > 700 C (Khlystov et al., 2017).

ε-Poly-L-lysine and γ-poly-glutamic acid are other examples of non-ribosomally synthesized polymers consisting of amino acids. They are examples of well-studied polymers, showing more than 3,000 hits for "poly-lysine" and more than 4,000 hits for "poly-glutamic acid" in a Web of Science search, compared to only 320 hits for "cyanophycin". All have great potential for use in many diverse areas–environmental pollution treatments, food preservation and multiple medical applications (Chen et al., 2021; Nair et al., 2021).

Climate change is a fact (Heesterman, 2020). The European Commission prepared a strategy to slow down the destruction of the Earth (European Comission, 2020), stressing the adoption of a "less waste, more value" policy. Replacing polymers derived from fossil fuels with biodegradable biobased polymers is a crucial part of this strategy. Cyanophycin is a biobased polymer with a great potential for applications in many areas (Frommeyer et al., 2016), including in medicine (Uddin et al., 2020) and food technology (Sallam and Steinbüchel, 2010). Despite the fact that cyanophycin's features do not allow this polymer to be used as a sole material, as for example polyhydroxyalkanoate (PHA), its biodegradability and environmentally friendly production encourages studies on widening its applicability. The availability of novel analogues of cyanophycin enables the determination of their features which may lead to the fulfillment of an industrial niche or the replacement of an existing but unsatisfactory solution. For instance, the modification of cyanophycin side chains with an alternative amino acid may not only yield novel polymers but may also lead to the production of dipeptides which could find other applications than aspartate-arginine (Sallam and Steinbüchel, 2010).

Cyanophycin Production in Various Microorganisms and Plants

Cyanophycin serves as a storage compound for nitrogen and carbon in cyanobacteria (Li et al., 2001; Du et al., 2019). The first literature data on cyanophycin was published in 1971, describing the isolation and characterization of cyanophycin from *Anabaena cylindrica*, a nitrogen-fixing cyanobacterium (Simon, 1971). This was followed by the discovery of cyanophycin in many other cyanobacteria, such as *Nostoc ellipsosporum*, *Scytonema*, *Synechococcus* and *Synechocystis* and also in other microorganisms, for example *Acinetobacteria* and *Bordetella* species (Frommeyer et al., 2016; Du et al., 2019). The occurrence of cyanophycin in many microorganisms is discussed in a recent detailed review (Du et al., 2019).

Cyanobacteria are not suitable for the large scale production of cyanophycin because the growth of photosynthetic bacteria is slow and only low cell densities are obtained (Du et al., 2019). In addition, the photoautotrophic growth of cyanobacteria is only possible in photobioreactors. Thus heterologous expression of cyanophycin synthetase genes (*cphA*) in heterotrophic microorganisms was widely studied. The main sources of the genes were: *Synechocystis sp.* PCC6803 ($cphA_{6803}$) (Frey et al., 2002), *Synechocystis sp.* PCC6308 ($cphA_{6308}$) (Aboulmagd et al., 2001), and *Anabaena sp.* PCC7120 ($cphA_{7120}$) (Voss et al., 2004a). Cyanophycin was heterologously produced for the first time in *E. coli* using *cphA* from *Synechocystis sp.* PCC6803. The genes were amplified from genomic DNA using PCR techniques and cloned into the pBluescript II SK + plasmid and transformed to *E. coli* strain DH5A. The yield of insoluble cyanophycin was around 100 mg/L (Ziegler et al., 1998).

Cyanophycin production at the 4.5 L scale was done with codon-optimized *cphA* gene using *E. coli* BL21 (DE3), obtaining 970 ± 80 mg/L cyanophycin (Khlystov et al., 2017). Large scale production was performed in a 500 L stirred-tank bioreactor. For this purpose *cphA* from *Synechocystis* sp. strain PCC6803 was expressed in *E. coli* DH1 on the pMa vector. The yield of cyanophycin biosynthesis achieved was 1.5 g/L (Frey et al., 2002). Cyanophycin synthetase from *Synechocystis sp.* strain PCC6308 was expressed in *E. coli* yielding a maximum cyanophycin content of 26.6% (w/w) of cell dry mass (Aboulmagd et al., 2000). In further studies, an addiction system was used to secure plasmid stability and applied to a recombinant *E. coli* HMS174(DE3) strain. This paid off with a cyanophycin content of 42% (w/w) (Kroll et al., 2011).

Other microorganisms have also been used for production of cyanophycin, for example *Ralstonia eutropha* and *Pseudomonas putida*, which are well established for PHA production (Voss et al., 2004b; Raberg et al., 2018). *P. putida* GPp104, *P. putida* KT2440, *R. eutropha* H16, *R. eutropha* PHB^{-}4 carrying the *Anabaena sp.* strain PCC7120 cyanophycin synthetase were tested and the highest cyanophycin yield was obtained with *P. putida* KT2440 (Voss et al., 2004b). Interestingly, *R. euthropha* H16 possess in its genome genes homologous to cyanophycin synthetase. However, no cyanophycin was detected when these genes from *R. euthropha* H16 were both overexpressed in its

natural host or heterologously expressed in *E. coli* (Adames et al., 2013).

Corynebacterium glutamicum is a bacterium that is used for the biotechnological production of various amino acids (Wendisch et al., 2016; Xiao et al., 2020). Therefore, it was investigated for the production of cyanophycin, however, with little success (2–3.6% of dry mass) (Aboulmagd et al., 2001). In addition the downstream process to isolate the polymer was difficult due to the rigidity of the cell walls (Aboulmagd et al., 2001). Other strains of *C. gutamicum* as well as various expression vectors and cyanophycin synthetases were later evaluated for this purpose with more success, resulting in cellular cyanophycin contents of approximately 14% of the dry mass (Wiefel et al., 2019b).

Yeast expression systems were also applied for cyanophycin synthesis. A particularly interesting idea was to use *Saccharomyces cerevisiae* to produce ethanol and cyanophycin simultaneously (Mooibroek et al., 2007; Könst et al., 2010). However, the yield of cyanophycin in *S. cerevisiae* was low in comparison to the *E. coli* system, amounting to only about 7% of the cellular dry mass (Steinle et al., 2008). Cyanophycin contents of up to 10.4% (wt/wt) were obtained when $CphA_{6308}$ was expressed in *Pichia pastoris*. Truncation at the carboxy terminus led to a 2.5-fold higher specific activity of cyanophycin synthetase and 14.3% cyanophycin at the maximum (Steinle et al., 2010). Glutamic acid at the C-terminus of $CphA_{6308}$ forms the M domain of the enzyme and its truncation probably led to conformational changes of the region thus causing the increase in activity.

In addition to microorganisms, transgenic plants were also constructed for cyanophycin production using agriculture. Two cultivars of *Nicotiana tabacum* carrying the *Thermosynecchococcus elongatus* BP-1 cyanophycin synthetase were used for this purpose yielding up to 9.4% dry weight cyanophycin (Nausch et al., 2016). Potato (*Solanum tuberosum*) is an alternative plant cyanophycin producer, however, the production yields were lower than that for tobacco cultivars, only amounting up to 7.5% dry weight (Schmidt et al., 2017). Although the yields are lower than for bacterial systems, it is arguable that plants are more suitable for the large scale production of cyanophycin due to their easier scalability and lower cost of cultivation (Nausch et al., 2015, 2016).

CYANOPHYCIN MODIFICATIONS

The availability of novel structures of cyanophycin enables the determination of their features, which may lead to the fulfillment of an industrial niche or the replacement of an existing but unsatisfactory material. There are two principal strategies to change the composition of cyanophycin and to obtain new variants of this polymer. One strategy relies on the biological system and on the cultivation conditions used to grow the cyanophycin producing organism. This *in vivo* approach yields cyanophycin with a different composition which is then accumulated in the producing cells. The second strategy begins from cyanophycin which was produced *in vivo*, but is then isolated from the cells and subjected to post-synthetic modification by enzymes and/or chemicals.

Changing Cyanophycin Composition *in vivo*

Cyanophycin from cyanobacteria is composed of nearly equimolar compositions of aspartic acid and arginine. Aspartic acid residues form the backbone of the polymer, while arginine residues are attached by their amino groups to the carboxyl group of each aspartate (Frommeyer et al., 2016; Du et al., 2019) (**Figure 1A**). However, the side chain of cyanophycin can be varied depending on the strain used for production and the conditions of cultivation, and most importantly, utilizing the low substrate specificity of most cyanophycin synthetases. For example, the purified $CphA_{MA19}$ was able to introduce canavanine instead of arginine in the side chain (Hai et al., 2002), while $CphA_{29413}$ incorporates a wider range of amino acids–lysine, ornithine, or citrulline (Berg et al., 2000; Du et al., 2019) (**Figures 1A–E**).

Lysine is an amino acid abundant in microbial cells and is more closely positioned on the metabolic map to the central metabolic pathways than arginine. It is therefore frequently added to cyanophycin chains at low concentrations in many microorganisms capable of synthesizing cyanophycin (Khlystov et al., 2017) (**Figure 1B**). *C. glutamicum* incorporates lysine into insoluble cyanophycin at around 5 mol%, while lysine is abundant in soluble cyanophycin, amounting to almost 50 mol%. The lysine content in cyanophycin influences its solubility. If its content is less than 4 mol%, cyanophycin does not become soluble even at 90 C, while cyanophycin with lysine contents above 31 mol% is soluble at 30 C (Wiefel and Steinbüchel, 2014). Amine groups on the lysine side chains form less hydrogen bonds than guanidine groups on arginine. In addition, lysine has a lower molecular weight than arginine, hence cyanophycin with an enhanced lysine content is more soluble (Khlystov et al., 2017).

Arginine can be replaced by glutamic acid in the side chain (**Figure 1G**) (Merritt et al., 1994; Wördemann et al., 2021). When *Synechocystis* sp. PCC 6308 was cultivated under nitrogen limiting conditions, no arginine was detected in cyanophycin, and instead glutamic acid was identified. The glutamic acid content decreased with increasing nitrogen supply (Merritt et al., 1994).

C. glutamicum developed for the production of target amino acids is able to incorporate lysine, citrulline ornithine and cadaverine into the side chain of cyanophycin, in particular while expressing the mutated $CphA_{6308}$. The highest ornithine content was almost 12 mol %; the highest citrulline content was about 3 mol% (Wördemann et al., 2021) (**Figure 1A–E**). Interestingly, *C. glutamicum* can also incorporate glutamic acid in the backbone of the polymer (**Figure 1H**) (Wiefel et al., 2019b).

A *Pseudomonas putida* strain is able to form citrulline from arginine (Kakimoto et al., 1971) and was used for production of cyanophycin with a modified content. The recombinant strain was able to produce cyanophycin with about 8% citrulline when the $CphA_{6308}$ cyanophycin synthetase was expressed. (Wiefel et al., 2011) (**Figure 1C**). Engineered *S. cerevisiae* strains

expressing cyanobacterial CphA were able to accumulate cyanophycins with up to 20 mol% of citrulline (strain with deleted argininosuccinate synthetase), 8 mol% of ornithine (**Figure 1E**) (strain with ornithine carbamoyl transferase deleted) and 16 mol% of Lys (with argininosuccinate lyase deleted) (Steinle et al., 2009).

In vitro Modifications of Cyanophycin

Beside *in vivo* variations of cyanophycin, the composition can also be varied *in vitro*. The composition of cyanophycin can be changed after its biosynthesis and subsequent isolation from the producing cells. For these post-synthetic modifications both enzymatic and chemical methods can be applied. Both strategies yield novel cyanophycin variants and thereby extend the number of available forms of cyanophycin.

Enzymatic Modifications

Enzymatic modifications of cyanophycin is a viable strategy to obtain new cyanophycin variants. The first modifications that should be mentioned is the use of cyanophycinases. These enzymes degrade the polymer and yield dipeptides. Cyanophycine derived dipeptides–mainly aspartate-arginine and aspartate-lysine–are highly bioavailable forms of amino acids. They have potentials for medical, nutrition or cosmetics applications (Sallam and Steinbüchel, 2010). Cyanophycinases are intracellular (CphB) or extracellular (CphE) enzymes. A bioinformatic analysis of bacterial strains revealed enzymes responsible for cyanophycin metabolism (Füser and Steinbüchel, 2007). Intracellular cyanophycinases occur in any bacterium accumulating cyanophycin in order to make the storage compound available to the cells again; extracellular cyanophycinases have also been found in various species including *Clostridium*, *Nitrosomonas*, *Nostoc*, *Pseudomonas*, *Ralstonia*, *Synechococcus* and others. These bacteria are able to use cyanophycin produced by other organisms if it is released from the decaying biomass (e.g., after a cyanobacteria blooming). A biotechnological process for the production of dipeptides using CphE from *Pseudomonas alcaligenes* has been developed (Sallam et al., 2009).

Arginine side chains of cyanophycin were treated with arginine deiminase (EC 3.5.3.15) from the European rabbit *Oryctolagus cuniculus* (Wiefel and Steinbüchel, 2016). This enzyme catalyzed reactions in which the imine group of arginine is converted to a ketone group. In nature this reaction occurs as a post-translational modification of peptide-bound arginine to citrulline (**Figure 1C**). The study demonstrated the possibility to modify the polymer enzymatically after its synthesis and to convert its side chain into citrulline.

Chemical Modifications

As mentioned above, cyanophycin can be hydrolyzed enzymatically by cyanophycinase. Chemical hydrolysis of this polymer was also studied, however, it requires much harsher conditions than its enzymatic counterpart. Acid hydrolysis yielded L-aspartic acid and L-arginine, while base hydrolysis allowed the release of L-arginine while polyaspartic acid is retained (Joentgen et al., 1998; Könst, 2011).

Lysine-rich cyanophycin produced in recombinant *E. coli* was subjected to treatment with *o*-methylisourea which yielded the guanidination of lysine residues that were converted to homoarginine (**Figure 1F**). The resulting polymer showed a similar solubility profile as insoluble cyanophycin and was soluble only at low or high pH. Such polymer can be degraded by CphE, yielding new dipeptides like aspartate-homoarginine (Frommeyer et al., 2014). Furthermore, it was proposed to introduce sulfur into lysine or arginine side chains, as it opens a path for further polymer modifications (Wiefel et al., 2019a). The reactions were conducted with methyl isocyanate and resulted in 50% conversion of lysine and 3% of arginine (**Figure 1I**). However, the yield of the reaction was much higher with dipeptides as substrates (72 and 96% respectively). N-acetylarginine and N-acetyllysine residues were obtained on the side chain of cyanophycin when the polymer was treated with acetic anhydride (Wiefel et al., 2019a) (**Figure 1J**). Cyanophycin was treated with formaldehyde to obtain a methylated version of the polymer (yielding a conversion of 84% for lysine and 15% for arginine residues) (**Figure 1K**). These modifications are expected to find applications in drug discovery research.

Cyanophycin as a Component of Hybrid Materials

Cyanophycin is too brittle to be used alone as an individual material, as is also the case for other biobased polymers such as PHA or poly (lactic acid) (Boey et al., 2021). However, it could be applied as a component of copolymers due to its zwitterionic features, or conjugated with other polymers (Khlystov et al., 2017).

Cyanophycin was also investigated for use in biomedical applications. Insoluble cyanophycin was dissolved with HCl and cross-linked with glutaraldehyde. In these experiments thin films of a nearly smooth surface were obtained. The thickness of the film was proportional to the amount of cyanophycin. Prior to the cross-linking the cyanophycin films were brittle and fragile, while after cross-linking the films exhibited a structure of stacking lamellae, and were transparent and yellowish (Tseng et al., 2016).

Soluble cyanophycin was tested for toxicity to Chinese Hamster ovary cells. Minimal immune response was caused, no toxicity was observed, and, moreover, the cyanophycin films supplied adequate conditions for cell growth. Thus cyanophycin has the potential to serve as biocompatible and biodegradable material for biomedicinal applications (Tseng et al., 2016). Following these findings, cyanophycin was conjugated with polyethylene glycol (PEG) (Tseng et al., 2018). Two levels of conjugation were obtained: one with a low and one with a high level of PEG. The materials were prepared by reacting the aldehyde group of the activated PEG and the amine group of lysine in cyanophycin in the presence of sodium cyanoborohydride. The authors were investigating the thermoresponse of cyanophycin and its conjugates, aiming at unravelling its potential in drug delivery. The conjugate with a high PEG level proved to be a promising material for the temperature-regulated release of drugs.

In further research, cyanophycin was combined with two different polyanionic biopolymers, hyaluronic acid (HA) and γ-polyglutamic acid (PG), yielding polyelectrolyte multilayers.

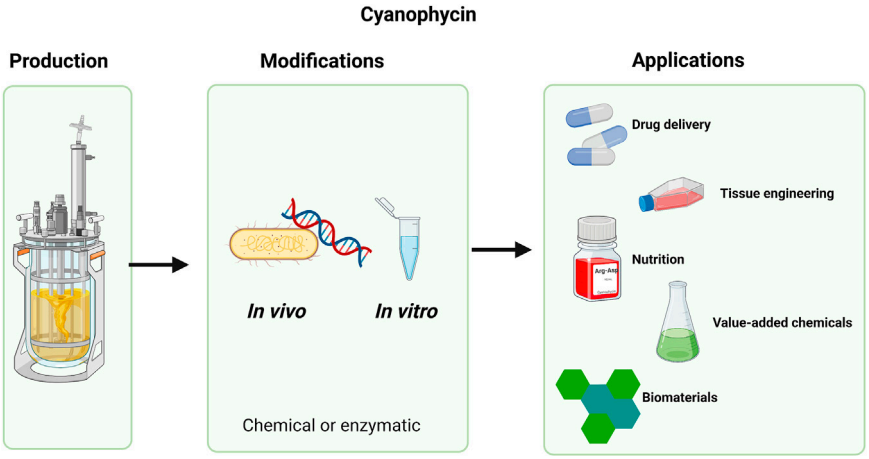

FIGURE 2 | Flow chart presenting the cyanophycin life cycle. From microbial production, through chemical or enzymatic modifications to valuable applications.

These were prepared by sequential adsorption of polyelectrolytes following the dip coat approach (Uddin et al., 2020). Both cyanophycin-PG and cyanophycin-HA films enabled growth, viability and enhanced cellular mobility when murine fibroblast cells were cultivated on them. Such features may be useful for tissue engineering.

CONCLUSIONS AND PERSPECTIVES

To date, the major applications of cyanophycin have yet to be established. However, its modification widens its possible applications and opens new perspectives (**Figure 2**). Khlystov et al., 2017 thoroughly characterized material properties of cyanophycin and suggested its usefulness as part of copolymers–cyanophycin could contribute to the final material with its strength. For example, cyanophycin could be used to toughen resins. Moreover, Tseng et al., 2016 showed that cross-linking cyanophycin led to decrease of brittleness, hence, this technique may also widen the applicability of cyanophycin.

The selective hydrolysis of cyanophycin can result in its conversion to polyaspartic acid, which can be used for the production of detergents, dishwasher soaps, as well as in biomedical applications (Du et al., 2019; Adelnia et al., 2021). Enzymatic degradation of cyanophycin leads to the formation of various dipeptides, mainly Asp-Arg or Asp-Lys. It could in the future also yield other dipeptides if the corresponding polymers are available in sufficient amounts. Dipeptides are bioavailable sources of amino acids. L-aspartic acid, L-arginine and L-lysine are used in numerous specimens for the treatment or prevention of various conditions, such as endocrine, cardiovascular or genitourinary disorders. The treatment of patients with both arginine and aspartate were reported to help to lower cholesterol levels, enhance wound healing, decrease erectile disfunction, and other beneficial results. Arginine and lysine are important in human and animal nutrition as their presence is correlated to cardiovascular functioning and the release of growth hormone (Sallam and Steinbüchel, 2010).

Cyanophycin can be included in the design of drugs and tissue engineering, as was recently demonstrated (Tseng et al., 2018; Uddin et al., 2020). Chemical and enzymatic modifications of cyanophycin allow the introduction of new functional groups into the polymer, thus expanding the area of possible applications (Wiefel et al., 2019a).

Another interesting proposed application focused on the concept of a cyanophycin biorefinery. Engineered *S. cerevisiae* would produce ethanol and cyanophycin simultaneously, subsequently the cyanophycin would be enzymatically or chemically hydrolyzed and converted to value-added chemicals. Cyanophycin hydrolysis yields arginine and aspartic acid. Using L-arginase (EC 3.5.3.1) the arginine of cyanophycin could first be converted to L-ornithine, and then L-ornithine could be a substrate for the production of other chemicals, for example nylon. This activity of L-arginase was shown only with free arginine (Könst et al., 2010). Similarly, aspartic acid could be converted to industrially important chemicals. For example, L-Aspartate α-decarboxylase (EC 4.1.1.11) catalyzes the reaction of aspartic acid with β-alanine, which could be further converted to acrylamide or acetonitrile (Könst, 2011).

The material properties of modified cyanophycin are not known. Most of the aforementioned modified polymers were not obtained in quantities large enough to perform full characterization. With enhanced yields of the modification reactions, sufficient amounts of products can be synthesized and tested. Consequently, new attractive applications may be found.

AUTHOR CONTRIBUTIONS

NK wrote and AS revised the manuscript.

FUNDING

The Project is carried out within the International Research Agendas PLUS programme of the Foundation for Polish Science, co-financed by The European Union under the European Regional Development Found (MAB PLUS/2019/11).

REFERENCES

Aboulmagd, E., Oppermann-Sanio, F. B., and Steinbüchel, A. (2000). Molecular Characterization of the Cyanophycin Synthetase from *Synechocystis* Sp. Strain PCC6308. *Arch. Microbiol.* 174, 297–306. doi:10.1007/s002030000206

Aboulmagd, E., Voss, I., Oppermann-Sanio, F. B., and Steinbüchel, A. (2001). Heterologous Expression of Cyanophycin Synthetase and Cyanophycin Synthesis in the Industrial Relevant Bacteria Corynebacterium Glutamicum and Ralstonia Eutropha and in Pseudomonas Putida. *Biomacromolecules* 2, 1338–1342. doi:10.1021/bm010075a

Adames, K., Euting, K., Bröker, A., and Steinbüchel, A. (2013). Investigations on Three Genes in *Ralstonia Eutropha* H16 Encoding Putative Cyanophycin Metabolizing Enzymes. *Appl. Microbiol. Biotechnol.* 97, 3579–3591. doi:10.1007/s00253-012-4599-6

Adelnia, H., Tran, H. D. N., Little, P. J., Blakey, I., and Ta, H. T. (2021). Poly(aspartic Acid) in Biomedical Applications: from Polymerization, Modification, Properties, Degradation, and Biocompatibility to Applications. *ACS Biomater. Sci. Eng.* 7, 2083–2105. doi:10.1021/acsbiomaterials.1c00150

Berg, H., Ziegler, K., Piotukh, K., Baier, K., Lockau, W., and Volkmer-Engert, R. (2000). Biosynthesis of the Cyanobacterial reserve Polymer Multi-L-Arginyl-Poly-L-Aspartic Acid (Cyanophycin). *Eur. J. Biochem.* 267, 5561–5570. doi:10.1046/J.1432-1327.2000.01622.X

Boey, J. Y., Mohamad, L., Khok, Y. S., Tay, G. S., and Baidurah, S. (2021). A Review of the Applications and Biodegradation of Polyhydroxyalkanoates and Poly(lactic Acid) and its Composites. *Polymers* 13, 1544. doi:10.3390/POLYM13101544

Chen, S., Huang, S., Li, Y., and Zhou, C. (2021). Recent Advances in Epsilon-Poly-L-Lysine and L-Lysine-Based Dendrimer Synthesis, Modification, and Biomedical Applications. *Front. Chem.* 9, 169. doi:10.3389/FCHEM.2021.659304

Du, J., Li, L., and Zhou, S. (2019). Microbial Production of Cyanophycin: From Enzymes to Biopolymers. *Biotechnol. Adv.* 37, 107400. doi:10.1016/j.biotechadv.2019.05.006

European Comission (2020). A New Circular Economy Action Plan. EUR-Lex 52020DC009. Available at: https://www.un.org/sustainabledevelopment/sustainable-consumption-production/(Accessed August 19, 2021).

Forchhammer, K., and Watzer, B. (2016). Microbiology Comment. *Microbiol. (United Kingdom)* 162, 727–729. doi:10.1099/mic.0.000260

Frey, K. M., Oppermann-Sanio, F. B., Schmidt, H., and Steinbüchel, A. (2002). Technical-scale Production of Cyanophycin with Recombinant Strains of *Escherichia coli*. *Appl. Environ. Microbiol.* 68, 3377–3384. doi:10.1128/AEM.68.7.3377-3384.2002

Frommeyer, M., Bergander, K., and Steinbüchel, A. (2014). Guanidination of Soluble Lysine-Rich Cyanophycin Yields a Homoarginine-Containing Polyamide. *Appl. Environ. Microbiol.* 80, 2381–2389. doi:10.1128/AEM.04013-13

Frommeyer, M., Wiefel, L., and Steinbüchel, A. (2016). Features of the Biotechnologically Relevant Polyamide Family "Cyanophycins" and Their Biosynthesis in Prokaryotes and Eukaryotes. *Crit. Rev. Biotechnol.* 36, 153–164. doi:10.3109/07388551.2014.946467

Füser, G., and Steinbüchel, A. (2007). Analysis of Genome Sequences for Genes of Cyanophycin Metabolism: Identifying Putative Cyanophycin Metabolizing Prokaryotes. *Macromol. Biosci.* 7, 278–296. doi:10.1002/mabi.200600207

Hai, T., Oppermann-Sanio, F. B., and Steinbüchel, A. (2002). Molecular Characterization of a Thermostable Cyanophycin Synthetase from the Thermophilic Cyanobacterium *Synechococcus* Sp. Strain MA19 and *In Vitro* Synthesis of Cyanophycin and Related Polyamides. *Appl. Environ. Microbiol.* 68, 93–101. doi:10.1128/AEM.68.1.93-101.2002

Heesterman, A. R. G. (2020). Containing the Risk of Catastrophic Climate Change. *Clean. Techn Environ. Pol.* 22, 1215–1227. doi:10.1007/S10098-020-01868-1

Holehouse, A. S., and Pappu, R. V. (2015). Encoding Phase Transitions. *Nat. Mater* 14, 1083–1084. doi:10.1038/nmat4459

Joentgen, W., Groth, T., Steinbüchel, A., Hai, T., and Oppermann, F. B. (1998). *Biotechnical Process for the Preparation of Aspartic Acid Homo- or Copolymers*. EU Patent. European Patent Office, EP0964740B1.

Kakimoto, T., Shibatani, T., Nishimura, N., and Chibata, I. (1971). Enzymatic Production of L -Citrulline by Pseudomonas Putida. *Appl. Microbiol.* 22, 992–999. doi:10.1128/am.22.6.992-999.1971

Khlystov, N. A., Chan, W. Y., Kunjapur, A. M., Shi, W., Prather, K. L. J., and Olsen, B. D. (2017). Material Properties of the Cyanobacterial reserve Polymer Multi-L-Arginyl-Poly-L-Aspartate (Cyanophycin). *Polymer* 109, 238–245. doi:10.1016/j.polymer.2016.11.058

Könst, P. M. (2011). "Production of Nitrogen Containing Chemicals from Cyanophycin". PhD thesis (Wageningen, Netherlands: Wageningen University).

Könst, P. M., Turras, P. M. C. C. D., Franssen, M. C. R., Scott, E. L., and Sanders, J. P. M. (2010). Stabilized and Immobilized *Bacillus Subtilis* Arginase for the Biobased Production of Nitrogen-Containing Chemicals. *Adv. Synth. Catal.* 352, 1493–1502. doi:10.1002/adsc.201000034

Kroll, J., Klinter, S., and Steinbüchel, A. (2011). A Novel Plasmid Addiction System for Large-Scale Production of Cyanophycin in *Escherichia coli* Using mineral Salts Medium. *Appl. Microbiol. Biotechnol.* 89, 593–604. doi:10.1007/s00253-010-2899-2

Li, H., Sherman, D., Bao, S., and Sherman, L. (2001). Pattern of Cyanophycin Accumulation in Nitrogen-Fixing and Non-nitrogen-fixing Cyanobacteria. *Arch. Microbiol.* 176, 9–18. doi:10.1007/S002030100281

Merritt, M. V., Sid, S. S., Mesh, L., and Allen, M. M. (1994). Variations in the Amino Acid Composition of Cyanophycin in the Cyanobacterium *Synechocystis* Sp. PCC 6308 as a Function of Growth Conditions. *Arch. Microbiol.* 162, 158–166. doi:10.1007/BF00314469

Mooibroek, H., Oosterhuis, N., Giuseppin, M., Toonen, M., Franssen, H., Scott, E., et al. (2007). Assessment of Technological Options and Economical Feasibility for Cyanophycin Biopolymer and High-Value Amino Acid Production. *Appl. Microbiol. Biotechnol.* 77, 257–267. doi:10.1007/s00253-007-1178-3

Nair, P., Navale, G. R., and Dharne, M. S. (2021). Poly-Gamma-Glutamic Acid Biopolymer: A Sleeping Giant With Diverse Applications and Unique Opportunities for Commercialization. *Biomass Conv. Bioref.* 34. doi:10.1007/S13399-021-01467-0

Nausch, H., Hausmann, T., Ponndorf, D., Hühns, M., Hoedtke, S., Wolf, P., et al. (2016). Tobacco as Platform for a Commercial Production of Cyanophycin. *New Biotechnol.* 33, 842–851. doi:10.1016/J.NBT.2016.08.001

Nausch, H., Huckauf, J., and Broer, I. (2015). Peculiarities and Impacts of Expression of Bacterial Cyanophycin Synthetases in Plants. *Appl. Microbiol. Biotechnol.* 100, 1559–1565. doi:10.1007/S00253-015-7212-Y

Raberg, M., Volodina, E., Lin, K., and Steinbüchel, A. (2018). Ralstonia eutrophaH16 in Progress: Applications beside PHAs and Establishment as Production Platform by Advanced Genetic Tools. *Crit. Rev. Biotechnol.* 38, 494–510. doi:10.1080/07388551.2017.1369933

Sallam, A., Kast, A., Przybilla, S., Meiswinkel, T., and Steinbüchel, A. (2009). Biotechnological Process for Production of β-Dipeptides from Cyanophycin on a Technical Scale and its Optimization. *Appl. Environ. Microbiol.* 75, 29–38. doi:10.1128/AEM.01344-08

Sallam, A., and Steinbüchel, A. (2010). Dipeptides in Nutrition and Therapy: Cyanophycin-Derived Dipeptides as Natural Alternatives and Their Biotechnological Production. *Appl. Microbiol. Biotechnol.* 87, 815–828. doi:10.1007/s00253-010-2641-0

Schmidt, K., Schmidtke, J., Mast, Y., Waldvogel, E., Wohlleben, W., Klemke, F., et al. (2017). Comparative Statistical Component Analysis of Transgenic, Cyanophycin-Producing Potatoes in Greenhouse and Field Trials. *Transgenic Res.* 26, 529–539. doi:10.1007/S11248-017-0022-5

Sharon, I., Haque, A. S., Grogg, M., Lahiri, I., Seebach, D., Leschziner, A. E., et al. (2021). Structures and Function of the Amino Acid Polymerase Cyanophycin Synthetase. *Nat. Chem. Biol.* 17, 1101–1110. doi:10.1038/s41589-021-00854-y

Simon, R. D. (1971). Cyanophycin Granules from the Blue-green Alga *Anabaena Cylindrica*: A reserve Material Consisting of Copolymers of Aspartic Acid and Arginine. *Proc. Natl. Acad. Sci.* 68, 265–267. doi:10.1073/pnas.68.2.265

Simon, R. D., Lawry, N. H., and Mclendon, G. L. (1980). Structural Characterization of the Cyanophycin Granule Polypeptide of *Anabaena Cylindrica* by Circular Dichroism and Raman Spectroscopy. *Biochim. Biophys. Acta (Bba) - Protein Struct.* 626, 277–281. doi:10.1016/0005-2795(80)90121-X

Simon, R. D. (1976). The Biosynthesis of Multi-L-Arginyl-poly(L-Aspartic Acid) in the Filamentous Cyanobacterium *Anabaena Cylindrica*. *Biochim. Biophys. Acta (Bba) - Enzymol.* 422, 407–418. doi:10.1016/0005-2744(76)90151-0

Steinle, A., Bergander, K., and Steinbüchel, A. (2009). Metabolic Engineering of *Saccharomyces cerevisiae* for Production of Novel Cyanophycins with an Extended Range of Constituent Amino Acids. *Appl. Environ. Microbiol.* 75, 3437–3446. doi:10.1128/AEM.00383-09

Steinle, A., Oppermann-Sanio, F. B., Reichelt, R., and Steinbüchel, A. (2008). Synthesis and Accumulation of Cyanophycin in Transgenic Strains of *Saccharomyces cerevisiae*. *Appl. Environ. Microbiol.* 74, 3410–3418. doi:10.1128/AEM.00366-08

Steinle, A., Witthoff, S., Krause, J. P., and Steinbüchel, A. (2010). Establishment of Cyanophycin Biosynthesis in *Pichia pastoris* and Optimization by Use of Engineered Cyanophycin Synthetases. *Appl. Environ. Microbiol.* 76, 1062–1070. doi:10.1128/AEM.01659-09

Tseng, W.-C., Fang, T.-Y., and Chen, S.-Y. (2016). Cellular Biocompatibility of Cyanophycin Substratum Prepared with Recombinant *Escherichia coli*. *Biochem. Eng. J.* 105, 97–106. doi:10.1016/j.bej.2015.09.012

Tseng, W.-C., Fang, T.-Y., Lin, Y.-C., Huang, S.-J., and Huang, Y.-H. (2018). Reversible Self-Assembly Nanovesicle of UCST Response Prepared with Multi-L-Arginyl-Poly-L-Aspartate Conjugated with Polyethylene Glycol. *Biomacromolecules* 19, 4585–4592. doi:10.1021/acs.biomac.8b01274

Uddin, Z., Fang, T. Y., Siao, J. Y., and Tseng, W. C. (2020). Wound Healing Attributes of Polyelectrolyte Multilayers Prepared with Multi- L -arginyl-poly- L -aspartate Pairing with Hyaluronic Acid and γ-Polyglutamic Acid. *Macromol. Biosci.* 20, 2000132. doi:10.1002/mabi.202000132

Voss, I., Diniz, S. C., Aboulmagd, E., and Steinbüchel, A. (2004a). Identification of the *Anabaena* Sp. Strain PCC7120 Cyanophycin Synthetase as Suitable Enzyme for Production of Cyanophycin in Gram-Negative Bacteria like *Pseudomonas Putida* and *Ralstonia Eutropha*. *Biomacromolecules* 5, 1588–1595. doi:10.1021/bm049861g

Voss, I., Diniz, S. C., Aboulmagd, E., and Steinbüchel, A. (2004b). Identification of the *Anabaena* Sp. Strain PCC7120 Cyanophycin Synthetase as Suitable Enzyme for Production of Cyanophycin in Gram-Negative Bacteria like *Pseudomonas Putida* and *Ralstonia Eutropha*. *Biomacromolecules* 5, 1588–1595. doi:10.1021/bm049861g

Wendisch, V. F., Jorge, J. M. P., Pérez-García, F., and Sgobba, E. (2016). Updates on Industrial Production of Amino Acids Using *Corynebacterium Glutamicum*. *World J. Microbiol. Biotechnol.* 32, 105. doi:10.1007/S11274-016-2060-1

Wiefel, L., Bachmann, F., Terwort, J., and Steinbüchel, A. (2019a). *In Vitro* modification of Bacterial Cyanophycin and Cyanophycin Dipeptides Using Chemical Agents towards Novel Variants of the Biopolymer. *Earth Syst. Environ.* 3, 637–650. doi:10.1007/s41748-019-00107-y

Wiefel, L., Bröker, A., and Steinbüchel, A. (2011). Synthesis of a Citrulline-Rich Cyanophycin by Use of *Pseudomonas Putida* ATCC 4359. *Appl. Microbiol. Biotechnol.* 90, 1755–1762. doi:10.1007/s00253-011-3224-4

Wiefel, L., and Steinbüchel, A. (2016). Enzymatic Modification of Soluble Cyanophycin Using the Type II Peptidyl Arginine Deiminase fromOryctolagus Cuniculus. *Macromol. Biosci.* 16, 1064–1071. doi:10.1002/mabi.201500433

Wiefel, L., and Steinbüchel, A. (2014). Solubility Behavior of Cyanophycin Depending on Lysine Content. *Appl. Environ. Microbiol.* 80, 1091–1096. doi:10.1128/AEM.03159-13

Wiefel, L., Wohlers, K., and Steinbüchel, A. (2019b). Re-evaluation of Cyanophycin Synthesis in *Corynebacterium Glutamicum* and Incorporation of Glutamic Acid and Lysine into the Polymer. *Appl. Microbiol. Biotechnol.* 103, 4033–4043. doi:10.1007/s00253-019-09780-5

Wördemann, R., Wiefel, L., Wendisch, V. F., and Steinbüchel, A. (2021). Incorporation of Alternative Amino Acids into Cyanophycin by Different Cyanophycin Synthetases Heterologously Expressed in *Corynebacterium Glutamicum*. *AMB Expr.* 11, 55. doi:10.1186/s13568-021-01217-5

Xiao, J., Wang, D., Wang, L., Jiang, Y., Xue, L., Sui, S., et al. (2020). Increasing L-Lysine Production in Corynebacterium Glutamicum by Engineering Amino Acid Transporters. *Amino Acids* 52, 1363–1374. doi:10.1007/S00726-020-02893-6

Ziegler, K., Diener, A., Herpin, C., Richter, R., Deutzmann, R., and Lockau, W. (1998). Molecular Characterization of Cyanophycin Synthetase, the Enzyme Catalyzing the Biosynthesis of the Cyanobacterial reserve Material Multi-L-Arginyl-Poly- L-Aspartate (Cyanophycin). *Eur. J. Biochem.* 254, 154–159. doi:10.1046/j.1432-1327.1998.2540154.x

Conflict of Interest: The authors declare that the research was conducted in the absence of any commercial or financial relationships that could be construed as a potential conflict of interest.

Publisher's Note: All claims expressed in this article are solely those of the authors and do not necessarily represent those of their affiliated organizations, or those of the publisher, the editors and the reviewers. Any product that may be evaluated in this article, or claim that may be made by its manufacturer, is not guaranteed or endorsed by the publisher.

frontiers in Bioengineering and Biotechnology

ORIGINAL RESEARCH
published: 14 December 2021
doi: 10.3389/fbioe.2021.810155

Effect of Freezing Process on the Microstructure of Gelatin Methacryloyl Hydrogels

Taotao Liu[1†], Yuzhuo Zhang[2†], Mingyue Sun[1†], Meiqi Jin[1], Wei Xia[1], Huazhe Yang[1] and Tianlin Wang[1*]*

[1]School of Intelligent Medicine, China Medical University, Shenyang, China, [2]Changchun Medical College, Changchun, China

Gelatin methacryloyl (GelMA) hydrogels have aroused considerable interests in the field of tissue engineering due to tunable physical properties and cell response parameters. A number of works have studied the impact of GelMA concentration, photo-initiator concentration, methacrylic anhydride (MA) concentration, cooling rate and temperature gradient on GelMA hydrogel generation, but little attention has been paid to the effect of the freezing temperatures and freezing time of GelMA prepolymer solution during preparation. In this study, GelMA hydrogels were synthesized with different freezing temperatures and time. It was found that the lower freezing temperatures and longer freezing time caused smaller pore sizes that realized higher cell viability and proliferation of MC3T3-E1 cells. The results showed that tunable microstructure of GelMA could be achieved by regulating the freezing conditions of GelMA, which provided a broad prospect for the applications of GelMA hydrogels in tissue engineering.

Keywords: GelMA, freezing temperature, freezing time, morphology, cell proliferation

OPEN ACCESS

Edited by:
Jianshe Hu,
Northeastern University, China

Reviewed by:
Yanhui Liu,
Qingdao University, China
Yanjin Lu,
Fujian Institute of Research on the Structure of Matter (CAS), China

***Correspondence:**
Huazhe Yang
hzyang@cmu.edu.cn
Tianlin Wang
tlwang@cmu.edu.cn

†These authors share first authorship

Specialty section:
This article was submitted to Biomaterials, a section of the journal Frontiers in Bioengineering and Biotechnology

Received: *06 November 2021*
Accepted: *29 November 2021*
Published: *14 December 2021*

Citation:
Liu T, Zhang Y, Sun M, Jin M, Xia W, Yang H and Wang T (2021) Effect of Freezing Process on the Microstructure of Gelatin Methacryloyl Hydrogels. Front. Bioeng. Biotechnol. 9:810155. doi: 10.3389/fbioe.2021.810155

INTRODUCTION

In recent years, many studies have focused on gelatin methacryloyl (GelMA) hydrogels, owing to the tunable physicochemical properties and good biocompatibility of the hydrogel (Yue et al., 2015; Sun et al., 2018; Basara et al., 2019; Liu et al., 2020; Elkhoury et al., 2021). GelMA hydrogel is a kind of photopolymer which is produced by the introduction of photosensitive groups on the side chains of gelatin (Lee et al., 2015a; Li et al., 2016; Sun et al., 2018). Solid GelMA hydrogel with good thermal stability can be obtained by photocrosslinking of GelMA prepolymer solution (Zhao et al., 2016; Kirsch et al., 2020). GelMA hydrogels possess arginine-glycine-aspartic acid (RGD) peptide sequences and matrix metalloproteinase (MMP) sequences, which favor cell adhesion and remodeling (Yue et al., 2015; Sun et al., 2018; Basara et al., 2019). Moreover, the porosities of GelMA hydrogels play an important role in the transport of oxygen and nutrients required by cells (Van Vlierberghe et al., 2007). Also, it has been demonstrated that the GelMA hydrogels at a relatively low concentration (i.e., ≤5% w/v) was more conducive for cell growth (Yin et al., 2018; Basara et al., 2019), but low concentration would lead to low compression modulus (Celikkin et al., 2018). Therefore, it is important to find a balance between supporting cell growth and possessing adequate mechanical properties since GelMA hydrogels have been widely used in tissue engineering (Zhang et al., 2018; Zheng et al., 2018; Wang et al., 2019). However, it is still a challenge to produce GelMA hydrogel scaffolds with proper pore sizes and mechanical properties for various tissue engineering applications (Celikkin et al., 2018; Zhang et al., 2018; Zheng et al., 2018; Gao et al., 2019; Wang et al., 2019).

One way to control the pore sizes of GelMA hydrogels is to adjust the concentration of GelMA or photo-initiator. For instance, Lee *et al.* (Lee et al., 2015b) and Celikkin *et al.* (Celikkin et al., 2018) confirmed that pore sizes would be affected by polymer concentration. Benton *et al.* (Benton et al., 2009) tuned the porosities, pore sizes and wall thicknesses of GelMA hydrogels indirectly by varying the photo-initiator concentration. Another way to change the pore sizes is to introduce other materials. For example, Wang *et al.* (Wang et al., 2014) combined GelMA with dextran glycidyl methacrylate (DexMA) to synthesize GelMA–DexMA copolymer hydrogels. They found that the pore sizes of GelMA–DexMA copolymer hydrogels would reduce as the degree of substitution (DS) of DexMA increased. In addition, the concentration of methacrylic anhydride (MA), the cooling rate and the temperature gradient could also affect pore sizes of GelMA hydrogels (Van Vlierberghe et al., 2007). Although the effects of these factors on the pore sizes of GelMA hydrogels have been demonstrated, the effect of the freezing temperatures and freezing time of GelMA prepolymer solution, which may have significant impacts on the pore sizes of the hydrogels, seem to be ignored.

In this study, the freezing temperatures and freezing time of GelMA prepolymer solution were studied and the influences of freezing conditions on pore sizes were evaluated. The effect of distinct pore sizes on swelling properties and mechanical properties was also investigated. Moreover, MC3T3-E1 cells were encapsulated in the GelMA hydrogels to study the cell proliferation.

MATERIALS AND METHODS

Materials

Gelatin (biochemical reagent) and 2-hydroxy-4′-(2-hydroxyethoxy)-2-methylpropiophenone (Irgacure 2,959, 98%) were purchased from Shanghai Yuanye Biotechnology Co., Ltd. Phosphate buffered saline (PBS, pH = 7.4, without calcium and magnesium) was purchased from Biological Industries. Methacrylic anhydride (MA, 94%) was purchased from Sigma-Aldrich. DME/F-12 1:1 (1X), fetal bovine serum (FBS), penicillin-streptomycin solution and trypsin 0.25% (1X) solution were purchased from Hyclone. 4% tissue cell fixative was purchased from Solarbio.

Synthesis of GelMA Prepolymers

The synthesis of gelatin methacryloyl (GelMA) hydrogel has been reported previously (Van den Bulcke et al., 2000; Chen et al., 2012). Briefly, GelMA prepolymers with different freezing temperatures and time were synthesized as follow: 20 g of gelatin was added into 200 ml of PBS and dissolved by stirring with a magnetic stirrer at 50°C and 240 rpm until completely dissolved. Then, 16 ml of methacrylic anhydride (MA) was added dropwise at 0.2 ml/min by using a micro syringe pump to the dissolved gelatin solution under continuous stirring. The mixed solution was allowed to react for 2 h by stirring at 50°C and 240 rpm using a magnetic stirrer. 50°ml of PBS was preheated to 50°C and then added into the mixed solution. After magnetic stirring for 10 min at 50°C, the reaction solution was placed in dialysis tubing and dialyzed in deionized water by stirring at 40°C and 500 rpm for 10 days to remove salts and unreacted MA. After dialysis, 400 ml of deionized water was added into the dialytic solution, heated to 40°C and stirred for 15 min. Finally, the solution was packed in 5 ml centrifuge tubes, and placed at −20°C, −40°C and −80°C for 2, 7, 12 and 17 days, respectively. Then, these samples were lyophilized for 4 days to obtain GelMA prepolymer (white foam) and stored in a drying dish at room temperature before use. In the end, 12 groups of samples were obtained with detailed freezing information listed in **Table 1**.

TABLE 1 | The 12 groups of samples with different freezing temperatures and time.

Group	Temperature (°C)	Time (day)
1#	−20	2
2#	−20	7
3#	−20	12
4#	−20	17
5#	−40	2
6#	−40	7
7#	−40	12
8#	−40	17
9#	−80	2
10#	−80	7
11#	−80	12
12#	−80	17

Preparation of GelMA Hydrogels

Freeze-dried GelMA prepolymers with different freezing temperatures and time were dissolved in PBS containing 1% (w/v) 2-hydroxy-4′-(2-hydroxyethoxy)-2-methylpropiophenone (Irgacure 2,959, 98%) as photoinitiator at room temperature and mixed by ultrasound. Then, the prepared solution was transferred to 2 ml centrifuge tube caps and exposed to ultraviolet (UV) light of 365 nm for 5 min. Finally, group 1#, 2#, 3# and 4# were frozen at −20°C, group 5#, 6#, 7# and 8# were frozen at −40°C, group 9#, 10#, 11# and 12# were frozen at −80°C for 6 h, respectively, and then lyophilized overnight to generate lyophilized GelMA hydrogels.

Fourier-Transform Infrared Spectroscopy

Fourier-transform infrared (FTIR) spectra of Freeze-dried GelMA hydrogels were recorded with a FTIR spectrometer (FTIR, Agilent Cary 630, United States). The samples and the KBr powder were mixed, and poured into a tableting mold to be pressed into a sheet. Every measurement includes 128 scans, $4cm^{-1}$ resolution and the Y-axis format for transmittance (Rahali et al., 2017).

Scanning Electron Microscope

The surface morphology of lyophilized GelMA hydrogels that had been sprayed with platinum was obtained from a scanning electron microscope (SEM, JSM-IT200, Japan) at 10 kV. The average pore size was analyzed with the SEM images (DursunUsal et al., 2019). No less than 30 pores were selected manually and randomly for each sample (Wang et al., 2018).

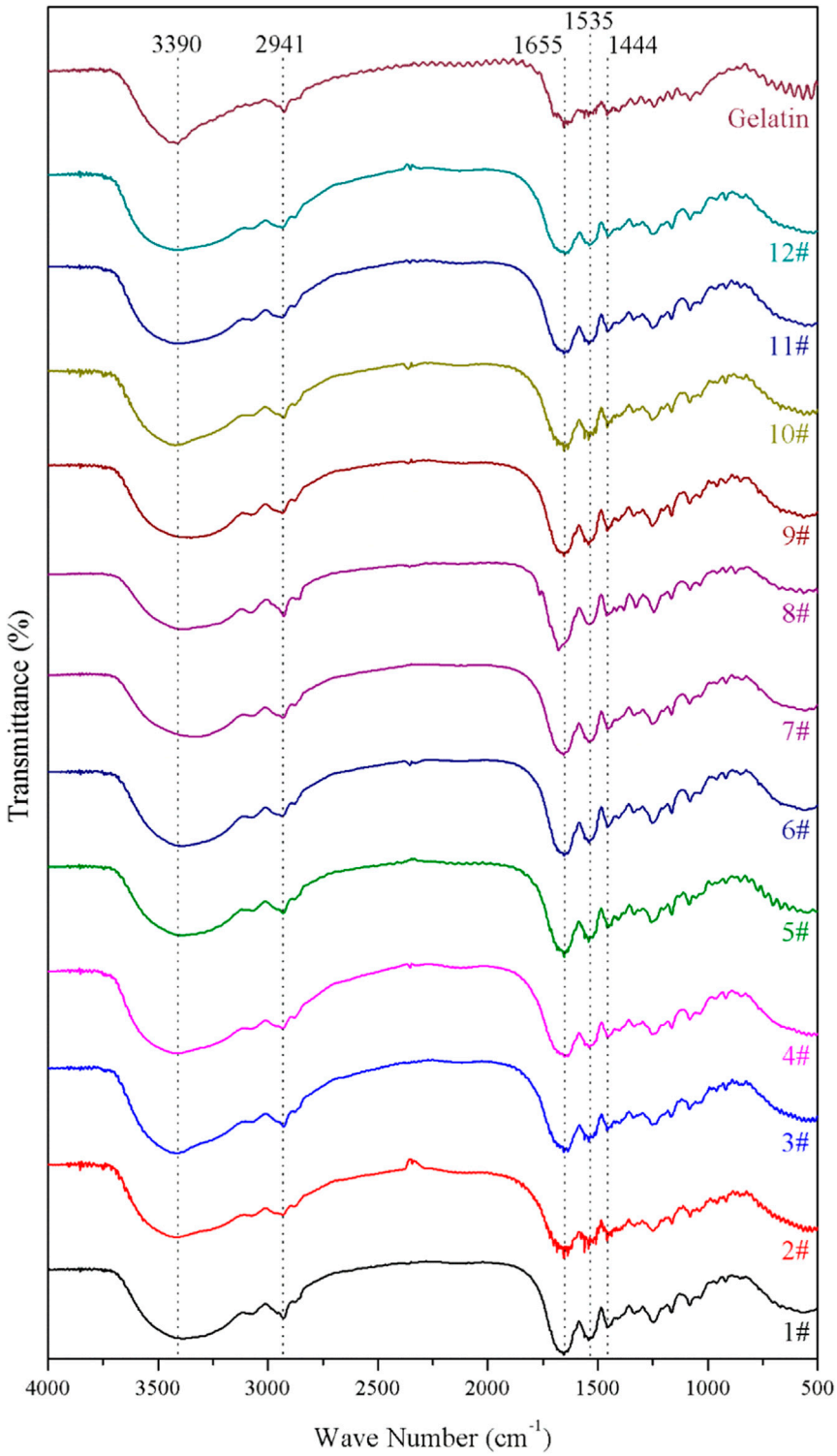

FIGURE 1 | The fourier-transform infrared (FTIR) spectra of the GelMA hydrogels with different freezing temperatures and time.

Swelling Ratio

Freeze-dried GelMA hydrogels were weighted to obtain the dry weight of GelMA hydrogels, as dryweight (W_d). Then, lyophilized GelMA hydrogels were immersed in PBS at room temperature, and the weight of GelMA hydrogels was measured after swelling for 30 min, 1, 2, 4, 8, 12, 24, and 48 h (the excess PBS on the sample surface was dried with filter paper before weighing), as wetweight (W_s).

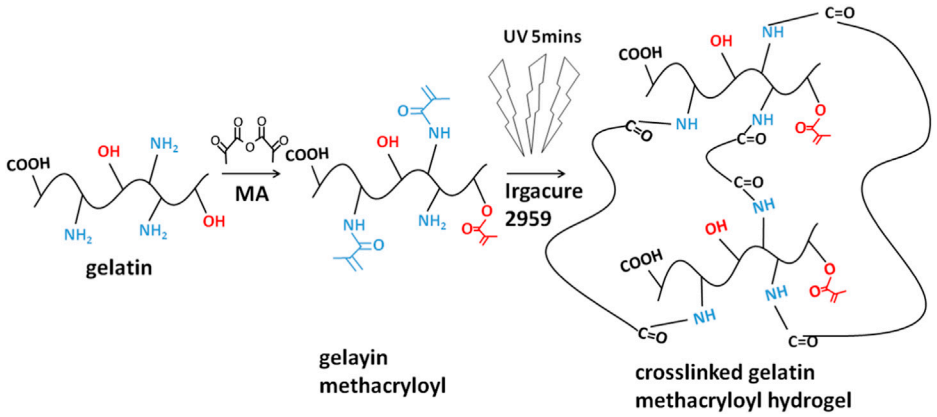

FIGURE 2 | The molecular formula of protein/peptide (gelatin) and MA-modified protein/peptide (GelMA).

The swelling ratio was calculated by the following equation (Rahali et al., 2017; Liu et al., 2019):

$$\text{swelling ratio} = \frac{W_s - W_d}{W_d} \times 100\% \quad (1)$$

Mechanical Properties

The mechanical properties of samples reaching swelling balance were tested using a biomechanical testing machine (Qixiang QX-W100, China). The samples were tested at a speed rate of 1 mm/min at room temperature. The compressive modulus was calculated from the slope of the linear region of the stress-strain curve that corresponds to 0–10% strain.

Cell Culture

2×10^5 MC3T3-E1 cells were encapsulated in different groups of GelMA (7.5 %) hydrogel-based scaffolds. After 1, and 3 days, the viability of cells was assessed by using AO/PI assay (Acridine Orange and Propidium Iodide, BestBio BB-4126-100 T). At each day after removing media, scaffolds were washed with PBS twice, and the AO and PI (Acridine Orange and Propidium Iodide) were mixed and added to each well and incubated for 20 min. Cell proliferation in different samples were detected using a laser scanning confocal microscope (LSCM, Zeisee LSM880).

Data Analysis

All results in this study were expressed as mean ± standard deviation. Data analysis was carried out by Student's *T* test and one-way analysis of variance (ANOVA), and the level of significance was set at $p < 0.05$.

RESULTS AND DISCUSSION

Component of GelMA Hydrogels

The fourier-transform infrared (FTIR) spectra of the GelMA hydrogels with different freezing temperatures and time are shown in **Figure 1**. According to the molecular formula (**Figure 2**) of gelatin and GelMA of the previous paper (Elkhoury et al., 2021) as can be seen from FTIR spectra, the absorption patterns of all samples were similar. The stretching vibration peak of -OH groups was observed at 3,305 cm^{-1}. Owing to the presence of methacryloyl groups in GelMA hydrogels, characteristic peaks of amide were observed. A strong absorption peak emerged at 1,655 cm^{-1}, which was due to the C=O stretching vibration of amide functional groups. The peak at 3,305 cm^{-1} was also contributed by the N-H stretching vibration, and the peak at 1,535 cm^{-1} was attributed to the N-H bending vibration. The peak at 2,941 cm^{-1} was due to the stretching vibration of C-H and the peak at 1,444 cm^{-1} represented the bending vibration of C-H (Sadeghi and Heidari, 2011; Rahali et al., 2017). Therefore, gelatin had been modified by MA successfully (Sadeghi and Heidari, 2011). According to the FTIR spectra, the chemical structure of GelMA hydrogels was not changed under varying freezing temperatures and time.

Morphology of GelMA Hydrogels

The interconnected pores of scaffolds could enhance cell proliferation by allowing nutrient and oxygen diffusion (Diao et al., 2019). Different pore sizes of porous scaffolds were controlled by different freezing conditions. The surface morphologies of lyophilized GelMA hydrogels with different freezing temperatures (−20°C, −40°C and −80°C) and time (2, 7, 12 and 17 days) are shown in **Figure 3**. Upon characterization with SEM, the average pore size for each sample was calculated and shown in **Figure 4**. In fact, some studies have proved that temperature was a key factor to affect the surface morphologies and pore sizes of hydrogels (Kang et al., 1999; Wu et al., 2013).

The effect of the freezing temperatures on the pore sizes of GelMA hydrogels was evident that lower temperatures promote smaller pore sizes (**Figures 3**, **4**). When GelMA hydrogels frozen at different temperatures for the same time, GelMA hydrogels frozen at −80°C exhibited smaller pores than hydrogels prepared at −20°C. The morphology and pore sizes of these GelMA hydrogels can be affected by the conditions of freezing temperatures. As showed in

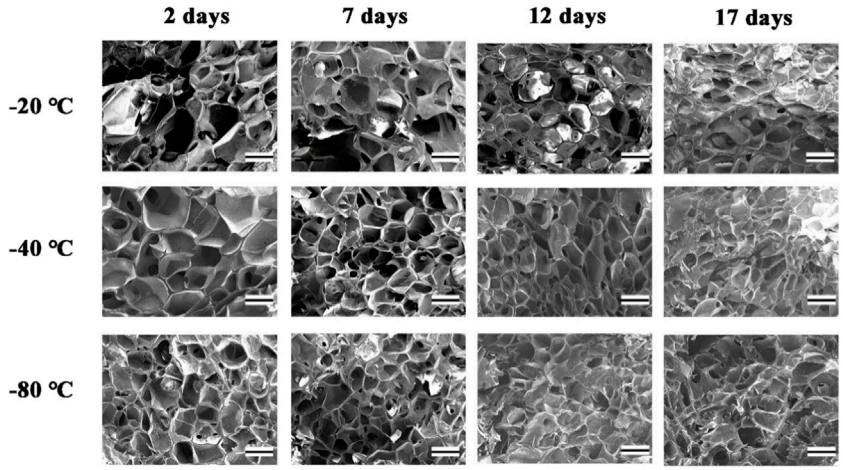

FIGURE 3 | The SEM of GelMA Hydrogels with different freezing temperatures and time. (Scale bars represent 200 μm in all images).

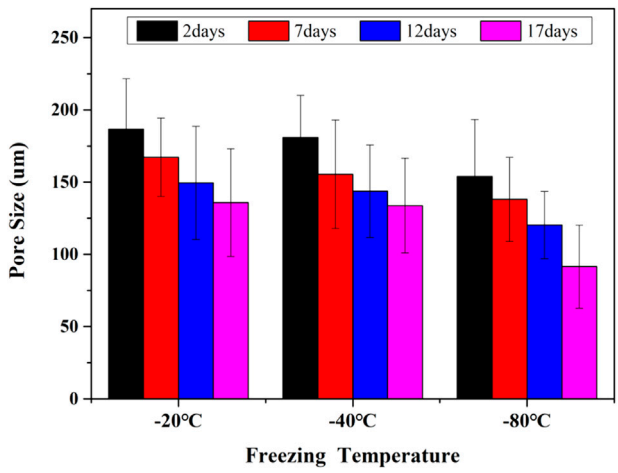

FIGURE 4 | The pore sizes of GelMA Hydrogels with different freezing temperatures and time.

Figure 5, during the freezing process, the solvent phase (deionized water) and the polymer phase (GelMA) were separately enriched to form a polymer network (Nam and Park, 1999). In order to reduce the free energy, the polymer phase underwent phase-to-phase migration to a high concentration region over time until a phase equilibrium was reached. The freezing conditions like freezing temperature have great influence on ice crystal morphology. At higher freezing temperature of GelMA hydrogels, slower freezing rate enhanced the formation of larger ice crystals. And the lower undercooling (difference between the freezing temperature and the actual temperature of the material) and the nucleation rate also resulted the larger pore sizes (Ni et al., 2016). At lower freezing temperature, the freezing rate augmented, and the larger undercooling led to the nucleation rate of ice crystals increased. The nucleation rate was larger than the growth rate of ice crystals, leading to the smaller ice crystals (Thiebaud et al., 2002; Ni et al., 2016). Finally, the pores were formed due to the vacuum sublimation during the process of lyophilization.

So, the pore sizes of the scaffolds reduced as the pre-freezing temperature decreased, which was due to that the ice crystals in the scaffolds became smaller as the temperature decreased.

The pore sizes of GelMA hydrogels are also directly impacted by freezing time. At the same temperature, the lower the freezing time, the higher the pore sizes of GelMA hydrogels. Upon characterization with SEM, the average pore size for each sample was calculated and shown in **Figures 3**, **4**. The average pore sizes of the GelMA hydrogels were 186.64 ± 34.96, 167.18 ± 27.16, 149.47 ± 39.12, and 135.80 ± 37.26 μm freezing at −20°C for 2, 7, 12 and 17 days. In this case, longer freezing time produce smaller pores sizes. Similarly, the pore sizes became smaller with longer freezing time when freezing at −40°C and −80°C. The results showed that the pore sizes of GelMA hydrogels could been controlled by freezing time, except for freezing temperatures.

Swelling Ratio and Mechanical Properties

The swelling properties of GelMA hydrogels depend on the pore sizes, the methacrylation degree, the amount of photoinitiator, and the solvent types (Rahali et al., 2017). It had been demonstrated in this work that the pore sizes of GelMA hydrogels treated in different conditions were different, so, the swelling properties were further studied. The swelling properties of GelMA hydrogels with different freezing temperatures and time are shown in **Figure 6**. According to **Figure 6A**, a rapid swelling was observed from 0 to 4 h, and the swelling reached equilibrium swelling after 24 h. The equilibrium swelling ratio in **Figure 6B** of group 1# - 12# at 24 h were 525.00 ± 13.03%, 514.02 ± 25.14%, 549.04 ± 54.06%, 513.71 ± 54.12%, 505.63 ± 15.75%, 536.27 ± 30.79%, 498.67 ± 37.88%, 525.35 ± 14.69%, 405.08 ± 50.17%, 516.59 ± 55.75%, 510.04 ± 4.59% and 489.06 ± 35.73%, respectively. And there was no significant difference in the equilibrium swelling ratio ($p > 0.05$). The differences in pore sizes in our samples made little contribution to the swelling

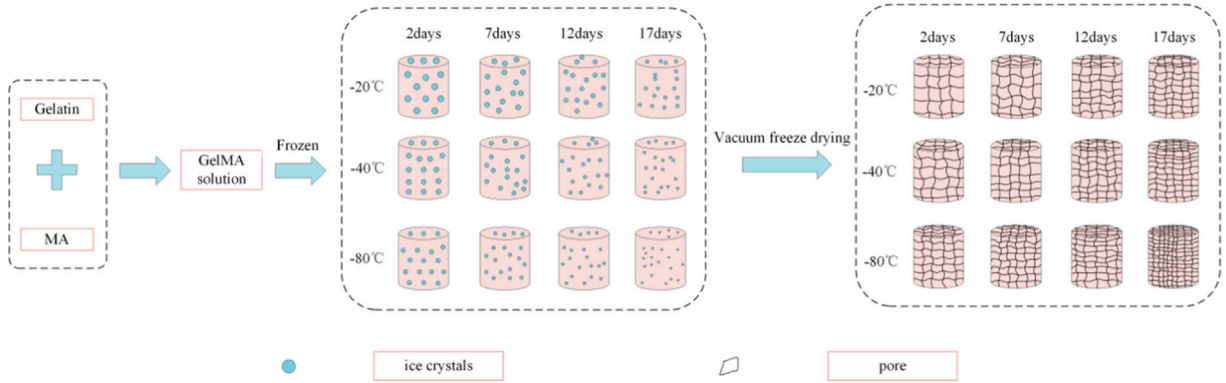

FIGURE 5 | Schematic illustration of the crystallization of GelMA hydrogels under different freezing time and temperatures.

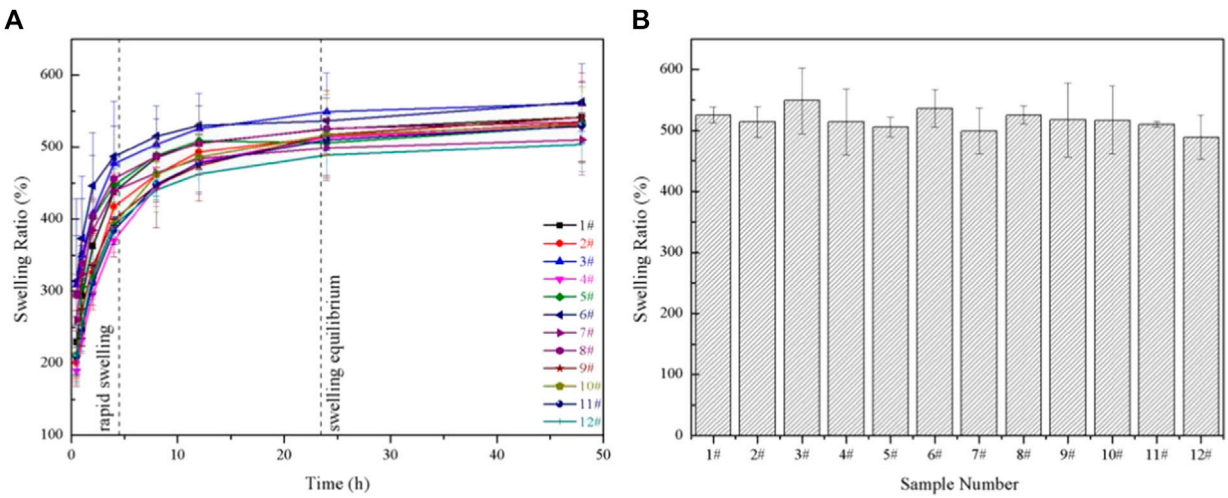

FIGURE 6 | (A) The swelling ratio of GelMA hydrogels with different freezing temperatures and time; **(B)** The equilibrium swelling ratio of GelMA hydrogels with different freezing temperatures and time in swelling 24 h.

properties. Therefore, the swelling properties of the GelMA hydrogels were not affected by changing freezing temperatures and time, which may be related to the degree of crosslinking was the same and the number of hydrophilic groups on the scaffolds unchanged.

The compressive properties of the GelMA hydrogel scaffolds treated under different freezing temperatures and time can be seen in **Figure 7**. The modulus of GelMA hydrogels increased with the reduction of freezing temperatures and the extension of freezing time, which was closely related to the decreased pore sizes of GelMA hydrogel scaffolds. It has been also reported that the mechanical strength of a porous scaffold depends mainly on its pore sizes, and smaller pores were helpful to enhance the biomechanical strength of engineered constructs (Felfel et al., 2019). During the freeze-drying course, the pore sizes decreased with the lower freezing temperatures and longer freezing time, also resulting in the higher compressive strength.

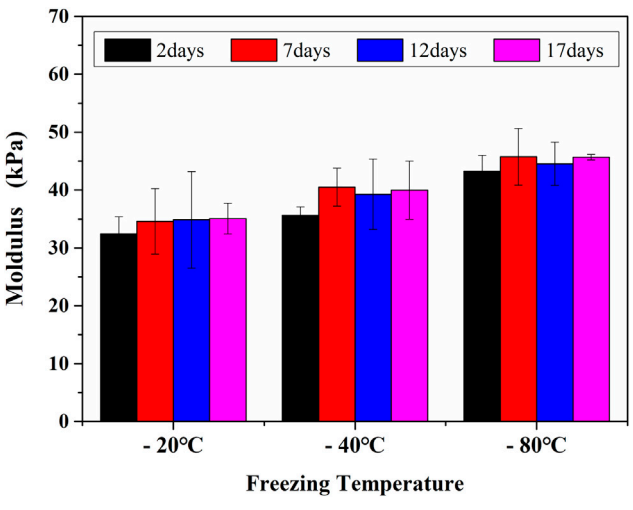

FIGURE 7 | The moldulus of GelMA hydrogels with different freezing temperatures and time.

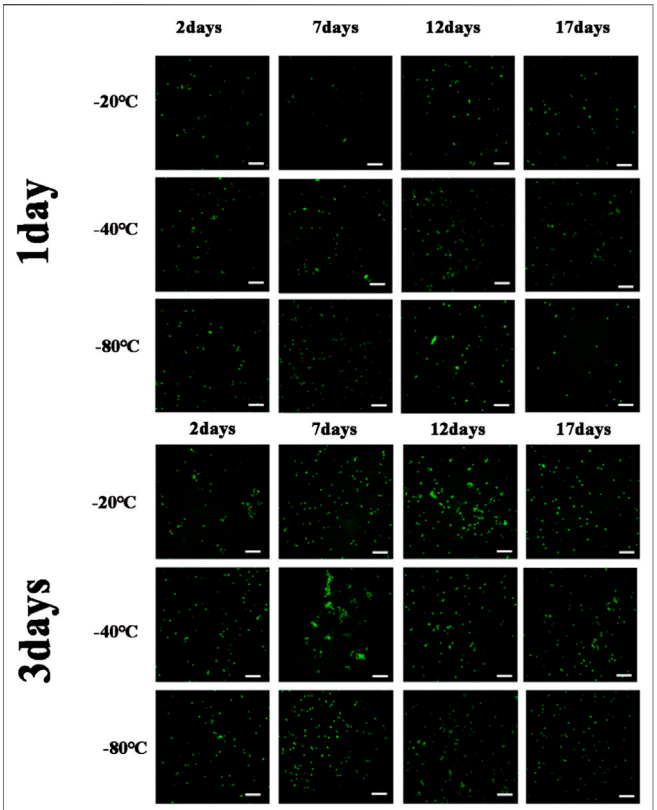

FIGURE 8 | LSCM images of live osteoblasts that were cultured with.

Growth of MC3T3-E1 Cells in GelMA Hydrogels

Figure 8 showed the cell viability and proliferation after 1 day and 3 days of cultivation, respectively. Cell viability was determined by green staining for living cells and red for dead cells during culture periods of 1 day and 3 days, and few dead cells were found. The results suggested that GelMA hydrogels could provide a good survival microenvironment for cells due to their ECM-mimetic properties (Monteiro et al., 2020). Consequently, the cell viability of long-term cultures with GelMA hydrogels was assumed to be perfect. As for GelMA hydrogels with larger pore sizes, the cell proliferation rate observed was lower than that observed with the smaller pore sizes. Because of MC3T3-E1 cells could only respond to submicron-scaled pore sizes (Zhang et al., 2017), MC3T3-E1 cells had better cell activity and cell proliferation as the pore sizes of GelMA hydrogels decreased for different freezing time and temperatures. As a result, by controlling the freezing conditions of GelMA hydrogels, the microenvironment suitable for MC3T3 cell was structured. Considering the different cells were suitable for different pore sizes, the tunable pore size hydrogels undoubtedly showed the broad prospect for 3D microenvironment of different types of cells.

GelMA hydrogels with different freezing temperatures and times at 1 day, 3 days (Scale bars represent 100 μm in all images).

CONCLUSION

GelMA hydrogels were synthesized with different freezing temperatures and time in this study, and the component, morphology, swelling ratio, mechanical properties and cell adhesion properties of the hydrogels were studied in detail. The pore sizes of the scaffold reduced as the pre-freezing temperature decreased and the freezing time increased. In addition, smaller pore sizes leading to higher MC3T3-E1cell proliferation rate. These results provided a broad prospect for synthesis of GelMA hydrogels with desired pore sizes as well as the appropriate pore sizes for different cells culture.

DATA AVAILABILITY STATEMENT

The original contributions presented in the study are included in the article/Supplementary Material, further inquiries can be directed to the corresponding authors.

AUTHOR CONTRIBUTIONS

Original article preparation: TL, YZ, and MS; cell experiments: MJ and WX; draft correction, supervision and editing: TW and HY. All authors listed have made substantial contribution to the article, which is acknowledged and confirmed by themselves. All authors have read and agreed on the final version of the article.

FUNDING

This research was funded by the project from the Natural Science Foundation of Liaoning Province of China (No. 2020-MS-166), Foundation of the Education Department of Liaoning Province in China (No. QN2019035), and the National Natural Science Foundation of China (No. 81500897).

REFERENCES

Basara, G., Yue, X., and Zorlutuna, P. (2019). Dual Crosslinked Gelatin Methacryloyl Hydrogels for Photolithography and 3D Printing. *Gels* 5 (3), 34. doi:10.3390/gels5030034

Benton, J. A., DeForest, C. A., Vivekanandan, V., and Anseth, K. S. (2009). Photocrosslinking of Gelatin Macromers to Synthesize Porous Hydrogels that Promote Valvular Interstitial Cell Function. *Tissue Eng. A* 15 (11), 3221–3230. doi:10.1089/ten.tea.2008.0545

Celikkin, N., Mastrogiacomo, S., Jaroszewicz, J., Walboomers, X. F., and Swieszkowski, W. (2018). Gelatin Methacrylate Scaffold for Bone Tissue Engineering: The Influence of Polymer Concentration. *J. Biomed. Mater. Res.* 106 (1), 201–209. doi:10.1002/jbm.a.36226

Chen, Y.-C., Lin, R.-Z., Qi, H., Yang, Y., Bae, H., Melero-Martin, J. M., et al. (2012). Functional Human Vascular Network Generated in Photocrosslinkable Gelatin

Methacrylate Hydrogels. *Adv. Funct. Mater.* 22 (10), 2027–2039. doi:10.1002/adfm.201101662

Diao, J. J., Ding, H. W., Huang, M. Q., Fu, X. L., Zou, F., Li, T. J., et al. (2019). Bone Defect Model Dependent Optimal Pore Sizes of 3D-Plotted Beta-Tricalcium Phosphate Scaffolds for Bone Regeneration. *Small Methods* 3 (11), 1900237. doi:10.1002/smtd.201900237

Dursun Usal, T., Yucel, D., and Hasirci, V. (2019). A Novel GelMA-pHEMA Hydrogel Nerve Guide for the Treatment of Peripheral Nerve Damages. *Int. J. Biol. macromolecules* 121, 699–706. doi:10.1016/j.ijbiomac.2018.10.060

Elkhoury, K., Morsink, M., Tahri, Y., Kahn, C., Cleymand, F., Shin, S. R., et al. (2021). Synthesis and Characterization of C2C12-Laden Gelatin Methacryloyl (GelMA) from marine and Mammalian Sources. *Int. J. Biol. Macromolecules* 183, 918–926. doi:10.1016/j.ijbiomac.2021.05.040

Felfel, R. M., Gideon-Adeniyi, M. J., Zakir Hossain, K. M., Roberts, G. A. F., and Grant, D. M. (2019). Structural, Mechanical and Swelling Characteristics of 3D Scaffolds from Chitosan-Agarose Blends. *Carbohydr. Polym.* 204, 59–67. doi:10.1016/j.carbpol.2018.10.002

Gao, F., Xu, Z., Liang, Q., Li, H., Peng, L., Wu, M., et al. (2019). Osteochondral Regeneration with 3D-Printed Biodegradable High-Strength Supramolecular Polymer Reinforced-Gelatin Hydrogel Scaffolds. *Adv. Sci. (Weinh)* 6 (15), 1900867. doi:10.1002/advs.201900867

Kang, H.-W., Tabata, Y., and Ikada, Y. (1999). Fabrication of Porous Gelatin Scaffolds for Tissue Engineering. *Biomaterials* 20 (14), 1339–1344. doi:10.1016/s0142-9612(99)00036-8

Kirsch, M., Rach, J., Handke, W., Seltsam, A., Pepelanova, I., Strauss, S., et al. (2020). Comparative Analysis of Mesenchymal Stem Cell Cultivation in Fetal Calf Serum, Human Serum, and Platelet Lysate in 2D and 3D Systems. *Front. Bioeng. Biotechnol.* 8, 598389. doi:10.3389/fbioe.2020.598389

Lee, B. H., Shirahama, H., Cho, N.-J., and Tan, L. P. (2015). Efficient and Controllable Synthesis of Highly Substituted Gelatin Methacrylamide for Mechanically Stiff Hydrogels. *RSC Adv.* 5 (128), 106094–106097. doi:10.1039/c5ra22028a

Lee, Y., Lee, J. M., Bae, P. K., Chung, I. Y., Chung, B. H., and Chung, B. G. (2015). Photo-crosslinkable Hydrogel-Based 3D Microfluidic Culture Device. *Electrophoresis* 36 (7-8), 994–1001. doi:10.1002/elps.201400465

Li, X., Chen, S., Li, J., Wang, X., Zhang, J., Kawazoe, N., et al. (2016). 3D Culture of Chondrocytes in Gelatin Hydrogels with Different Stiffness. *Polymers (Basel)* 8 (8), 269. doi:10.3390/polym8080269

Liu, J. Y., Li, L., Suo, H. R., Yan, M. L., Yin, J., and Fu, J. Z. (2019). 3D Printing of Biomimetic Multi-Layered GelMA/nHA Scaffold for Osteochondral Defect Repair. *Mater. Des.* 171, 107708. doi:10.1016/j.matdes.2019.107708

Liu, T., Weng, W., Zhang, Y., Sun, X., and Yang, H. (2020). Applications of Gelatin Methacryloyl (GelMA) Hydrogels in Microfluidic Technique-Assisted Tissue Engineering. *Molecules* 25 (22), 5305. doi:10.3390/molecules25225305

Monteiro, M. V., Gaspar, V. M., Ferreira, L. P., and Mano, J. F. (2020). Hydrogel 3D *In Vitro* Tumor Models for Screening Cell Aggregation Mediated Drug Response. *Biomater. Sci.* 8 (7), 1855–1864. doi:10.1039/c9bm02075f

Nam, Y. S., and Park, T. G. (1999). Biodegradable Polymeric Microcellular Foams by Modified Thermally Induced Phase Separation Method. *Biomaterials* 20 (19), 1783–1790. doi:10.1016/s0142-9612(99)00073-3

Ni, X., Ke, F., Xiao, M., Wu, K., Kuang, Y., Corke, H., et al. (2016). The Control of Ice crystal Growth and Effect on Porous Structure of Konjac Glucomannan-Based Aerogels. *Int. J. Biol. Macromolecules* 92, 1130–1135. doi:10.1016/j.ijbiomac.2016.08.020

Rahali, K., Ben Messaoud, G., Kahn, C. J. F., Sanchez-Gonzalez, L., Kaci, M., Cleymand, F., et al. (2017). Synthesis and Characterization of Nanofunctionalized Gelatin Methacrylate Hydrogels. *Int. J. Mol. Sci.* 18 (12), 2675. doi:10.3390/ijms18122675

Sadeghi, M., and Heidari, B. (2011). Crosslinked Graft Copolymer of Methacrylic Acid and Gelatin as a Novel Hydrogel with pH-Responsiveness Properties. *Materials* 4 (3), 543–552. doi:10.3390/ma4030543

Sun, M., Sun, X., Wang, Z., Guo, S., Yu, G., and Yang, H. (2018). Synthesis and Properties of Gelatin Methacryloyl (GelMA) Hydrogels and Their Recent Applications in Load-Bearing Tissue. *Polymers (Basel)* 10 (11), 1298. doi:10.3390/polym10111290

Thiebaud, M., Dumay, E. M., and Cheftel, J.-C. (2002). Pressure-shift Freezing of O/w Emulsions: Influence of Fructose and Sodium Alginate on Undercooling, Nucleation, Freezing Kinetics and Ice crystal Size Distribution. *Food Hydrocolloids* 16 (6), 527–545. doi:10.1016/s0268-005x(01)00133-3

Van den Bulcke, A. I., Bogdanov, B., De Rooze, N., Schacht, E. H., Cornelissen, M., and Berghmans, H. (2000). Structural and Rheological Properties of Methacrylamide Modified Gelatin Hydrogels. *Biomacromolecules* 1 (1), 31–38. doi:10.1021/bm990017d

Van Vlierberghe, S., Cnudde, V., Dubruel, P., Masschaele, B., Cosijns, A., De Paepe, I., et al. (2007). Porous Gelatin Hydrogels: 1. Cryogenic Formation and Structure Analysis. *Biomacromolecules* 8 (2), 331–337. doi:10.1021/bm060684o

Wang, H., Zhou, L., Liao, J., Tan, Y., Ouyang, K., Ning, C., et al. (2014). Cell-laden Photocrosslinked GelMA-DexMA Copolymer Hydrogels with Tunable Mechanical Properties for Tissue Engineering. *J. Mater. Sci. Mater. Med.* 25 (9), 2173–2183. doi:10.1007/s10856-014-5261-x

Wang, Y., Ma, M., Wang, J., Zhang, W., Lu, W., Gao, Y., et al. (2018). Development of a Photo-Crosslinking, Biodegradable GelMA/PEGDA Hydrogel for Guided Bone Regeneration Materials. *Materials (Basel)* 11 (8), 1345. doi:10.3390/ma11081345

Wang, Y., Ma, M., Zhang, L., Gao, Y., Zhang, B., and Guo, Y. (2019). Fabrication of Bi-layer Photocrosslinked GelMA/PEGDA Fibrous Membrane for Guided Bone Regeneration Materials. *Mater. Lett.* 249, 112–115. doi:10.1016/j.matlet.2019.04.076

Wu, J., Zhao, Q., Liang, C., and Xie, T. (2013). Enzymatically Degradable Oxidized Dextran-Chitosan Hydrogels with an Anisotropic Aligned Porous Structure. *Soft Matter* 9 (46), 11136–11142. doi:10.1039/c3sm52070f

Yin, J., Yan, M., Wang, Y., Fu, J., and Suo, H. (2018). 3D Bioprinting of Low-Concentration Cell-Laden Gelatin Methacrylate (GelMA) Bioinks with a Two-step Cross-Linking Strategy. *ACS Appl. Mater. Inter.* 10 (8), 6849–6857. doi:10.1021/acsami.7b16059

Yue, K., Trujillo-de Santiago, G., Alvarez, M. M., Tamayol, A., Annabi, N., and Khademhosseini, A. (2015). Synthesis, Properties, and Biomedical Applications of Gelatin Methacryloyl (GelMA) Hydrogels. *Biomaterials* 73, 254–271. doi:10.1016/j.biomaterials.2015.08.045

Zhang, J., Sun, L., Luo, X., Barbieri, D., de Bruijn, J. D., van Blitterswijk, C. A., et al. (2017). Cells Responding to Surface Structure of Calcium Phosphate Ceramics for Bone Regeneration. *J. Tissue Eng. Regen. Med.* 11 (11), 3273–3283. doi:10.1002/term.2236

Zhang, X., Kim, G. J., Kang, M. G., Lee, J. K., Seo, J. W., Do, J. T., et al. (2018). Marine Biomaterial-Based Bioinks for Generating 3D Printed Tissue Constructs. *Mar. Drugs* 16 (12), 484. doi:10.3390/md16120484

Zhao, X., Lang, Q., Yildirimer, L., Lin, Z. Y., Cui, W., Annabi, N., et al. (2016). Photocrosslinkable Gelatin Hydrogel for Epidermal Tissue Engineering. *Adv. Healthc. Mater.* 5 (1), 108–118. doi:10.1002/adhm.201500005

Zheng, J., Zhao, F., Zhang, W., Mo, Y., Zeng, L., Li, X., et al. (2018). Sequentially-crosslinked Biomimetic Bioactive Glass/gelatin Methacryloyl Composites Hydrogels for Bone Regeneration. *Mater. Sci. Eng. C* 89, 119–127. doi:10.1016/j.msec.2018.03.029

Conflict of Interest: The authors declare that the research was conducted in the absence of any commercial or financial relationships that could be construed as a potential conflict of interest.

Publisher's Note: All claims expressed in this article are solely those of the authors and do not necessarily represent those of their affiliated organizations, or those of the publisher, the editors and the reviewers. Any product that may be evaluated in this article, orclaim that may be made by its manufacturer, is not guaranteed or endorsed by the publisher.

frontiers in Bioengineering and Biotechnology

REVIEW
published: 22 December 2021
doi: 10.3389/fbioe.2021.792929

Recent Advances of Biomedical Materials for Prevention of Post-ESD Esophageal Stricture

*Yuchen Bao[1], Zhenguang Li[1], Yingze Li[1], Tao Chen[2], Yu Cheng[1] and Meidong Xu[2]**

[1]Translational Medical Center for Stem Cell Therapy and Institute for Regenerative Medicine, Institute for Translational Nanomedicine, Shanghai East Hospital, Tongji University School of Medicine, Shanghai, China, [2]Endoscopy Center, Shanghai East Hospital, Tongji University School of Medicine, Shanghai, China

Esophageal stricture commonly occurs in patients that have suffered from endoscopic submucosal dissection (ESD), and it makes swallowing difficult for patients, significantly reducing their life qualities. So far, the prevention strategies applied in clinical practice for post-ESD esophageal stricture usually bring various inevitable complications, which drastically counteract their effectiveness. Nowadays, with the widespread investigation and application of biomedical materials, lots of novel approaches have been devised in terms of the prevention of esophageal stricture. Biomedical polymers and biomedical-derived materials are the most used biomedical materials to prevent esophageal stricture after ESD. Both of biomedical polymers and biomedical-derived materials possess great physicochemical properties such as biocompatibility and biodegradability. Moreover, some biomedical polymers can be used as scaffolds to promote cell growth, and biomedical-derived materials have biological functions similar to natural organisms, so they are important in tissue engineering. In this review, we have summarized the current approaches for preventing esophageal stricture and put emphasis on the discussion of the roles biomedical polymers and biomedical-derived materials acted in esophageal stricture prevention. Meanwhile, we proposed several potential methods that may be highly rational and feasible in esophageal stricture prevention based on other researches associated with biomedical materials. This review is expected to offer a significant inspiration from biomedical materials to explore more effective, safer, and more economical strategies to manage post-ESD esophageal stricture.

Keywords: endoscopic submucosal dissection (ESD), esophageal stricture, tissue engineering, biomedical polymer, biomedical derived materials

OPEN ACCESS

Edited by:
Hongli Mao,
Nanjing Tech University, China

Reviewed by:
Goutam Thakur,
Manipal Institute of Technology, India
Gefei Wang,
Jinling Hospital, China

****Correspondence:***
Meidong Xu
1800512@tongji.edu.cn

Specialty section:
This article was submitted to Biomechanics, a section of the journal Frontiers in Bioengineering and Biotechnology

Received: *11 October 2021*
Accepted: *22 November 2021*
Published: *22 December 2021*

Citation:
Bao Y, Li Z, Li Y, Chen T, Cheng Y and Xu M (2021) Recent Advances of Biomedical Materials for Prevention of Post-ESD Esophageal Stricture. Front. Bioeng. Biotechnol. 9:792929. doi: 10.3389/fbioe.2021.792929

INTRODUCTION

Esophageal cancer, a malignant tumor occurring in the esophagus, has the seventh highest incidence and the sixth highest mortality rate worldwide (Sung et al., 2021). Although the overall 5-year survival of malignant esophageal cancer is less than 20% in Asian people, early esophageal cancer patients can obtain good prognosis if merely the mucosal layer or superficial submucosal layer is invaded (Siegel et al., 2017). With the remarkable development of endoscopic technology, endoscopic submucosal dissection (ESD) has been acknowledged as the standard therapy in clinics for early esophageal cancer because of minimally invasive tumor excision for minimizing the risk of deterioration (Shah and Gerdes 2015). The ESD employs high-frequency electrosurgical

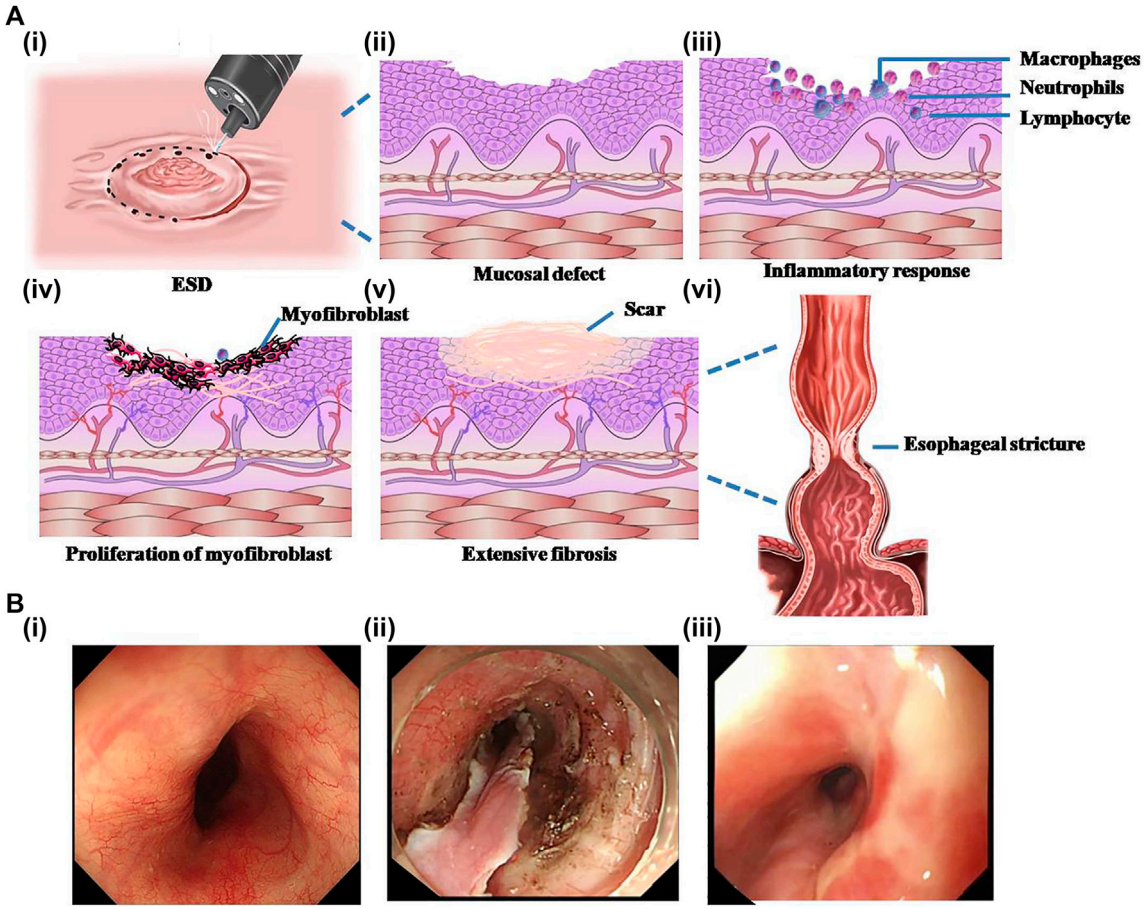

FIGURE 1 | Schematic representation of the formation process of esophageal stricture after endoscopic submucosal dissection (ESD) and the endoscopic photographs of esophageal stricture. **(A)** The schematic diagram of the formation of esophageal stricture. **(i)** ESD surgery. **(ii)** Irregular mucosal defect left after surgery. **(iii)** Acute inflammatory reaction in exposed mucosal wounds. **(iv)** Massive proliferation of myofibroblasts after inflammation accompanied by angiogenesis in the submucosa. **(v)** Extensive fibrosis of the esophageal mucosal wound forming a scar. **(vi)** Scar formation and contracture at the wound result in esophageal stricture. **(B)** Endoscopic pictures of the esophagus. **(i)** Normal esophagus. **(ii)** Esophagus with mucosal layer stripped by ESD. **(iii)** Stricture-forming esophagus. Reproduced from Chu et al. (2019). Copyright (2019), with permission from Springer Nature.

knife and special equipment under the endoscope to gradually peel off the gastrointestinal lesion from the normal submucosa to achieve complete resection of the lesions, reducing local recurrence and metastasis (Fujishiro et al., 2009; Mochizuki et al., 2012). Meanwhile, ESD shows optimistic results in the evaluation of postoperative efficacy. It is recorded that the *en bloc* resection rate and complete resection rate of esophageal ESD is 90%–100% and 90%–97.4%, respectively (Takahashi et al., 2010; Nishizawa and Suzuki 2020). In general, ESD is an economical, safe, and reliable method to remove superficial lesions of the digestive tract.

However, there are still some complications that occurred during or after ESD, such as bleeding, perforation, and stricture. Esophageal stricture, which presents as a significant tortuosity of the esophageal lumen and is difficult to pass through by conventional gastroscopy, is a particularly common and serious postoperative complication (Lew and Kochman 2002; Ono et al., 2009), significantly reducing the living quality of patients for its serious consequences such as reflux and inhalation pneumonia. The incidence of post-operative esophageal stricture would reach 90% if patients suffer from mucosal defects over three-quarters of the circumferential of the esophagus (Nishizawa and Suzuki 2020). Unlike other complications such as bleeding and perforation, skilled operation is not able to fundamentally prevent the occurrence of esophageal stricture.

It has been found that esophageal stricture usually occurs within 2–4 weeks after mucosal resection (Mizuta et al., 2009; Ono et al., 2009). Though the specific mechanism of esophageal stricture after ESD has not been completely illuminated, many experiments have indicated that mucosal defect is the initial and most important condition in the process of esophageal stricture (Honda et al., 2010; Pech et al., 2014). Although it has been confirmed that the wound over three-quarters of the esophageal circumference after ESD would cause obvious esophageal stricture (Ono et al., 2009; Chu et al., 2019), the longitudinal length of the esophageal mucosal defect and the depth of the lesions are also reliable risk factors for the occurrence of postoperative stricture (Alvarez Herrero et al., 2011). The

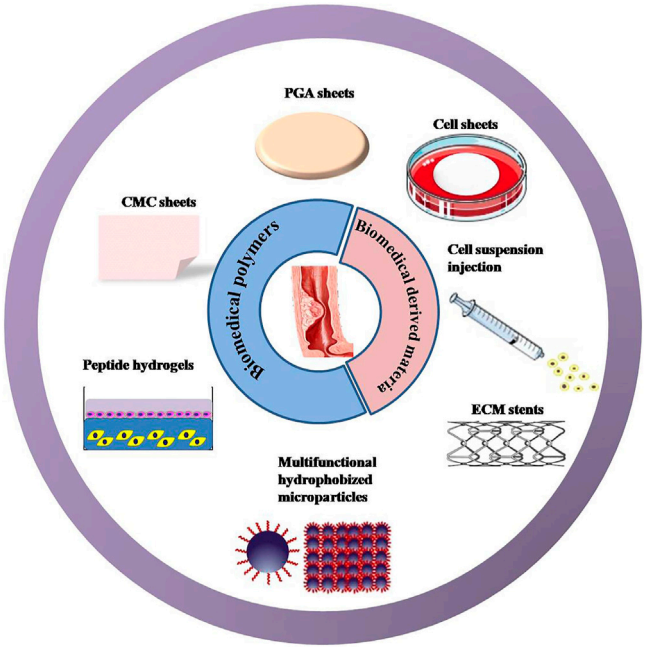

FIGURE 2 | New strategies that have been reported to prevent post-ESD esophageal stricture. Approaches involve biomedical polymers: including polyglycolic acid (PGA)/carboxymethyl cellulose (CMC) sheets, peptide hydrogels, and multifunctional hydrophobized microparticles. Methods covering the biomedical-derived materials incorporating cell sheets, cell suspension, and extracellular matrix (ECM) stents.

esophageal mucosal defect caused by ESD will promote inflammatory response and subsequently enter into the staggered and complicated wound-repairing process (Radu et al., 2004), which can be simply divided into three phases: inflammatory response, epithelial proliferation, and extracellular matrix remodeling (**Figure 1**) (Broughton et al., 2006). The wound-healing process after endoscopic mucosal resection (EMR) has been observed in an animal experiment conducted by Honda et al. (2010). The inflammation at defect lesions disappeared after 1 week of operation, and then new blood vessels and fibrous tissues proliferated significantly, accompanied by epithelial cells growing and migrating from the edge of the lesions. More than 1 month after EMR, the mucosal defect was gradually covered by squamous epithelium, and the submucosa was replaced by large and dense collagen fibers. Meanwhile, the muscle fibers of the muscularis propria gradually atrophied and eventually became fibrotic, reducing the elasticity and compliance of the esophageal wall. Besides, the massive proliferation of collagen fibers and extensive fibrosis can form scarring tissues, resulting in further esophageal stricture. Therefore, effective prevention methods of esophageal stricture can be approached from the following aspects: inhibiting initial inflammatory response, promoting epithelial regeneration, and inhibiting fibrosis.

The main methods currently used in clinics for treating or preventing post-ESD esophageal stricture include balloon dilation, stent dilation, and pharmaceutical prophylaxis. Although these methods are effective to some extent, they also bring certain different extents of complications, which seriously affect the physical and mental health of patients. Thus, it is essential to optimize and explore new methods for the prevention of esophageal stricture. In recent decades, tissue engineering has been considered as the most potential technology for regenerative medicine, in which biomedical materials are employed as scaffold to support cell migration, adhesion, proliferation, and differentiation due to their unique properties including good biocompatibility and biodegradability, stable chemical properties, and mechanical properties matching the tissues. In the application of esophageal stricture prevention after ESD, biomedical materials derived from polymers and natural tissues can be used as tissue engineering scaffold to support mucosal epithelial cell adhesion and proliferation and promote esophageal mucosal repairing.

In this review, we are going to integrate approaches involving biomedical materials that have been reported for the management of esophageal stricture (**Figure 2**). Furthermore, novel preventive strategies are proposed based on the extensive investigations and applications of biocompatible and biodegradable polymers. These proposed innovations may be reasonable and practicable by inhibiting inflammatory response, promoting epithelial regeneration, or reducing excessive fibrosis on the base of intervention to the formation of esophageal stricture. As an ultimate aim of the review, we hope the comprehensive analysis of these strategies and in-depth thinking will provide a strong reference value for engineering more effective and safe systems to drastically reduce the incidence of esophageal stricture after ESD.

CURRENT CLINICAL APPROACHES FOR THE PREVENTION OF POST-ESD ESOPHAGEAL STRICTURE

Up to now, many methods of preventing or treating esophageal stricture have been widely applied in clinical practice, including pharmacological treatments and mechanical manipulation, such as endoscopic dilation and endoscopic stent implantation (Ezoe et al., 2011; Yamaguchi et al., 2011; Machida et al., 2012; Ye et al., 2016). However, these methods bring certain different extents of complications. Endoscopic balloon dilatation (EBD) usually needs to be underwent multiple times to prevent re-stricture and may result in bleeding, perforation, bacteremia, and other complications, which are time-consuming and bring great pain to patients. Endoscopic stents mainly include metal stents and biodegradable stents. Metal stents have a certain preventive effect on stricture after ESD, but they may cause complications such as stent displacement, gastrointestinal bleeding, perforation, and granulation hyperplasia (Bakken et al., 2010). Contrastively, biodegradable stents represented by polylactic acid show good biocompatibility and ideal degradability, while it has poor capacity of self-expansion and weak mechanical strength, accompanied by complicated placement procedure. Saito et al. (2008) reported that the stent would dislocate in 10–21 days with the biodegradation of polylactic acid, while the effectiveness of

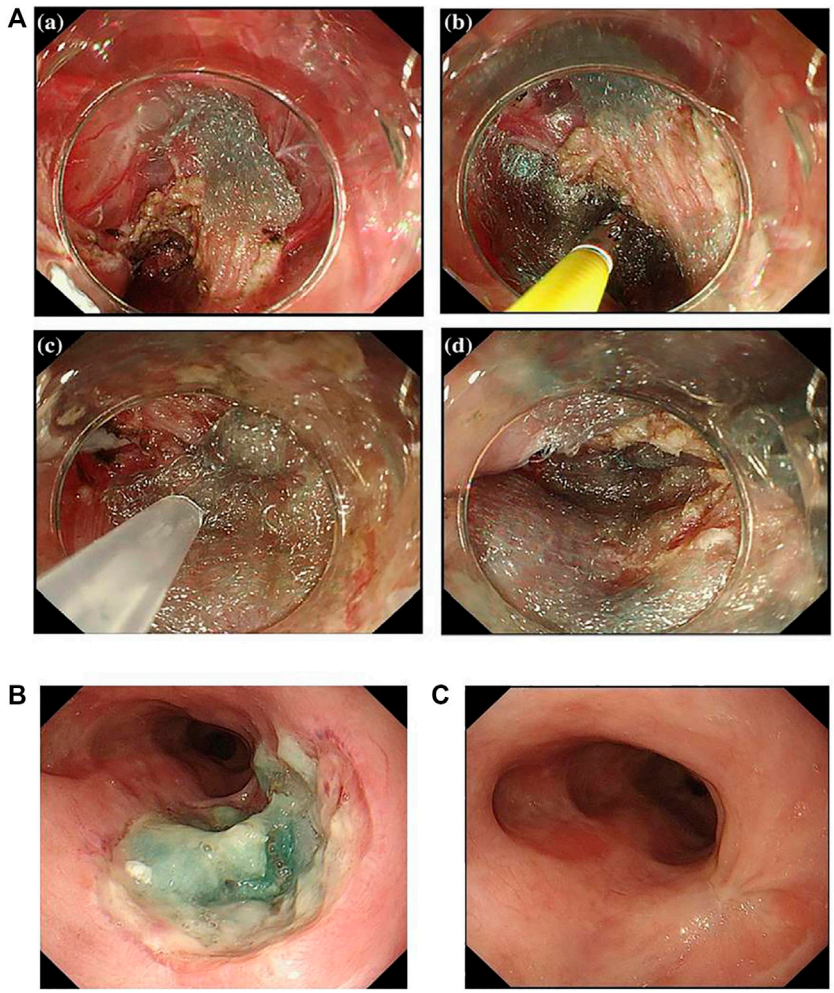

FIGURE 3 | Newly proposed healing dressings based on biocompatible biomedical polymers. **(A)** Esophageal perforation was completely covered by PGA sheets. **(B)** The endoscopic image of the esophageal perforation with PGA sheets after 6 days of ESD. **(C)** The endoscopic image of the esophagus after 3 months of ESD. Reproduced from Seehawong et al. (2019). Copyright (2019), with permission from Springer Nature.

stents in preventing stricture in such a short period of time is doubtful. Steroids are common anti-inflammatory drugs, and they are widely used in clinical practice to inhibit inflammatory response (Rhen and Cidlowski 2005; Mori et al., 2013). However, the use of systemic steroids is frequently accompanied by adverse reactions such as immunosuppression, osteoporosis, and other hormone-induced diseases. Even local injection of steroids could also bring complications related to puncture operations, such as esophageal perforation, esophageal abscess, mediastinal abscess, pleural effusion, and gastrointestinal bleeding. What is worse, steroids are poorly utilized in local injection (Rajan et al., 2005; Lee et al., 2013).

BIOMEDICAL POLYMERS

Biomedical polymers used for esophageal stricture prevention can be categorized as synthetic polymers and naturally derived polymers according to their material sources. Synthetic polymers are artificially synthesized by chemical or physical means. Naturally derived polymers are made from natural polymers produced by living organisms with appropriate modifications. Naturally derived polymers have better biocompatibility and biodegradability than synthetic polymers.

Synthetic Polymers

Polyglycolic Acid Sheets

Polyglycolic acid (PGA) sheets are biodegradable fabric dressings made of polyglycolic acid. They are biocompatible and can be fully absorbed within 5 months. PGA is the first biomedical synthetic polymer used in clinical medicine, and they have a high degree of crystallinity to make a large tensile elastic modulus as well as excellent mechanical properties (Budak et al., 2020). Therefore, PGA and its derivatives have been employed in medical fields such as drug delivery and dental and orthopedic systems (Takimoto et al., 2014; Sakaguchi et al., 2016; Sharma and Sharma 2018), and PGA sheets, as a form of tissue engineering scaffold, are widely used in gastrointestinal field. In Japan, PGA

sheets have been used to promote wound healing after resection of oral tumors (Inokuchi et al., 2017). In the recent decade, PGA sheets (Neoveil; Gunze Co., Kyoto, Japan) are applied in endoscopic technology for the closure of perforations and postoperative homeostasis. Seehawong et al. (2019) used PGA sheets combined with fibrin glue to treat esophageal perforation after ESD (**Figure 3A**). They found that PGA sheets and fibrin glue facilitated the regeneration of mucosal tissues after ESD in a 74-year-old female, and perforations were all closed by PGA sheets without obvious leakage after 6 days of operation (**Figure 3B**). After 3 months of ESD, the esophageal ulcer repaired completely without formation of esophageal stricture (**Figure 3C**). Sakaguchi et al. (2015) conducted a research in which 11 patients received submucosal injection of steroids immediately after esophageal ESD, and then PGA was shielded on the esophageal defect. At last, they found that the incidence of esophageal stricture was reduced without requirement for EBD (Sakaguchi et al., 2015). Chai et al. (2018) found that the combination of PGA and stent dilation could significantly suppress the esophageal stricture compared to using individual stent in 70 patients (incidence was 20.5%:46.9%). To sum up, PGA sheets combined with fibrin glue have been proved to be effective to prevent post-ESD stricture. Though PGA has many advantages in the prevention of esophageal stricture, it is difficult for them to stay at the defect site for a long time. In some circumstances, some patients may be allergic to the degradation products of PGA. Besides, the risk of infection and bleeding during the application still needs to be discussed.

Peptide Hydrogels

Peptide hydrogel is a kind of hydrogel formed by cross-linked polymer chains of polypeptides or polypeptide derivatives (Zhou et al., 2009). It can be classified as chemical cross-linked peptide hydrogel and physical peptide hydrogel according to the formation type (Jonker et al., 2012). Physical peptide hydrogels are made by the intra- and intermolecular self-assembly, which derived from non-covalent interactions, including hydrogen bonding, electrostatic interactions, hydrophobic interactions, and so on (Tsonchev et al., 2004; Paramonov et al., 2006; de Groot et al., 2007; Bowerman et al., 2011; Koutsopoulos 2016). Therefore, physical peptide hydrogels are also considered to be self-assembling peptide hydrogels (SAPHs). Because self-assembling peptide hydrogels are formed gradually from molecules to nanofibers and then to the final network, the preparation process has a strong influence on the structure and properties of SAPHs. The peptide constituent gives SAPHs excellent properties of biocompatibility and biodegradability. Moreover, the preparation of SAPHs does not involve crosslinking reagents or organic solvents virtually, which makes SAPHs one of the promising options for biomedical applications, and SAPHs are injectable owing to the shear thinning property (Bakota et al., 2011; Lian et al., 2016; Zhang et al., 2017; Nguyen et al., 2018; Zhang et al., 2018; Gong et al., 2019). Besides, the structure of SAPHs is similar to the extracellular matrix, so they can be used as a scaffold in cell culture and tissue engineering, indicating a great potential of SAPHs in promoting repair of esophageal defects after ESD (Wan et al., 2016). Therefore, synthetic peptide hydrogels can be a disposal for preventing esophageal stricture in some way. Kumar et al. (2017) purchased a library of synthetic SAPHs from a company. Each hydrogel was different in terms of peptide sequence, stiffness, and overall charge (Kumar et al., 2017). These synthetic SAPHs supported bioactivities and functions of esophageal cells, realizing epithelialization and stratification during *in vitro* three-dimensional co-culture (**Figure 4**). In their study, mouse esophageal epithelial cells (mOECs) were seeded on the surface of peptide hydrogels (**Figure 4A**), while rat esophageal stromal fibroblasts (rOSFs) were incorporated into peptide hydrogels (**Figure 4A, B**). After a series of experimental evaluations, they found that the behaviors of mOECs such as morphology, proliferation, the formation of epithelial cell layers, and migration activity were influenced by distinctive properties of different hydrogels (**Figure 4A–D**). Similarly, the stiffness, charge, and mechanical properties of peptide hydrogels also affected responses of rOSFs (**Figure 4B–D**). The optimal composite hydrogel systems for 3D co-culture were favorable to both cell types and could successfully support the formation of a functional, uninterrupted epithelial sheet within a few days of incubation. However, the study was conducted merely at the cellular level, so the preventive effect and safety of these synthetic SAPHs need to be further studied in in-depth research.

Naturally Derived Polymers

Carboxymethyl Cellulose Sheets

Cellulose is a plant-derived polymer, and it is a renewably abundant resource in nature. Carboxymethyl cellulose (CMC) is obtained by carboxymethylation of cellulose. CMC sheets are biocompatible and biodegradable suture materials composed of modified hyaluronic acid and CMC, and they are harmless to people. Up to now, some clinical studies have demonstrated the effect of CMC sheets in wound healing (Bristow and Montz 2005; Huang et al., 2013). Tang et al. (2018b) covered small CMC sheets on the mucosal defects of the esophagus after ESD in pigs, and they found that the incidence of esophageal stricture in the CMC sheet treatment group was lower than that in the control group (71.4% vs 100%), with better food tolerance in the CMC sheet group (**Figure 5**). In the study, they delivered a CMC sheet above the mucosal defect by biopsy forceps to cover the defect fully in pigs (**Figure 5A**). Two weeks later, the pigs were killed, and the esophagus of each pig was excised and cultured to observe and evaluate esophageal stricture. As shown in **Figure 5B**, after 2 weeks of the implementation of ESD, severe esophageal stricture was seen in the control group, while the esophagus with treatment of CMC only showed slight stenosis. After histological evaluation of the esophagus in the CMC treatment and control groups, it was found that the fibrosis degree in the submucosa of the esophagus in the control group was significantly higher than that in the CMC-treated group (**Figure 5C**). They suggested that CMC sheets had an anti-fibrosis effect by regulating the expression of transforming growth factor beta (TGF-β1), which is a kind of growth factor associated with fibrosis (Sporn and Roberts 1989). Besides, the mucosal regeneration of the esophagus in the CMC-treated group

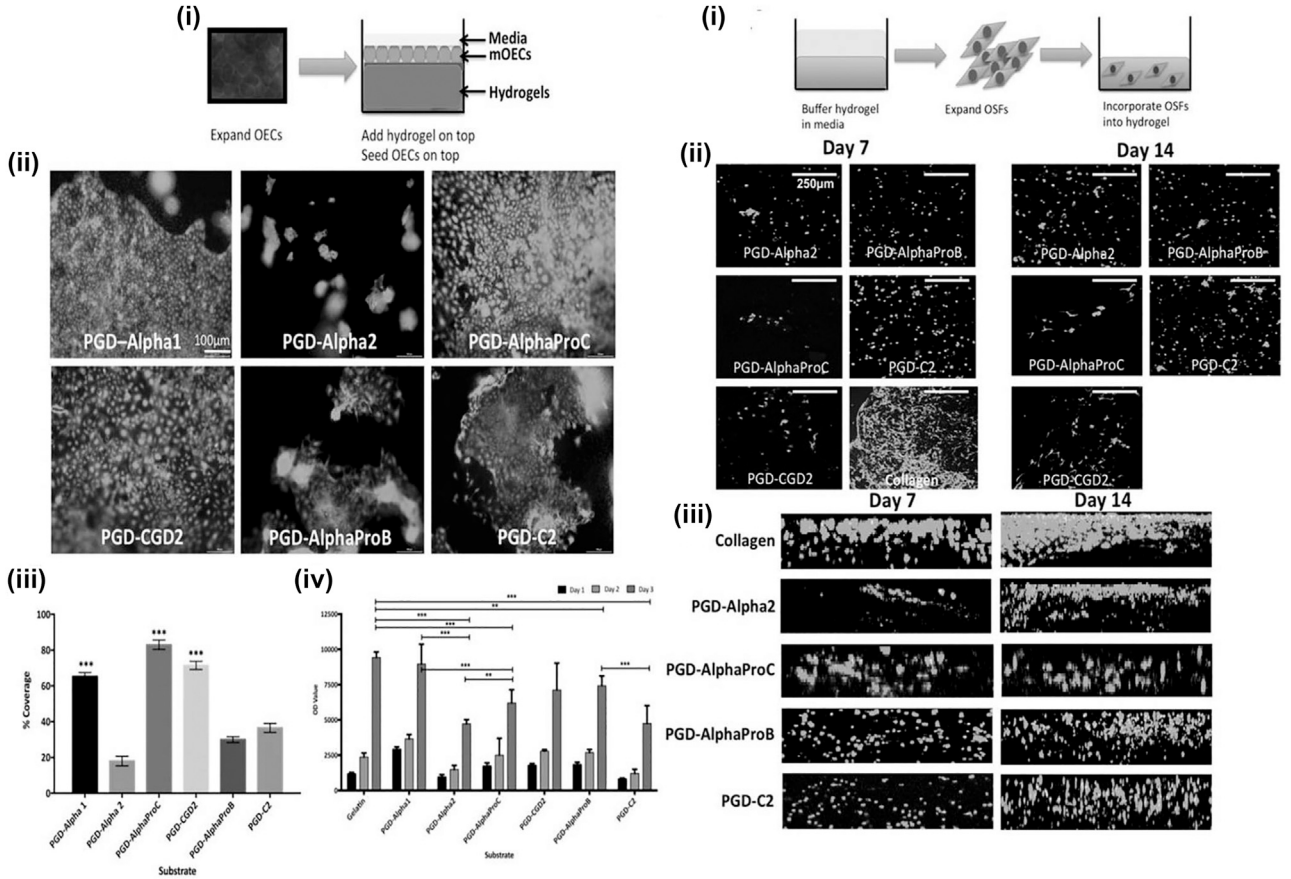

FIGURE 4 | The behaviors of mouse esophageal epithelial cells (mOECs) and rat esophageal stromal fibroblasts (rOSFs) cultured on the surface of peptide hydrogels **(A)** and embedded within peptide hydrogels **(B)**. **[A (i)]** Schematic diagram of mOECs cultured on the surface of peptide hydrogels. **[A (ii)]** The viability and proliferation of mOECs cultured on different peptide hydrogel surfaces for 3 days. **[A (iii, iv)]** The assessment of metabolic viability of mOECs cultured on the surface of different peptide hydrogels at different time points. **[B (i)]** Schematic diagram of rOSFs cultured into peptide hydrogels. **[B (ii)]** The viability and proliferation of rOSFs cultured into different peptide hydrogels. **[B (iii)]** The distribution of rOSFs within the different peptide hydrogels at the culture time point of 7 and 14 days. Reproduced from Kumar et al. (2017). Copyright (2017), with permission from John Wiley and Sons.

was better than that in the control group (**Figure 5D**). Similar to PGA sheets, CMC sheets could play the role of biophysical barriers to protect the wound. The essence of mucopolysaccharides possessed by CMC allows them to adhere to the mucosal defect within minutes after being exposed to moisture. Gago et al. (2003) made a comparative cell experiment and concluded that the ability of CMC sheets to reduce fibrosis probably stems from its function as a physical barrier, though the exact mechanism has not been elucidated. These studies proved that CMC sheets have a certain effect on preventing esophageal stricture with safety after ESD. However, researchers discover that CMC sheets formed barriers for approximately 7 days but no more than 14 days due to their good biodegradability, and the short duration of action of CMC sheets can weaken the fibrosis inhibition effect. Besides, CMC sheets cannot achieve a strong and long adhesion to tissues. Last but not the least, a short-term study may be insufficient for elucidating the mechanism of CMC sheets to suppress the wound fibrosis and evaluating the effect on preventing esophageal stricture. Furthermore, larger samples are necessary and more basic research need to be done to demonstrate the efficacy and mechanism of action of CMC sheets before clinical application.

Multifunctional Colloidal Dressing

A multifunctional colloidal dressing was prepared by Nishiguchi et al. (2019) to accelerate wound healing after ESD (**Figure 6**). The wound dressing was composed of hydrophobic microparticles (hMPs), which were prepared as follows: gelatin (Gltn), which is produced by the partial hydrolysis of collagen from the organism, was modified with aliphatic aldehyde to synthesize hydrophobically modified Gltn (hm-Gltn), and then, granulation of hm-Gltn was realized using the spray drying method before being formed into dried hMPs by thermal crosslinking route. The dried hMPs swelled in esophageal exudates when they were sprayed to the artificial defects, and aggregation of hMPs formed a hydrogel layer on the surface of post-ESD wound to enter the subsequent treatment cycle (**Figure 6A**). Multi-functionality of hMPs under wet environments based on hydrophobic interaction included tissue adhesiveness, acceleration of blood coagulation,

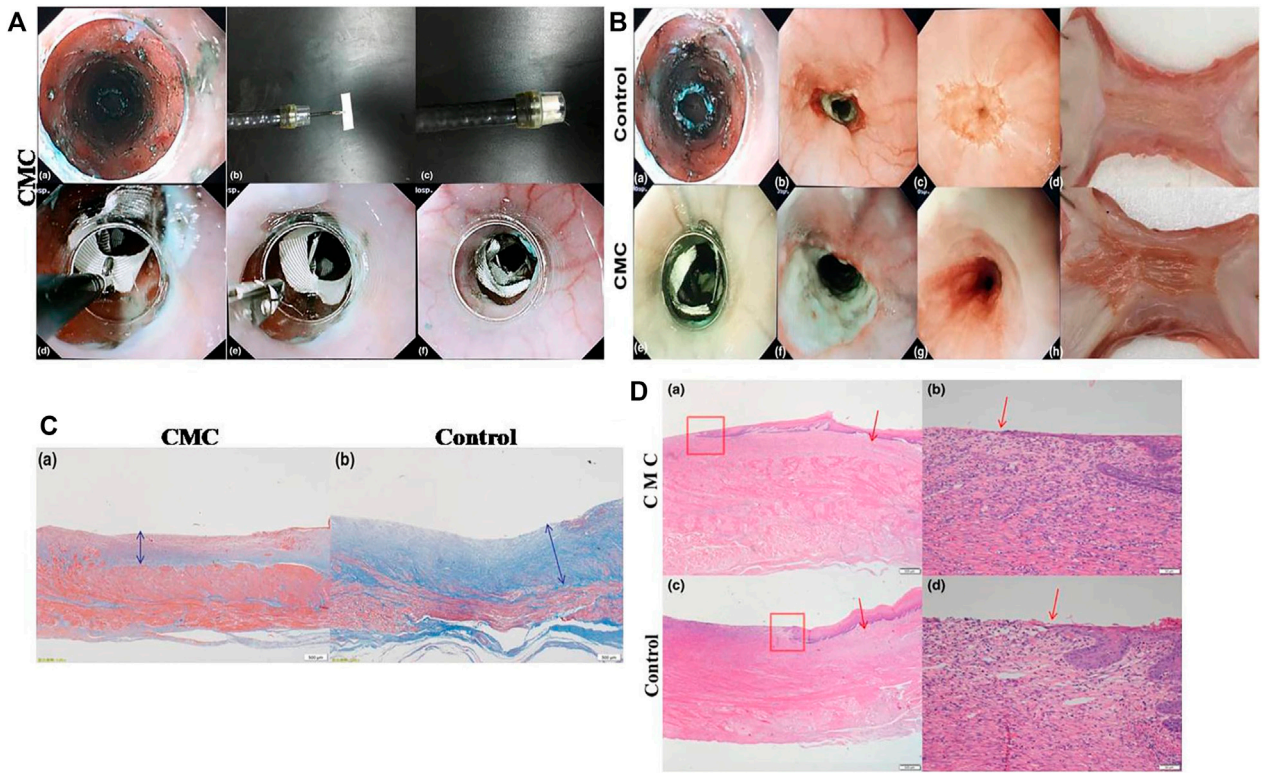

FIGURE 5 | The application of CMC sheet to prevent esophageal stricture after ESD. **(A)** The process of delivering CMC sheet to the defect of the esophagus. **(B)** The comparison of the esophagus between the control group and the CMC group. **(C)** The comparison of fibrosis thickness (blue double-headed arrow) in the submucosa of the esophagus between the CMC-treated group and the control group. **(D)** The comparison of regenerated epithelial lengths of the esophagus between the CMC-treated group and the control group (red boxes designate the boundary between the regenerated mucosal layer and original mucosa, and red arrows refer to the edge of the regenerating mucosal epithelium). The esophageal mucosal epithelium regeneration in the CMC group was better than that in control group. Reproduced from Tang et al. (2018b). Copyright (2018), with permission from John Wiley and Sons.

enhanced epithelialization, controlled inflammation, and enhanced angiogenesis. The adhesion strength of colloidal dressing substantially enhances as the alkyl chain length of aliphatic aldehyde increases at a certain extent. While the balance between hydrophobicity and hydrophilicity of hMPs is critical for achieving strong adhesion to live tissues, hydrophobically modified polymers can elicit blood coagulation reaction by facilitating physical crosslinking of blood component (Dowling et al., 2011; Rao et al., 2013). In their studies, researchers found that hMPs could aggregate with fibrin networks under a scanning electron microscope (SEM). So, they supposed that hydrophobic moieties on the particle surface might also interact with platelets and red blood cells besides fibrin networks, inducing a hemostatic effect of hMPs when they were sprayed to the esophageal wound. They also detected that these hMPs probably provided suitable scaffolds for growing of epithelial cells because of significant hydrophobicity and stiffness. In addition, the scaffold composed of hMPs was able to deliver and release vascular endothelial growth factor, which promoted angiogenesis (Yoshizawa et al., 2015). Moreover, the study discovered that the hydrogel layer transformed from hMPs in gastric ESD model of swine could suppress the fibrosis of gastric mucosa *via* interacting with cells, and ECM proteins multiply based on hydrophobic interactions. The number of inflammatory cells in the submucosa sprayed with hMPs obviously decreased compared to the control group. Meanwhile, the expression of α-smooth muscle actin (α-SMA) and type I collagen was significantly inhibited. Besides, the expression of von Willebrand factor (vWF) increased obviously in the hMP-treated group, indicating that the spraying of hMPs contributed to the growth and remodeling of blood vessels in the submucosa (**Figure 6B**). Above all, this sprayable wound dressing composed of naturally derived polymers exhibits multiple functions for wound healing based on hydrophobic interactions between polymers and biological tissues, establishing a good foundation for its clinical translation.

BIOMEDICAL-DERIVED MATERIALS

Biomedical-derived materials are originated from natural biological tissues that have undergone special treatments. Biological tissues may be taken from homologous or heterologous animal bodies. Special treatments include mild treatments such as fixation, sterilization, and eliminating antigenicity. Biomedical-derived materials have biological

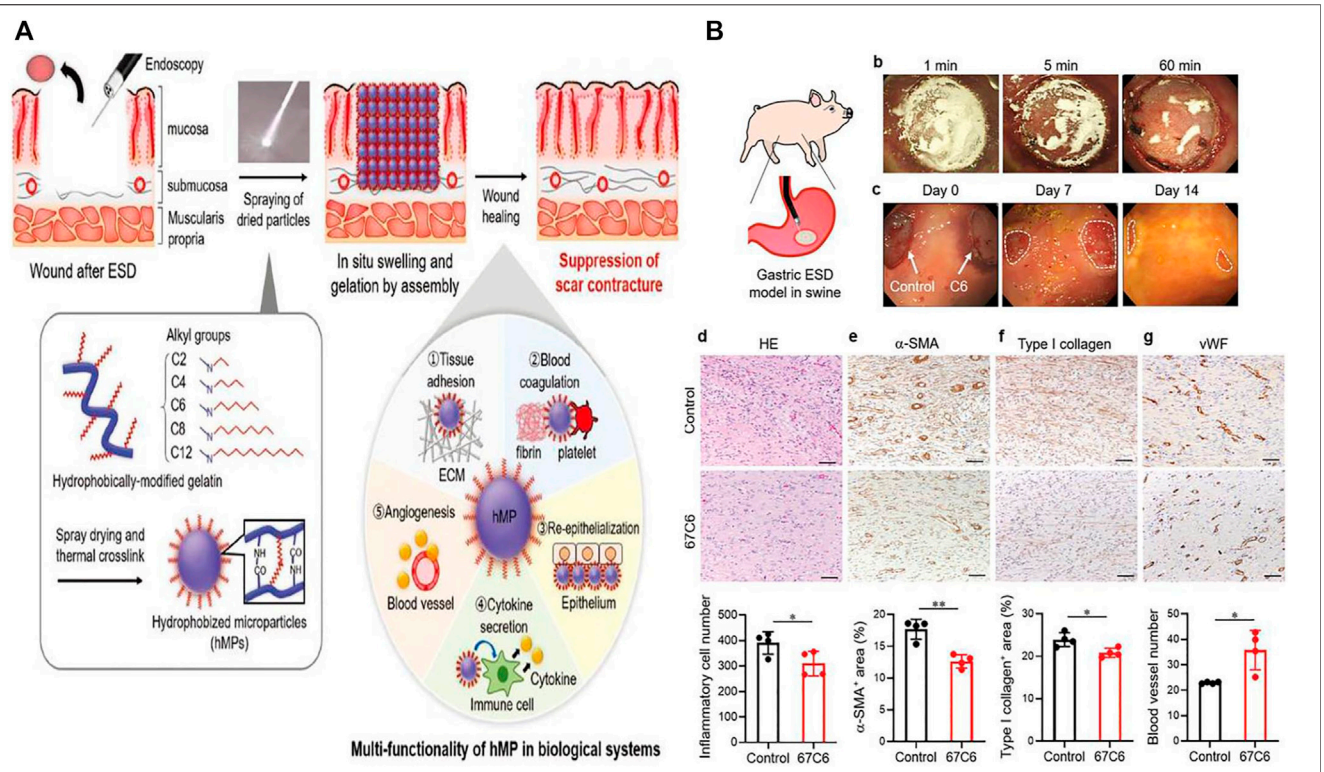

FIGURE 6 | The preparation and application of colloidal wound dressings to facilitate ulcer healing after ESD. **(A)** The schematic diagram of multifunctional hydrophobic colloidal dressings for wound repair. **(B)** Hydrophobic colloidal dressings effectively suppressed wound fibrosis after ESD in the swine stomach model. Reproduced from Nishiguchi et al. (2019). Copyright (2019), with permission from John Wiley and Sons.

functions similar to those of natural organisms, and they play an important role in tissue repair. Therefore, biomedical-derived materials can be regarded as potentially ideal materials to be employed to prevent esophageal stricture.

The Transplantation of Cell Sheets

Cell sheet transplantation is a tissue engineering technology in which isolated cells are cultured at special conditions *in vitro*, retaining cell junctions and extracellular matrix in maximum. Specifically, after cells have been inoculated densely, cell sheet layers are formed by stimulating secretion of extracellular matrix, typically five to eight layers, and the intact extracellular matrix promotes cell growth. Cell sheets can act as barriers for defects to avoid being affected by food and other substances flowing through the esophagus. In the meantime, cell sheets may secrete various cytokines and growth factors to promote the proliferation of epithelial cells and wound repair. What is more, most cell sheets are originating from autologous cells, so there is no severe inflammatory reaction when they are applied to the surface of the wound. Cells and the extracellular matrix within the sheet can form interconnections with tissues through multiple pathways or interactions, enhancing adhesive strength between the cell sheet and the esophageal wound. As far as previous studies are concerned, cell sheets contain oral mucosal epithelial cell (OMEC) sheets (Ohki and Yamamoto 2020), compound cell sheets composed of OMECs and small intestinal submucosa (SIS) (Wei et al., 2009), and autologous skin epidermal cell sheets (Kanai et al., 2012). Ohki et al. (2012) discovered the promising potential of autologous OMEC transplantation to prevent esophageal stricture after ESD the earliest (**Figure 7**). Firstly, they harvested OMECs originating from patients' oral cavity at normal condition in advance. Then, they treated cell sheets with temperature plunges to 20°C, and these cell sheets were transplanted to mucosal defects by endoscopy in patients immediately after ESD. After being transplanted to the defects, cell sheets adhered to the esophageal wounds, and they proliferated to form integral stratified epithelium. Wei et al. (2009) prepared the compound sheets composed of canine OMECs and porcine SIS, then they transplanted compound sheets on canine esophageal defects after ESD. After 1 month, the wounds treated by compound sheets completely repaired without inflammatory response. Additionally, the esophageal mucosal surface was as smooth as normal (Wei et al., 2009). Kanai et al. (2012) implanted cell sheets originating from porcine autologous skin epidermal cells into the post-ESD esophageal defect. As a comparison, another four pigs that underwent ESD without any treatments were given as control. After 2 weeks, the weight of pigs in the cell sheet group increased significantly compared to that in the control group, and there was no obvious esophageal stricture and inflammatory response (Kanai et al., 2012).

Above all, cell sheet technology seems indeed effective for preventing esophageal stricture after ESD by facilitating cell

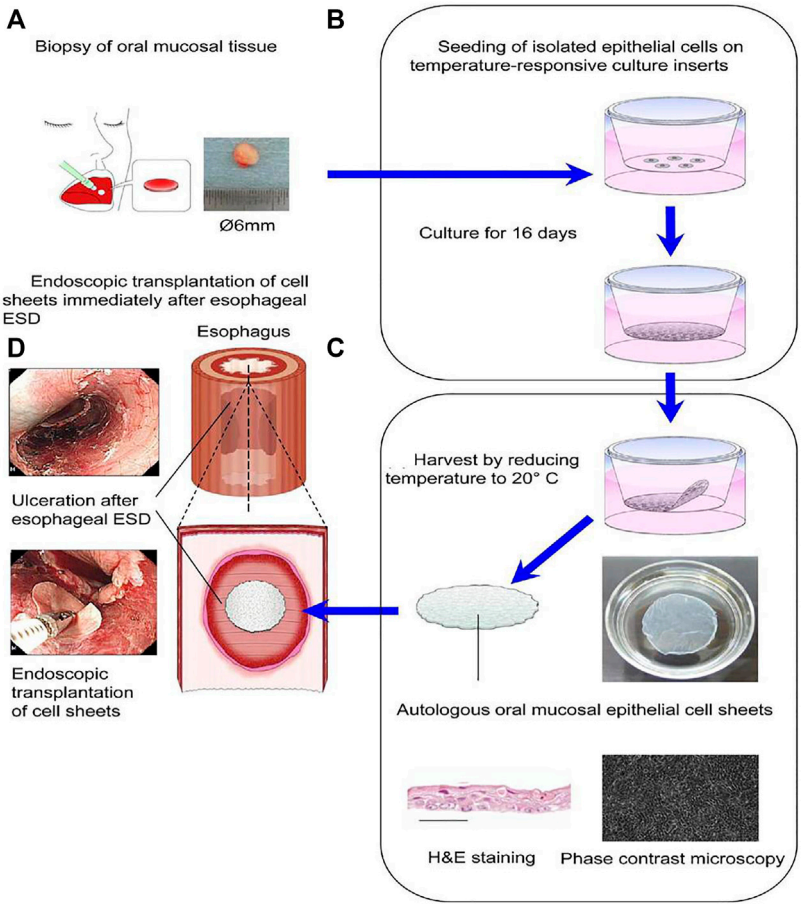

FIGURE 7 | The treatment of the esophageal defect after ESD by transplantation of cell sheets composed of autologous oral mucosal epithelial cells. **(A)** Oral mucosal epithelial cells (OMECs) were taken from the patients' oral cavity. **(B)** The OMECs were seeded on temperature-responsive culture inserts and cultured for 16 days. **(C)** Cell sheets composed of OMECs were harvested by reducing temperature to 20°C. **(D)** Cell sheets composed of OMECs were transplanted immediately on the esophageal defect under endoscopy after ESD. Reproduced from Ohki and Yamamoto (2020). Copyright (2020), with permission from Elsevier.

proliferation and promoting wound repair. Though reassuring advantages of cell sheets in preventing post-ESD esophageal stricture are shown, there are still some drawbacks and shortcomings. Firstly, the cell sheet technology has a high cost, and the preparation procedure *in vitro* is considerably complicated. Secondly, esophageal peristalsis and eating actions may cause cell sheets falling off, so how to anchor the transplanted cell sheets for a long time is a tough challenge. Thirdly, cell sheets must be prepared and preserved in a sterile condition; therefore, preserving cell sheets in a sterile environment for a long time is also a troublesome problem.

Endoscopic Injection of Cell Suspension

Owing to the relative simplicity, some scholars began to pay attention to cell suspension that can be injected endoscopically. During the process, autologous cells would be injected into defects (as illustrated in **Figure 8**), expecting to promote re-epithelialization and wound healing, so cell suspension can effectively prevent the occurrence of esophageal stricture in a way. The autologous cell suspension includes OMEC suspension, skin keratinocyte suspension, and adipose tissue-derived stromal cell (ADSC) suspension. Sakurai et al. (2007) injected autologous OMECs into the esophageal defects after ESD and achieved satisfying results. They made two postoperative defects in the esophagus of a pig. One was injected with autologous OMEC suspension into the submucosal layer immediately, and the other one was not treated. Two weeks later, there was no scarring stenosis in the injection group. The esophageal mucosa was smooth and the regenerating epithelium was completed. In the control group, there was scarring stenosis without the coverage of mucosal epithelium. Zuercher et al. (2013) reported that autologous skin keratinocyte suspension could prevent esophageal stricture effectively after EMR in sheep. Honda et al. (2011) used ADSCs to prevent esophageal stricture after EMR (**Figure 8**). They injected ADSC suspension into esophageal defects in five dogs under endoscopy after EMR (**Figure 8A, B**), and another five dogs were left untreated. After 2 months, serious esophageal stenosis occurred in the control group, while there was only a mild esophageal stricture in the injection group (Honda et al., 2011). The pathological findings of the esophagus showed that the mucosal layer of the esophagus was significantly

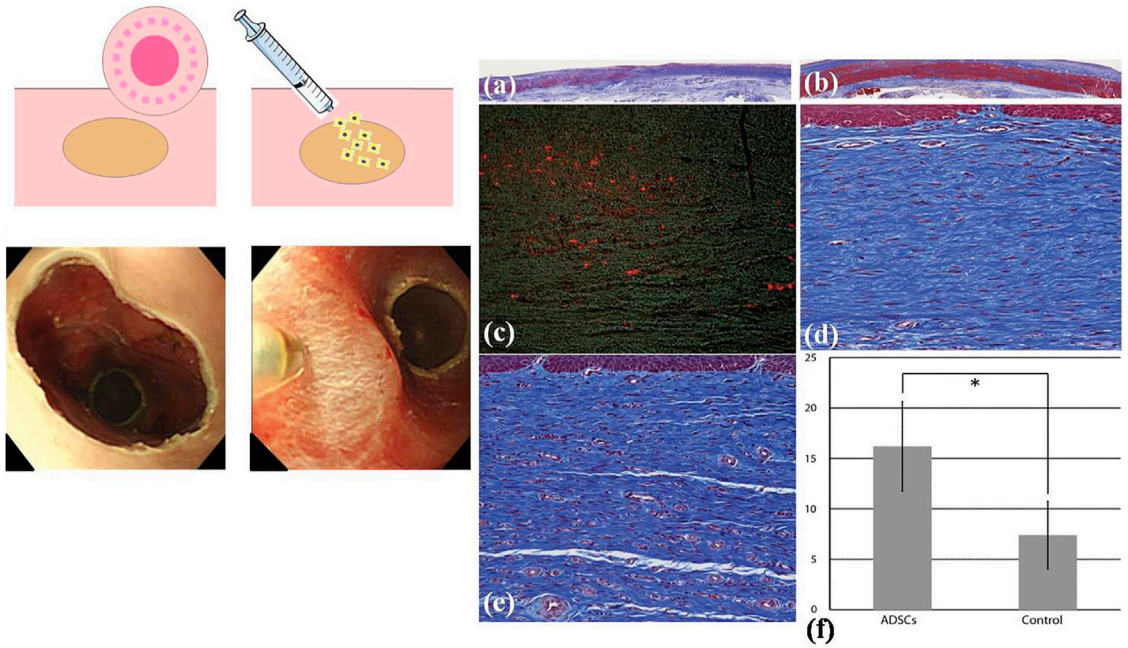

FIGURE 8 | Adipose tissue-derived stromal cellADSC) injection to prevent esophageal stricture. **(A)** The schematic diagram of cell injection. **(B)** The esophageal defect left after EMR and ADSCs were injected into the submucosa of the esophagus. **(C)** The pathological analysis of the esophagus. **[C (i)]** The esophageal mucosa tissue in the control group (Masson trichrome). **[C (ii)]** The esophageal mucosa tissue in the ADSC-treated group. **[C (iii)]** Stain-labelled ADSCs (red color) in the submucosa of the esophagus in the cell injection group. **[C (iv)]** Submucosal layer of the esophagus in the control group. **[C (v)]** Submucosal layer of the esophagus in the ADSC-treated group. **[C (vi)]** The comparison of the number of microvessels in esophageal submucosa between the control group and the ADSC-injected group. Reproduced from Honda et al. (2011). Copyright (2011), with permission from Elsevier.

damaged, and the submucosa was obviously fibrotic with few microvessels in the control group, while in the ADSC-injected group, the mucosa regenerated well, and there were more neovascularizations in the submucosa (**Figure 8C**). Above all, the effect of cell suspension injection has been partly displayed in some animal experiments. However, the mechanism of cell suspension injection has not been completely elucidated. There are two possible acting mechanisms: firstly, stratified epithelium may be formed owing to the proliferation of transplanted cells; secondly, transplanted cells may induce the secretion of cytokines and other nutrients needed by mucosal cells, promoting the migration of surrounding epithelial cells to the defect (Horch et al., 2005; Honda et al., 2011). Though cell suspension injection is simple and accessible without the need for lots of time and expenses, the limited isolated cells and low utilization need to be seriously considered. In addition, there is no research on the relationship between ADSCs and the remaining cancer cells, so it is still controversial whether injection of cell suspension into the wound will increase the risk of tumor recurrence, especially for the wounds with residual tumor cells.

Extracellular Matrix Stents

The extracellular matrix (ECM) is a kind of macromolecule synthesized by cells and secreted outside the cells, and they are distributed on the surface of cells or between the cells. ECM mainly consist of polysaccharides, proteins, and proteoglycans. They can form complex grid structures spontaneously to support and connect cells. Besides, ECM contains a large number of signaling molecules that are actively involved in the control of cell growth, polarity, shape, migration, and metabolic activities. Attributed to the structure and biological functions of the ECM, they can be made into an artificial biological scaffold. The excellent physical and chemical properties of ECM make ECM stents have no pro-inflammatory effect and adapt well to biological tissues. A large number of cellular active components contained in ECM stents also promote tissue repair. Nieponice et al. (2009) applied ECM stents to prevent esophageal stricture after EMR in dogs (**Figure 9**). The study group treated with ECM stents had no presentation of esophageal stricture, while esophageal stricture occurred in the control group without implantation of ECM stents, accompanied by regenerated epithelium failing to cover mucosal defects with partial inflammatory response. However, there are few clinical trials at present, so there is a long and stiff road for ECM stents before being widely applied in clinical practice.

Autologous Transplantation

With the aim of getting protection from physical barriers and promoting repair for esophageal wound, autologous esophageal mucosal transplantation has also been put forward, and it demonstrates a partial preventive effect in very limited clinical trials (Hochberger et al., 2014; Liao et al., 2018; Chai et al., 2019). In the process, researchers perform removal of normal esophageal mucosa and transplant it to the defect left by ESD. Hence,

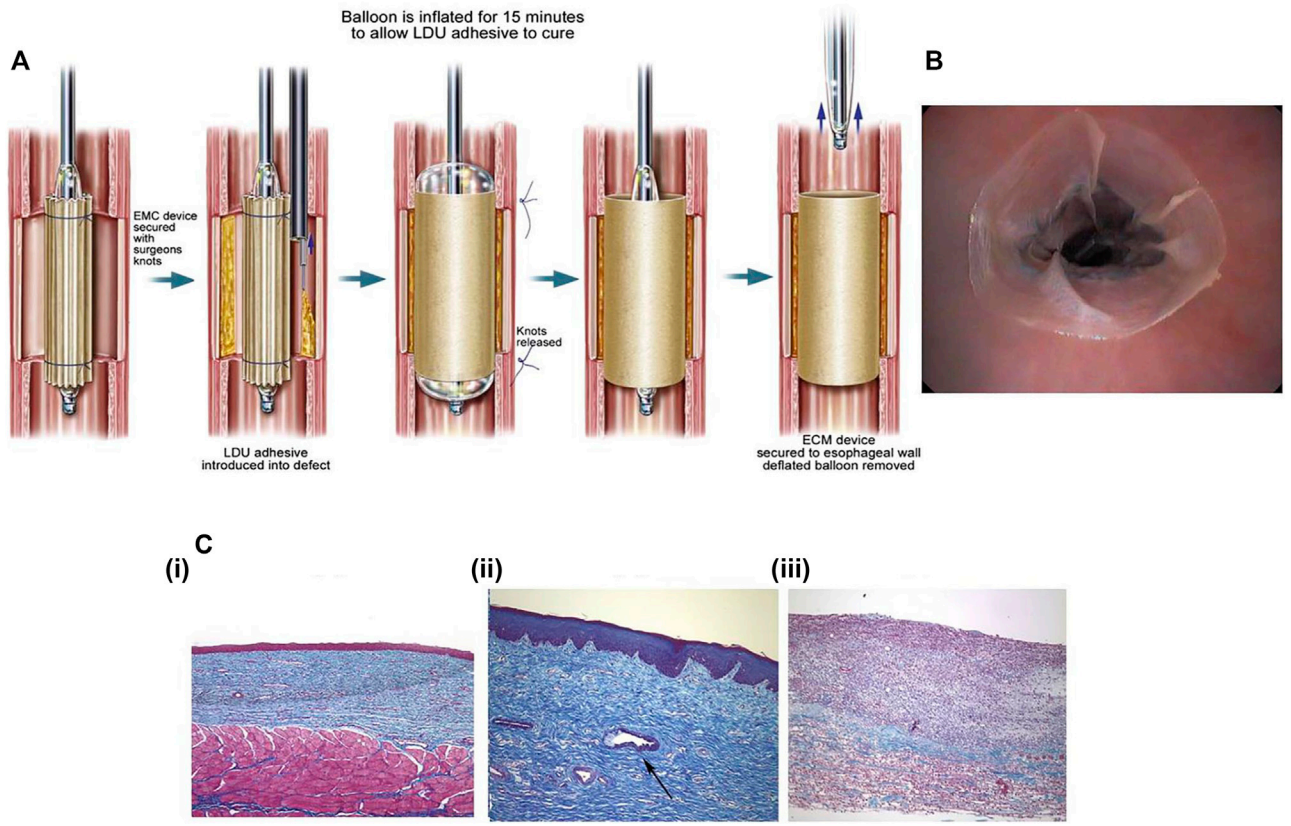

FIGURE 9 | The ECM stents that have been reported to prevent esophageal stricture. **(A)** The schematic diagram of deployment of ECM stent with the internal supporting of balloons. **(B)** Endoscopic image of the ECM stent applied to post-EMR esophageal defect. **(C)** The histological assessment of the esophagus after 2 months of the deployment of ECM stents. **[C (i)]** The esophageal mucosa treated by ECM stents has intact squamous epithelium. **[C (ii)]** The gland formation in the submucosa of the esophagus treated with ECM stents. **[C (iii)]** The significant fibrosis with extensive infiltration of inflammatory cells in the esophageal submucosa in the control group. Reproduced from Nieponice et al. (2009). Copyright (2009), with permission from Elsevier.

autologous esophageal mucosal transplantation is a tissue-shielding method, and it contains physical and biochemical factors of the native extracellular matrix. In certain aspects, autologous transplantation is similar to cell sheet. In summary, autologous esophageal mucosal patches can not only protect the esophageal wound as physical barriers but also promote angiogenesis and cell regeneration at the defect. Nevertheless, the corresponding clinical research sample of autologous transplantation needs to be expanded to study the feasibility, effectiveness, and safety further.

PROSPECT OF BIOMEDICAL POLYMERS AND POTENTIAL TECHNOLOGY

Overall, many methods involving various biomedical materials have been introduced to prevent esophageal stricture after ESD, in which some have been widely used in the clinics and some are still under basic research. However, each method has its own advantages and limitations (**Table 1**). In clinical practice, steroid precautions, particularly systemic application, is currently one of the most common approaches to prevent post-ESD esophageal stricture. Tissue engineering technology demonstrates the prospect of restorative treatment. Autologous transplantation avoids immune rejection response. Other novel strategies like PGA sheets, CMC sheets, peptide hydrogels, and colloidal dressings have opened up new paths in preventing esophageal stricture based on the exploration of polymers.

With the rapid development of biomedical polymers, several new approaches may be possible routes to prevent esophageal stricture. These polymers have ideal properties of biocompatibility and biodegradability to achieve their practicability. In addition, they can be combined with pharmacological prophylaxis and tissue engineering technology. Herein, we put forward two drug-loading (or other formulation) platforms: microneedles and hydrogel dressings. We study the practicality and feasibility of each system according to their inherent properties. Also, we analyze the application prospects after having discovered their strengths and weaknesses, respectively.

Microneedle Technology

Microneedles (MNs) have been utilized for medical treatment due to their ease of use over the past two decades. With their

TABLE 1 | The advantages and limitations of strategies having been reported to prevent esophageal stricture after ESD.

	Approaches	Advantages	Limitations
Mechanical methods	Endoscopic balloon dilation	Sustaining long clinical use with quick effect	Demanding multiple dilatations; spending much time; uncomfortable to patients; and having the risk of bleeding, bacteremia, perforation, and re-stricture
	Metal stent implantation	Safe and effective to prevent esophageal stenosis	Prone to be displaced and having complications of bleeding and perforation
	Biodegradable stent implantation	No long-term complications, no need for manual removal, and can avoid re-injury of the esophagus	Poor capability of self-expansion, weak mechanical strength, and the placing process is complicated
Pharmaceutical prevention	Systemic steroid	Strong anti-inflammation and fibrosis-inhibition effect, very convenient, and accessible for patients to take	May induce many systematic side effects and lacking efficacy to esophageal mucosal defects
	Local injection of steroid	Powerful for inhibiting inflammation and decreasing the systematic side effects	Susceptible to complications related to injection operation
	Other medicine injections	Having an inhibitory effect on inflammation and fibrosis	Optimal dosage and usage time need to be clarified
Approaches involving biomedical polymers	PGA sheets	Successful to cover the defect and promote the regeneration of mucosal tissue	Difficult to stay at the defect for a long time, some patients may be allergic to them, and the feasibility and usefulness remain to be discussed for defects accompanied by bleeding
	Peptide hydrogels	Supporting the formation of functional and continued epithelial cell sheet	The study is performed on an *in vitro* model and how to utilize the hydrogel/dressing *in vivo* is to be discussed
	CMC sheets	Biocompatible and biodegradable and exhibit some preventive effects in several studies	Larger sample size and longer observation period are needed
	Colloidal dressing	Accelerating blood coagulation in defect, enhancing epithelialization, interacting with immune cells, and promoting angiogenesis	Experiments are done on animals at most currently, so safety and effectiveness are to be studied further
Methods covering biomedical-derived materials	Cell sheets	Promoting esophageal mucosal repair and inhibiting the degree of mucosal fibrosis	Accessible to falling off and having the risk of infection, huge costs, and the preparation process is cumbersome
	Autologous cell suspension	Simple and accessible to perform without requiring lots of time and economical expenses	Limited number of isolated cells and low utilization efficiency and having the risk of tumor recurrence
	Extracellular matrix stents	Having little pro-inflammatory effect, adapting well to esophageal defects, and containing a large number of cellular active components to promote tissue repair	There are few clinical trials
Autologous transplantation	Autologous gastro-esophageal mucosal/esophageal mucosal/skin transplantation	Having no inflammatory response and the grafting process is accessible	Lack of clinical samples

advantages of possessing capacities of injection and transdermal drug delivery, MNs have been proven to increase transdermal drug delivery efficiency significantly by penetrating though intrinsic tissue barriers in a minimally invasive manner, and they attract more and more attention from the medical field in recent years (Alexander et al., 2012). With the optimization of MN technology, non-transdermal MNs have demonstrated some effect in the management of diseases of the eyes, blood vessels, oral cavity, and mucosal tissues in animals (Lee et al., 2020). Lee et al. (2014) prepared a MN cuff (MNC) device to deliver anti-proliferation pharmaceuticals to vascular media and adventitia to prevent neointimal hyperplasia after grafting surgery. The MNCs were designed to wrap the exterior of the blood vessels, and the internal surface of MNCs contained an array of MNs, which is coated with drug formulation on tips. MNCs were installed on the blood vessels by embedding MNs, which were displayed onto the inner surface of MNC, into the walls of the blood vessels. Subsequently, the pharmaceuticals incorporated into the tips of MNs would be slowly and continuously released into the blood vessels, which guaranteed the sustained release and long-term effect of drugs. As a classical drug delivery system, MNs can load not only pharmaceuticals but also cells. Tang et al. (2018a) engineered a polymeric MN system integrated with cardiac stem/stromal cells (CSCs) for the treatment of myocardial infarction (MI). The MN-CSC system possesses certain superiorities compared with conventional patches. For instance, the MNs would serve as channels to allow for communications between CSCs in the patch and the host myocardium in heart tissues. The heart could provide CSCs in transplanted patch with nutrients. Meanwhile, CSCs in MN patch could release paracrine factors to repair myocardial tissues. Their study demonstrated that the MN-CSC patch brought bright prospect to facilitate effective treatment of MI by promoting angio-myogenesis and myocardial regeneration. After the treatment by MN-CSC, the myocardial functions gradually recovered. On the basis of the great application potential of

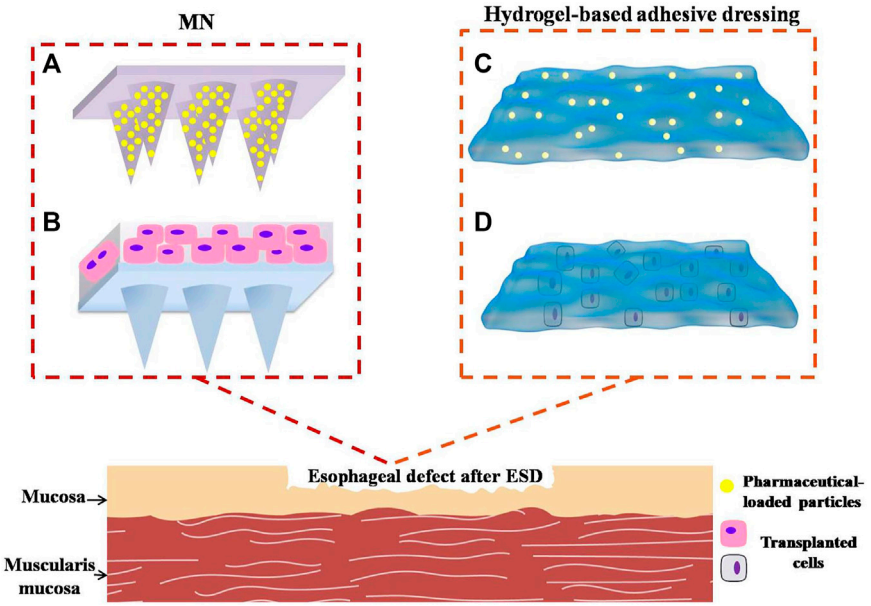

FIGURE 10 | Novel potential strategies involve polymeric materials to prevent post-ESD esophageal stricture. **(A)** Microneedles loading anti-inflammatory or anti-fibrosis drugs into the needle body. **(B)** Microneedles incorporating active functional cells. **(C)** Hydrogel-based adhesive dressing loading pharmaceuticals. **(D)** Hydrogel adhesives incorporating transplanted cells.

non-transdermal MNs, the strategy of engineering polymeric MNs loading pharmaceuticals or other cytokines to prevent esophageal stricture can be put forward. The MNs can be attached to the surface of esophageal wound after ESD through mechanical interlocking (**Figure 10A**). Compared with ordinary needles, MNs have relatively soft insertions into the defects without sharp stimulations, which avoid serious complications such as perforation, bleeding, and other symptoms of the esophagus. This kind of MN-array system has two major functions, releasing drugs or cytokines to exert the appropriate pharmacological actions and forming a physical barrier like sheets to avoid irritation from food and other fluids passing through the esophagus.

In terms of drug release modalities, MNs can be divided into three types: burst release, prolonged release, and responsive release. According to the properties of anti-inflammatory drugs and duration of local inflammation reaction in esophageal wounds, the prolonged release and responsive release are preferred. Prolonged release means sustained delivery of pharmaceuticals, and this delivery mode helps to maintain a steady range of drug concentrations in the surrounding tissues for a considerable period. Generally, therapeutic agents can be incorporated into degradable microspheres or nanoparticles to realize the sustained release. For instance, Yang et al. (2019) made hydrogel-based MNs including the mesenchymal stem cell-derived exosomes and UK5099-loaded PLGA nanoparticles. The hydrogel-based MNs achieved a sustained release of UK5099 and exosomes for the duration of more than 10 days in a mouse model (Yang et al., 2019). The drug-loaded nanoparticles were evenly distributed within the bodies of MNs instead of just being localized on the surface of MNs. This engineering method could contribute to the slow release of the drug because of the gradual degradation of the polymeric matrices of MNs. Apart from this, the MN system can respond to the changes in the surrounding environment (including physical, chemical, and biological changes) to release the agents. By controlling the switch and intensity of the external stimulus, it is possible to control the release of pharmaceuticals in a timed, quantitative, and localized manner. Responsive delivery platforms are divided into closed-loop and open-loop systems (Jamaledin et al., 2020). Closed-loop control systems switch on and switch off drug release in a self-regulated manner to automatically achieve a circulating state, without any external intervention. For instance, glucose-responsive "closed-loop" insulin delivery systems mimicking the function of pancreatic cells possess a great potential to improve the health status and life qualities of people with diabetes (Ravaine et al., 2008; Bratlie et al., 2012). In their study, a glucose-monitoring module was combined with a sensor-triggered insulin-releasing module. A glucose-responsive insulin delivery strategy using a MN-array patch containing glucose-responsive vesicles (GRV) loaded with insulin and glucose oxidase enzyme was designed by some researchers. The components of GRVs contained a hydrophobic section, which transformed into hydrophilic composition under enzymatic hypoxic conditions. After that, GRVs dissociated and subsequently released the loaded insulin to lower blood glucose levels. If blood glucose was normal, significant enzymatic hypoxic conditions could not occur and hypoxia-sensitive GRVs would not dissociate to release insulin. In this way, precise regulation of blood glucose was guaranteed by GRV-loaded MN-array patch (Yu et al., 2015). Open-loop

systems are known as an externally regulated-dependent platform (Kost and Langer 2001). They utilize external stimuli such as light, heat, magnetism, electricity, or mechanical stress to control loading release. Unlike closed-loop-responsive systems, stimuli are artificially added in the open-loop-responsive systems, and the stimuli will last for some time (such as light, magnetism, and heat). Closed-loop-responsive system allows for precise and rapid regulation of loading release, therefore, closed-loop-responsive MNs are frequently devised and studied.

When the MN patch is inserted on the surface of post-ESD defect under endoscope, pharmaceutical-loaded nanoparticles can be released into defect. The sustained release of pharmaceuticals will suppress inflammation or fibrosis. Polymeric MNs can degrade *in vivo* over time, eliminating the need for secondary endoscopic manipulation. Pharmaceuticals can also be released responsively to the inflammatory environment, which requires that the drug-loaded device should contain specific groups that are sensitive to inflammation-related enzymes or inflammatory factors. In the post-ESD esophageal environment, when the inflammation reaction is serious and local inflammatory mediators are numerous, the MN delivery system can sense the significant inflammation and release anti-inflammatory pharmaceuticals immediately to suppress the inflammation. When the inflammatory reaction becomes mild, MNs would correspondingly decrease the loading release. In such contexts, maximum efficacy and minimization of side effects can be realized. When inflammation is safely and effectively suppressed, the esophageal stricture would be further prevented.

What is more, esophageal mucosal epithelial cells, OMECs, ADSCs, autologous skin epidermal cells, and skin keratinocyte can be incorporated into the MN patch. These cells would proliferate and secrete some growth factors or other nutrients into defects to nourish mucosal cells and facilitate wound healing (**Figure 10B**).

Above all, with advances and optimizations of preparation processing, flexible, biocompatible, and degradable MN-array devices integrating sustained release or responsive release of drugs have a strong potential to prevent esophageal stricture. However, there is no report of MNs being used directly in the esophagus until now, which may be attributed to the special structure and functions of the esophagus. Apart from this, MN device is attached to the defect surface by mechanical cross-linking, so food passing through the esophagus may also affect the fixation of the MN system. Most importantly, a large number of studies are necessary to confirm the safety and biocompatibility of MNs in human bodies. Therefore, the selection of polymers to prepare a MN delivery system and the development of engineering technology demand comprehensive and in-depth explorations.

Hydrogel-Based Wound Dressing

Hydrogels are soft materials possessing three-dimensional cross-linked network structures with flexible physical and chemical properties, which are similar to the natural ECM. In the recent decade, hydrogels have attracted worldwide attention, especially in drug delivery and tissue engineering. They have versatile characteristics: porous structures enable hydrogels to provide sufficient gas or nutrient exchange between the wound and the surrounding environment; a capacity to hold large amounts of water or biomedical fluids makes the hydrogel relatively comfortable for patients; good biocompatibility ensures safety; nice elasticity enables the hydrogel to be prepared with various shapes and sizes to conform to different wounds; and network structures render hydrogels able to reserve therapeutic nanoparticles and other biomedical reagents within them (Huang et al., 2017; Koehler et al., 2018; Li et al., 2020). In addition, the degradability of hydrogels reduces the pain of patients and avoids secondary tissue damages (Stern and Cui 2019). In recent years, hydrogel-based dressings have been developed to meet the requirements of wound healing because of the strong adhesion besides the advantages of hydrogels mentioned above. In some wounds accompanied with a high level of inflammatory exudate, hydrogel-based dressings can absorb exudates to facilitate the debridement process. In general, hydrogels composed of biocompatible and biodegradable biomedical materials can be optimized into ideal wound dressings. A variety of widespread biomedical polymers have been employed to engineer hydrogel-based dressings, such as chitosan, hyaluronic acid (HA), gelatin, polyethylene glycol, alginate, and several other less-common polymers (Chen et al., 2018; Dimatteo et al., 2018; Koehler et al., 2018; Qu et al., 2018).

Enlightened by the adhesion phenomena of natural organisms, researchers have developed hydrogels with different adhesion mechanisms for wound dressings. For instance, marine mussels can form strong adhesions to wet surfaces through mussel foot protein (mfp) secreted by foot filaments. The main component of mfp is L-DOPA (3,4-dihydroxyphenylalanine), which is rich in catechol structures (Ahn et al., 2015). By means of imitating specific features of marine mussels, the mfp-like adhesion component can be introduced into hydrogels *via* grafting catechol groups into the polymer chains. These catechol groups would bring many physical and chemical interaction forces to make hydrogel dressings adhere strongly to tissue surfaces, including van der Waals forces, metal chelation, hydrogen bonds, π-π stacking, Schiff base reaction, and Michael addition reaction (Burzio and Waite 2000; Li et al., 2010; Wang et al., 2017; Zhou et al., 2020). Lee et al. (2010) fabricated injectable and thermo-sensitive hydrogels based on HA and Pluronic through using rapid and robust catechol-thiol reactions. In study, HA conjugated with dopamine was mixed with thiol-bonded Pluronic F127 copolymer to produce a cross-linked composite gel based on typical Michael addition reaction. The HA/Pluronic hydrogels could be injected in a sol state at room temperature, but immediately turn into a robust gel at body temperature. The composite gel exhibited excellent tissue-adhesion capacities with superior stability *in vivo*. Moreover, the catechol-based adhesives have been proven to possess good dehydration effect, and they can form strong adhesion on wet tissues (Wei et al., 2016).

Besides using polymers containing the catechol group, other chemical groups are equally capable to build covalent bondings between hydrogels and the amine groups on tissue surfaces. Qu et al. (2018) synthesized an injectable hydrogel adhesive

composed of quaternized chitosan and benzaldehyde-terminated Pluronic® F127 (PF127-CHO) under physiological conditions, in which a Schiff base was constructed between the aldehyde group in PF127-CHO and the amine group on the tissue surface, so the hydrogel adhesive could adhere to the skin tissues. Bu et al. (2019) prepared a clearly defined tetra-armed poly-(ethylene glycol) (Tetra-PEG) hydrogel sealant *via* ammonolysis. The sealant owned competencies of fast gelating speed, strong tissue adhesion, and high mechanical strength. The active ester of succinimidyl succinate on the polymer chain reacted with the amino group on tissues and made the hydrogel attach to the skin. Some other adhesion mechanisms such as topological adhesion and electrostatic interaction also have a good adhesion effect, though the preparation process should be further improved to avoid toxicity (Cho et al., 2019; Krishnadoss et al., 2019). Khalil et al. (2020) prepared an antibacterial adhesive hydrogel loaded with micelles containing ciprofloxacin (CPX) for the treatment of corneal injuries with risk of infection. The results showed that the loading of CPX did not affect the stiffness, biocompatibility, and adhesive strength of hydrogels, suggesting a potential solution to seal corneal wounds without being infected. You et al. (2021) designed poly (2-ethyl-2-oxazoline-co-2-butenyl-2-oxazoline) (POx) hydrogels encapsulating mesenchymal stromal cells (MSCs). The thiol-ene crosslinked hydrogels exhibited great tissue adhesive strength. In a rat model of myocardial infarction, the epicardial placement of MSC-loaded POx hydrogels promoted the recovery of cardiac structure and functions with decreased interstitial fibrosis and increased formation of neovasculars. All these studies demonstrated that hydrogel adhesives engineered by a variety of natural or synthetic polymers can be utilized for effective delivery of drugs and cells.

As for wet esophageal defect after ESD, the hydrogel adhesives are expected to play dramatic roles in the prevention of esophageal stricture. Firstly, hydrogel adhesive can be adhered to the esophageal wound firmly and tightly owing to the powerful adhesions originating from different mechanisms. Secondly, they possess ideal physical and chemical properties to support defects and promote wound healing. Thirdly, steroids or anti-fibrotic drugs can be loaded into the hydrogel adhesive in the form of drug carriers (**Figure 10C**) to achieve sustained release of pharmaceuticals, such as micelles, vesicles, or other nanoparticles. OMECs, ADSCs, or other skin keratinocytes can also be incorporated into hydrogel adhesives to facilitate mucosal repairing and epithelialization (**Figure 10D**). Above all, the hydrogel adhesive has a great potential to be applied to manage post-ESD defect, despite the compatibility and biodegradability needing further improvement. In prospect, we expect to observe the safety and efficacy of hydrogel adhesives for the prevention of esophageal strictures in more animal studies and preclinical trials.

SUMMARY AND CONCLUSION

Esophageal stricture is a common and serious post-ESD complication, but until now, there is no standard consensus to effectively manage it. In clinical practice, preventing this complication in advance improves the patients' prognosis and life qualities compared to intervening after it has developed. However, these methods often bring inevitable and serious complications such as bleeding, esophageal perforation, tissue adhesion, and other related symptoms. In this review, we have summarized the preventive strategies of esophageal stricture involving biomedical materials that have been reported in recent decades. Firstly, we have described the mechanism of the formation of esophageal stricture; secondly, we introduced novel preventive methods covering biomedical materials; thirdly, we put forward some prospective strategies related to biomedical polymers. Generally, the basic requirements for biomedical materials include good biocompatibility, biodegradability, safety, and stable chemical properties. In addition to these features mentioned above, some biomedical polymers and biomedical-derived materials possess network structures similar to those of natural ECM, providing scaffolds that facilitate cell adhesion, proliferation, and differentiation. Besides, they have good mechanical properties, matching the structural mechanics of the natural tissues. Additionally, some biomedical materials have superior surface physico-chemical properties to form specific adhesion on tissue surfaces, and they can load functional biological agents. The approaches employing these biomedical materials demonstrate some preventive effect and safety in post-ESD esophageal stricture. In particular, PGA sheets and CMC sheets have been studied in a very small number of clinical patients. Therefore, the safety and feasibility of biomedical polymers need to be explored further. Other prospective technologies engineered by various natural or synthetic polymers, like chitosan, hyaluronic acid, and so on, also require systematic and comprehensive observational studies *in vitro* and *in vivo* before being performed into clinical trials. Above all, biomedical materials provide important and far-reaching inspiration for the prevention of esophageal strictures after ESD, especially biomedical polymers and biomedical-derived materials. Nevertheless, there are some non-negligible bottlenecks for their clinical applications, such as specific immunogenicity, sensitization to patients, slightly poor histocompatibility, and incomplete degradability. All these issues are anticipated to be resolved basically in the near future. We believe that biomedical materials are promising to play a pivotal role to prevent esophageal stricture after ESD safely and effectively.

AUTHOR CONTRIBUTIONS

YB, ZL, and YL mainly conceived and listed the outline of the review. YB mainly wrote the review. TC, YC, and MX contributed to review modification and editing. All authors contributed to the article and approved the submitted version.

FUNDING

This work was supported by the National Natural Science Foundation of China (82072684) and the Shanghai Committee of Science and Technology (18140900100).

REFERENCES

Ahn, B. K., Das, S., Linstadt, R., Kaufman, Y., Martinez-Rodriguez, N. R., Mirshafian, R., et al. (2015). High-Performance Mussel-Inspired Adhesives of Reduced Complexity. *Nat. Commun.* 6, 8663. doi:10.1038/ncomms9663

Alexander, A., Dwivedi, S., AjazuddinGiri, T. K., Saraf, S., Saraf, S., et al. (2012). Approaches for Breaking the Barriers of Drug Permeation Through Transdermal Drug Delivery. *J. Controlled Release.* 164, 26–40. doi:10.1016/j.jconrel.2012.09.017

Alvarez Herrero, L., Pouw, R., van Vilsteren, F., ten Kate, F., Visser, M., Seldenrijk, C., et al. (2011). Safety and Efficacy of Multiband Mucosectomy in 1060 Resections in Barrett's Esophagus. *Endoscopy.* 43, 177–183. doi:10.1055/s-0030-1256095

Bakken, J. C., Wong Kee SongSong, L. M. L. M., de Groen, P. C., and Baron, T. H. (2010). Use of a Fully Covered Self-Expandable Metal Stent for the Treatment of Benign Esophageal Diseases. *Gastrointest. Endosc.* 72, 712–720. doi:10.1016/j.gie.2010.06.028

Bakota, E. L., Wang, Y., Danesh, F. R., and Hartgerink, J. D. (2011). Injectable Multidomain Peptide Nanofiber Hydrogel as a Delivery Agent for Stem Cell Secretome. *Biomacromolecules.* 12, 1651–1657. doi:10.1021/bm200035r

Bowerman, C. J., Liyanage, W., Federation, A. J., and Nilsson, B. L. (2011). Tuning β-Sheet Peptide Self-Assembly and Hydrogelation Behavior by Modification of Sequence Hydrophobicity and Aromaticity. *Biomacromolecules.* 12, 2735–2745. doi:10.1021/bm200510k

Bratlie, K. M., York, R. L., Invernale, M. A., Langer, R., and Anderson, D. G. (2012). Materials for Diabetes Therapeutics. *Adv. Healthc. Mater.* 1, 267–284. doi:10.1002/adhm.201200037

Bristow, R. E., and Montz, F. J. (2005). Prevention of Adhesion Formation After Radical Oophorectomy Using a Sodium Hyaluronate-Carboxymethylcellulose (HA-CMC) Barrier. *Gynecol. Oncol.* 99, 301–308. doi:10.1016/j.ygyno.2005.06.057

Broughton, G., 2nd, Janis, J. E., and Attinger, C. E. (2006). The Basic Science of Wound Healing. *Plast. Reconstr. Surg.* 117, 12S–34S. doi:10.1097/01.prs.0000225430.42531.c2

Bu, Y., Zhang, L., Sun, G., Sun, F., Liu, J., Yang, F., et al. (2019). Tetra-PEG Based Hydrogel Sealants for *In Vivo* Visceral Hemostasis. *Adv. Mater.* 31, e1901580. doi:10.1002/adma.201901580

Budak, K., Sogut, O., and Sezer, U. A. (2020). A Review on Synthesis and Biomedical Applications of Polyglycolic Acid. *J. Polym. Res.* 27, 208. doi:10.1007/s10965-020-02187-1

Burzio, L. A., and Waite, J. H. (2000). Cross-Linking in Adhesive Quinoproteins: Studies With Model Decapeptides. *Biochemistry.* 39, 11147–11153. doi:10.1021/bi0002434

Chai, N.-L., Feng, J., Li, L.-S., Liu, S.-Z., Du, C., Zhang, Q., et al. (2018). Effect of Polyglycolic Acid Sheet Plus Esophageal Stent Placement in Preventing Esophageal Stricture After Endoscopic Submucosal Dissection in Patients With Early-Stage Esophageal Cancer: A Randomized, Controlled Trial. *World J. Gastroenterol.* 24, 1046–1055. doi:10.3748/wjg.v24.i9.1046

Chai, N., Zou, J., Linghu, E., Chai, M., Li, L., Wang, X., et al. (2019). Autologous Skin-Grafting Surgery to Prevent Esophageal Stenosis After Complete Circular Endoscopic Submucosal Tunnel Dissection for Superficial Esophageal Neoplasms. *Am. J. Gastroenterol.* 114, 822–825. doi:10.14309/ajg.0000000000000169

Chen, T., Chen, Y., Rehman, H. U., Chen, Z., Yang, Z., Wang, M., et al. (2018). Ultratough, Self-Healing, and Tissue-Adhesive Hydrogel for Wound Dressing. *ACS Appl. Mater. Inter.* 10, 33523–33531. doi:10.1021/acsami.8b10064

Cho, H., Wu, G., Christopher Jolly, J., Fortoul, N., He, Z., Gao, Y., et al. (2019). Intrinsically Reversible Superglues via Shape Adaptation Inspired by Snail Epiphragm. *Proc. Natl. Acad. Sci. USA.* 116, 13774–13779. doi:10.1073/pnas.1818534116

Chu, Y., Chen, T., Li, H., Zhou, P., Zhang, Y., Chen, W., et al. (2019). Long-Term Efficacy and Safety of Intralesional Steroid Injection Plus Oral Steroid Administration in Preventing Stricture After Endoscopic Submucosal Dissection for Esophageal Epithelial Neoplasms. *Surg. Endosc.* 33, 1244–1251. doi:10.1007/s00464-018-6404-9

de Groot, N. S., Parella, T., Aviles, F. X., Vendrell, J., and Ventura, S. (2007). Ile-phe Dipeptide Self-Assembly: Clues to Amyloid Formation. *Biophysical J.* 92, 1732–1741. doi:10.1529/biophysj.106.096677

Dimatteo, R., Darling, N. J., and Segura, T. (2018). *In Situ* forming Injectable Hydrogels for Drug Delivery and Wound Repair. *Adv. Drug Deliv. Rev.* 127, 167–184. doi:10.1016/j.addr.2018.03.007

Dowling, M. B., Kumar, R., Keibler, M. A., Hess, J. R., Bochicchio, G. V., and Raghavan, S. R. (2011). A Self-Assembling Hydrophobically Modified Chitosan Capable of Reversible Hemostatic Action. *Biomaterials.* 32, 3351–3357. doi:10.1016/j.biomaterials.2010.12.033

Ezoe, Y., Muto, M., Horimatsu, T., Morita, S., Miyamoto, S. i., Mochizuki, S., et al. (2011). Efficacy of Preventive Endoscopic Balloon Dilation for Esophageal Stricture After Endoscopic Resection. *J. Clin. Gastroenterol.* 45, 222–227. doi:10.1097/mcg.0b013e3181f39f4e

Fujishiro, M., Kodashima, S., Goto, O., Ono, S., Niimi, K., Yamamichi, N., et al. (2009). Endoscopic Submucosal Dissection for Esophageal Squamous Cell Neoplasms. *Dig. Endosc. : official J. Jpn. Gastroenterological Endosc. Soc.* 21, 109–115. doi:10.1111/j.1443-1661.2009.00837.x

Gago, L., Saed, G. M., and Chauhan, S. (2003). Seprafilm (Modified Hyaluronic Acid and Carboxymethylcellulose) Acts as a Physical Barrier. *Fertil. sterility.* 80, 612–616. doi:10.1016/s0015-0282(03)00767-2

Gong, C., Sun, S., Zhang, Y., Sun, L., Su, Z., Wu, A., et al. (2019). Hierarchical Nanomaterials via Biomolecular Self-Assembly and Bioinspiration for Energy and Environmental Applications. *Nanoscale.* 11, 4147–4182. doi:10.1039/c9nr00218a

Hochberger, J., Koehler, P., Wedi, E., Gluer, S., Rothstein, R. I., Niemann, H., et al. (2014). Transplantation of Mucosa from Stomach to Esophagus to Prevent Stricture After Circumferential Endoscopic Submucosal Dissection of Early Squamous Cell. *Gastroenterology.* 146, 906–909. doi:10.1053/j.gastro.2014.01.063

Honda, M., Hori, Y., Nakada, A., Uji, M., Nishizawa, Y., Yamamoto, K., et al. (2011). Use of Adipose Tissue-Derived Stromal Cells for Prevention of Esophageal Stricture After Circumferential EMR in a Canine Model. *Gastrointest. Endosc.* 73, 777–784. doi:10.1016/j.gie.2010.11.008

Honda, M., Nakamura, T., Hori, Y., Shionoya, Y., Nakada, A., Sato, T., et al. (2010). Process of Healing of Mucosal Defects in the Esophagus After Endoscopic Mucosal Resection: Histological Evaluation in a Dog Model. *Endoscopy.* 42, 1092–1095. doi:10.1055/s-0030-1255741

Horch, R. E., Kopp, J., Kneser, U., Beier, J., and Bach, A. D. (2005). Tissue Engineering of Cultured Skin Substitutes. *J. Cell. Mol. Med.* 9, 592–608. doi:10.1111/j.1582-4934.2005.tb00491.x

Huang, H., Deng, M., Jin, H., Dirsch, O., and Dahmen, U. (2013). Preventing Intra-abdominal Adhesions With a Sodium Hyaluronate Carboxymethylcellulose Membrane Enabled Visualization of Hepatic Microcirculation. *Int. J. Surg.* 11, 935–943. doi:10.1016/j.ijsu.2013.06.842

Huang, Q., Zou, Y., Arno, M. C., Chen, S., Wang, T., Gao, J., et al. (2017). Hydrogel Scaffolds for Differentiation of Adipose-Derived Stem Cells. *Chem. Soc. Rev.* 46, 6255–6275. doi:10.1039/c6cs00052e

Inokuchi, S., Rokutanda, S., Yanamoto, S., Naruse, T., Sakamoto, Y., and Umeda, M. (2017). Experimental Study and Clinical Application of Polyglycolic Acid Sheet with Fibrin Glue for Oral Soft Tissue Surgery. *J. Oral Maxillofacial Surg. Med. Pathol.* 29, 295–300. doi:10.1016/j.ajoms.2017.02.006

Jamaledin, R., Makvandi, P., and Yiu, C. K. Y. (2020). Engineered Microneedle Patches for Controlled Release of Active Compounds: Recent Advances in Release Profile Tuning. *Adv. Ther-germany.* 3, 2000171. doi:10.1002/adtp.202000171

Jonker, A. M., Löwik, D. W. P. M., and van Hest, J. C. M. (2012). Peptide- and Protein-Based Hydrogels. *Chem. Mater.* 24, 759–773. doi:10.1021/cm202640w

Kanai, N., Yamato, M., Ohki, T., Yamamoto, M., and Okano, T. (2012). Fabricated Autologous Epidermal Cell Sheets for the Prevention of Esophageal Stricture after Circumferential ESD in a Porcine Model. *Gastrointest. Endosc.* 76, 873–881. doi:10.1016/j.gie.2012.06.017

Khalil, I. A., Saleh, B., Ibrahim, D. M., Jumelle, C., Yung, A., Dana, R., et al. (2020). Ciprofloxacin-Loaded Bioadhesive Hydrogels for Ocular Applications. *Biomater. Sci.* 8, 5196–5209. doi:10.1039/d0bm00935k

Koehler, J., Brandl, F. P., and Goepferich, A. M. (2018). Hydrogel Wound Dressings for Bioactive Treatment of Acute and Chronic Wounds. *Eur. Polym. J.* 100, 1–11. doi:10.1016/j.eurpolymj.2017.12.046

Kost, J., and Langer, R. (2001). Responsive Polymeric Delivery Systems. *Adv. Drug Deliv. Rev.* 46, 125–148. doi:10.1016/s0169-409x(00)00136-8

Koutsopoulos, S. (2016). Self-assembling Peptide Nanofiber Hydrogels in Tissue Engineering and Regenerative Medicine: Progress, Design Guidelines, and Applications. *J. Biomed. Mater. Res.* 104, 1002–1016. doi:10.1002/jbm.a.35638

Krishnadoss, V., Melillo, A., Kanjilal, B., Hannah, T., Ellis, E., Kapetanakis, A., et al. (2019). Bioionic Liquid Conjugation as Universal Approach to Engineer Hemostatic Bioadhesives. *ACS Appl. Mater. Inter.* 11, 38373–38384. doi:10.1021/acsami.9b08757

Kumar, D., Workman, V. L., and O'Brien, M. (2017). Peptide Hydrogels-A Tissue Engineering Strategy for the Prevention of Oesophageal Strictures. *Adv. Funct. Mater.* 27, 1702424. doi:10.1002/adfm.201702424

Lee, K., Goudie, M. J., Tebon, P., Sun, W., Luo, Z., Lee, J., et al. (2020). Non-Transdermal Microneedles for Advanced Drug Delivery. *Adv. Drug Deliv. Rev.* 165-166, 41–59. doi:10.1016/j.addr.2019.11.010

Lee, K. J., Park, S. H., Lee, J. Y., Joo, H. C., Jang, E. H., Youn, Y.-N., et al. (2014). Perivascular Biodegradable Microneedle Cuff for Reduction of Neointima Formation After Vascular Injury. *J. Controlled Release.* 192, 174–181. doi:10.1016/j.jconrel.2014.07.007

Lee, W. J., Jung, H.-Y., Kim, D. H., Lee, J. H., Choi, K. D., Song, H. J., et al. (2013). Intralesional Steroid Injection to Prevent Stricture After Near-Circumferential Endosopic Submucosal Dissection for Superficial Esophageal Cancer. *Clin. Endosc.* 46, 643–646. doi:10.5946/ce.2013.46.6.643

Lee, Y., Chung, H. J., Yeo, S., Ahn, C.-H., Lee, H., Messersmith, P. B., et al. (2010). Thermo-sensitive, Injectable, and Tissue Adhesive Sol-Gel Transition Hyaluronic Acid/Pluronic Composite Hydrogels Prepared From Bio-Inspired Catechol-Thiol Reaction. *Soft Matter.* 6, 977–983. doi:10.1039/b919944f

Lew, R. J., and Kochman, M. L. (2002). A Review of Endoscopic Methods of Esophageal Dilation. *J. Clin. Gastroenterol.* 35, 117–126. doi:10.1097/00004836-200208000-00001

Li, J., Yu, F., Chen, G., Liu, J., Li, X.-L., Cheng, B., et al. (2020). Moist-Retaining, Self-Recoverable, Bioadhesive, and Transparent *In Situ* Forming Hydrogels to Accelerate Wound Healing. *ACS Appl. Mater. Inter.* 12, 2023–2038. doi:10.1021/acsami.9b17180

Li, S.-C., Chu, L.-N., Gong, X.-Q., and Diebold, U. (2010). Hydrogen Bonding Controls the Dynamics of Catechol Adsorbed on a TiO 2 (110) Surface. *Science.* 328, 882–884. doi:10.1126/science.1188328

Lian, M., Chen, X., Lu, Y., and Yang, W. (2016). Self-Assembled Peptide Hydrogel as a Smart Biointerface for Enzyme-Based Electrochemical Biosensing and Cell Monitoring. *ACS Appl. Mater. Inter.* 8, 25036–25042. doi:10.1021/acsami.6b05409

Liao, Z., Liao, G., Yang, X., Peng, X., Zhang, X., Xie, X., et al. (2018). Transplantation of Autologous Esophageal Mucosa to Prevent Stricture After Circumferential Endoscopic Submucosal Dissection of Early Esophageal Cancer (With Video). *Gastrointest. Endosc.* 88, 543–546. doi:10.1016/j.gie.2018.04.2349

Machida, H., Tominaga, K., Minamino, H., Sugimori, S., Okazaki, H., Yamagami, H., et al. (2012). Locoregional Mitomycin C Injection for Esophageal Stricture after Endoscopic Submucosal Dissection. *Endoscopy.* 44, 622–625. doi:10.1055/s-0032-1306775

Mizuta, H., Nishimori, I., Kuratani, Y., Higashidani, Y., Kohsaki, T., and Onishi, S. (2009). Predictive Factors for Esophageal Stenosis after Endoscopic Submucosal Dissection for Superficial Esophageal Cancer. *Dis. esophagus : official J. Int. Soc. Dis. Esophagus.* 22, 626–631. doi:10.1111/j.1442-2050.2009.00954.x

Mochizuki, Y., Saito, Y., Tanaka, T., Nitta, N., Yamada, H., Tsujikawa, T., et al. (2012). Endoscopic Submucosal Dissection Combined With the Placement of Biodegradable Stents for Recurrent Esophageal Cancer After Chemoradiotherapy. *J. Gastrointest. Canc.* 43, 324–328. doi:10.1007/s12029-011-9283-z

Mori, H., Rafiq, K., Kobara, H., Fujihara, S., Nishiyama, N., Oryuu, M., et al. (2013). Steroid Permeation into the Artificial Ulcer by Combined Steroid Gel Application and Balloon Dilatation: Prevention of Esophageal Stricture. *J. Gastroenterol. Hepatol.* 28, 999–1003. doi:10.1111/jgh.12154

Nguyen, P. K., Gao, W., Patel, S. D., Siddiqui, Z., Weiner, S., Shimizu, E., et al. (2018). Self-Assembly of a Dentinogenic Peptide Hydrogel. *ACS omega.* 3, 5980–5987. doi:10.1021/acsomega.8b00347

Nieponice, A., McGrath, K., Qureshi, I., Beckman, E. J., Luketich, J. D., Gilbert, T. W., et al. (2009). An Extracellular Matrix Scaffold for Esophageal Stricture Prevention After Circumferential EMR. *Gastrointest. Endosc.* 69, 289–296. doi:10.1016/j.gie.2008.04.022

Nishiguchi, A., Sasaki, F., Maeda, H., Kabayama, M., Ido, A., and Taguchi, T. (2019). Multifunctional Hydrophobized Microparticles for Accelerated Wound Healing After Endoscopic Submucosal Dissection. *Small.* 15, e1901566. doi:10.1002/smll.201901566

Nishizawa, T., and Suzuki, H. (2020). Long-Term Outcomes of Endoscopic Submucosal Dissection for Superficial Esophageal Squamous Cell Carcinoma. *Cancers (Basel).* 12, 2849. doi:10.3390/cancers12102849

Ohki, T., and Yamamoto, M. (2020). Esophageal Regenerative Therapy Using Cell Sheet Technology. *Regenerative Ther.* 13, 8–17. doi:10.1016/j.reth.2020.04.009

Ohki, T., Yamato, M., Ota, M., Takagi, R., Murakami, D., Kondo, M., et al. (2012). Prevention of Esophageal Stricture After Endoscopic Submucosal Dissection Using Tissue-Engineered Cell Sheets. *Gastroenterology.* 143, 582–588. doi:10.1053/j.gastro.2012.04.050

Ono, S., Fujishiro, M., Niimi, K., Goto, O., Kodashima, S., Yamamichi, N., et al. (2009). Predictors of Postoperative Stricture After Esophageal Endoscopic Submucosal Dissection for Superficial Squamous Cell Neoplasms. *Endoscopy.* 41, 661–665. doi:10.1055/s-0029-1214867

Paramonov, S. E., Jun, H.-W., and Hartgerink, J. D. (2006). Self-Assembly of Peptide–Amphiphile Nanofibers: The Roles of Hydrogen Bonding and Amphiphilic Packing. *J. Am. Chem. Soc.* 128, 7291–7298. doi:10.1021/ja060573x

Pech, O., May, A., Manner, H., Behrens, A., Pohl, J., Weferling, M., et al. (2014). Long-Term Efficacy and Safety of Endoscopic Resection for Patients With Mucosal Adenocarcinoma of the Esophagus. *Gastroenterology.* 146, 652–660. doi:10.1053/j.gastro.2013.11.006

Qu, J., Zhao, X., Liang, Y., Zhang, T., Ma, P. X., and Guo, B. (2018). Antibacterial Adhesive Injectable Hydrogels With Rapid Self-Healing, Extensibility and Compressibility as Wound Dressing for Joints Skin Wound Healing. *Biomaterials.* 183, 185–199. doi:10.1016/j.biomaterials.2018.08.044

Radu, A., Grosjean, P., Fontolliet, C., and Monnier, P. (2004). Endoscopic Mucosal Resection in the Esophagus With a New Rigid Device: an Animal Study. *Endoscopy.* 36, 298–305. doi:10.1055/s-2004-814205

Rajan, E., Gostout, C., Feitoza, A., Herman, L., Knipschield, M., Burgart, L., et al. (2005). Widespread Endoscopic Mucosal Resection of the Esophagus With Strategies for Stricture Prevention: a Preclinical Study. *Endoscopy.* 37, 1111–1115. doi:10.1055/s-2005-870531

Rao, Z., Sasaki, M., and Taguchi, T. (2013). Development of Amphiphilic, Enzymatically-Degradable PEG-Peptide Conjugate as Cell Crosslinker for Spheroid Formation. *Colloids Surf. B: Biointerfaces.* 101, 223–227. doi:10.1016/j.colsurfb.2012.06.033

Ravaine, V., Ancla, C., and Catargi, B. (2008). Chemically Controlled Closed-Loop Insulin Delivery. *J. Controlled Release.* 132, 2–11. doi:10.1016/j.jconrel.2008.08.009

Rhen, T., and Cidlowski, J. A. (2005). Antiinflammatory Action of Glucocorticoids - New Mechanisms for Old Drugs. *N. Engl. J. Med.* 353, 1711–1723. doi:10.1056/nejmra050541

Saito, Y., Tanaka, T., Andoh, A., Minematsu, H., Hata, K., Tsujikawa, T., et al. (2008). Novel Biodegradable Stents for Benign Esophageal Strictures Following Endoscopic Submucosal Dissection. *Dig. Dis. Sci.* 53, 330–333. doi:10.1007/s10620-007-9873-6

Sakaguchi, Y., Tsuji, Y., Ono, S., Saito, I., Kataoka, Y., Takahashi, Y., et al. (2015). Polyglycolic Acid Sheets With Fibrin Glue Can Prevent Esophageal Stricture After Endoscopic Submucosal Dissection. *Endoscopy.* 47, 336–340. doi:10.1055/s-0034-1390787

Sakaguchi, Y., Tsuji, Y., Yamamichi, N., Fujishiro, M., and Koike, K. (2016). Successful Closure of a Large Perforation during Colorectal Endoscopic Submucosal Dissection by Application of Polyglycolic Acid Sheets and Fibrin Glue. *Gastrointest. Endosc.* 84, 374–375. doi:10.1016/j.gie.2016.03.787

Sakurai, T., Miyazaki, S., Miyata, G., Satomi, S., and Hori, Y. (2007). Autologous Buccal Keratinocyte Implantation for the Prevention of Stenosis After EMR of the Esophagus. *Gastrointest. Endosc.* 66, 167–173. doi:10.1016/j.gie.2006.12.062

Seehawong, U., Morita, Y., Nakano, Y., Iwasaki, T., Krutsri, C., Sakaguchi, H., et al. (2019). Successful Treatment of an Esophageal Perforation That Occurred during Endoscopic Submucosal Dissection for Esophageal Cancer Using

Polyglycolic Acid Sheets and Fibrin Glue. *Clin. J. Gastroenterol.* 12, 29–33. doi:10.1007/s12328-018-0900-2

Shah, P. M., and Gerdes, H. (2015). Endoscopic Options for Early Stage Esophageal Cancer. *J. Gastrointest. Oncol.* 6, 20–30. doi:10.3978/j.issn.2078-6891.2014.096

Sharma, A., and Sharma, G. (2018). Biomaterials And Their Applications. *Aip Conf. Proc.*, 080041. doi:10.1063/1.5032847

Siegel, R. L., Miller, K. D., and Jemal, A. (2017). Cancer Statistics, 2017. *CA: a Cancer J. clinicians.* 67, 7–30. doi:10.3322/caac.21387

Sporn, M. B., and Roberts, A. B. (1989). Transforming Growth Factor-β. *Jama.* 262, 938–941. doi:10.1001/jama.1989.03430070086036

Stern, D., and Cui, H. (2019). Crafting Polymeric and Peptidic Hydrogels for Improved Wound Healing. *Adv. Healthc. Mater.* 8, e1900104. doi:10.1002/adhm.201900104

Sung, H., Ferlay, J., and Siegel, R. L. (2021). Global Cancer Statistics 2020: GLOBOCAN Estimates of Incidence and Mortality Worldwide for 36 Cancers in 185 Countries. *CA: A Cancer Journal for Clinicians*. Hoboken, New Jersey: Wiley Online Library.

Takahashi, H., Arimura, Y., Masao, H., Okahara, S., Tanuma, T., Kodaira, J., et al. (2010). Endoscopic Submucosal Dissection Is superior to Conventional Endoscopic Resection as a Curative Treatment for Early Squamous Cell Carcinoma of the Esophagus (With Video). *Gastrointest. Endosc.* 72, 255–264. doi:10.1016/j.gie.2010.02.040

Takimoto, K., Imai, Y., and Matsuyama, K. (2014). Endoscopic Tissue Shielding Method With Polyglycolic Acid Sheets and Fibrin Glue to Prevent Delayed Perforation After Duodenal Endoscopic Submucosal Dissection. *Dig. Endosc.* 26 (Suppl. 2), 46–49. doi:10.1111/den.12280

Tang, J., Wang, J., Huang, K., Ye, Y., Su, T., Qiao, L., et al. (2018a). Cardiac Cell-Integrated Microneedle Patch for Treating Myocardial Infarction. *Sci. Adv.* 4, eaat9365. doi:10.1126/sciadv.aat9365

Tang, J., Ye, S., Ji, X., Liu, F., and Li, Z. (2018b). Deployment of Carboxymethyl Cellulose Sheets to Prevent Esophageal Stricture After Full Circumferential Endoscopic Submucosal Dissection: A Porcine Model. *Dig. Endosc.* 30, 608–615. doi:10.1111/den.13070

Tsonchev, S., Schatz, G. C., and Ratner, M. A. (2004). Electrostatically-Directed Self-Assembly of Cylindrical Peptide Amphiphile Nanostructures. *J. Phys. Chem. B.* 108, 8817–8822. doi:10.1021/jp037731g

Wan, S., Borland, S., Richardson, S. M., Merry, C. L. R., Saiani, A., and Gough, J. E. (2016). Self-Assembling Peptide Hydrogel for Intervertebral Disc Tissue Engineering. *Acta Biomater.* 46, 29–40. doi:10.1016/j.actbio.2016.09.033

Wang, R., Li, J. Z., and Chen, W. (2017). A Biomimetic Mussel-Inspired Epsilon-Poly-L-Lysine Hydrogel With Robust Tissue-Anchor and Anti-Infection Capacity. *Adv. Funct. Mater.* 27, 1604894. doi:10.1002/adfm.201604894

Wei, R.-Q., Tan, B., Tan, M.-Y., Luo, J.-C., Deng, L., Chen, X.-H., et al. (2009). Grafts of Porcine Small Intestinal Submucosa With Cultured Autologous Oral Mucosal Epithelial Cells for Esophageal Repair in a Canine Model. *Exp. Biol. Med. (Maywood).* 234, 453–461. doi:10.3181/0901-rm-5

Wei, W., Petrone, L., Tan, Y., Cai, H., Israelachvili, J. N., Miserez, A., et al. (2016). An Underwater Surface-Drying Peptide Inspired by a Mussel Adhesive Protein. *Adv. Funct. Mater.* 26, 3496–3507. doi:10.1002/adfm.201600210

Yamaguchi, N., Isomoto, H., Nakayama, T., Hayashi, T., Nishiyama, H., Ohnita, K., et al. (2011). Usefulness of Oral Prednisolone in the Treatment of Esophageal Stricture After Endoscopic Submucosal Dissection for Superficial Esophageal Squamous Cell Carcinoma. *Gastrointest. Endosc.* 73, 1115–1121. doi:10.1016/j.gie.2011.02.005

Yang, G., Chen, Q., Wen, D., Chen, Z., Wang, J., Chen, G., et al. (2019). A Therapeutic Microneedle Patch Made From Hair-Derived Keratin for Promoting Hair Regrowth. *Acs Nano.* 13, 4354–4360. doi:10.1021/acsnano.8b09573

Ye, L.-P., Zheng, H.-H., Mao, X.-L., Zhang, Y., Zhou, X.-B., and Zhu, L.-H. (2016). Complete Circular Endoscopic Resection Using Submucosal Tunnel Technique Combined With Esophageal Stent Placement for Circumferential Superficial Esophageal Lesions. *Surg. Endosc.* 30, 1078–1085. doi:10.1007/s00464-015-4301-z

Yoshizawa, K., Mizuta, R., and Taguchi, T. (2015). Enhanced Angiogenesis of Growth Factor-Free Porous Biodegradable Adhesive Made With Hexanoyl Group-Modified Gelatin. *Biomaterials.* 63, 14–23. doi:10.1016/j.biomaterials.2015.06.003

You, Y., Kobayashi, K., Colak, B., Luo, P., Cozens, E., Fields, L., et al. (2021). Engineered Cell-Degradable Poly(2-Alkyl-2-Oxazoline) Hydrogel for Epicardial Placement of Mesenchymal Stem Cells for Myocardial Repair. *Biomaterials.* 269, 120356. doi:10.1016/j.biomaterials.2020.120356

Yu, J., Zhang, Y., Ye, Y., DiSanto, R., Sun, W., Ranson, D., et al. (2015). Microneedle-array Patches Loaded With Hypoxia-Sensitive Vesicles Provide Fast Glucose-Responsive Insulin Delivery. *Proc. Natl. Acad. Sci. USA.* 112, 8260–8265. doi:10.1073/pnas.1505405112

Zhang, W., Lin, D., Wang, H., Li, J., Nienhaus, G. U., Su, Z., et al. (2017). Supramolecular Self-Assembly Bioinspired Synthesis of Luminescent Gold Nanocluster-Embedded Peptide Nanofibers for Temperature Sensing and Cellular Imaging. *Bioconjug. Chem.* 28, 2224–2229. doi:10.1021/acs.bioconjchem.7b00312

Zhang, Y., Zhang, H., Zou, Q., Xing, R., Jiao, T., and Yan, X. (2018). An Injectable Dipeptide-Fullerene Supramolecular Hydrogel for Photodynamic Antibacterial Therapy. *J. Mater. Chem. B.* 6, 7335–7342. doi:10.1039/c8tb01487f

Zhou, M., Smith, A. M., Das, A. K., Hodson, N. W., Collins, R. F., Ulijn, R. V., et al. (2009). Self-Assembled Peptide-Based Hydrogels as Scaffolds for Anchorage-Dependent Cells. *Biomaterials.* 30, 2523–2530. doi:10.1016/j.biomaterials.2009.01.010

Zhou, Y., Kang, L., Yue, Z., Liu, X., and Wallace, G. G. (2020). Composite Tissue Adhesive Containing Catechol-Modified Hyaluronic Acid and Poly-L-Lysine. *ACS Appl. Bio Mater.* 3, 628–638. doi:10.1021/acsabm.9b01003

Zuercher, B. F., George, M., Escher, A., Piotet, E., Ikonomidis, C., Andrejevic, S. B., et al. (2013). Stricture Prevention after Extended Circumferential Endoscopic Mucosal Resection by Injecting Autologous Keratinocytes in the Sheep Esophagus. *Surg. Endosc.* 27, 1022–1028. doi:10.1007/s00464-012-2509-8

Conflict of Interest: The authors declare that the research was conducted in the absence of any commercial or financial relationships that could be construed as a potential conflict of interest.

Publisher's Note: All claims expressed in this article are solely those of the authors and do not necessarily represent those of their affiliated organizations, or those of the publisher, the editors, and the reviewers. Any product that may be evaluated in this article, or claim that may be made by its manufacturer, is not guaranteed or endorsed by the publisher.

frontiers in Materials

REVIEW
published: 10 February 2022
doi: 10.3389/fmats.2022.815930

Research Progress of Biodegradable Polymers in Repairing Achilles Tendon Injury

Jinchi Zhang[1,2†], Wange Wang[1†], Xinan Zhang[1], Liqun Yang[2]* and JinChao Zhang[3]*

[1]College of Kinesiology, Shenyang Sport University, Shenyang, China, [2]NHC Key Laboratory of Reproductive Health and Medical Genetics (China Medical University) and Liaoning Key Laboratory of Reproductive Health, Liaoning Research Institute of Family Planning (The Affiliated Reproductive Hospital of China Medical University), Shenyang, China, [3]School of Physical Education, Harbin Normal University, Harbin, China

Achilles tendon injury has become a common sports injury clinically, and its treatment and rehabilitation are essential, while the regenerative capacity of the Achilles tendon in adult mammals is limited. Therefore, it is necessary to promote the repair and remodelling of the Achilles tendon through efficient interventions. Biodegradable polymer materials are one of the most popular in the treatment and repair of soft tissues, ligaments, muscles, and organs injured by organisms to enhance the function of their wounded sites. Thus, it plays a specific role in "compensation" and is widely used in clinical medicine and rehabilitation. This review summarized the progress of poly (ε-caprolactone), polylactic acid, poly (lactic-co-glycolic acid), poly (trimethylene carbonate) (PTMC), and polydioxanone (PDS) in repairing Achilles tendon injury, indicating that the biodegradable polymers have succeeded in improving and treating Achilles tendon injuries. However, some problems such as lack of good affinity with cells and uncontrollable degradation of the biodegradable polymers should be overcome in repairing Achilles tendon injury. Therefore, the development of modified biodegradable polymers to make them an ideal repair material that meets the requirements is vital in improving Achilles tendon injuries. With the continuous development and close cooperation of life sciences and material sciences, excellent materials for repairing Achilles tendon injuries will undoubtedly be produced. The treatment of Achilles tendon injuries will be more straightforward, which will be a boon for many athletes.

Keywords: biodegradable polymers, Achilles tendon injury, poly (ε-caprolactone), poly (lactic acid), poly (lactide-co-glycolide), poly (trimethylene carbonate), polydioxanone

OPEN ACCESS

Edited by:
Yilong Cheng,
Xi'an Jiaotong University, China

Reviewed by:
Ernesto Reverchon,
University of Salerno, Italy
He Liu,
Jilin University, China

****Correspondence:***
Liqun Yang
yanglq@lnszjk.com.cn
Xinan Zhang
zhangxa2725@163.com

†These authors have contributed equally to this work

Specialty section:
This article was submitted to Biomaterials, a section of the journal Frontiers in Materials

Received: *16 November 2021*
Accepted: *04 January 2022*
Published: *10 February 2022*

Citation:
Zhang J, Wang W, Zhang X, Yang L and Zhang J (2022) Research Progress of Biodegradable Polymers in Repairing Achilles Tendon Injury. Front. Mater. 9:815930. doi: 10.3389/fmats.2022.815930

INTRODUCTION

The Achilles tendon is the largest and most powerful tendon in the human body, laying the foundation for our lower limb activities. Achilles tendon injury often occurs during the process of physical training. The damage of soft tissue and muscle ligaments around the Achilles tendon, causing the loss of lower limb muscle strength, flexibility, and other functions. If the Achilles tendon fracture is severe and surgical treatment is needed. Tendon injury is common in sports and other rigorous sports, leading to dysfunction, and disability for months or years (Dams et al., 2019). In addition to direct damage, more than 70% of the Achilles tendon breaks are more involved in sports, especially the ball and track and field (Ganestam et al., 2016). Complications after an Achilles tendon

rupture are not uncommon. The tendon rupture was the most common. The postoperative Achilles tendon re-rupture rate was approximately 1.7–5.6% (Cerrato and Switaj, 2017). The most common method of tendon injury is autologous transplantation. However, these lead to morbidity and further weakness (Jayasree et al., 2019).

In recent years, tissue engineering based on biomedical materials has given hope to repairing Achilles tendon injuries. Previous work showed that collagen is a popular scaffold material for tendon tissue engineering because tendons are principally composed of collagen (Garvin et al., 2003; Juncosa-Melvin et al., 2006). Although other naturally derived scaffolds researched for tendon applications have included chitosan-based hyaluronan hybrid polymer fibres (Funakoshi et al., 2005) and alginate–chitosan polyion hybrid fibrous complex (Majima et al., 2005), a significant focus has been targeted on synthetic degradable materials, such as PGA (Cao et al., 2006) and PLGA (Moffat et al., 2009). Revercho et al. had critically analyzed the biodegradable polyester like polyglycolic acid (PGA), polylactic acid (PLA), and their copolymer for tendon tissue engineering (Reverchon et al., 2012). They demonstrated the degradation products of polyesters, such as glycolic acid and lactic acid, are metabolites present in the human body, while the main disadvantage is that the degradation products are acidic and will cause inflammation. In addition, the hydrophobic structure of biodegradable polyesters may cause problems for cell adhesion. In contrast, poly (ε-caprolactone) (PCL), polydioxanone (PDS), or poly (trimethylene carbonate) (PTMC) degrades with non-acidic products, avoiding the problem of pH drop. Hence, biodegradable polymers' selection and performance regulation will significantly impact the repair effect of Achilles tendon injury, which also attracts extensive interest.

In this review, the most widely studied biodegradable polymers, including polyesters, such as PLA and PLGA, and PTMC, PDS, are listed as representatives to summarize the progress in the application of biodegradable polymers in the repair of Achilles tendon injuries. It will provide detailed theoretical guidance for the selection and development of scaffold materials with good performance, and promote tissue recovery and regeneration of the Achilles tendon injury, making it a reality for patients to return to families and society healthily.

EFFECT OF PCL ON THE REPAIR OF THE ACHILLES TENDON INJURY

Poly (ε-caprolactone) (PCL), has a highly effective therapeutic effect as a biomedical polymeric material combined with cells to treat Achilles tendon injuries. Cai et al. (2020) combined PCL-SF/PLCL fabric scaffolds with marrow stem cells from rabbit bone to promote healing of injured tendons. It has been found that PCL-SF/PLCL copolymer has good tissue regeneration ability. It will be a potentially valuable biomedical polymer material widely used in tendon tissue engineering.

It is worth noting that using a variety of biomedical polymers as composite scaffold materials can play a double role in repairing Achilles tendon injuries with half the effort. It was concluded that the Band-Aid with 50% Wharton's jelly (WJ)-derived extracellular matrix (ECM) combined with PCL electrospinning had the fastest therapeutic effect on cell proliferation and differentiation, indicating that it was beneficial to nerve regeneration after Achilles tendon rupture and improved the activity of muscle tissue (Li et al., 2017). Schoenenberger et al. (2018) prepared PCL fibre scaffolds with highly aligned or randomly oriented by electrospinning and cultured human tendon fibroblasts (TFs) on them. The results showed that highly aligned PCL scaffolds tended to down-regulate the expression of matrix metalloproteinases (MMPs) because of their high catabolic activity; Czarnecki et al. (2012) similarly investigated the feasibility of PCL-modified composite fibre-carbon scaffolds and analyzed their mechanical properties and ability to support the growth and proliferation of human dermal fibroblasts. The results showed that PCL-modified composite fibrous scaffold had similar mechanical properties to the acellular dermal matrix to support fibroblast adhesion and proliferation. The results demonstrated that PCL, as the main component of the fibrous scaffold, can play a role in inhibiting cell adhesion and rapid proliferation physiologically and can be used as a biomedical polymer material in clinical studies.

In addition to the above composite fibre scaffold, the Achilles tendon can also be repaired directly using the interaction between biomaterials and cells. Wang has developed a bioactive polymer membrane for guided bone regeneration (GBR) by interacting bone marrow stromal cells (BMSCs) with PCL and functionalizing stromal cell-derived factor-1a (SDF-1a). The cultured biofilm can be applied to the injured bone and joint. The results suggest that SDF-1a-loaded PCL electrospun membranes are bioactive and valuable for optimizing the clinical application of GBR strategies (Ji et al., 2013).

To simulate the natural tendon tissue structure, Jayasree et al. (2019) prepared a woven multiscale fibrous scaffold composed of PCL micro/collagen bFGF nanofibers and coated with sodium alginate to prevent peritendinous adhesions. The release kinetics of bFGF showed sustained release of growth factors for 20 days. The results showed that mPCL-nCol-bFGF had higher cell proliferation and expression of tenogenic markers than mPCL-nCol. The results also showed that PCL nanofibers scaffold loaded with essential fibroblast growth factor (bFGF) could recover some physiological indexes around the Achilles tendon of rabbit tendon. It could be used as a biomedical polymer material to repair Achilles tendon injury.

Chen et al. (2017) studied the physicochemical properties of random PCL (RP) nanofibers, random PCL/SF (RPSF) nanofibers, and aligned PCL/SF (APSF) nanofibers, and used RPSF and APSF scaffolds to repair rabbit Achilles tendon defects. Histological sections were stained with Hematoxylin-eosin (H&E) and Masson's trichrome at 6 and 12 weeks. The results showed that the migration and proliferation of rabbit dermal fibroblasts (RDFBs) on the arranged nanofiber scaffolds tended to stretch in a parallel direction along with the arrangement of nanofibers, which was conducive to promoting soft tissue healing around Achilles tendon defects and improving the effectiveness and reliability of the scaffolds *in vitro*. In addition, scaffolds made of SF can also be applied to the regenerative repair of other tissues,

for example, renewable bone, eye, nerve, skin, tendon, ligament, and cartilage (Jao et al., 2016).

As a biodegradable fibrous membrane, the biomedical polymer can make full use of its biological characteristics such as repair of Achilles tendon and rapid degradation rate, which is conducive to reducing the number of inflammatory factors around Achilles tendon injury can play a role in preventing soft tissue adhesion. Some experts have studied the applicability of PCL film for repairing the Achilles tendon gap in the rat model. The results showed that the biomechanical and morphological changes were similar in the PCL membrane repair Achilles tendinopathy group after 8 weeks of surgery (Kazimoğlu et al., 2003). It indicated that the biodegradable PCL membrane group had the best therapeutic effect on the Achilles tendon and demonstrated the practical therapeutic effect of PCL in repairing Achilles tendon injury.

It has been reported that Lee et al. (2019) also improved the healing of collagenase-induced Achilles tendinitis in rabbits by preparing diclofenac immobilized polycaprolactone (DFN/PCL) fibre sheets. The study results demonstrated that the long-term diclofenac delivery system using PCL fibre sheets strongly affects collagenase-induced Achilles tendinitis rabbit model and tendon recovery. By investigating the effect of PCL ultrafine fibres arranged in three dimensions on the growth behaviour of fibroblasts, it was found that microfibers were able to support the proliferation of human dermal fibroblasts for more than 7 days (An et al., 2012). This super fibre can be considered a scaffold study for applying biomedical polymer materials in tissue engineering and will be an effective clinical treatment option for athletes with Achilles tendon injuries.

Others have combined composite fibrous materials with stem cells to prepare new biomedical polymer materials to promote soft tissue regeneration around the Achilles tendon, enhance cell activity, and avoid pathological changes in the injured tendon tissue. Dong et al. (2021) found that a biopolymer scaffold composed of polycaprolactone/silk fibroin (PCL/SF) copolymers could reduce the adhesion of tissues around the Achilles tendon, thereby promoting the healing of Achilles tendon injuries. Bosworth et al. (2013) used three different polycaprolactone fibre-based electrospinning scaffolds (two-dimensional random sheets, two-dimensional alignment sheets, and three-dimensional bundles.) to repair injured tendons. The results showed that the three-dimensional bundle showed the most excellent tensile performance, significantly stiffer than the two-dimensional arrangement and two-dimensional random fibres. It can be used as a biomaterial for artificial grafts, and considered the polymer material of choice to treat Achilles tendon ruptures.

The study of Achilles tendon reconstruction is a hot topic. Immunohistochemical and biomechanical analysis of the tendon regeneration process using braided tendon implants for Achilles tendon reconstruction in rabbits showed that both polylactic acid and chitin composite tendons had good initial strength and increased fibrous tissue length. It also plays a compliant role in reconstructing the Achilles tendon, indicating that these polymer materials have great potential in artificial tendons (Sato et al., 2000). Hu et al. (2013) prepared PCL biofilms using an improved melt moulding/leaching technique and evaluated their physical and mechanical properties and *in vitro* degradation rates, while biomechanical analysis was carried out after repairing the Achilles tendon of rabbits after repair rupture. The results showed that the internal fixation technique of strengthening tendon repair with PCL biofilm could significantly improve the tensile strength of the Achilles tendon repair site, which laid a foundation for early postoperative rehabilitation.

As mentioned above, PCL has good biocompatibility and has great application potential in repairing Achilles tendon injuries as one of the ideal repair materials. However, PCL is a semi-crystalline polymer; its degradation rate *in vivo* is prolonged and affected by crystallinity. The higher the crystallinity, the slower the degradation. How to adjust the all-around performance of PCL, make it have a controllable degradation rate to match the degradation rate with the speed of tissue regeneration is a problem that needs to be addressed in the application of PCL to repair Achilles tendon injuries. In addition, whether the crystalline degradation fragments of PCL can induce inflammation is also a question worthy of attention.

EFFECT OF PLA ON ACHILLES TENDON REPAIR

Polylactic acid (PLA) has been widely used in regenerative medicine as an absorbable, biodegradable polymer. Due to its excellent biological characteristics, PLA has also attracted more and more attention in repairing Achilles tendon injuries. Liu et al. (2015) produced the electrospun PLA nanofibers with controllable coiling. Studies have shown that electrospinning PLA has controllability and can play a therapeutic effect in restoring tendon injury. It is common to prepare PLA composite scaffold materials to repair Achilles tendon injury, as coupled with the intervention of various cytokines, the regeneration of the Achilles tendon and the proliferation and differentiation function cells will be promoted. Vuornos et al. (2016) reported that human adipose-derived stem cells (hASCs) could form a uniform cell layer on woven PLA scaffolds under the culture of a tenogenic medium, and effectively differentiate into tendon tissue.

Unlike the fibrous scaffolds loaded with hASCs described above, Wang et al. (2017) compared the effect of cell-free scaffolds, allogeneic scaffolds and autologous cell implantation scaffolds on the tissue recovery. The allogeneic scaffold material was PGA with PLA fibres woven in a ratio of 4:2. The study results found that the degree of tissue recovery in the allogeneic group was better than the other two groups, and the degradation rate of the scaffold *in vivo* was much faster; Deng et al. (2014) also used a composite tendon scaffold consisting of a PGA unwoven fibre medial and a PGA/PLA wool woven mesh lateral to provide mechanical strength. The results showed that adipose-derived stem cells (ASCs) combined with biomaterials could rapidly heal the ruptured tendon, produce new granulation tissue, and gradually form mature new tendons. The results indicate that

ASCs have a huge promoting effect in tissue remodelling and tendon regeneration.

In addition to the above composite scaffold materials, PLA also can be used to prepare new hollow braided prosthetic material that can be degraded *in vivo* to repair Achilles tendon injury. Araque-Monrós et al. (2013) designed a new renewable absorbable tendon and ligament prosthesis through PLA hollow braided bands, finfding that L929 lineage fibroblasts combined with PLA braid could prevent tissue adhesion and promote the continuous proliferation and renewal of cells. Chen et al. (2009) reported that the regeneration limitations of injured biological tissues have been solved by using the characteristics of cells in combination with material scaffolds for tendon and ligament injuries.

PLA has good biological characteristics, will not have adverse effects on the body, and plays an essential role in repairing Achilles tendon injury. Song et al. (2015a) used PLA and PCL electrospinning membranes with different degradation kinetics to study the anti-adhesion effect on Achilles tendon repair. The results showed that the electrospun PLA membrane group's anti-adhesion ability and tendon repairability were significantly better than those of the PCL membrane group.

At present, Achilles tendon rupture requires the fixation of an external splint, and the traditional sling will cause muscle spasms. Blaya F et al. prepared splints made of made of PLA and FilaFlex to ensure comfort and corrosion resistance (Blaya et al., 2019). Some researchers have prepared anti-adhesion films by co-spinning beeswax (Wax) with PLA. In the rat Achilles tendon adhesion model, the beeswax/PLA film group had the least histologically surrounding adhesions at the repair site, which indicated that the anti-adhesive effect of beeswax/PLA copolymer on the Achilles tendon was significant and could be considered to prevent the adhesion of Achilles tendon soft tissue (Zou et al., 2020).

From autologous transplantation to "compensatory" replacement of grafts with medical polymer materials, this will be a significant advance in applying medical polymer materials, but the histocompatibility of this biomedical polymer material to the human body, and whether there will be eosinophilic substances need to be further studied. To promote the broad application of PLA in the repair of Achilles tendon injuries, eliminating the inflammation caused by acid degradation products is a critical issue that needs attention. Another issue that needs to be considered is how to increase the affinity of PLA and cells to improve cell adhesion and proliferation viability.

EFFECT OF PLGA ON ACHILLES TENDON REPAIR

The scaffold materials composed of PLGA combined with cells are also reoprted in Achilles tendon injury. For example, the complex of stem cells (MSCs), fibrin glue, and woven PLGA to repair the tendon defects of gastrocnemius tendon and patella have shown that the tensile modulus of the gastrocnemius tendon reaches 62% of normal tissue 12 weeks after implantation (Awad et al., 2003; Ouyang et al., 2003).

It is a relatively novel tissue engineering method to encapsulate the bioactive substance on reinforced degradable knitted fibres, combined with cellular components for repairing Achilles tendon injuries. Sahoo et al. (2010) encapsulated bFGF on a slowly degrading knitted PLGA microfiber filament scaffold to fabricate a new biohybrid fibre scaffold system. It has been found that this hybrid polymer scaffold can promote the attachment and proliferation of intercellular progenitor cells (MPC) and allow the cells to grow on PLGA fibre scaffolds, fully indicating that PLGA is very potential for repairing and regenerating tendons; Ouyang et al. (2002) reported the application of woven PLGA scaffold seeded with bone marrow stromal cells (bMSC) in improving Achilles tendon injury in rabbits. bMSC/PLGA-treated tendon repair had eosinophilic tissue formation after stent implantation, which indicated that this biological scaffold produced cell proliferation and regeneration in the soft tissue around the Achilles tendon, resulting in treatment around the Achilles tendon injury. However, acidic substances will produce an acidic environment around the Achilles tendon, which is not conducive to the healing of the Achilles tendon.

Some experts prepared silk fibroin-PLGA mesh scaffolds, filling with type I collagen and rabbit autologous bone marrow stem cells. Implantation of these scaffolds into rabbit Achilles tendon defect sites resulted in the formation of granulation tissue exhibited by the regenerated Achilles tendon, indicating that necrotic tissue was being repaired and inflammatory factors were reduced (Zhang et al., 2015). Choi et al. (2020) prepared lactoferrin-immobilized, heparin-anchored PLGA nanoparticles and delivered them to rat Achilles tendon sites with Achilles tendinitis. The collagen and factor around the tendon increased, showing that PLGA nanoparticles have an excellent therapeutic effect on Achilles tendinitis.

Yan et al. (2021) concluded that fibroblast growth factor (bFGF) can promote tendon healing, and they prepared PLGA electrospun membrane loaded with ibuprofen (IBU) and bFGF to treat Achilles tendon injuries in animals. The study showed that the PLGA electrospun film loaded with bFGF and IBU significantly reduced inflammatory factors and increased collagen fibres at the Achilles tendon healing area. Weng et al. (2020) studied the use of electrospinning to develop antibiotics loaded ultrafine materials. It was found that PLGA nanofibers released effective concentrations of epinomycin more than 40 days after surgery. At 1.5 weeks, the maximum intensity levels of control tendons were lower than that of healthy tendons. At 3 weeks, the doxycycline group showed a top tendon strength level comparable to the healthy tendon group. The control group did not receive a doxycycline nanofiber membrane, and the maximum intensity was poor compared to the other two groups. Six weeks after surgery, the tendon strength was comparable in all three groups, while the values in the doxycycline group were slightly more significant than the other groups, and the rats also showed better mobility and stronger tendons after surgery.

In addition to using sustained-release systems, some scholars have used new bioactive scaffolds to transplant multifunctional stem cells to repair Achilles tendon injury. Zhao et al. (2019) integrated MSC sheets and bFGF into PLGA/bFGF-fibrin gel

scaffolds, promoting the proliferation, and differentiation of MSCs into tendons and synergistically promoting the reconstruction of injured tendons. Histological observation of regenerated tendons at 8 weeks after transplantation showed that the PLGA/bFGF-fibrin gel scaffold integrated with MSC sheets and bFGF had more interwoven collagen fibres compared with the PLGA/MSCs and PLGA/bFGF groups, while the control group had a lower content of fibrocytes and myofibers. Therefore, the transplantation of PLGA/MSCs/bFGF into injured tendon sites in humans can promote the remodelling of necrotic cells around tendons, improve the degree of tendon injury, and promote the repair and regeneration of tendons.

It is a novel idea to use PLGA hydrogel as a carrier in tissue engineering to repair Achilles tendon injury. The use of hydrogel can improve the body's compatibility and promote the removal of necrotic tissue. Yuan et al. (2015) injected 5-Fuloaded PLGA-PEG-PLGA hydrogel into the severed Achilles tendon on the right side of the rat. Studies have shown that 5-Fu-loaded PLGA hydrogel can effectively inhibit the adhesion and contracture of Achilles tendon soft tissue, providing a solid guarantee for clinical research of Achilles tendon injury. Similarly, the unit model treated with PLGA film prepared by electrospinning also showed better inhibition of tissue adhesion and tissue repair ability (Song et al., 2015b).

Making appropriate improvements in the performance of biomedical polymer materials and combining various cells to repair Achilles tendon injuries will improve the repair efficiency of Achilles tendon injuries. El Khatib et al. (2020) determined the biological characteristics of sheep amniotic epithelial cells by changing time and distance by treating PLGA with highly aligned microfibers using cold atmospheric plasma (CAP). The results showed that the hydrophilicity and cellular characteristics of PLGA microfibers were improved by treating PLGA microfibers with CAP in the range of 1.3 m.

In addition to the use of biomedical polymer materials, the combined use of drugs for the intervention of Achilles tendon injury will maximize its repair function. Chen et al. (2020) prepared Collagen Hybridizing Peptide (CHP)-modified PLGA nanoparticles and delivered them to mouse Achilles tendons using rapamycin (RAPA) as a drug model. The results showed that CHP-PLGA-RAPA nanoparticles reflected histocompatibility and affinity when repairing Achilles tendon injuries, allowing rapid repair of injured Achilles tendon tissues.

Although numerous studies have shown that PLGA is a promising material for repairing Achilles tendon injuries, the production of acid degradation products and the lack of active groups that interact with cells are still the main factors limiting its wide application in the repair of Achilles tendon injury. Blending or graft modification with natural polymers may be an effective strategy to solve the above problems, which will inevitably become a research hotspot in this field.

EFFECT OF PTMC ON ACHILLES TENDON REPAIR

Poly (trimethylene carbonate) (PTMC) is formed by ring-opening condensation of trimethylene carbonate monomer, which has non-toxicity, good cytocompatibility, and degradability.

Li et al. (2020) studied nanofibrous PCL/PTMC-MA biopolymer scaffolds. The results showed that the mechanical properties of polymer composite scaffolds composed of PTMC combined with PCL increased significantly, which prevented tissue adhesion and promoted cell proliferation and differentiation.

Shieh et al. (1990) prepared polymer material fibres from random copolymers of 90% DMTMC and 10% TMC. They retain excellent biomechanical properties and have appropriate biodegradability. It lays a foundation for the proliferation and migration of rabbit Achilles tendon cells and further improves the activity of stromal cells. Duek et al. (2014) used P (LDLA-TMC) membrane as a protective membrane and implanted it into adjacent tissues in New Zealand rabbits to prevent their adhesion. The results showed that the proliferation and differentiation of cells were accompanied by scar formation around the soft tissue, indicating that the P (LDLA-TMC) membrane has a specific anti-adhesion effect in repairing Achilles tendon injury.

PTMC does not produce acidic degradation products during *in vivo* degradation, allowing a reduction in the number of inflammatory factors around the Achilles tendon and removing necrotic scar tissue. Although PTMC overcomes the disadvantages of producing eosinophilic substances, its application in repairing Achilles tendon injuries is less studied, and there are still some problems that need to be solved urgently. For example, further study is required to ensure that stem cells can play a full role in PTMC scaffold materials and are evenly distributed on the material surface without shedding.

EFFECT OF PDS ON ACHILLES TENDON REPAIR

Polydioxanone (PDS) has non-toxicity, contamination, complete degradation, and good mechanical properties. Using PDS loaded fibroblasts to suture the Achilles tendon injury site can promote fibroblasts to exert their unique properties and heal Achilles tendon injury. He et al. (2002) seeded fetal skin fibroblasts into the human amniotic extracellular matrix (HA-ECM) and wrapped them around the Achilles tendon injury suture sutured by PDS. The immunohistochemical results showed that the labelled seed fibroblasts grew well. The rate and quality of Achilles tendon recombination in the experimental group were better than those in the control group, indicating the use of PDS is used helpful for the repair of Achilles tendon injury.

Unlike the above studies, Moshiri et al. (2015) fabricated a collagen implant (CI) as a simulated tendon, simulated the accessory tendon with a PDS sheath, and then embedded bovine platelet gel (BPG) as an active source of growth factors in rabbits Achilles tendon defects. Studies have found that activated platelets in the scaffold release significantly higher growth factors than the control group, and the turnover of peritendinous fibrocytes and remodelling of the Achilles

tendon have also been further improved. Oryan et al. (2014) also studied the effect of 3D collagen and collagen/PDS implantation on rabbit Achilles tendon defect model by observing the histopathology and ultrastructural structure of injured Achilles tendon and intact Achilles tendon. It has been shown that the implantation of 3D collagen and collagen/PDS accelerates the production of new tendons in the defect area and restores the average functional level of the Achilles tendon.

PDS has excellent mechanical and mechanical properties, playing a role in consolidating acute Achilles tendon rupture in humans. Gebauer et al. (2007) conducted a comparative experiment of the surgical suture in patients with acute Achilles tendon. The results showed that the Bunnell method had primary suture stability than the Kessler method, and PDS had higher suture strength. It indicates that PDS as a suture material can help connect the broken end of the human Achilles tendon and play a role in fixation and support. Ji et al. (2015) compared the effect of PDSII and Ethibond W4843 surgical sutures in treating acute Achilles tendon rupture. By postoperative observation, the two suture biomedical materials had an almost consistent therapeutic effect in incision infection and re-rupture rate, but in the follow-up score, the wound healing effect of PDSII was slightly inferior to Ethibond. Yildirim et al. (2006) found that the two PDS sutures had the highest tendon stress, indicating that PDS has the loading capacity and excellent elastic properties, plays a tight junction role in the healing of fresh Achilles tendon, and provides practical help for the tissue healing and cell regeneration of Achilles tendon rupture.

Some scholars have also reported that using PDS and non-use of PDS as carrier substances for repairing the Achilles tendon will have different therapeutic effects. Meimandi-Parizi et al. (2013) used collagen and collagen-PDS implants to reconstruct Achilles tendon defects. Studies have shown that with the introduction of PDS materials, the biomechanical properties of the experimental group have been significantly improved, the necrotic tissue around the injured tendon has been reduced, and the soft tissue adhesion around the Achilles tendon has also been effectively inhibited.

In summary, PDS has the advantages of good degradability and biocompatibility and is now widely used in the field of clinical medicine, such as surgical sutures, which can provide vital help for the future of Achilles tendon rupture and promote the rapid recovery of the mechanical characteristics and functional level of the Achilles tendon.

EFFECT OF OTHER MATERIALS ON ACHILLES TENDON REPAIR

Pietschmann et al. (2013) prepared Polyglycolic acid (PGA) scaffolds for bridge Achilles tendon rupture in rats. The study results showed that the application of MSC significantly improved the healing rate of the Achilles tendon compared with the PGA scaffold alone group.

Nguyen et al. (2020) studied the effect of polyethene (PE) sutures in repairing human Achilles tendon rupture and evaluated the mechanical properties of the suture. The results showed that PE could be used as a medical polymer material to suture human Achilles tendon rupture, but the tensile resistance and degradability are general.

Cai et al. (2018) seeded allogeneic bone marrow stem cells (BMSCs) were on polyethylene terephthalate (PET) scaffolds and then implanted into rabbit unilateral Achilles tendon defects. The results showed that 12 weeks after surgery, the BMSCs-PET group was significantly more substantial than the control PET group in terms of type I and III collagen fibres and mechanical characteristics. In addition, researchers have simulated the fibrous structure of Achilles tendons with different structures of polypropylene (PP) and PET, and PET Achilles tendons showed some anti-fatigue and appropriate creep characteristics (Morais et al., 2020). Unlike the above studies, Gall et al. (2009) investigated the mechanical stability of polypropylene (PP) shapes in repairing distal Achilles tendon ruptures in dogs. The results showed that PP could be used as a medical polymer material to repair the Achilles tendon after surgery.

CONLUSION

The ideal scaffold material is still a critical issue for tendon tissue engineering. The research results of scaffold materials will directly promote the development of tendon tissue engineering and have broad clinical application prospects. In this review, we summarized the progress of biodegradable polymers, such as PCL, PLA, PLGA, PTMC, and PDS, in treating Achilles tendon injury. The biodegradable polymers loaded with stem cells or drugs can significantly improve the Achilles tendon injury repair effect. Although the research and application of scaffold materials derived from biodegradable polymers in tendon tissue engineering have succeeded, the currently used materials may have biocompatibility and degradability problems or have defects such as poor mechanical properties complex in processing and moulding. There are still some problems in applying biodegradable polymers to repair Achilles tendon injury that needs to be further explored; for example, are the adverse effects of biodegradable polymers on human function significant? Can the patient be helped to maximize functional recovery? Can tissue-engineered scaffold materials produce relatively ideal therapeutic results in humans and animal models? Are there differences in physiological and biomechanical properties between regenerated and native Achilles tendons? The above problems still need further study to be solved. Therefore, developing synthetic materials and modified natural materials to make them an ideal scaffold material that meets the requirements is an essential direction of repairing Achilles tendon injury. With the continuous development and close cooperation of life sciences and material sciences, ideal materials for repairing Achilles tendon injuries will undoubtedly be produced. The treatment of Achilles tendon

injuries will be more straightforward, which will be a boon for many athletes.

AUTHOR CONTRIBUTIONS

JZ and WW wrote this article and equally contributed to this work; JCZ revised this article; XZ and LY checked and review this article.

FUNDING

This work was supported by the Liaoning Revitalization Talents Program (XLYC1807142), the Department of Science and Technology of Liaoning Province (2018225079), the Educational Department of Liaoning Province (ZF2019040), and the Shenyang Science and Technology Bureau (RC190426).

REFERENCES

An, J., Chua, C. K., Leong, K. F., Chen, C.-H., and Chen, J.-P. (2012). Solvent-free Fabrication of Three Dimensionally Aligned Polycaprolactone Microfibers for Engineering of Anisotropic Tissues. *Biomed. Microdevices* 14 (5), 863–872. doi:10.1007/s10544-012-9666-3

Araque-Monrós, M. C., Gamboa-Martínez, T. C., Santos, L. G., Bernabé, S. G., Pradas, M. M., and Estellés, J. M. (2013). New Concept for a Regenerative and Resorbable Prosthesis for Tendon and Ligament: Physicochemical and Biological Characterization of PLA-Braided Biomaterial. *J. Biomed. Mater. Res. A.* 101 (11), 3228–3237. doi:10.1002/jbm.a.34633

Awad, H. A., Boivin, G. P., Dressler, M. R., Smith, F. N. L., Young, R. G., and Butler, D. L. (2003). Repair of Patellar Tendon Injuries Using a Cell-Collagen Composite. *J. Orthop. Res.* 21 (3), 420–431. doi:10.1016/s0736-0266(02)00163-8

Blaya, F., Pedro, P. S., Pedro, A. B. S., Lopez-Silva, J., Juanes, J. A., and D'Amato, R. (2019). Design of a Functional Splint for Rehabilitation of Achilles Tendon Injury Using Advanced Manufacturing (AM) Techniques. Implementation Study. *J. Med. Syst.* 43 (5), 122–215. doi:10.1007/s10916-019-1247-z

Bosworth, L. A., Alam, N., Wong, J. K., and Downes, S. (2013). Investigation of 2D and 3D Electrospun Scaffolds Intended for Tendon Repair. *J. Mater. Sci. Mater. Med.* 24 (6), 1605–1614. doi:10.1007/s10856-013-4911-8

Cai, J., Yang, Y., Ai, C., Jin, W., Sheng, D., Chen, J., et al. (2018). Bone Marrow Stem Cells-Seeded Polyethylene Terephthalate Scaffold in Repair and Regeneration of Rabbit Achilles Tendon. *Artif. Organs* 42 (11), 1086–1094. doi:10.1111/aor.13298

Cai, J., Xie, X., Li, D., Wang, L., Jiang, J., Mo, X., et al. (2020). A Novel Knitted Scaffold Made of Microfiber/nanofiber Core-Sheath Yarns for Tendon Tissue Engineering. *Biomater. Sci.* 8 (16), 4413–4425. doi:10.1039/d0bm00816h

Cao, D., Liu, W., Wei, X., Xu, F., Cui, L., and Cao, Y. (2006). *In Vitro* tendon Engineering with Avian Tenocytes and Polyglycolic Acids: a Preliminary Report. *Tissue Eng.* 12 (5), 1369–1377. doi:10.1089/ten.2006.12.1369

Cerrato, R., and Switaj, P. (2017). Using Arthroscopic Techniques for Achilles Pathology. *Foot Ankle Clin.* 22 (4), 781–799. doi:10.1016/j.fcl.2017.07.007

Chen, J., Xu, J., Wang, A., and Zheng, M. (2009). Scaffolds for Tendon and Ligament Repair: Review of the Efficacy of Commercial Products. *Expert Rev. Med. Devices* 6 (1), 61–73. doi:10.1586/17434440.6.1.61

Chen, C.-H., Chen, S.-H., Kuo, C.-Y., Li, M.-L., and Chen, J.-P. (2017). Response of Dermal Fibroblasts to Biochemical and Physical Cues in Aligned Polycaprolactone/silk Fibroin Nanofiber Scaffolds for Application in Tendon Tissue Engineering. *Nanomaterials* 7 (8), 219. doi:10.3390/nano7080219

Chen, Y., Shen, W., Tang, C., Huang, J., Fan, C., Yin, Z., et al. (2020). Targeted Pathological Collagen Delivery of Sustained-Release Rapamycin to Prevent Heterotopic Ossification. *Sci. Adv.* 6 (18), eaay9526. doi:10.1126/sciadv.aay9526

Choi, H. J., Choi, S., Kim, J. G., Song, M. H., Shim, K.-S., Lim, Y.-M., et al. (2020). Enhanced Tendon Restoration Effects of Anti-inflammatory, Lactoferrin-Immobilized, Heparin-Polymeric Nanoparticles in an Achilles Tendinitis Rat Model. *Carbohydr. Polym.* 241, 116284. doi:10.1016/j.carbpol.2020.116284

Czarnecki, J. S., Lafdi, K., Joseph, R. M., and Tsonis, P. A. (2012). Hybrid Carbon-Based Scaffolds for Applications in Soft Tissue Reconstruction. *Tissue Eng. Part. A.* 18 (9-10), 946–956. doi:10.1089/ten.TEA.2011.0533

Dams, O. C., van den Akker-Scheek, I., Diercks, R. L., Wendt, K. W., Zwerver, J., and Reininga, I. H. F. (2019). Surveying the Management of Achilles Tendon Ruptures in the Netherlands: Lack of Consensus and Need for Treatment Guidelines. *Knee Surg. Sports Traumatol. Arthrosc.* 27 (9), 2754–2764. doi:10.1007/s00167-018-5049-5

Deng, D., Wang, W., Wang, B., Zhang, P., Zhou, G., Zhang, W. J., et al. (2014). Repair of Achilles Tendon Defect with Autologous ASCs Engineered Tendon in a Rabbit Model. *Biomaterials* 35 (31), 8801–8809. doi:10.1016/j.biomaterials.2014.06.058

Dong, L., Li, L., Song, Y., Fang, Y., Liu, J., Chen, P., et al. (2021). MSC-derived Immunomodulatory Extracellular Matrix Functionalized Electrospun Fibers for Mitigating Foreign-Body Reaction and Tendon Adhesion. *Acta Biomater.* 133, 280–296. doi:10.1016/j.actbio.2021.04.035

Duek, J. R., Riquetto, M. L., Jesus, D. C., Sabongi, J. J., Barbo, M. d. L. P. B., Duek, E. A. d. R., et al. (2014). Membrana de PLDLA-TMC como Protetor na Regeneração Do Tendão Calcâneo. Estudo *In Vivo* em Coelhos. *Polímeros* 24 (3), 360–366. doi:10.4322/polimeros.2014.021

El Khatib, M., Mauro, A., Wyrwa, R., Di Mattia, M., Turriani, M., Di Giacinto, O., et al. (2020). Fabrication and Plasma Surface Activation of Aligned Electrospun PLGA Fiber Fleeces with Improved Adhesion and Infiltration of Amniotic Epithelial Stem Cells Maintaining Their Teno-Inductive Potential. *Molecules* 25 (14), 3176. doi:10.3390/molecules25143176

Funakoshi, T., Majima, T., Iwasaki, N., Suenaga, N., Sawaguchi, N., Shimode, K., et al. (2005). Application of Tissue Engineering Techniques for Rotator Cuff Regeneration Using a Chitosan-Based Hyaluronan Hybrid Fiber Scaffold. *Am. J. Sports Med.* 33 (8), 1193–1201. doi:10.1177/0363546504272689

Gall, T. T., Santoni, B. G., Egger, E. L., Puttlitz, C. M., and Rooney, M. B. (2009). *In Vitro* biomechanical Comparison of Polypropylene Mesh, Modified Three-Loop Pulley Suture Pattern, and a Combination for Repair of Distal Canine Achilles' Tendon Injuries. *Vet. Surg.* 38 (7), 845–851. doi:10.1111/j.1532-950x.2009.00598.x

Ganestam, A., Kallemose, T., Troelsen, A., and Barfod, K. W. (2016). Increasing Incidence of Acute Achilles Tendon Rupture and a Noticeable Decline in Surgical Treatment from 1994 to 2013. A Nationwide Registry Study of 33,160 Patients. *Knee Surg. Sports Traumatol. Arthrosc.* 24 (12), 3730–3737. doi:10.1007/s00167-015-3544-5

Garvin, J., Qi, J., Maloney, M., and Banes, A. J. (2003). Novel System for Engineering Bioartificial Tendons and Application of Mechanical Load. *Tissue Eng.* 9 (5), 967–979. doi:10.1089/107632703322495619

Gebauer, M., Beil, F. T., Beckmann, J., Sárváry, A. M., Ueblacker, P., Ruecker, A. H., et al. (2007). Mechanical Evaluation of Different Techniques for Achilles Tendon Repair. *Arch. Orthop. Trauma Surg.* 127 (9), 795–799. doi:10.1007/s00402-007-0325-8

He, Q., Li, Q., Chen, B., and Wang, Z. (2002). Repair of Flexor Tendon Defects of Rabbit with Tissue Engineering Method. *Chin. J. Traumatol.* 5 (4), 200–208.

Hu, J. Z., Zhou, Y. C., Huang, L. H., and Lu, H. B. (2013). Development of Biodegradable Polycaprolactone Film as an Internal Fixation Material to Enhance Tendon Repair: an *In Vitro* Study. *BMC Musculoskelet. Disord.* 14 (1), 246–248. doi:10.1186/1471-2474-14-246

Jao, D., Mou, X., and Hu, X. (2016). Tissue Regeneration: a Silk Road. *J. Funct. Biomater.* 7 (3), 22. doi:10.3390/jfb7030022

Jayasree, A., Kottappally Thankappan, S., Ramachandran, R., Sundaram, M. N., Chen, C.-H., Mony, U., et al. (2019). Bioengineered Braided Micro-nano (Multiscale) Fibrous Scaffolds for Tendon Reconstruction. *ACS Biomater. Sci. Eng.* 5 (3), 1476–1486. doi:10.1021/acsbiomaterials.8b01328

Ji, W., Yang, F., Ma, J., Bouma, M. J., Boerman, O. C., Chen, Z., et al. (2013). Incorporation of Stromal Cell-Derived Factor-1α in PCL/gelatin Electrospun Membranes for Guided Bone Regeneration. *Biomaterials* 34 (3), 735–745. doi:10.1016/j.biomaterials.2012.10.016

Ji, Y., Ma, X., Wang, X., Huang, J., Zhang, C., and Chen, L. (2015). Different Sutures in the Surgical Treatment of Acute Closed Achilles Tendon Rupture. *Indian J. Surg.* 77 (3), 936–940. doi:10.1007/s12262-014-1068-8

Juncosa-Melvin, N., Boivin, G. P., Galloway, M. T., Gooch, C., West, J. R., and Butler, D. L. (2006). Effects of Cell-To-Collagen Ratio in Stem Cell-Seeded Constructs for Achilles Tendon Repair. *Tissue Eng.* 12 (4), 681–689. doi:10.1089/ten.2006.12.681

Kazimoğlu, C., Bölükbaşi, S., Kanatli, U., Senköylü, A., Altun, N. S., Babaç, C., et al. (2003). A Novel Biodegradable PCL Film for Tendon Reconstruction: Achilles Tendon Defect Model in Rats. *Int. J. Artif. Organs* 26 (9), 804–812.

Lee, T. H., Kim, S. E., Lee, J. Y., Kim, J. G., Park, K., and Kim, H.-J. (2019). Wrapping of Tendon Tissues with Diclofenac-Immobilized Polycaprolactone Fibrous Sheet Improves Tendon Healing in a Rabbit Model of Collagenase-Induced Achilles Tendinitis. *J. Ind. Eng. Chem.* 73, 152–161. doi:10.1016/j.jiec.2019.01.018

Li, P. H., Liu, S. Y., Huang, J. X., Peng, J., Lu, S., and Guo, Q. (2017). *In Vitro* preparation and Characterization of Dual Biomimetic Electrospun Wharton's Jelly-Derived Extra Cellular Matrix/polycaprolactone Sub-micron Fibrous Band-Aid for superior Achilles Tendon Recovery. *Int. J. Clin. Exp. Med.* 10, 11563–11573.

Li, X., Chen, H., Xie, S., Wang, N., Wu, S., Duan, Y., et al. (2020). Fabrication of Photo-Crosslinkable Poly(Trimethylene Carbonate)/Polycaprolactone Nanofibrous Scaffolds for Tendon Regeneration. *Int. J. Nanomedicine* 15, 6373–6383. doi:10.2147/ijn.s246966

Liu, W., Lipner, J., Moran, C. H., Feng, L., Li, X., Thomopoulos, S., et al. (2015). Generation of Electrospun Nanofibers with Controllable Degrees of Crimping through a Simple, Plasticizer-Based Treatment. *Adv. Mater.* 27 (16), 2583–2588. doi:10.1002/adma.201500329

Majima, T., Funakosi, T., Iwasaki, N., Yamane, S.-T., Harada, K., Nonaka, S., et al. (2005). Alginate and Chitosan Polyion Complex Hybrid Fibers for Scaffolds in Ligament and Tendon Tissue Engineering. *J. Orthopaedic Sci.* 10 (3), 302–307. doi:10.1007/s00776-005-0891-y

Meimandi-Parizi, A., Oryan, A., and Moshiri, A. (2013). Tendon Tissue Engineering and its Role on Healing of the Experimentally Induced Large Tendon Defect Model in Rabbits: a Comprehensive *In Vivo* Study. *PloS one* 8 (9), e73016. doi:10.1371/journal.pone.0073016

Moffat, K. L., Kwei, A. S.-P., Spalazzi, J. P., Doty, S. B., Levine, W. N., and Lu, H. H. (2009). Novel Nanofiber-Based Scaffold for Rotator Cuff Repair and Augmentation. *Tissue Eng. A* 15 (1), 115–126. doi:10.1089/ten.tea.2008.0014

Morais, D. S., Cruz, J., Fangueiro, R., Lopes, H., Guedes, R. M., and Lopes, M. A. (2020). Mechanical Behavior of Ropes Based on Polypropylene (PP) and Poly(ethylene Terephthalate) (PET) Multifilament Yarns for Achilles Tendon Partial Substitution. *J. Mech. Behav. Biomed. Mater.* 106, 103734. doi:10.1016/j.jmbbm.2020.103734

Moshiri, A., Oryan, A., and Meimandi-Parizi, A. (2015). Synthesis, Development, Characterization and Effectiveness of Bovine Pure Platelet Gel-Collagen-Polydioxanone Bioactive Graft on Tendon Healing. *J. Cel. Mol. Med.* 19 (6), 1308–1332. doi:10.1111/jcmm.12511

Nguyen, T. P., Keyt, L. K., Herfat, S., Gordon, L., and Palanca, A. (2020). Biomechanical Study of a Multifilament Stainless Steel cable Crimp System versus a Multistrand Ultra-high Molecular Weight Polyethylene Polyester Suture Krackow Technique for Achilles Tendon Rupture Repair. *J. Foot Ankle Surg.* 59 (1), 86–90. doi:10.1053/j.jfas.2019.01.022

Oryan, A., Moshiri, A., Parizi, A. M., and Maffulli, N. (2014). Implantation of a Novel Biologic and Hybridized Tissue Engineered Bioimplant in Large Tendon Defect: an *In Vivo* Investigation. *Tissue Eng. Part. A.* 20 (3-4), 447–465. doi:10.1089/ten.TEA.2013.0053

Ouyang, H. W., Goh, J. C. H., Mo, X. M., Teoh, S. H., and Lee, E. H. (2002). The Efficacy of Bone Marrow Stromal Cell-Seeded Knitted PLGA Fiber Scaffold for Achilles Tendon Repair. *Ann. N Y Acad. Sci.* 961 (1), 126–129. doi:10.1111/j.1749-6632.2002.tb03064.x

Ouyang, H. W., Goh, J. C. H., Thambyah, A., Teoh, S. H., and Lee, E. H. (2003). Knitted Poly-Lactide-Co-Glycolide Scaffold Loaded with Bone Marrow Stromal Cells in Repair and Regeneration of Rabbit Achilles Tendon. *Tissue Eng.* 9 (3), 431–439. doi:10.1089/107632703322066615

Pietschmann, M. F., Frankewycz, B., Schmitz, P., Docheva, D., Sievers, B., Jansson, V., et al. (2013). Comparison of Tenocytes and Mesenchymal Stem Cells Seeded on Biodegradable Scaffolds in a Full-Size Tendon Defect Model. *J. Mater. Sci. Mater. Med.* 24 (1), 211–220. doi:10.1007/s10856-012-4791-3

Reverchon, E., Baldino, L., Cardea, S., and De Marco, I. (2012). Biodegradable Synthetic Scaffolds for Tendon Regeneration. *Muscles Ligaments Tendons J.* 2 (3), 181–186.

Sahoo, S., Toh, S. L., and Goh, J. C. H. (2010). A bFGF-Releasing silk/PLGA-Based Biohybrid Scaffold for Ligament/tendon Tissue Engineering Using Mesenchymal Progenitor Cells. *Biomaterials* 31 (11), 2990–2998. doi:10.1016/j.biomaterials.2010.01.004

Sato, M., Maeda, M., Kurosawa, H., Inoue, Y., Yamauchi, Y., and Iwase, H. (2000). Reconstruction of Rabbit Achilles Tendon with Three Bioabsorbable Materials: Histological and Biomechanical Studies. *J. Orthopaedic Sci.* 5 (3), 256–267. doi:10.1007/s007760050161

Schoenenberger, A. D., Foolen, J., Moor, P., Silvan, U., and Snedeker, J. G. (2018). Substrate Fiber Alignment Mediates Tendon Cell Response to Inflammatory Signaling. *Acta Biomater.* 71, 306–317. doi:10.1016/j.actbio.2018.03.004

Shieh, S.-J., Zimmerman, M. C., and Parsons, J. R. (1990). Preliminary Characterization of Bioresorbable and Nonresorbable Synthetic Fibers for the Repair of Soft Tissue Injuries. *J. Biomed. Mater. Res.* 24 (7), 789–808. doi:10.1002/jbm.820240702

Song, Z., Shi, B., Ding, J., Zhuang, X., Zhang, X., Fu, C., et al. (2015). A Comparative Study of Preventing Postoperative Tendon Adhesion Using Electrospun Polyester Membranes with Different Degradation Kinetics. *Sci. China Chem.* 58 (7), 1159–1168. doi:10.1007/s11426-015-5425-7

Song, Z.-m., Shi, B., Ding, J.-x., Zhuang, X.-l., Zhang, X.-n., Fu, C.-f., et al. (2015). Prevention of Postoperative Tendon Adhesion by Biodegradable Electrospun Membrane of Poly(lactide-Co-Glycolide). *Chin. J. Polym. Sci.* 33 (4), 587–596. doi:10.1007/s10118-015-1611-5

Vuornos, K., Björninen, M., Talvitie, E., Paakinaho, K., Kellomäki, M., Huhtala, H., et al. (2016). Human Adipose Stem Cells Differentiated on Braided Polylactide Scaffolds Is a Potential Approach for Tendon Tissue Engineering. *Tissue Eng. Part. A.* 22 (5-6), 513–523. doi:10.1089/ten.tea.2015.0276

Wang, W., Deng, D., Wang, B., Zhou, G., Zhang, W., Cao, Y., et al. (2017). * Comparison of Autologous, Allogeneic, and Cell-free Scaffold Approaches for Engineered Tendon Repair in a Rabbit Model-A Pilot Study. *Tissue Eng. Part. A.* 23 (15-16), 750–761. doi:10.1089/ten.TEA.2016.0447

Weng, C.-J., Lee, D., Ho, J., and Liu, S.-J. (2020). Doxycycline-Embedded Nanofibrous Membranes Help Promote Healing of Tendon Rupture. *Int. J. Nanomedicine* 15, 125–136. doi:10.2147/ijn.s217697

Yan, Z., Meng, X., Su, Y., Chen, Y., Zhang, L., and Xiao, J. (2021). Double Layer Composite Membrane for Preventing Tendon Adhesion and Promoting Tendon Healing. *Mater. Sci. Eng. C* 123, 111941. doi:10.1016/j.msec.2021.111941

Yildirim, Y., Saygi, B., Kara, H., Cabukoğlu, C., and Esemenli, T. (2006). Tendon Holding Capacities of the Suture Materials Used in Repairing Achilles Tendon Rupture. *Acta Orthop. Traumatol. Turc.* 40 (2), 164–168.

Yuan, B., He, C., Dong, X., Wang, J., Gao, Z., Wang, Q., et al. (2015). 5-Fluorouracil Loaded Thermosensitive PLGA-PEG-PLGA Hydrogels for the Prevention of Postoperative Tendon Adhesion. *RSC Adv.* 5 (32), 25295–25303. doi:10.1039/c5ra01307k

Zhang, W., Yang, Y., Zhang, K., Li, Y., and Fang, G. (2015). Weft-knitted Silk-Poly(lactide-Co-Glycolide) Mesh Scaffold Combined with Collagen Matrix and Seeded with Mesenchymal Stem Cells for Rabbit Achilles Tendon Repair. *Connect. Tissue Res.* 56 (1), 25–34. doi:10.3109/03008207.2014.976309

Zhao, T., Qi, Y., Xiao, S., Ran, J., Wang, J., Ghamor-Amegavi, E. P., et al. (2019). Integration of Mesenchymal Stem Cell Sheet and bFGF-Loaded Fibrin Gel in Knitted PLGA Scaffolds Favorable for Tendon Repair. *J. Mater. Chem. B* 7 (13), 2201–2211. doi:10.1039/c8tb02759e

Zou, J., Lu, M., Chen, S., Cai, C., Yao, Z., Cui, W., et al. (2020). Beeswax-inspired Superhydrophobic Electrospun Membranes for Peritendinous Anti-adhesion. *Mater. Sci. Eng. C* 116, 111166. doi:10.1016/j.msec.2020.111166

Conflict of Interest: The authors declare that the research was conducted in the absence of any commercial or financial relationships that could be construed as a potential conflict of interest.

Publisher's Note: All claims expressed in this article are solely those of the authors and do not necessarily represent those of their affiliated organizations, or those of the publisher, the editors and the reviewers. Any product that may be evaluated in this article, or claim that may be made by its manufacturer, is not guaranteed or endorsed by the publisher.

frontiers in Bioengineering and Biotechnology

ORIGINAL RESEARCH
published: 04 March 2022
doi: 10.3389/fbioe.2022.856986

In Vitro Study of Degradation and Cytocompatibility of Ceramics/PLA Composite Coating on Pure Zinc for Orthopedic Application

Shenghui Su[1], *Qiangqiang Tang*[2] *and Dongbin Qu*[1,3]*

[1]Division of Spine Surgery, Department of Orthopaedics, Nanfang Hospital, Southern Medical University, Guangzhou, China, [2]School of Materials Science and Engineering, South China University of Technology, Guangzhou, China, [3]Department of Orthopaedic Surgery, Zengcheng Branch of Nanfang Hospital, Southern Medical University, Guangzhou, China

Zinc and its alloys are considered to be next-generation materials for fabricating absorbable biomedical devices. However, cytotoxicity has been reported to be associated with rapid degradation. To address these issues, a composite coating (PLA/Li-OCP) consisting of $CaHPO_4$ conversion coating (Ca-P) and polylactic acid (PLA) decorated with Li-octacalcium phosphate particles was constructed on pure zinc. The immersion tests showed that the presence of Ca-P coating and PLA/Li-OCP coating on pure zinc could reduce the pH value. Compared with Ca-P coating, the introduction of the PLA/Li-OCP film on the Ca-P-coated samples could enhance the corrosion resistance, and there was one order of magnitude decrease in the corrosion current density. The cytocompatibility assay suggested that the PLA/Li-OCP coating favored the cell viability and upregulated the expression of related osteogenic-genes including RUNX2, OCN, and BMP. Therefore, the presence of the PLA/Li-OCP coating on pure zinc could effectively improve the degradation rate and cytocompatibility of pure zinc.

Keywords: zinc, biodegradation behavior, cytocompatibility, PLA film, pH

OPEN ACCESS

Edited by:
Liqun Yang,
China Medical University, China

Reviewed by:
Yujing Liu,
Changsha University of Science and Technology, China
Yingchao Su,
Stony Brook University, United States

***Correspondence:**
Dongbin Qu
nfyy_qu@126.com

Specialty section:
This article was submitted to Biomaterials, a section of the journal Frontiers in Bioengineering and Biotechnology

Received: *18 January 2022*
Accepted: *28 January 2022*
Published: *04 March 2022*

Citation:
Su S, Tang Q and Qu D (2022) In Vitro Study of Degradation and Cytocompatibility of Ceramics/PLA Composite Coating on Pure Zinc for Orthopedic Application. Front. Bioeng. Biotechnol. 10:856986. doi: 10.3389/fbioe.2022.856986

INTRODUCTION

Biodegradable metals such as iron, magnesium, and zinc are steadily considered to be next-generation materials for manufacturing absorbable biomedical devices due to their good mechanical properties. Currently, magnesium and iron have been studied widely because of their low elastic modulus and excellent biocompatibility. However, one of the issues against magnesium-based alloys for their clinical application is due to their rapid degradation rate and subsequent evolution of hydrogen gas in the human body environment, whereas the degradation rate of iron is very slow (Liu et al., 2018; Kabir et al., 2021; Mo et al., 2021). In contrast, the corrosion potential of zinc is between magnesium and iron, meaning that the corrosion rate of zinc falls in between that of magnesium and iron (Tong et al., 2020). Meanwhile, bone formation is closely related to zinc. Zinc deficiency would cause growth failure, neuropathy, dystocia, hypothermia, etc. (Chabosseau & Rutter, 2016). Given this, zinc and its alloys are very suitable for clinical usage, which has gained extensive interest in 2013 after the report of a landmark research from Bowen et al. (2013). According to their study, they implanted pure zinc in the rat abdominal aorta to simulate the degradation behavior of stents and found that zinc showed ideal degradation behavior in rat blood vessels compared with magnesium and iron alloys *in vivo* and that corrosion product also had good

biocompatibility. Therefore, they reported that zinc and its alloys are a promising candidate as a bioabsorbable stent in the next generation.

However, cytotoxicity has been reported to be associated with the Zn^{2+} concentration released from zinc and its alloys (Murni et al., 2015; Alves et al., 2017). For example, Ma et al. demonstrated that a certain concentration of zinc ion, approximately 6.50 ppm, could inhibit cell proliferation. Peng et al. (2021) revealed that almost few cells could stay alive when the cell was directly exposed to the zinc surface (Zhu M et al., 2019). In this case, a perceived drawback of zinc is that higher concentrations of Zn^{2+} released from zinc-based alloy would induce cytotoxicity response to different cells including osteoblast. Therefore, promoting zinc and its alloys' transfer to clinical applications still face the key issue that the high concentration of zinc ions accumulated around zinc-based implants would deteriorate the biocompatibility of implant (Zhu M et al., 2019).

Surface modification is an impactful strategy to enhance the biocompatibility of the implant by controlling the release rate of zinc ions (Pathak & Pandey, 2020; Pezzato et al., 2020; Sheng et al., 2020; Serdechnova et al., 2021). For this purpose, many studies have been focused on the improvement of bioactivity and biodegradability *via* developing surface treatments, such as PEO coating, chemical conversion coating, electrochemical deposition coating, and polymer coating (Peng et al., 2021). Conversion coating has been widely used to enhance corrosion resistance and upgrade bioactivity and biocompatibility of magnesium and its alloys by reacting magnesium with electrolyte in the bath, which is considered to be an efficient, feasible, easily applicable cost-effective way of protecting zinc and its alloys (Hafeez et al., 2020). Moreover, the calcium and zinc phosphate conversion coatings with intrinsic bioactivity and biocompatibility are proverbially produced on many biomaterials thanks to their similar composition to carbonated apatite in natural bone tissue (Guo et al., 2020; Hafeez et al., 2020). Attempts have been conducted to produce kinds of conversion coatings on zinc and its alloys (Gao et al., 2021; Zhang et al., 2020). For example, Mo et al. (2021) fabricated a zinc phosphate (ZnP) coating with decorating alendronate on zinc to improve the degradation rate and the bio-functionality and found that the coating not only improves the release rate of zinc ions but also showed the ability with balancing osteo-functionality of anti-osteoclast and pro-osteoblast response. Zhang et al. (2020) designed and fabricated a zinc-phosphate (ZnP) coating containing graphene oxide (GO) on pure zinc to control the degradation behavior of next-generation bioabsorbable implant and found that a Zn alloy scaffold with Ca-P coating could modulate Zn2+ release rate and demonstrated that the Ca-P coating could contribute to the osteogenic differentiation of BMSCs (Zhuang et al., 2021). However, the main drawback of the conversion coatings is that there is the presence of pores and cracks on the coatings, which would cause the solution to permeate into the substrate (Su et al., 2019).

Preparing a polymer film on the conversion coatings with defects can address this issue. Ostrowski et al. (2013) sealed microcracks of the MAO coating by PLLA film. Lu et al. (2011) prepared a PLA film on the Ca-P conversion coating to propose a composite coating on AZ91alloy. Their results indicated that this composite coating could reduce the biodegradation (Kannan & Liyanaarachchi, 2013). Electrochemical tests showed that the composite coating can effectively improve the polarization resistance of AZ91. et al. modified the pure zinc with the film of poly (L-lactic acid) (PLLA). The *in vivo* study suggested that the PLLA could reduce the corrosion resistance of pure zinc (Shamoli et al., 2017). Moreover, to further improve the bioactivity of the polymer films on the conversion coatings, some studies reported that bioactive elements and matters were loaded into the polymer film to promote osteogenic differentiation. doped the Li element into the MAO coating to enhance the osteogenic differentiation. The *in vitro* study suggested that the osteogenic-related gene expression was upregulated by the Li addition (Lin et al., 2021). Galli et al. noted that the differentiation of bone marrow MSCs on the titanium was improved by the Li addition on coating *via* the wnt/β-catenin signal. González-García & Monje (2013) doped octacalcium phosphate (OCP, $Ca_8H_2(PO_4)_6{\cdot}5H_2O$) into the nanofibers consisting of poly(lactic-co-glycolic acid) (PLGA)/poly(caprolactone) (PCL) *via* electrospinning, and found that the nanofibers with doping OCP could upregulate the gene expression of bone-specific markers (Wang et al., 2019). Heydari et al. fabricated a novel scaffold consisting of polycaprolactone (PCL) and OCP particles. The results showed that OCP particles favored the growth of the osteoblast (Heydari et al., 2017).

Currently, the considerable attraction with zinc mainly lies in the design and development of zinc-based alloys (Ren et al., 2019; Yin et al., 2019; Zhu S et al., 2019; Tong et al., 2020), focusing on the improvement of mechanical properties, and biocompatibility evaluation. However, there are rather few studies on improving corrosion resistance and cytocompatibility for biomedical zinc *via* surface modification. Herein, the calcium phosphate conversion coatings were produced on pure zinc, following doping with a polylactic acid (PLA) with decorating Li-OCP particles to improve the biocompatibility. The microstructure, biodegradable rate, and cytocompatibility were studied to estimate the feasibility of pure zinc with Ca-P coating for clinical application.

EXPERIMENTAL DETAILS

Materials Preparation

A zinc bar (Zn ≥ 99.99%) was cut into disk specimens with dimensions of Φ10 × 2 mm. These samples were ground with sandpapers to 2000#, ultrasonically cleaned with deionized water, respectively, and then dried in a drying cabinet. Whereafter, the samples were exposed to an acidic calcium phosphate electrolyte consisting of 0.12 M NaH_2PO_4, 0.20 M $CaCl_2$, and 0.10 M $Na_2EDTA{\cdot}2H_2O$ with the pH of 3.50 for 6 h at 100°C in autoclaves. Then, the obtained Ca-P-coated samples were washed 3 times using deionized water and dried. The Li-OCP particles were fabricated by the following method: 0.009 mol NH_4PO_3 and 0.03 mol CH_4N_2O were mixed in 300 ml of

distilled water for 30 min at room temperature (named A solution), while 0.01188 mol calcium acetate and 0.00012 mol of lithium chloride were mixed in 300 ml of distilled water for 30 min at room temperature (named B solution). Subsequently, solution B was added to solution A and stirred for 5 min (solution C). Solution C was heated to 90°C in a water bath with stirring for 2 h. The Li-OCP particles were obtained after the reaction. The PLA powders and Li-OCP particles were mixed and PLA was dissolved in chloroform solvent to fabricate the PLA/Li-OCP solution. Then, the Ca-P-coated samples were dipped in PLA/Li-OCP solution and pulled out rapidly to produce the PLA/Li-OCP coating on the Ca-P-coated samples (named PLA/Li-OCP-coated sample). The weight ratio of the PLA powders and Li-OCP particles was 400:1.

Coating Analysis

A scanning electron microscope was used to observe the morphologies of coated zinc. The chemical compositions and phase of the Ca-P coatings were analyzed by energy spectroscopy (EDS) and x-ray diffraction, with the radiation source being Cu-K α with a scanning speed of 5°. The chemical valence state of coatings was characterized by x-ray photoelectron spectroscopy (XPS, ESCALAB 250Xi, Thermo Fisher) equipped with a monochromatic Al-K α (1,486.60 eV). The C1s peak located at the binding energy of 284.80 eV was used for the charge correction. The wettability of coatings was analyzed by a contact angle meter.

Immersion Test

The corrosion rate of the coated samples was studied *via* immersion test in simulated body fluid (SBF) solution at 37 ± 0.50°C for 21 days. The volume of solution to the immersed area of the surface was 1.25 ml/cm^2. To imitate a dynamic circulation environment in the human body, the SBF solution was refreshed every 3 days. At each time point, the pH value was recorded by a pH meter. After 21 days of immersion, the immersed coated zinc was washed by deionized water and dried in air. Scanning electron microscopy was used to observe the morphology.

Electrochemical Tests

The corrosion resistance of coated zinc was measured *via* potential polarization curve and electrochemical impedance spectroscopy (EIS) using a Princeton Model 273A electrochemical work station in SBF solution. In the electrochemical test, the pure zinc and coated zinc were used as the working electrode, platinum sheet was used as the auxiliary electrode, and saturated mercuric electrode was used as the parameter electrode. In the dynamic potential polarization test, an applied potential ranged from −0.50 V to +1.50 V relative to OCP with a scanning velocity of 1 mV/s. The frequency ranging from 105 Hz to 10–2 Hz was used applying 10 mV perturbation in the EIS test.

Cell Viability

Pre-osteoblast cell lines MC3T3-E1 were used to analyze the cytotoxicity. The MC3T3-E1 were cultured with studied samples in Dulbecco's modified Eagle's medium (DMEM) containing 100 U/ml penicillin, 10% fetal bovine serum (FBS), and 100 μg/mg streptomycin in an incubator with humid 5% CO_2. The cytotoxicity was measured using MTT according to operating instructions. The studied coated zinc and uncoated zinc were soaked in DMEM to extract the immersion at 37°C for 3 days. The cells with a density of 5× 10^4/well were seeded in a 96-well plate for 1, 3, and 5 days, respectively. The medium was refreshed every day. According to the manufacturer's protocol, the cell viability in terms of optical density (OD) values was obtained at a wavelength of 490 nm in a microplate reader. Meanwhile, 5×10^4 cells/ml were seeded on samples in 24-well plates and cultured for 3 days to assess the cell morphology attached to studied samples. After that, the cells attached to the samples were rinsed with PBS solution, and then fixed on the surface of samples using 4% paraformaldehyde at 25°C for 25 min and subsequently rinsed with PBS. Thereafter, the cell microfilament was stained by 1.0% (v/v) FITC-phalloidin dye for 30 min, and then nuclei were stained by 1 mg/ml DAPI for 10 min at 37°C. The cell morphology was analyzed by a fluorescence microscope.

Expression of Osteogenic Genes

The mRNA expression of osteogenic differentiation-related genes including RUNX2, BMP, and OCN was detected by quantitative PCR (qPCR) analysis. The cells MC3T3-E1 with a density of 5 × 10^4/well were cultured with studied samples in DMEM in a 24-well plate for 3 and 5 days. According to operating instructions, the mRNA expression of osteogenic genes including RUNX2, BMP, and OCN was analyzed by qPCR each time.

Statistical Analysis

The one-way ANOVA was used for statistical analysis. There is a significance between the studied groups when $p < 0.05$.

RESULTS

Coating Analysis

Figures 1A–F show the morphology of pure zinc, the Ca-P-coated samples, and PLA/Li-OCP-coated samples. As for the pure zinc without coating, scratches could be found on the pure zinc after being ground with sandpapers to 2000# (**Figure 1A,B**). With Ca-P coating treatment, at low magnification (**Figure 1C**), the coatings on pure zinc formed at different temperatures seem compact and dense without evident defects, indicating that the Ca-P coatings could be successfully formed on the pure zinc substrate. At high magnification (**Figure 1D**), numerous good crystals could be detected in all coatings, but the morphology of those coatings was different. In the case of the PLA/Li-OCP-coated samples, the morphology of Ca-P coating was covered by the PLA/Li-OCP coating. Moreover, the nano Li-OCP particles cannot be well observed in the PLA coating. The EDS results obtained from zones I and II are listed in **Table 1**, which suggested that the ratio of Ca/P for the Ca-P coating was close to 1, and the C element appeared in the PLA/Li-OCP coating, which belonged to PLA. However, the Li element cannot be detected by EDS because Li would emit an x-ray signal that exists at a relatively low

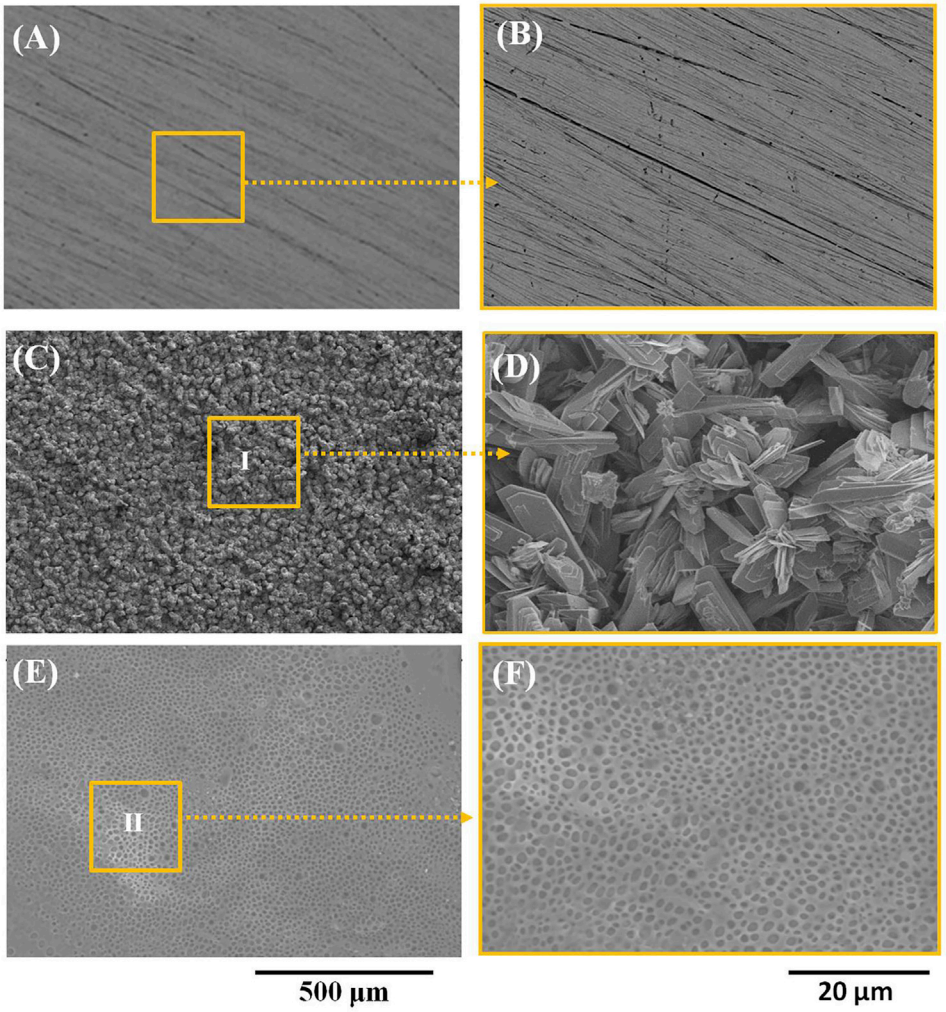

FIGURE 1 | (A, B) The microstrucutres of pure zinc, **(C, D)** Ca-P-coated samples, and **(E, F)** PLA/Li-OCP-coated samples.

TABLE 1 | Results of EDS obtained from zones I and II in **Figure 1 C,E**, respectively.

Element (At. %)	Ca-P coated	PLA/Li-OCP coated
O K	75.89 ± 3.88	43.95 ± 6.32
CK	n.a.	42.94 ± 8.69
P K	13.30 ± 0.26	7.19 ± 3.75
CaK	10.81 ± 0.54	4.64 ± 4.73

intensity of less than 55 eV. This is because the conventional EDS detectors absorb 100% of x-rays of approximately 55 eV (Lin et al., 2021).

Figure 2A shows the results of the contact angle of studied samples. Hydrophilicity is one of the indicators to assess the ability of cell adhesion on the implant in the initial stage. As can be seen, the value of contact angle of pure zinc was 121.54 ± 0.81°, and the values of contact angle for the Ca-P- and PLA/Li-OCP-coated samples were 61.12° ± 1.43 and 80.68° ± 1.05°, respectively, indicating that there was no significant difference in the water contact angle among the coatings obtained by different temperatures. Thus, the presence of coatings on the zinc could decrease the water contact angle, suggesting that the coating could improve the hydrophilicity of the surface compared to pure zinc. **Figure 2B** shows the XRD of the samples with and without coatings. The main phase of the Ca-P coatings was dicalcium phosphate anhydrous $CaHPO_4$, whose ratio of Ca/P was consistent with the EDS results in **Table 1**. When the zinc was exposed to the electrolyte, heterogeneous nucleation of CaH_2EDTA began to occur on the substrate. Meanwhile, upon processing the hydrothermal treatment, the increasing temperature promoted the precipitation of the CaH_2EDTA crystal on the zinc surface. However, the further increasing temperature resulted in the dissolution of CaH_2EDTA crystals, releasing calcium ions. Then, the calcium ions react with dihydrogen phosphate ions to form

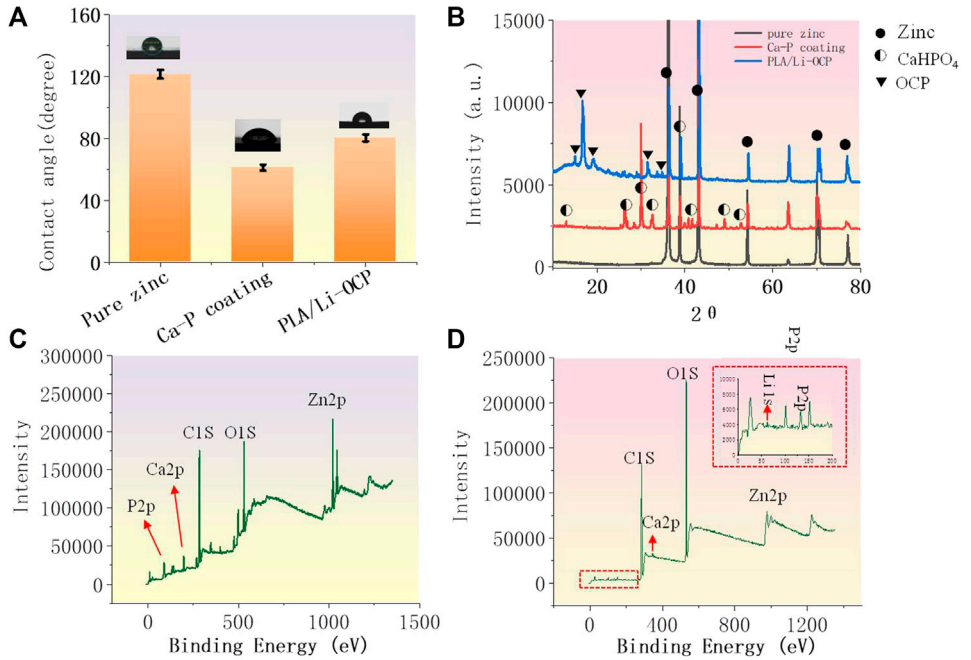

FIGURE 2 | (A) The contact angle of studied samples; **(B)** the XRD patterns; **(C, D)** the total XPS spectrum of the Ca-P coating and PLA/Li-OCP coating.

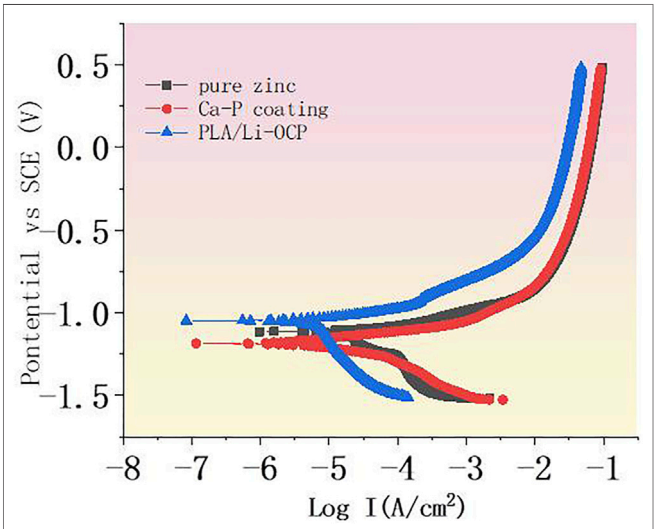

FIGURE 3 | The potentiodynamic polarization curves of coated zinc and pure zinc.

$$CaEDTA^{2-} + H^{+} \rightleftharpoons CaHEDTA^{-} \quad (3\text{–}1)$$

$$CaHEDTA^{-} + H^{+} \rightleftharpoons CaH_2EDTA \downarrow \quad (3\text{–}2)$$

$$CaH_2EDTA \rightleftharpoons Ca^{2+} + H_2EDTA^{2-} \quad (3\text{–}3)$$

$$Ca^{2+} + HPO_4^{2-} \rightleftharpoons CaHPO_4 \downarrow \quad (3\text{–}4)$$

$CaHPO_4$, as a kind of biological CaP ceramics, shows excellent biocompatibility to the bone, and has been used as a coating to improve the proliferation and maturation of osteoblastic cells (Chow, 1999). As for the PLA/Li-OCP-coated samples, the main phase of the coating was $Ca_8H_2(PO_4)_6{\cdot}5H_2O$. The total spectrum of the Ca-P coating in **Figure 2C** shows that the peaks of O1s, Zn2p, Ca2p, and P2p were detected, while Li 1s was found in PLA/Li-OCP coating except for O1s, Zn2p, Ca2p, and P2p in **Figure 2D**; this indicated that the Li was doped into the OCP particles.

TABLE 2 | The corresponding corrosion parameters including corrosion potential and the corrosion current density.

Sample	I_{corr} (A/cm^2)	E_{corr} (V)
Pure zinc	(8.26 ± 0.54) × 10^{-5}	−1.12 ± 0.03
Ca-P coating	(1.32 ± 0.81) × 10^{-5}	−1.18 ± 0.12
PLA/Li-OCP	(6.56 ± 0.25) × 10^{-6}	−1.03 ± 0.07

Electrochemical Tests

The potentiodynamic polarization curves are shown in **Figure 3**, and the corrosion potential (E_{corr}) and the corrosion current density (I_{corr}) are listed in **Table 2**. Compared with the pure zinc, there was no significant difference in the E_{corr} between the pure zinc and Ca-P-coated samples, but the E_{corr} for the PLA/Li-OCP sample shifted to positive. The E_{corr} value of the bare zinc was −1.12 ± 0.03 V, and the E_{corr} value for the Ca-P-treated sample and PLA/Li-OCP samples was −1.18 ± 0.12 V and −1.03 ± 0.07 V, respectively. In thermodynamics, the positive shift of corrosion potential indicated that the corrosion tendency of pure zinc was inhibited by the presence of coatings on the substrate. Meanwhile, I_{corr} in the coated specimens was decreased compared with the bare zinc, in which the PLA/Li-OCP sample exhibited the lowest corrosion current density. This indicated that the PLA/Li-OCP coatings could effectively act as a barrier and block the infiltration

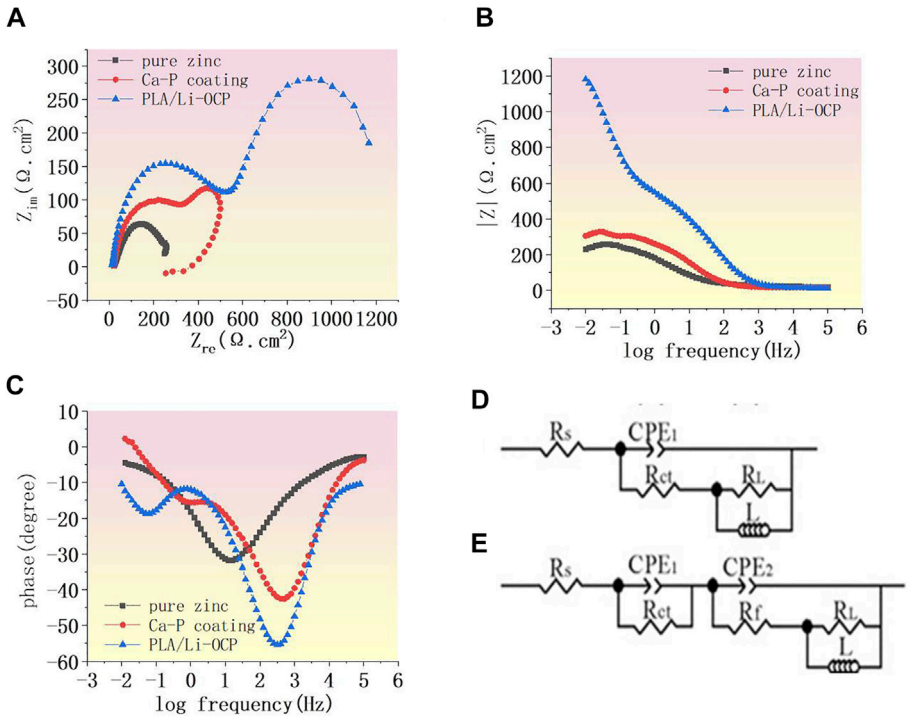

FIGURE 4 | (A) Nyquist curves of studied samples, **(B)** Bode curves of impedance and **(C)** Bode curves of phase angle, and **(D, E)** equivalent circuit.

of electrolytes into the substrate. With regard to the coated samples, the I_{corr} of the Ca-P-coated sample was reduced from 8.26 × 10^{-5} A/cm^2 of pure zinc to 1.32 × 10^{-5} A/cm^2. When treated with PLA/Li-OCP on the Ca-P-coated sample, the I_{corr} was further reduced to 6.56 × 10^{-6} A/cm^2. As mentioned above, the PLA/Li-OCP-coated samples had the best corrosion resistance.

The EIS was used to further study the corrosion resistance of the coated samples. **Figure 4A** shows the Nyquist curves of studied specimens without coatings in SBF solution. In all cases, two semicircle-like curves were found in the Nyquist curves. In high frequency, the capacitive loop generally corresponds to the charge transfer resistance of corrosion products. Herein, the capacitive loop was assigned to the Ca-P coatings, while this capacitive loop in high frequency was attributed to the corrosion product for the bare zinc (Jamesh et al., 2015). The capacitive loop represented the adsorption process during corrosion. In the lower-frequency region, as a rule, the diameter of the semicircle-like curves can be represented by the polarization resistance of the coatings. In **Figure 4A**, the PLA/Li-OCP sample exhibited the biggest diameter of the semicircle-like curves, whereas pure zinc showed the smallest diameter of the semicircle-like curves. The Bode-impendence plots in **Figure 4B** show that a remarkable increase of impedance value was obtained in the coated samples compared with the bare zinc. The impedance for pure zinc, Ca-P, and PLA/Li-OCP-coated samples was ~242.13, ~336.65, and ~1200 Ω cm^2, respectively. As expected, the PLA/Li-OCP samples exhibited the greatest impedance at the lowest-frequency zone, indicating that the PLA/Li-OCP samples had the best corrosion resistance. Moreover, all the samples revealed an inductive character at the lower frequencies, a characteristic of pitting corrosion (Wu et al., 2017). The bode-phase plots in **Figure 4C** demonstrate that there was a significant increase in the phase angle in the medium-frequency region as the treatment temperature increased. The phase angle was reduced from −30.25° of pure zinc to −55° of the PLA/Li-OCP sample. Besides, two time constants can be found in the coated samples. Normally, in the high frequencies, the time constant is assigned to double-layer capacitance and the corresponding charge transfer resistance, while one is related to the film resistance of the corrosion product in low frequency (Wojciechowski et al., 2016). The equivalent electrical circuit was applied to fit the EIS spectra (**Figures 4D,E**). R_s means the solution resistance. CPE1 and R_{ct} are the constant phase element (CPE) and corrosion product resistance, while the constant phase element and the inner layer resistance were represented by CPE2 and R_f, respectively (Jamesh et al., 2015). Moreover, the capacitance to remit the "scatter effect" at the interface between electrode and solution was replaced by CPE with a symbol of Q. In general, higher values of R_{ct} and R_f mean a greater corrosion resistance of the sample. A lower CPE1 value represents a lower corrosion area on the surface, while a higher CPE2 means the relatively thin and incompact film on the metal. The corresponding results fitted from the circuit elements are listed in **Table 3**, which was a good fit confirmed by chi-square (χ^2) values of about 10^{-3}. The values of R_{ct} of the coated zinc for the Ca-P- and PLA/Li-OCP-coated samples were 275.34 and 275.34 Ω cm^2, respectively, which were greater than 276.82 Ω cm^2 of pure zinc; the values of R_f of the coated zinc for the Ca-P- and PLA/Li-OCP-coated samples were 25.34 and 156.47 × 10^3 Ω cm^2, respectively, indicating that the corrosion resistance of the inner layer was increased with temperature; besides, lower CPE1

TABLE 3 | The corresponding results fitted from the circuit element.

Samples	R_S ($\Omega.cm^2$)	R_{ct} ($\Omega.cm^2$)	$Y0_1$ ($\mu\Omega^{-1}\cdot sn\cdot cm^{-2}$) $\times10^{-5}$	n1	R_f (Ωcm^2) $\times10^3$	$Y0_2$ ($\mu\Omega^{-1}\cdot sn\cdot cm^{-2}$) 2×10^{-4}	n2	R_L ($\Omega.cm^2$)	L(H) $\times10^{-3}$
Pure zinc	20.33 ± 2.31	276.82 ± 55.87	5.22 ± 0.83	0.75 ± 0.09	—	7.022 ± 0.64	0.72 ± 0.08	257.34 ± 41.62	1.04 ± 0.36
Ca-P coating	16.95 ± 1.85	275.34 ± 42.17	3.15 ± 1.68	0.71 ± 0.13	0.025 ± 0.01	2.03 ± 0.22	0.76 ± 0.04	442.46 ± 64.21	8.52 ± 1.08
PLA/Li-OCP	18.87 ± 6.31	469.12 ± 50.64	2.74 ± 3.65	0.84 ± 0.07	156.47 ± 0.78	3.82 ± 0.98	0.89 ± 0.02	198.26 ± 24.74	0.74 ± 0.07

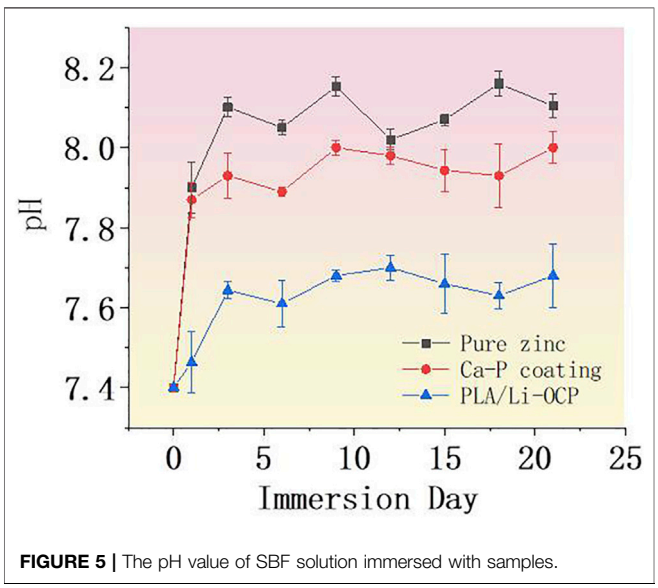

FIGURE 5 | The pH value of SBF solution immersed with samples.

and CPE2 values were also found in the coated zinc, indicating a near-capacitive behavior of the zinc modified by coatings. It is observed that the R_{ct} resistance of the coating was significantly larger than the R_f resistance of the outer layer, suggesting that the compact coating can favor more effective protection on the substrate from corrosion.

Immersion Test

The pH values of SBF soaked with studied samples with and without coatings for 21 days are presented in **Figure 5A**. When the zinc and its alloys are exposed to the electrolyte, the chemical reaction listed as the following would have occurred (Ma et al., 2015; Hernandez-Escobar et al., 2019):

$$\text{Anodic reaction: } Zn \rightarrow Zn^{2+} + 2e^- \quad (3\text{–}5)$$

$$\text{Cathodic reaction: } H_2O + 1/2O_2 \rightarrow 2OH^- \quad (3\text{–}6)$$

$$\text{Total reaction: } Zn^{2+} + 2OH^- Zn \rightarrow (OH)_2 \quad (3\text{–}7)$$

Proceeding with the anode reaction, the degradation of zinc and its alloys begins to occur. Most of the OH^-in the cathode reaction would react with Zn^{2+} ions to form zinc hydroxide on the surface of pure zinc, while the rest of the OH^-would cause an increase of pH value in the surrounding environment, which will promote the deposition of insoluble calcium and phosphorus salt on the zinc surface. The SBF solution immersed with the bare zinc exhibited the highest pH value approaching 7.89 on the first day, which sharply increased for 9 days, and then reduced after 12 days of immersion. With the deposition of the complex corrosion products on zinc surface, a relatively dense protective film dominantly consisting of zinc hydroxide would result in the decrease of corrosion rate. With the extension of the immersion time, the thicker corrosion layer further reduced the corrosion rate of zinc. At the same time, a degradation behavior occurred, resulting in the damage of the corrosion product layer. Then, the electrolyte infiltrated into the substrate to proceed with the degradation. This phenomenon could be reflected by the fluctuant pH curve, suggesting an alternative in pit corrosion, generation, and degradation of corrosion products on zinc. In the initial immersion time, the pH values of the SBF solutions immersed with CaP-coated samples significantly decreased, indicating that all the coatings could improve the degradation rate of pure zinc. Noticeably, it can be seen that there was a different degradation behavior among the coated samples. As for the Ca-P-coated samples, the pH value began to increase when the samples were immersed for 1 day. This suggested that some electrolyte permeated into the substrate. In contrast, the PLA/Li-OCP samples showed the lowest pH value concerning the other groups, indicating that more compact and stable coatings were deposited on pure zinc. After 12 days, the pH was gradually reduced and approached a lower level for the coated zinc. Moreover, a more fluctuant profile of the pH values in the bare zinc was observed with respect to the zinc with Ca-P coatings. With regard to coated samples, such a phenomenon was not evident in the coated groups, especially for the PLA/Li-OCP group.

Figures 6A–G display the morphology of the studied samples immersed in SBF for 21 days, and the corresponding EDS patterns are shown in **Figure 6G**. It can be seen that lots of pits were displayed in pure zinc, indicating that pure zinc suffered from pitting corrosion, as seen in **Figure 6A,D**; moreover, the EDS patterns obtained from *point a* and *b* in **Figure 6D** suggested that the corrosion products consisted of Ca and P. In the case of the Ca-P-coated sample in **Figure 6B**, a crack could be observed on the coating, as marked by the ellipse, and the EDS patterns from *point c* in **Figure 6E** indicated that this region should be assigned to the corrosion products. This is because the Zn element appeared in this region compared with *point b*. The presence of Zn demonstrated that the occurrence of pit corrosion resulted in the released zinc ions from the substrate reacting with calcium phosphate to form corrosion products, suggesting that the protection of Ca-P coating locally became invalid, resulting in the electrolyte permeating into the substrate. Concerning the PLA/Li-OCP coating (**Figure 6C**), there was still a compact and dense PLA coating without obvious

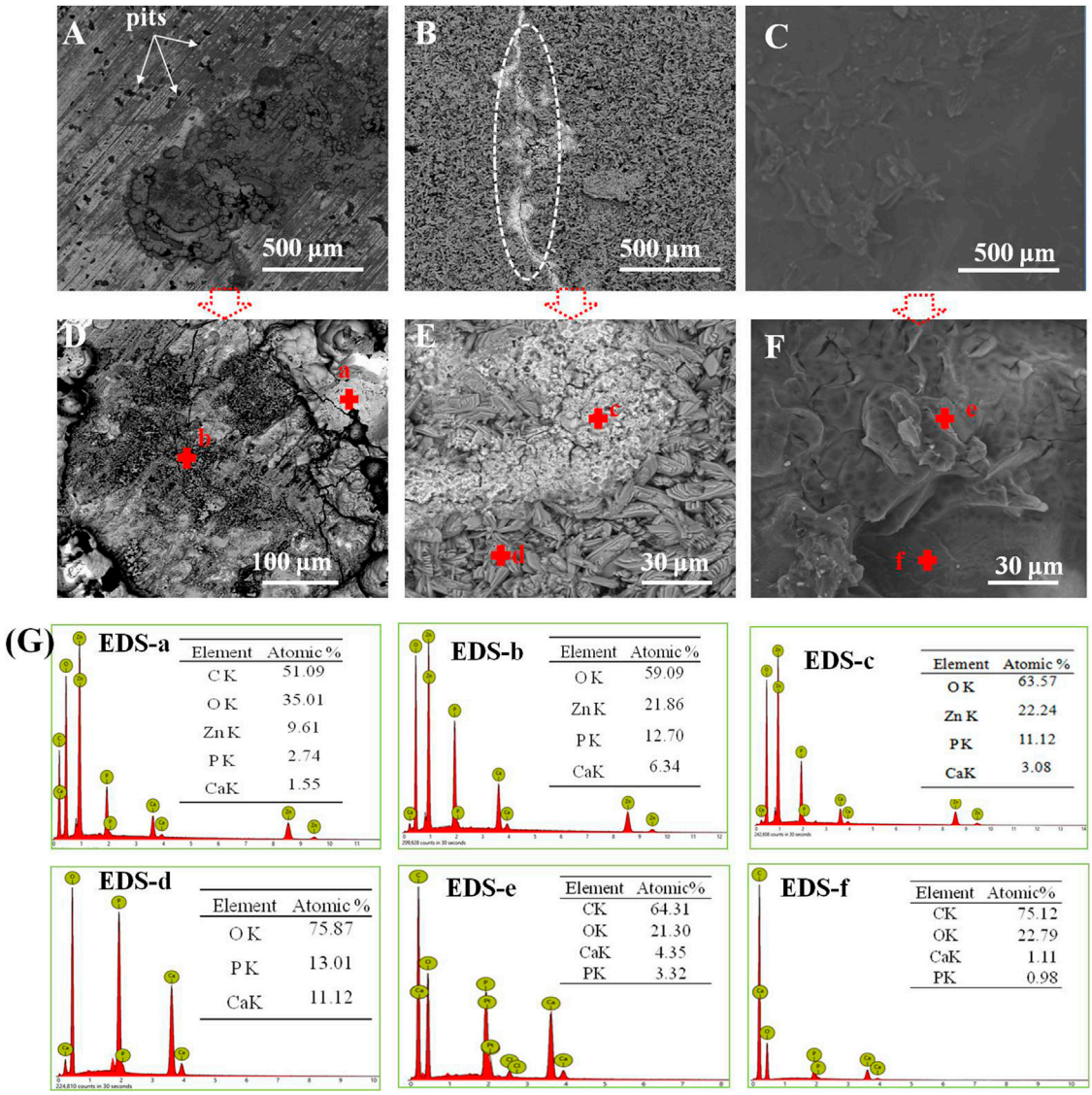

FIGURE 6 | (A–G) The microstructures of the studied samples immersed in SBF for 21 days and the corresponding EDS patterns in panel **(G)**: **(A, D)** pure zinc; **(B, E)** Ca-P coating; **(C, F)** PLA/Li-OCP coating.

defects on the substrate. This suggested that the PLA coating could provide ample protection to prevent the electrolyte from infiltrating the substrate. This is further confirmed by the EDS patterns in *point e* in **Figure 6F**, which showed that no Zn element was found in the coating, and a small amount of Ca and P was found, indicating sufficient protection from the coating although there was degradation of the PLA coatings.

Cell Activity and Osteogenesis Differentiation

The cell viability after cells were seeded on studied samples with and without coatings for 1, 3, and 5 days is shown in **Figure 7**. It can be seen that there was almost no cell activity when the cells were exposed to the bare zinc during culture time, which suggested severe cytotoxicity of the material. This could be attributed to the high zinc ion concentration and pH value that induced cell apoptosis. In contrast, such a case was improved in that cell activity could be detected when the cells were co-cultured with the coated samples. As for the Ca-P-treated group, the maximum cell viability was found on the first day and then the value of viability slightly decreased with time. The cell viability for the PLA/Li-OCP group was higher than that of the Ca-P-treated samples at any time point, and the cell viability gradually increased after 3 and 5 days of culture. This revealed that the PLA/Li-OCP sample showed the greatest cytocompatibility with the ability for cell proliferation due to the degradable rate being considerably improved by the coating obtained at this temperature. **Figure 8** shows photographs of MC3T3-E1 cells exposed on the studied samples for 3 days. In

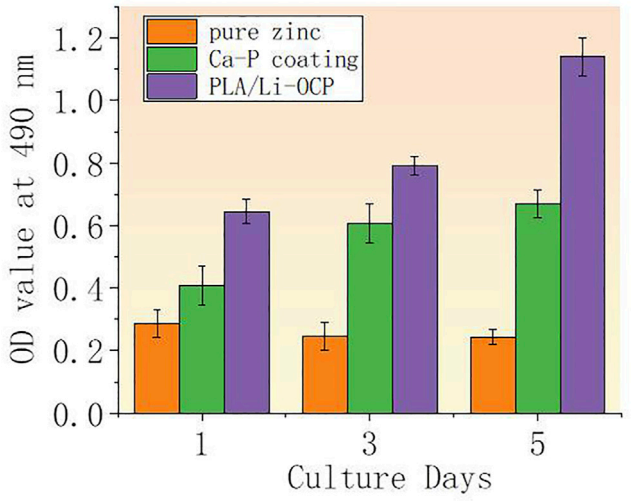

FIGURE 7 | (A) OD value after MC3T3-E cells being seeded on studied samples for 1, 3, and 5 days (**$p < 0.05$).

Figure 8, alive cells failed to adhere to the pure zinc surface, showing lytic morphology, a characteristic of dead cells. This case was slightly changed in the Ca-P-coated samples. In contrast, these conditions were changed by the presence of PLA/Li-OCP coatings. It can be seen that the cells attached to the PLA/Li-OCP coatings show a healthy spreading morphology, indicating that the PLA/Li-OCP coatings could favor the attachment and proliferation of cells. This observation coincided with the results of cell activity.

To further evaluate the effect of coating on cell proliferation, RT-PCR was applied to measure the related osteogenic genes at the mRNA level including runt-related transcription factor 2 (RUNX2), osteocalcin (OCN), and bone morphogenetic protein (BMP). **Figures 9A–C** show the expression levels of RUNX2, BMP, and OCN after cells were cultured with samples for 3 and 5 days. As expected, the expression of all related osteogenic genes in the bare zinc was much low during culture time, whereas fabricating the Ca-P coatings on the zinc could slightly enhance the expression of related osteogenic genes. After 3 days of culture, the expression of RUNX2 and BMP on Ca-P-treated samples was higher than that on the pure zinc, and the PLA/Li-OCP samples present the greatest gene expression among the other groups. After 5 days of culture, the expression of the osteogenic genes in PLA/Li-OCP-treated samples was higher than that of the Ca-P-treated samples and pure zinc. As mentioned above, the PLA/Li-OCP coating could improve the osteogenic activity and osteogenesis of pure zinc.

DISCUSSION

Once an implant is fixed in the body, cells subsequently adhere to the implant for cell proliferation and differentiation, and cell

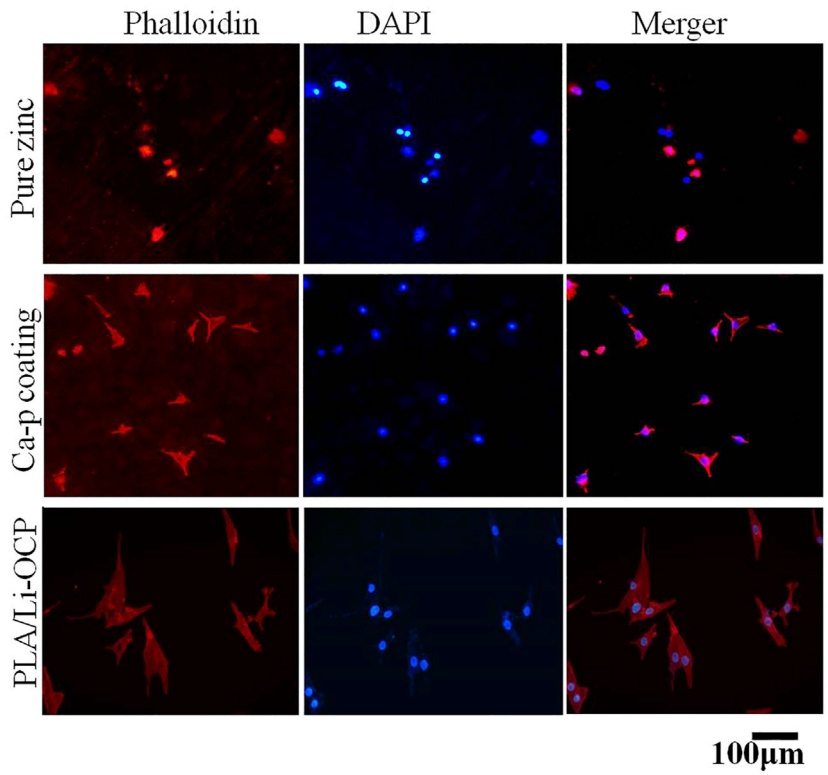

FIGURE 8 | Immunofluorescence-stained osteoblasts on samples after 3 days of culture.

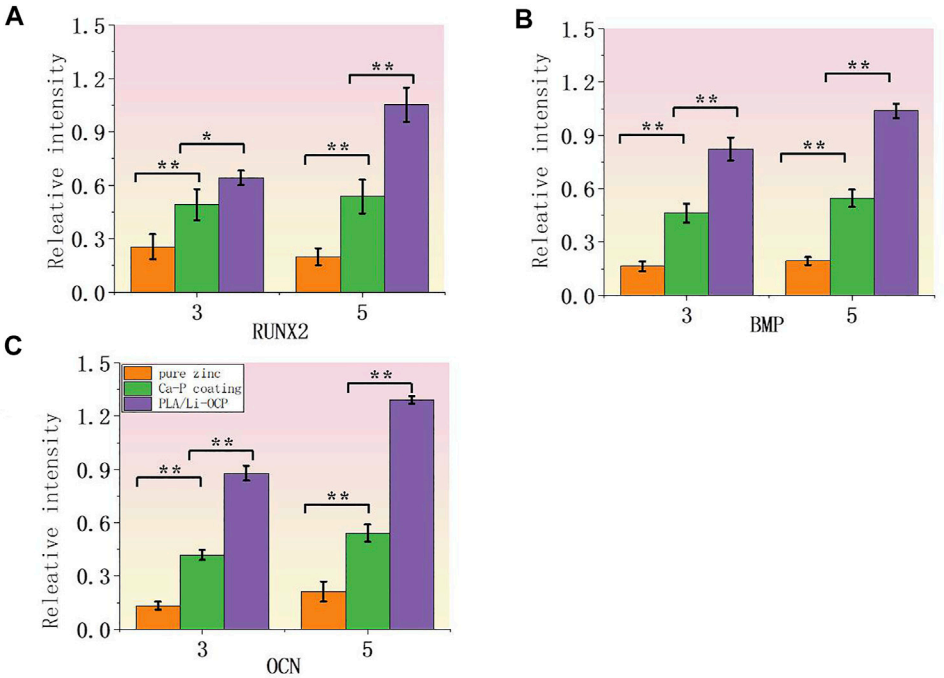

FIGURE 9 | Expression of related osteogenic genes: **(A)** RUNX2, **(B)** BMP, and **(C)** OCN (*$p > 0.05$, **$p < 0.05$).

adhesion has a close relationship with the cultural environment induced by the materials. Therefore, material without cytotoxicity to the cells is a prerequisite for the healing of the bone defect. For zinc and its alloys, one of the main obstacles to transfer to clinical application is the locally accumulated zinc ions in the initial stage of the degradation process, which inhibits the cell adhesion to the materials. Although zinc is required for bone formation, there is a piece of increasing evidence showing that an excessive release of zinc ions from an implant would induce cytotoxicity. Yuan et al. (2019), who investigated the effect of zinc ions on the endothelial cellular responses, demonstrated that a low concentration of zinc ions less than 80 μM could contribute to cell adhesion and proliferation. However, when the zinc ions exceed 80 μM, a negative side to the cell viability would occur (Ma et al., 2015). According to the study from Murni et al., the high zinc ion concentration released from the Zn–3Mg alloy could inhibit electron transport in uncoupled mitochondria (Murni et al., 2015). This drawback was improved by introducing PLA/Li-OCP coating on pure zinc in this study. The important observation that aids understanding of this improvement is the decrease in pH value and releasing concentration of zinc ions. Moreover, the protective effect of coatings on the substrate was enhanced with increasing treatment temperature. As analysis from immersion and electrochemical tests shows, the PLA/Li-OCP coating exhibited the best protective effect. During immersion, herein, three stages of degradation could be proposed for the Ca-P coating, namely, coating degradation, local pit corrosion of substrate, and deposition of corrosion products. In the coating degradation stage, the coatings began to degrade when the sample was exposed to the electrolyte. The local degradation of coating provided sites for solution infiltration into the substrate, causing the local pit corrosion of substrate, accompanied by the release of OH^- and zinc ions. This phenomenon could be indicated by the elevated pH value and zinc ion concentration. Subsequently, a locally high concentration of zinc ions reacted with the OH^- and the phosphate radical to form corrosion products, which, in turn, deposited on the coatings, leading to the decrease of pH value and zinc ion concentration. In fact, the degradation behaviors of all the coatings were different in PBS solution, as the protective effect of coatings is related to microstructure and thickness (Hiromoto, Tomozawa, & Maruyama, 2013). For example, the increasing pH value in the Ca-P-treated group occurred after 5 days, which should be due to the unstable coating obtained at low temperature, and early damage of coating was present. On the contrary, the pH value of the PLA/Li-OCP group remained more stable due to the compact coatings (Pan et al., 2009). The presence of the PLA coating could further prevent the solution from permeating into the substrate.

Accordingly, the cell activity on different coatings suggested that the coated zinc showed good cell proliferation compared with the bare zinc. As such, the outcome from real-time PCR indicated that the pure zinc modified with Ca-P coating and PLA/Li-OCP coating could upregulate the osteogenic gene expression including RUNX2, OCN, and BMP. These findings indicated that the coated zinc could favor osteogenic differentiation in the early and late osteogenesis process. On the one hand, the improvement of cytocompatibility should be attributed to the decrease in local zinc ions, which provides a healthy microenvironment for cell attachment and differentiation. That is, the Ca-P and PLA/Li-

OCP coating acted as a barrier to close the corrosive liquid of zinc matrix and modulated the degradation rate. This inhibitory effect promoted the generation of a friendly microenvironment for cell proliferation and differentiation, because the cell medium was refreshed every day. On the other hand, the reduced pH value also helps cell adhesion and differentiation, since cell adhesion on biomaterials is closely relevant for the alkaline microenvironment (Lin et al., 2021). In **Figure 5**, it can be found that the pH value of pure zinc on the first day approached 7.98, whereas the pH value of Ca-P and PLA/Li-OCP samples was 7.78 and 7.42. The decrease in pH value by the introduction of Ca-P coating was the other factor promoting cell differentiation. Noticeably, the presence of the Ca and Li elements in the coating may also be a factor to favor the enhancement of cytocompatibility. Ninety-nine percent of the Ca element in the body is present in normal bone tissue, and Ca ions can recruit a certain number of bone growth precursor cells to the damaged site by activating calmodulin signaling and activation of ERK1/2 and PI3K/Akt pathway, thereby stimulating the adhesion, proliferation, and differentiation of human osteocyte (Hu et al., 2019; Gao et al., 2021). Moreover, lithium (Li) ions, as a trace element in the human body, were considered to play an important role in organisms (Lin et al., 2021). According to Chen et al., osteogenic differentiation was found to be promoted by adding Li ions in the inflammatory microenvironment (Chen et al., 2013). In addition, it has to be mentioned that the OCP also contributed to enhancing biocompatibility. Many studies have observed that the OCP-based materials favor the bone regenerative properties *via* promoting the osteoblast differentiation from precursor cells *in vitro* (Suzuki, 2013). However, we have to mention that the promotion of cell activity favored by the presence of PLA/Li-OCP coating on pure zinc may be complex, which is the result of synergism of dynamic change of zinc ion, pH, and the existing Ca and P ion. Therefore, an in-depth investigation should be performed *in vitro* and *in vivo* in further studies.

CONCLUSION

In this study, a composite coating consisting of $CaHPO_4$ conversion coating (Ca-P) and PLA decorated with Li-octacalcium phosphate particles (PLA/Li-OCP) was constructed on pure zinc to improve degradation and cytocompatibility. The presence of the PLA/Li-OCP coatings elaborated an effective barrier to prevent the electrolyte from infiltrating the substrate. The enhanced corrosion resistance significantly reduced the pH value, resulting in improving the cytocompatibility. Moreover, the improvement of degradation also upregulated the expression of related osteogenic genes including RUNX2, OCN, and BMP. Therefore, the PLA/Li-OCP conversion coating was a promising coating to improve degradation rate and cytocompatibility.

DATA AVAILABILITY STATEMENT

The original contributions presented in the study are included in the article/Supplementary Material. Further inquiries can be directed to the corresponding author.

AUTHOR CONTRIBUTIONS

Conceptualization, SS; methodology, SS and QT; formal analysis, SS and QT; data curation, SS and QT; writing—original draft preparation, SS; writing—review and editing, DQ.

FUNDING

This work was financially supported by the National Natural Science Foundation of China (Grant No. 81272022) and Innovation Foundation of Zengcheng, Guangzhou, China (Grant No. 185. 2019).

REFERENCES

Alves, M. M., Prosek, T., Santos, C. F., and Montemor, M. F. (2017). *In Vitro* degradation of ZnO Flowered Coated Zn-Mg Alloys in Simulated Physiological Conditions. *Mater. Sci. Eng. C* 70, 112–120. doi:10.1016/j.msec.2016.08.071

Bowen, P. K., Drelich, J., and Goldman, J. (2013). Zinc Exhibits Ideal Physiological Corrosion Behavior for Bioabsorbable Stents. *Adv. Mater.* 25 (18), 2577–2582. doi:10.1002/adma.201300226

Chabosseau, P., and Rutter, G. A. (2016). Zinc and Diabetes. *Arch. Biochem. Biophys.* 611, 79–85. doi:10.1016/j.abb.2016.05.022

Chen, X., Hu, C., Wang, G., Li, L., Kong, X., Ding, Y., et al. (2013). Nuclear Factor-Kb Modulates Osteogenesis of Periodontal Ligament Stem Cells through Competition with β-catenin Signaling in Inflammatory Microenvironments. *Cell Death Dis* 4 (2), e510. doi:10.1038/cddis.2013.14

Chow, L. C. (1999). Calcium Phosphate Cements: Chemistry, Properties, and Applications. *MRS Proc.* 599, 27–37. doi:10.1557/proc-599-27

Gao, J., Su, Y., and Qin, Y.-X. (2021). Calcium Phosphate Coatings Enhance Biocompatibility and Degradation Resistance of Magnesium alloy: Correlating *In Vitro* and *In Vivo* Studies. *Bioactive Mater.* 6 (5), 1223–1229. doi:10.1016/j.bioactmat.2020.10.024

González-García, R., and Monje, F. (2013). The Reliability of Cone-beam Computed Tomography to Assess Bone Density at Dental Implant Recipient Sites: a Histomorphometric Analysis by Micro-CT. *Clin. Oral Implants Res.* 24 (8), 871–879.

Guo, Y., Jia, S., Qiao, L., Su, Y., Gu, R., Li, G., et al. (2020). Enhanced Corrosion Resistance and Biocompatibility of Polydopamine/dicalcium Phosphate Dihydrate/collagen Composite Coating on Magnesium alloy for Orthopedic Applications. *J. Alloys Compd.* 817, 152782. doi:10.1016/j.jallcom.2019.152782

Hafeez, M. A., Farooq, A., Zang, A., Saleem, A., and Deen, K. M. (2020). Phosphate Chemical Conversion Coatings for Magnesium Alloys: a Review. *J. Coat. Technol. Res.* 17 (4), 827–849. doi:10.1007/s11998-020-00335-2

Hernández-Escobar, D., Champagne, S., Yilmazer, H., Dikici, B., Boehlert, C. J., and Hermawan, H. (2019). Current Status and Perspectives of Zinc-Based Absorbable Alloys for Biomedical Applications. *Acta Biomater.* 97, 1–22. doi:10.1016/j.actbio.2019.07.034

Heydari, Z., Mohebbi-Kalhori, D., and Afarani, M. S. (2017). Engineered Electrospun Polycaprolactone (PCL)/octacalcium Phosphate (OCP) Scaffold for Bone Tissue Engineering. *Mater. Sci. Eng. C* 81, 127–132. doi:10.1016/j.msec.2017.07.041

Hiromoto, S., Tomozawa, M., and Maruyama, N. (2013). Fatigue Property of a Bioabsorbable Magnesium alloy with a Hydroxyapatite Coating Formed by a

Chemical Solution Deposition. *J. Mech. Behav. Biomed. Mater.* 25, 1–10. doi:10.1016/j.jmbbm.2013.04.021

Hu, C., Ashok, D., Nisbet, D. R., and Gautam, V. (2019). Bioinspired Surface Modification of Orthopedic Implants for Bone Tissue Engineering. *Biomaterials* 219, 119366. doi:10.1016/j.biomaterials.2019.119366

Jamesh, M. I., Wu, G., Zhao, Y., McKenzie, D. R., Bilek, M. M. M., and Chu, P. K. (2015). Electrochemical Corrosion Behavior of Biodegradable Mg-Y-RE and Mg-Zn-Zr Alloys in Ringer's Solution and Simulated Body Fluid. *Corrosion Sci.* 91, 160–184. doi:10.1016/j.corsci.2014.11.015

Kabir, H., Munir, K., Wen, C., and Li, Y. (2021). Recent Research and Progress of Biodegradable Zinc Alloys and Composites for Biomedical Applications: Biomechanical and Biocorrosion Perspectives. *Bioactive Mater.* 6 (3), 836–879. doi:10.1016/j.bioactmat.2020.09.013

Kannan, M. B., and Liyanaarachchi, S. (2013). Hybrid Coating on a Magnesium alloy for Minimizing the Localized Degradation for Load-Bearing Biodegradable Mini-Implant Applications. *Mater. Chem. Phys.* 142 (1), 350–354. doi:10.1016/j.matchemphys.2013.07.028

Lin, J.-z., Chen, W.-d., Tang, Q.-q., Cao, L.-y., and Su, S.-h. (2021). Lithium-modified MAO Coating Enhances Corrosion Resistance and Osteogenic Differentiation for Pure Magnesium. *Surf. Inter.* 22, 100805. doi:10.1016/j.surfin.2020.100805

Liu, L., Meng, Y., Dong, C., Yan, Y., Volinsky, A. A., and Wang, L.-N. (2018). Initial Formation of Corrosion Products on Pure Zinc in Simulated Body Fluid. *J. Mater. Sci. Technol.* 34 (12), 2271–2282. doi:10.1016/j.jmst.2018.05.005

Lu, P., Fan, H., Liu, Y., Cao, L., Wu, X., and Xu, X. (2011). Controllable Biodegradability, Drug Release Behavior and Hemocompatibility of PTX-Eluting Magnesium Stents. *Colloids Surf. B: Biointerfaces* 83 (1), 23–28. doi:10.1016/j.colsurfb.2010.10.038

Ma, J., Zhao, N., and Zhu, D. (2015). Endothelial Cellular Responses to Biodegradable Metal Zinc. *ACS Biomater. Sci. Eng.* 1 (11), 1174–1182. doi:10.1021/acsbiomaterials.5b00319

Mo, X., Qian, J., Chen, Y., Zhang, W., Xian, P., Tang, S., et al. (2021). Corrosion and Degradation Decelerating Alendronate Embedded Zinc Phosphate Hybrid Coating on Biodegradable Zn Biomaterials. *Corrosion Sci.* 184, 109398. doi:10.1016/j.corsci.2021.109398

Murni, N. S., Dambatta, M. S., Yeap, S. K., Froemming, G. R. A., and Hermawan, H. (2015). Cytotoxicity Evaluation of Biodegradable Zn-3Mg alloy toward normal Human Osteoblast Cells. *Mater. Sci. Eng. C* 49, 560–566. doi:10.1016/j.msec.2015.01.056

Ostrowski, N. J., Lee, B., Roy, A., Ramanathan, M., and Kumta, P. N. (2013). Biodegradable Poly(lactide-Co-Glycolide) Coatings on Magnesium Alloys for Orthopedic Applications. *J. Mater. Sci. Mater. Med.* 24 (1), 85–96. doi:10.1007/s10856-012-4773-5

Pan, H. B., Li, Z. Y., Lam, W. M., Wong, J. C., Darvell, B. W., Luk, K. D. K., et al. (2009). Solubility of Strontium-Substituted Apatite by Solid Titration. *Acta Biomater.* 5 (5), 1678–1685. doi:10.1016/j.actbio.2008.11.032

Pathak, D. K., and Pandey, P. M. (2020). An Experimental Investigation of the Fabrication of Biodegradable Zinc-Hydroxyapatite Composite Material Using Microwave Sintering. *Proc. Inst. Mech. Eng. C: J. Mech. Eng. Sci.* 234 (14), 2863–2880. doi:10.1177/0954406220910445

Peng, F., Lin, Y., Zhang, D., Ruan, Q., Tang, K., Li, M., et al. (2021). Corrosion Behavior and Biocompatibility of Diamond-like Carbon-Coated Zinc: An *In Vitro* Study. *ACS Omega* 6 (14), 9843–9851. doi:10.1021/acsomega.1c00531

Pezzato, L., Settimi, A. G., Cerchier, P., Gennari, C., Dabalà, M., and Brunelli, K. (2020). Microstructural and Corrosion Properties of PEO Coated Zinc-Aluminized (ZA) Steel. *Coatings* 10 (5), 448. doi:10.3390/coatings10050448

Ren, T., Gao, X., Xu, C., Yang, L., Guo, P., Liu, H., et al. (2019). Evaluation of As-extruded Ternary Zn-Mg-Zr Alloys for Biomedical Implantation Material: *In Vitro* and *In Vivo* Behavior. *Mater. Corrosion* 70 (6), 1056–1070. doi:10.1002/maco.201810648

Serdechnova, M., Blawert, C., Karpushenkov, S., Karpushenkava, L., Shulha, T., Karlova, P., et al. (2021). Properties of ZnO/ZnAl2O4 Composite PEO Coatings on Zinc alloy Z1. *Surf. Coat. Technol.* 410, 126948. doi:10.1016/j.surfcoat.2021.126948

Sheng, Y., Yang, J., Zhao, X., Liu, H., Cui, S., Chen, L., et al. (2020). Development and *In Vitro* Biodegradation of Biomimetic Zwitterionic Phosphorylcholine Chitosan Coating on Zn1Mg Alloy. *ACS Appl. Mater. Inter.* 12 (49), 54445–54458. doi:10.1021/acsami.0c16662

Shomali, A. A., Guillory, R. J., Seguin, D., Goldman, J., and Drelich, J. W. (2017). Effect of PLLA Coating on Corrosion and Biocompatibility of Zinc in Vascular Environment. *Surf. Innov.* 5 (4), 211–220. doi:10.1680/jsuin.17.00011

Su, Y., Cockerill, I., Zheng, Y., Tang, L., Qin, Y.-X., and Zhu, D. (2019). Biofunctionalization of Metallic Implants by Calcium Phosphate Coatings. *Bioactive Mater.* 4, 196–206. doi:10.1016/j.bioactmat.2019.05.001

Suzuki, O. (2013). Octacalcium Phosphate (OCP)-based Bone Substitute Materials. *Jpn. dental Sci. Rev.* 49 (2), 58–71. doi:10.1016/j.jdsr.2013.01.001

Tong, X., Zhang, D., Lin, J., Dai, Y., Luan, Y., Sun, Q., et al. (2020). Development of Biodegradable Zn-1Mg-0.1RE (RE = Er, Dy, and Ho) Alloys for Biomedical Applications. *Acta Biomater.* 117, 384–399. doi:10.1016/j.actbio.2020.09.036

Wang, Z., Liang, R., Jiang, X., Xie, J., Cai, P., Chen, H., et al. (2019). Electrospun PLGA/PCL/OCP Nanofiber Membranes Promote Osteogenic Differentiation of Mesenchymal Stem Cells (MSCs). *Mater. Sci. Eng. C* 104, 109796. doi:10.1016/j.msec.2019.109796

Wojciechowski, J., Szubert, K., Peipmann, R., Fritz, M., Schmidt, U., Bund, A., et al. (2016). Anti-corrosive Properties of Silane Coatings Deposited on Anodised Aluminium. *Electrochimica Acta* 220, 1–10. doi:10.1016/j.electacta.2016.10.080

Wu, P.-p., Xu, F.-j., Deng, K.-k., Han, F.-y., Zhang, Z.-z., and Gao, R. (2017). Effect of Extrusion on Corrosion Properties of Mg-2Ca-χAl (χ = 0, 2, 3, 5) Alloys. *Corrosion Sci.* 127, 280–290. doi:10.1016/j.corsci.2017.08.014

Yin, Y. X., Zhou, C., Shi, Y. P., Shi, Z. Z., Lu, T. H., Hao, Y., et al. (2019). Hemocompatibility of Biodegradable Zn-0.8 wt% (Cu, Mn, Li) Alloys. *Mater. Sci. Eng. C Mater. Biol. Appl.* 104, 109896. doi:10.1016/j.msec.2019.109896

Yuan, W., Li, B., Chen, D., Zhu, D., Han, Y., and Zheng, Y. (2019). Formation Mechanism, Corrosion Behavior, and Cytocompatibility of Microarc Oxidation Coating on Absorbable High-Purity Zinc. *ACS Biomater. Sci. Eng.* 5 (2), 487–497. doi:10.1021/acsbiomaterials.8b01131

Zhang, L., Tong, X., Lin, J., Li, Y., and Wen, C. (2020). Enhanced Corrosion Resistance via Phosphate Conversion Coating on Pure Zn for Medical Applications. *Corrosion Sci.* 169, 108602. doi:10.1016/j.corsci.2020.108602

Zhu, M., Lu, Y., Zhang, C., Li, L., Xie, M., Lin, J., et al. (2019). Facile Fabrication of Mg-Based Coating to Improve the Biodegradable Behavior and Cytocompatibility of Pure Zinc. *Surf. Coat. Technol.* 372, 209–217. doi:10.1016/j.surfcoat.2019.05.034

Zhu, S., Wu, C., Li, G., Zheng, Y., and Nie, J.-F. (2019). Creep Properties of Biodegradable Zn-0.1Li alloy at Human Body Temperature: Implications for its Durability as Stents. *Mater. Res. Lett.* 7 (9), 347–353. doi:10.1080/21663831.2019.1610106

Zhuang, Y., Liu, Q., Jia, G., Li, H., Yuan, G., and Yu, H. (2021). A Biomimetic Zinc Alloy Scaffold Coated with Brushite for Enhanced Cranial Bone Regeneration. *ACS Biomater. Sci. Eng.* 7 (3), 893–903. doi:10.1021/acsbiomaterials.9b01895

Conflict of Interest: The authors declare that the research was conducted in the absence of any commercial or financial relationships that could be construed as a potential conflict of interest.

Publisher's Note: All claims expressed in this article are solely those of the authors and do not necessarily represent those of their affiliated organizations, or those of the publisher, the editors, and the reviewers. Any product that may be evaluated in this article, or claim that may be made by its manufacturer, is not guaranteed or endorsed by the publisher.

frontiers in Bioengineering and Biotechnology

ORIGINAL RESEARCH
published: 15 March 2022
doi: 10.3389/fbioe.2022.859280

The Biodegradability and *in Vitro* Cytological Study on the Composite of PLGA Combined With Magnesium Metal

Xue Wang[1,2], *Hui Sun*[1,2], *Mang Song*[1,2], *Guangqi Yan*[1,2]* *and Qiang Wang*[1,2]

[1]School and Hospital of Stomatology, China Medical University, Shenyang, China, [2]Liaoning Provincial Key Laboratory of Oral Diseases, Shenyang, China

The main goal of this study was to develop a novel poly (lactic-co-glycolic acid) (PLGA) composite biodegradable material with magnesium (Mg) metal to overcome the acidic degradation of PLGA and to investigate the cytocompatibility and osteogenesis of the novel material. PLGA composites with 5 and 10 wt% Mg were prepared. The samples were initially cut into 10 mm × 10 mm films, which were used to detect the pH value to evaluate the self-neutralized ability. Murine embryo osteoblast precursor (MC3T3-E1) cells were used for *in vitro* experiments to evaluate the cytotoxicity, apoptosis, adhesion, and osteogenic differentiation effect of the composite biodegradable material. pH monitoring showed that the average value of PLGA with 10 wt% Mg group was closer to the normal physiological environment than that of other groups. Cell proliferation and adhesion assays indicated no significant difference between the groups, and all the samples showed no toxicity to cells. As for cell apoptosis detection, the rate of early apoptotic cells was proportional to the ratio of Mg. However, the ratios of the experimental groups were lower than those of the control group. Alkaline phosphatase activity staining demonstrated that PLGA with 10 wt% Mg could effectively improve the osteogenic differentiation of MC3T3-E1 cells. In summary, PLGA with 10 wt% Mg possessed effective osteogenic properties and cytocompatibility and therefore could provide a wide range of applications in bone defect repair and scaffold-based tissue engineering in clinical practice.

Keywords: PLGA, magnesium, biomaterial, bone defect, osteogenesis

OPEN ACCESS

Edited by:
Shuai Jiang,
Max Planck Institute for Polymer Research, Germany

Reviewed by:
Yanjin Lu,
Fujian Institute of Research on the Structure of Matter (CAS), China
Xiao Lin,
Soochow University, China
Chunguang Yang,
Institute of Metal Research (CAS), China

***Correspondence:**
Guangqi Yan
782751362@qq.com

Specialty section:
This article was submitted to Biomaterials, a section of the journal Frontiers in Bioengineering and Biotechnology

Received: *21 January 2022*
Accepted: *11 February 2022*
Published: *15 March 2022*

Citation:
Wang X, Sun H, Song M, Yan G and Wang Q (2022) The Biodegradability and in Vitro Cytological Study on the Composite of PLGA Combined With Magnesium Metal. Front. Bioeng. Biotechnol. 10:859280. doi: 10.3389/fbioe.2022.859280

INTRODUCTION

Bone defects resulting from performing procedures for the head–neck cysts or tumors are common clinical problems. Therefore, synthesis of biomaterials with biocompatibility and controlled degradability to repair bone defects has always been a hot topic in the maxillofacial field (Phasuk et al., 2018; Zhang et al., 2019).

Poly (lactic-co-glycolic acid) (PLGA) possesses good biocompatibility, suitable mechanical strength, and controlled degradability, and is widely used in pharmaceutical and medical engineering materials (Omezli et al., 2015; Martins et al., 2018). PLGA, which has mechanical and degradable characteristics that can be regulated by varying the lactic acid (LA) to glycolic acid (GA) ratio (Makadia and Siegel, 2011; Gentile et al., 2014), has been used to produce biodegradable sutures and orthopedic fixation plates according to these characteristics (Hutmacher, 2000; Goth

et al., 2012). Moreover, PLGA can inhibit the infiltration of macrophages, which are beneficial for bone regeneration and repairs (Ren et al., 2021). However, PLGA degradation can lead to an acidic environment in local tissues, which affects bone tissue regeneration and slows down the degradation rate of the material (Fu et al., 2000; Zhao et al., 2021).

In recent years, magnesium (Mg) and its alloys as metal biomaterials have attracted considerable attention because of their lightweight, bone-like mechanical, and osteoconductive properties (Landi et al., 2008; Hort et al., 2010; Farraro et al., 2014; Chakraborty Banerjee et al., 2019). Some authors have reported that Mg and its alloys have been used in orthopedic appliances in patients with bone defects (Staiger et al., 2006). The advantages also include antibacterial properties because of the alkaline environment with a local high pH value after Mg degradation. However, Mg degrades rapidly *in vivo*, and uncontrolled degradation increases the pH value of the local environment, which affects the process of osteogenic differentiation (Jana et al., 2021). With regard to the uncontrolled degradation of Mg, other studies have investigated coating bulk Mg alloys with PLGA, poly (L-lactic acid), or poly (ε-caprolactone) to control the degradation rate of the alloy (Wong et al., 2010; Guo et al., 2011; Ostrowski et al., 2013; Johnson et al., 2016). Furthermore, Yu et al. develop a composite bioactive scaffold composed of polylactide-coglycolide and tricalcium phosphate incorporating osteogenic, bioactive magnesium metal powder (Yu et al., 2019). These coatings decrease short-term degradation rate and increase cell attachment and viability. The cellular studies showed that the composites with higher Mg particle concentration showed higher cell viability, cytocompatibility, migration, and osteogenesis differentiation. Most recently, many authors reported similar coating techniques and high-quality coating materials on their articles (Chen et al., 2018; Tang et al., 2022).

Based on the physicochemical complementary characteristics of PLGA and Mg, we aimed to develop a novel PLGA/Mg composite biodegradable material. We hypothesized that 1) Mg degradation products can neutralize the acidic byproducts in the process of decomposing PLGA and 2) the PLGA/Mg composite biomaterial can promote osteogenesis. To identify a better ratio of PLGA and Mg, 5 and 10 wt% Mg were added to PLGA to form the composite material. Immersion tests and pH value monitoring were performed to evaluate the degradability and self-neutralizing ability of the composite material. Cell proliferation, attachment, apoptosis, and osteogenesis assays were performed *in vitro*.

MATERIALS AND METHODS

Synthesis of PLGA

The PLGA copolymers with a molar ratio of 50/50 were synthesized as follows. Equal molar amounts of L-lactide (LLA) and glycolide were charged in a polymerization tube, and the catalyst solution (0.2 mol, 1/5,000 eq.) was then added to the reaction mixture. The tube was purged with dry nitrogen and kept under vacuum for 2 h to remove all volatiles. The tube was heat-sealed under vacuum, and copolymerization was carried out at 130 ± 2°C for 3 days. After the reaction, the tube was broken, the copolymer was dissolved in chloroform, further purified in ice-cold methanol, and dried under vacuum to a constant weight.

Preparation of PLGA/Mg Composite Biomaterials

PLGA (10 g) was dissolved in dichloromethane at a ratio of 1:5 g/ml, and pure Mg powder (50 μm average diameter) provided by Institute of Metal Research, Chinese Academy of Sciences was then added to the polymer solution to form composites with 5 and 10 wt% Mg metal. The solution was vortexed for 30 min before casting into a polytetrafluoroethylene dish and left to air dry at 4°C for 3 days. After solvent evaporation, the films were dried to a constant weight under vacuum. The dried films were cut into strips 10 mm long and 10 mm wide.

pH Value Monitoring

The samples were divided into three groups: P group, P5% Mg group, and P10% Mg group. Each sample was cut into 10 mm × 10 mm films and then placed into a phosphate-buffered saline (PBS) solution. The surface for each sample was immersed in the PBS buffer solution. The change in the pH of PBS solution was detected every day. The test included 7 days of continuous pH value monitoring. Finally, the pH value of each sample was calculated for three times, and the average value was recorded for future analysis.

In Vitro Experiments

Cell Culture

Murine calvarial preosteoblast (MC3T3-E1) cells were cultured in Alpha modified Eagle medium (α-MEM; Hyclone Corporation, United States) supplemented with 10% fetal bovine serum (Clark, Virginie Ledoyen, United States), 100 U/mL penicillin, and 0.1 mg/ml streptomycin. The cells were stored in an incubator at 37°C with 5% CO_2. Trypsin (0.25%; Sigma Corporation, United States) was used to digest and passage the cells. MC3T3-E1 cells were used to assess cell cytotoxicity, adhesion, apoptosis, and osteogenic regeneration.

Cell Cytotoxicity Test

Cell cytotoxicity tests were performed using the CCK-8 kit (US Everbright Inc., Silicon Valley, United States). Cells were incubated in 96-well cell culture plates (Corning, NY, United States) at a density of 2 × 103 cells/well. After 24 h of cell attachment, the medium was replaced with 100 μL of the extracts, and the control groups were replaced with normal culture medium. Each group had five biological replicates. The 96-well cell culture plates were incubated at 37°C in a humidified atmosphere with 5% CO_2 for 24 h, 3, 5, and 7 days. Subsequently, 100 μL of α-MEM with 10% CCK-8 was added to each well, and the 96-well cell culture plates were incubated with CCK-8 solution at 37°C for 4 h. The spectrophotometric absorbance of the samples was measured using a microplate reader (Infinite M200, Tecan, Austria) at 450 nm. All tests were repeated three

times. Relative growth rate (RGR) was used to evaluate the biocompatibility of the composite material. The formula for calculating RGR was as follows: RGR = $OD_e/OD_c \times 100\%$. OD_e is the average OD value of the experimental group. OD_c is the average OD value of the control group. Cell toxicity grade (CTG) was based on the value of RGR, referring to the standard United States Pharmacopeia (Jin et al., 2013). A material was considered non-toxic when the RGR value of the sample was greater than 80 and the CTG grade was 0 or 1 according to the criterion (Vincent et al., 2018).

Cell Apoptosis

Flow cytometry (Becton Dickinson Corporation, United States) was performed to determine the apoptosis rate of MC3T3-E1 cells cultured with samples in the three groups. Each group included three samples, which were cleaned and sterilized. The samples were then placed in 12-well plates for the subsequent procedure. MC3T3-E1 cells with 50–60% confluence in a culture flask were seeded in 12-well plates with sterilized samples at a density of 5×10^4 cells/well for 24 h. The medium was then replaced every 48 h. Annexin V-FITC/PI double staining was performed at 1, 3, and 7 days after planting the cells using the Annexin V-FITC/PI double staining kit (US Everbright Corporation, United States) according to the manufacturer's instructions. Early apoptotic cells were localized in the lower right quadrant of the dot-plot graph.

Cell Adhesion Activity Assay

To determine the cell adhesion activity of the samples in the three groups, an adhesion assay was performed. The samples used for this assay in each group were initially sterilized before detection. The MC3T3-E1 cells were then seeded onto the samples in 12-well plates at a density of 5×10^3/well for 1, 2, and 3 days. Subsequently, the samples were washed with phosphate buffer solution three times, followed by fixation with 2.5% glutaraldehyde for 4 h. After washing with PBS solution, the samples were dehydrated using alcohol with 30, 50, 75, 95, and 100% concentrations in sequence. Rhodamine-phalloidin and DAPI staining were performed to visualize the cytoskeleton and cell nuclei, respectively. Fluorescence microscopy (Nikon, Tokyo, Japan) was used to observe the results.

Alkaline Phosphatase Activity Staining

ALP staining was used to test mineralization activity (Golub et al., 1992). MC3T3-E1 cells were seeded onto the sample surfaces at a density of 5×10^4 cells/well in 12-well plates. After 24 h, the medium was replaced with osteogenic medium (α-MEM culture medium supplemented with 10 mM beta-glycerophosphate [Sigma, St. Louis, MO], 50 mg/ml ascorbic acid [Sigma], and 10^{-8} M dexamethasone [Sigma]), which was changed every 2 days for 7 and 14 days. The samples were washed twice with PBS solution, followed by fixation with 4% paraformaldehyde for 10 min. BCIP/NBT staining was performed to detect osteogenic activity according to the manufacturer's instructions for the BCIP/NBT ALP staining kit (Beyotime, Shanghai, China). The results were observed using a fluorescence microscope (Nikon, Japan).

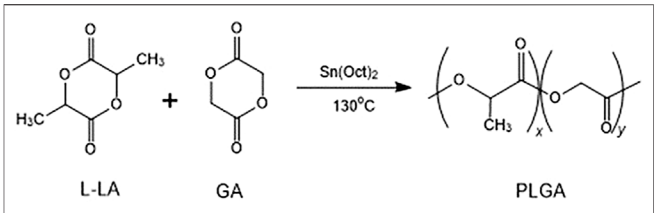

FIGURE 1 | The synthetic route of PLGA.

Statistical Analysis

All experiments were performed at least in triplicate. Data were analyzed using GraphPad Prism software (version 6.0; GraphPad Software, San Diego, CA, United States) and are shown as mean ± standard deviation. Statistical analysis was performed using SPSS 21.0 software. One-way analysis of variance followed by Tukey's post-test was performed in this study. Statistical significance was set at $p < 0.05$.

RESULTS AND DISCUSSION

Characterization of PLGA

PLGA was synthesized by bulk ring-opening copolymerization of LLA and GA in the presence of $SnOct_2$ as a catalyst at 130°C. The synthesis of PLGA is illustrated in **Figure 1**. ^{1}H NMR (δ, ppm from TMS in $CDCl_3$):1.52 ($-CH_3$, LA unit), 5.20 (−CH<, LA unit), and 4.85 ($-CH_2-$, GA unit). The LA/GA ratios in the PLGA copolymer were calculated by comparing the ratios of absorbances at 5.20 ppm (−CH<, LA unit) and 4.85 ppm ($-CH_2-$, GA unit), which were found to be 46.4/53.6 in the copolymer. The larger fraction of GA in the copolymer than that charged in the monomer feed was due to the higher reactivity of GA in comparison with LLA.

The molecular weight and polydispersity of the PLGA copolymers were determined using GPC, showing a polydispersity of 1.70 and a molecular weight of 1.05×10^5 g/mol. The thermal properties of the PLGA copolymer were determined using DSC and TGA. The TGA thermogram of PLGA showed that the polymer began to degrade at 272°C, and the DSC studies showed that the PLGA copolymer was amorphous with only one glass transition temperature of 32.6°C.

Characterization of PLGA/Mg Composite Biomaterials

Distribution of magnesium particle in the composite with different culture time was determined using scanning electron microscope (SEM, Zeiss, Germany) coupled with energy dispersive spectrum (EDS) (**Figure 2**). The green fluorescence pots represented magnesium element. It indicated that magnesium element had been added to the

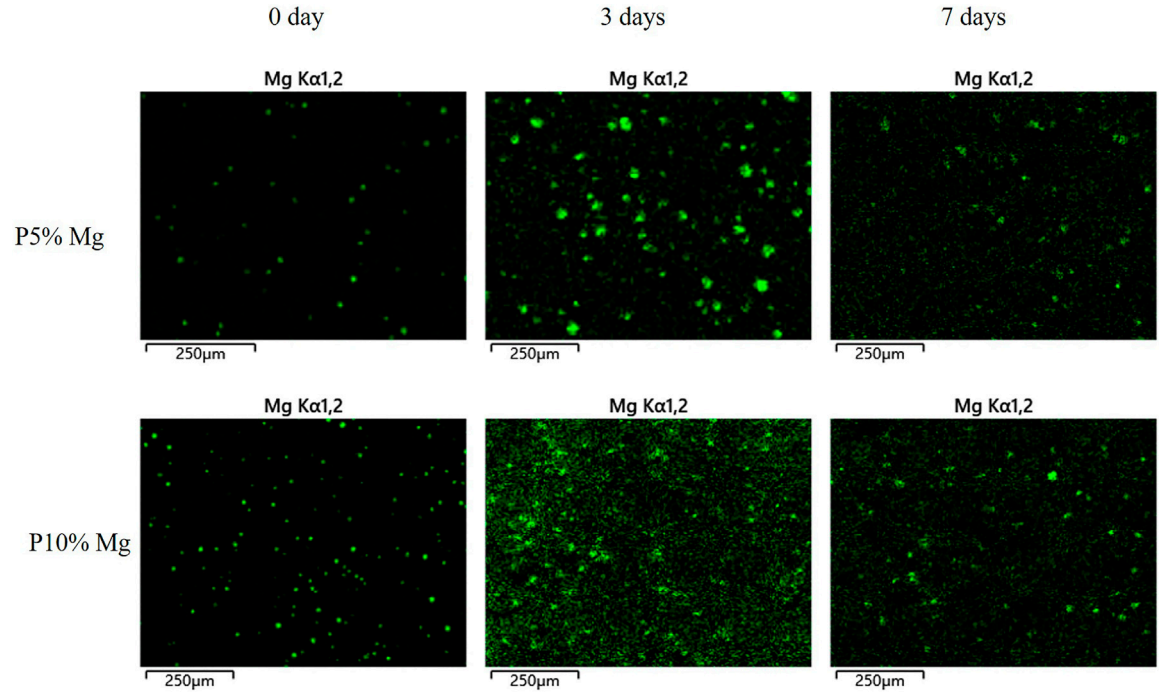

FIGURE 2 | EDS-mapping analysis of the surfaces of P5% Mg and P10% Mg for 0, 3, and 7 days.

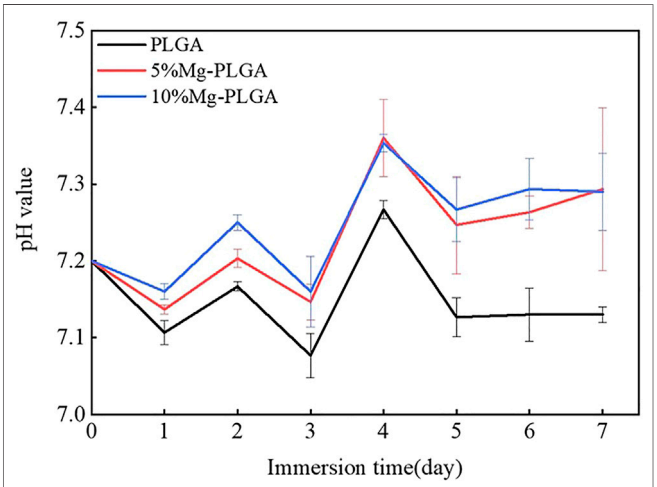

FIGURE 3 | Results of pH value monitoring. The peak value of three groups appeared on the fourth day. From the fifth day on, the pH value of three groups leveled out gradually. With the increasing of the ratio of the magnesium, the pH value increased correspondingly between the P5% Mg group and P10% Mg group. The average value of the P10%Mg group was closer to the normal physiological value.

composite material to distribute regularly on the surface at 0 day and continuously played important role over time. More magnesium element could be detected on the P10% Mg group. At the time point of 3 and 7 days, magnesium element could be observed which indicated that magnesium degraded gradually during the culture time. The results confirmed the conclusion of constant degradation of magnesium element.

Immersion Test for pH Value Monitoring

The pH value of the normal physiological environment was between 7.35 and 7.45. **Figure 3** shows the results of the pH monitoring. The general trend from day 1 to day 7 was consistent among the three groups. For the PLGA group, the peak value, which was lower than the normal value, appeared on the fourth day, and the average value was lower than that of the P5% Mg and P10% Mg groups. With the increase in the ratio of Mg, the pH value increased correspondingly between the P5% Mg and P10% Mg groups. The average value of the P10% Mg group was closer to the normal physiological value. From the fifth day onwards, the pH values of the three groups leveled out gradually.

In Vitro Experiments

Cell Cytotoxicity

Figure 4A shows the proliferation of MC3T3-E1 cells cultured with samples. The OD values of all groups gradually increased over time. No statistically significant differences were found between the groups ($p < 0.05$). **Figure 4B** shows the results for the CTG. For the P group, the average RGR value was greater than 100 from day 1 to day 7. For the P5% Mg and P10% Mg groups, the average RGR value was greater than 80 from day 1 to day 7, except 104.58% ± 0.08, which appeared on the second day in the P5% Mg group. The CTGs of the P, P5% Mg, and P10% Mg groups were 0, 0, 1, and 1, respectively. None of the samples showed toxicity to the cells.

A

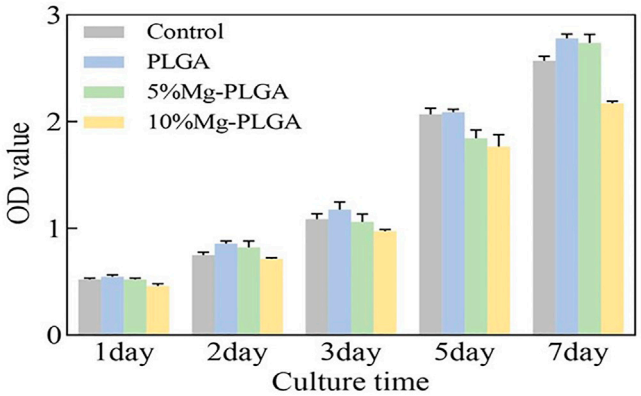

B

	PLGA		5%Mg-PLGA		10%Mg-PLGA	
	RGR	Grade	RGR	Grade	RGR	Grade
1day	104.89%±0.03	0	99.97%±0.03	1	87.98%±0.05	1
2day	114.25%±0.03	0	104.58%±0.08	0	95.21%±0.01	1
3day	108.34%±0.07	0	97.82%±0.07	1	89.73%±0.01	1
5day	100.98%±0.01	0	89.10%±0.04	1	85.40%±0.05	1
7day	104.89%±0.03	0	99.97%±0.03	1	87.98%±0.05	1

FIGURE 4 | Results of cell proliferation and cell cytotoxicity. **(A)** The results of the proliferation of MC3T3-E1 cells cultured with samples. The OD value of all the groups gradually increased over time. There were no statistically significant for the differences between groups ($p < 0.05$). **(B)** The results of the cell toxicity grade (CTG). The CTG of the P group, P5% Mg group, and P10% Mg group showed 0, 0 or 1, and 1, respectively according to the standard United States Pharmacopeia. It indicated that all the samples showed no toxicity to cells.

Cell Apoptosis

The scatter plot of flow cytometry is shown in **Figure 5**. It shows the results of the apoptosis rates of MC3T3-E1 cells co-cultured with samples for 1, 3, and 7 days. Early apoptotic, dead, and late apoptotic cells were localized in the lower right, upper left, and upper right quadrants of a dot-plot graph, respectively. The early apoptosis rates of the negative, P, P5% Mg, and P10% Mg groups after 1 day in co-culture were 10.5, 5.1, 6.4, and 8.2%, respectively. After 3 days in co-culture, the early apoptosis rates of the control, P, P5% Mg, and P10% Mg groups were 2, 1.7, 1.8, and 2%, respectively. After 7 days in co-culture, the early apoptosis rates of the negative, P, P5% Mg, and P10% Mg groups were 1.7, 0.5, 0.8, and 1.2%, respectively. With the increase in the ratio of Mg, the early apoptosis rates of the P5% Mg and P10% Mg groups increased correspondingly compared with the P group, but lower than that of the control group. The rates of early apoptotic cells were proportional to the ratio of Mg.

Cell Adhesion

Figure 6 shows the cytoskeletons and nuclei of MC3T3-E1 cells cultured with samples for 1, 2, and 3 days. The cytoskeletal fluorescence was stained with phalloidin, and the nucleus was stained with DAPI. No significant difference was found for cell shape and number between groups, which was the same as the results of cell proliferation mentioned above. Therefore, it can be concluded that the samples in the P, P5% Mg, and P10% Mg groups were favorable for the initial attachment and spreading of cells. Finally, the results indicated that adding Mg at a ratio of less than 10% would not inhibit cell adhesion compared with the control P group.

ALP Activity Staining

Figure 7 shows the ALP staining of MC3T3-E1 cells cultured with PLGA, PLGA with 5% Mg, and PLGA with 10% Mg for 7 and 14 days. At 7 days after osteogenic induction, with the increase in the ratio of Mg, ALP activity increased gradually with increasing dark staining in the figure. In addition, no significant difference was found between the control and PLGA groups. The same trend was observed at 14 days after osteogenic induction.

DISCUSSION

Bone defects resulting from trauma, inflammation, and cancer are common therapeutic problems in the field of oral and maxillofacial surgery (Mardas et al., 2014). Autologous/allogenic grafting procedures are usually performed as an effective method to complete bone repair in clinical practice (Wei et al., 2020). However, the most common disadvantage after the procedure is injury to the donor site. In recent years, biomaterials have been accepted as a potential alternative to standard autologous/allogenic grafting procedures to achieve clinically successful bone regeneration (Thrivikraman et al., 2017). Among the biomaterials, PLGA as a biodegradable

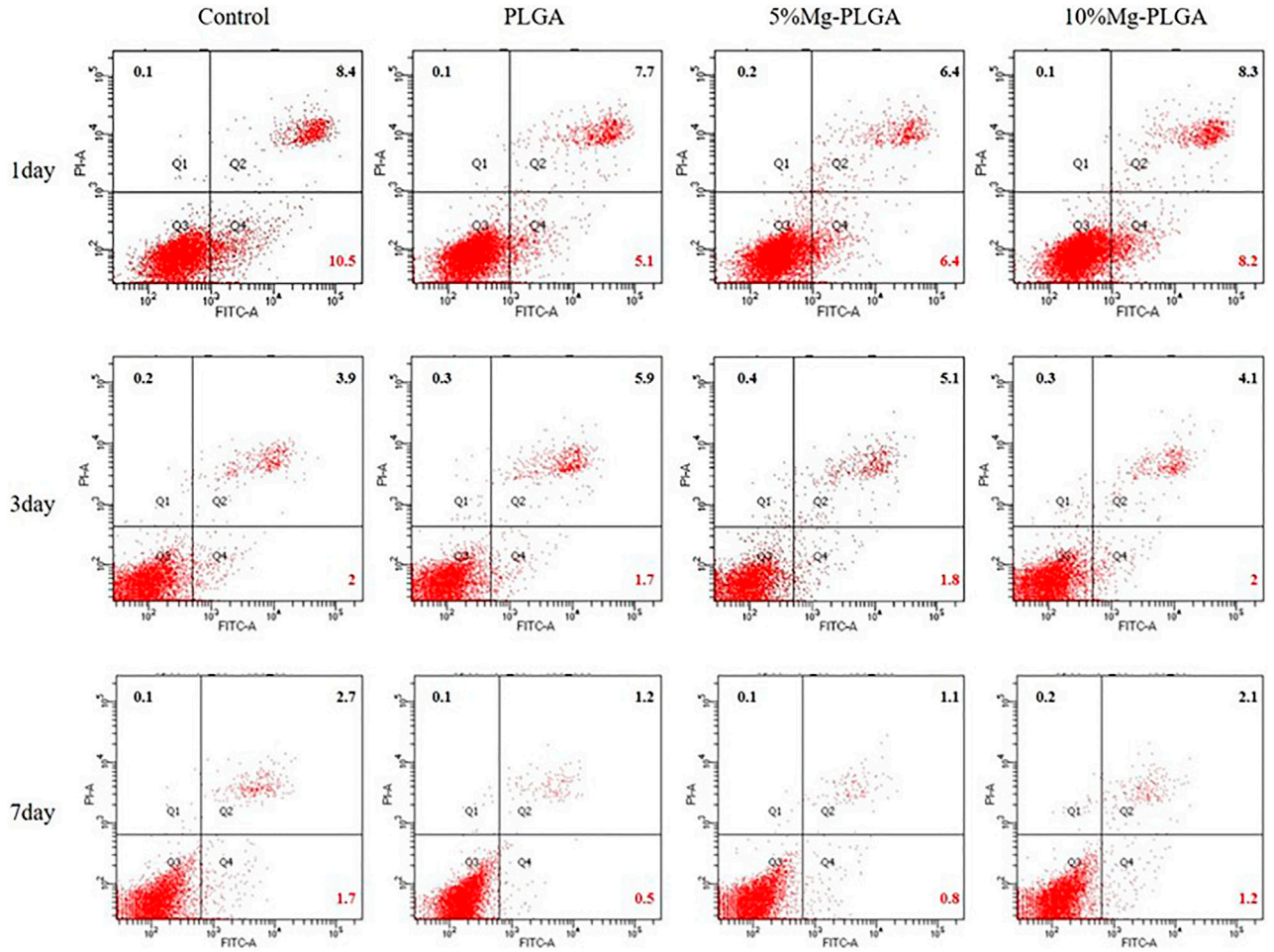

FIGURE 5 | The apoptosis rates of MC3T3-E1 cells cocultured with the samples for 1, 3, and 7 days. Early apoptotic, dead and late apoptotic cells were localized in the lower right (Q4), upper left (Q1), and upper right (Q2) quadrant of a dot-plot graph respectively. It showed that with the increasing of the ratio of the magnesium, the early apoptosis rate of P5% Mg group and P10% Mg group increased correspondingly compared with P group at each time point, but lower than control group. The rates of the early apoptotic cells were basically proportional to the ratio of the magnesium.

polyester has received attention because of its excellent biocompatibility and tunable physicochemical properties. It has been used to produce biodegradable sutures and orthopedic fixation devices for surgical procedures (Middleton and Tipton, 2000). However, the acidic products produced during the degradation of PLGA limit its widespread use as a bone repair material. Mg, as a metallic biomaterial, possesses numerous advantages, such as biodegradability, biocompatibility, and mechanical properties, similar to those of bone. However, its disadvantages include low corrosion resistance against living body conditions, rapid loss of mechanical integrity, hydrogen evolution, and alkalization during degradation (Ding, 2016). Therefore, the current study aimed to combine the physicochemical properties of PLGA and Mg to develop a composite biodegradable material. Some researchers have reported the application of PLGA combined with Mg by coating PLGA on the surface of Mg or 3D printing synthetic material (Brown et al., 2015; Liu et al., 2015). In contrast to the above reports, we improved the forming method of materials and examined cell cytotoxicity, cell adhesion, and osteogenic properties.

pH Value Monitoring

The degradation products of pure Mg included H_2 gases and released ions (Mg^{2+}, OH^-) obeying the following formula (Amukarimi and Mozafari, 2021; Jana et al., 2021):

$$Mg \rightarrow Mg^2 + 2e$$
$$2H_2O + 2e \rightarrow 2OH^- + H2$$
$$Mg^2 + 2OH^- \rightarrow Mg(OH)_2$$

The major degradants of PLGA were oligomers, such as LA and GA, at the initial stage, while displaying an initial increase in pH. Li et al. reported that the degradable oligomers for PLGA 50 were L_4G_2 oligomers and for PLGA 80 were G_{10} and L_7at the initial stage (Li et al., 2018). As degradation proceeded, we proposed that the formation of basic $Mg(OH)_2$ through Mg degradation would react with the acidic byproducts of PLGA

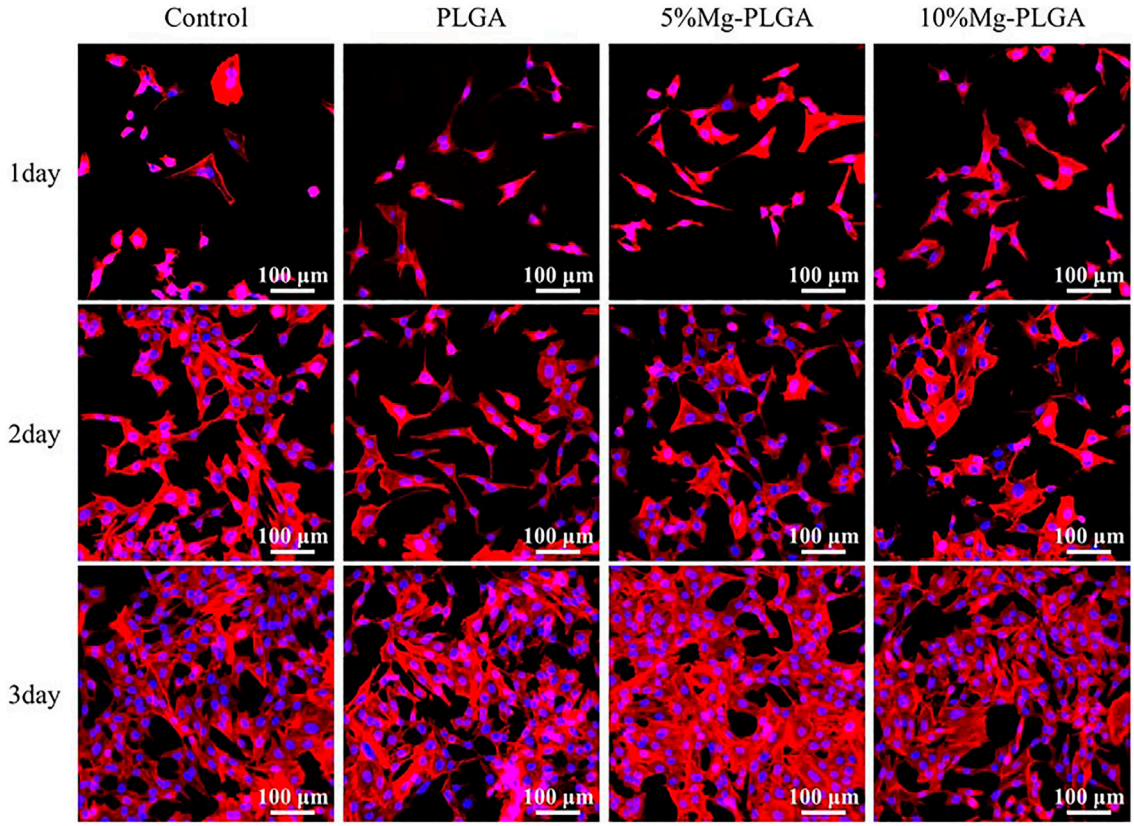

FIGURE 6 | It showed the cytoskeletons and the nucleus of the MC3T3-E1 cells cultured on samples for 1, 2, and 3 days. It indicated that there was no significant difference for cell shape and number between groups. The samples in P group, P5% Mg group, and P10% Mg group were favorable to initial attachment and spreading of cells.

to complete pH neutralization and promote osteogenic osteogenesis. The results of our study confirmed this hypothesis. The increase in pH can be attributed to the degradation of exposed Mg particles because these particles spontaneously react with water to produce Mg hydroxide (Pogorielov et al., 2017). We then observed subsequent neutralization resulting from acidic degradation of PLGA. In the current study, the 10 wt% Mg group maintained a pH value closer to the normal value. Therefore, with the increase in the ratio of Mg in the composite material, the reaction time of the Mg and acidic byproducts of PLGA would be longer. The microenvironment of the composite biomaterials with 10 wt% Mg maintained a longer neutralized status and possessed better osteogenesis than 5 wt% Mg.

In Vitro Experiment

In the current study, the cytocompatibility of the PLGA/Mg composite biodegradable material was investigated using cell proliferation and cytotoxicity tests. The results of the cell proliferation assay showed no significant difference between the groups, and the composite biodegradable material would not be deleterious to cell viability. The same trend was observed in the cell adhesion assay. These results are in accordance with Zhao et al.'s conclusions. Zhao et al. reported PLA/Mg composites for orthopedic implants and evaluated the influence of Mg on the degradation and biocompatibility of PLA. The cytotoxicity results showed that the PLA/Mg composites exhibit no toxicity in osteoblastic cell culture (Zhao et al., 2017). However, by summarizing the data of the CCK-8 test, the average OD values of the composite biodegradable material groups were lower than those of the PLGA and control groups and higher than those of the PLGA with 5 wt% Mg group and PLGA with 10 wt% Mg group. These findings could be due to the formation of hydrogen gas pockets within the composite materials during the degradation of Mg, which inhibited the proliferation of cells, and the amount of gas pockets increased with the increase in the ratio of Mg. Therefore, the ratio of Mg was controlled to less than 10% in the current study. Sayuri et al. reported that the cells proliferate the fastest *in vitro* after the addition of 10 mM Mg^{2+}, but cell proliferation is inhibited at higher concentrations (Mg^{2+} > 20 mM). This cytotoxicity has also been reported for other metal ions (Na, Cr, Mo, Al, Ta, Co, Ni, Fe, Cu, Mn, and V) in osteoblasts (Hallab et al., 2002; Yoshizawa et al., 2014).

Programmed cell death is called apoptosis, which is a normal physiological process of cell death. Apoptosis process is controlled by genes, which are important for maintaining the stability of the intracellular environment (Chen et al., 2014; Shih

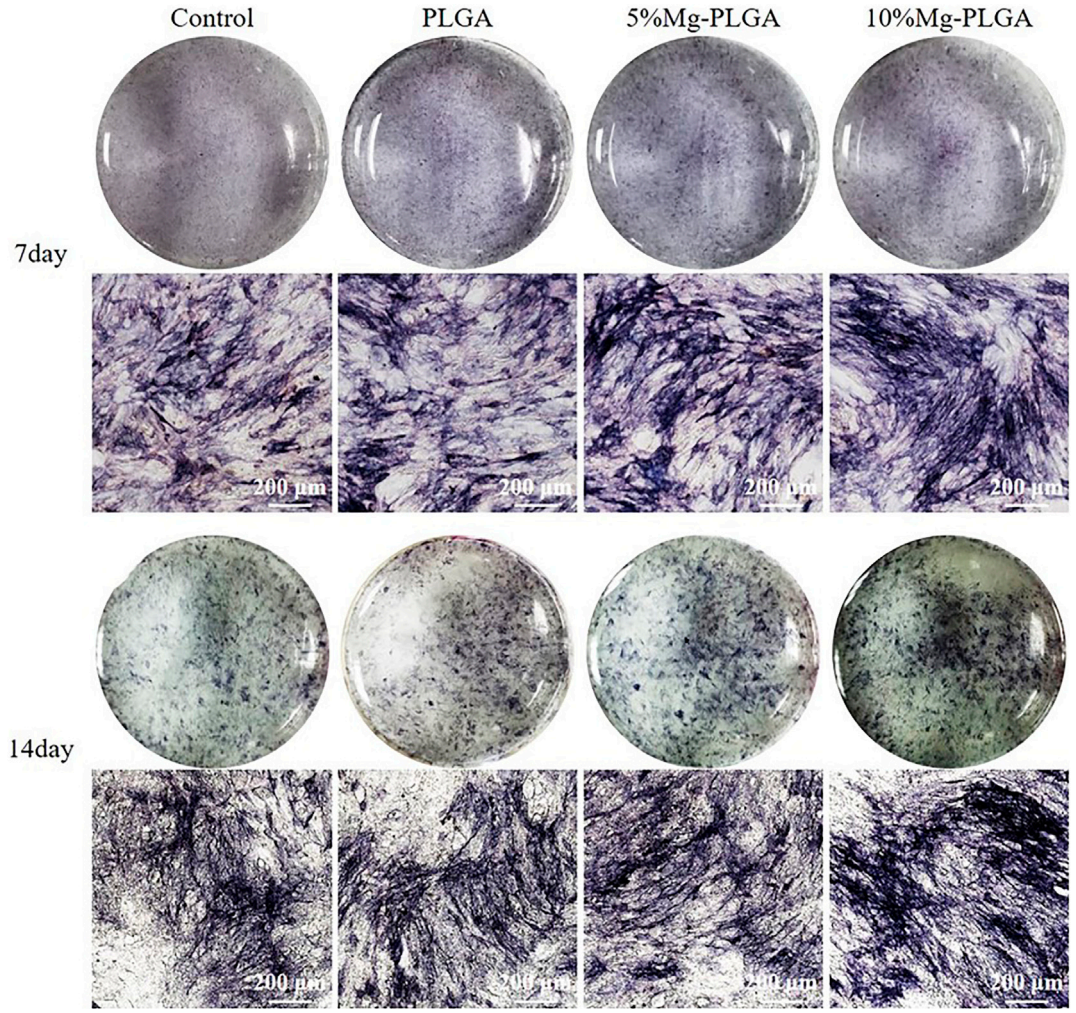

FIGURE 7 | It showed the ALP staining of MC3T3 cells cultured with PLGA, PLGA with 5% magnesium, and PLGA with 10% magnesium for 7 and 14 days, respectively. With the increasing of the ratio of magnesium, ALP activity increased correspondingly.

et al., 2015). Researchers usually use the apoptosis rate to reflect the ability of cells to adapt to different surfaces. The apoptosis rate reflects the state of cells on the material surface. Flow cytometry is now a widely used method for analyzing the expression of cell surface and intracellular molecules (Bolton and Roederer, 2009; Maecker, 2009; Zaritskaya et al., 2010). Our current data showed that the early apoptosis rate in the lower right quadrants in the three groups was lower than that in the control group, but the rate increased significantly among the experimental groups with the increase in Mg concentration at different time points. The possible reasons include the existence of mental Mg particles that induce cell apoptosis. The other reason could be attributed to oxidative stress response during Mg hydroxide formation on the material surface, promoting osteoblast apoptosis.

In the current study, the data of ALP activity staining and q-PCR supported the conclusion that higher Mg concentrations promote osteogenic regeneration. However, with the increase in the concentration of Mg, cell proliferation is inhibited. Hence, Mg ion concentration should be controlled within a certain range. This was the reason why the quality ratio of Mg in the composite material did not exceed 10 wt%. Our results are consistent with those reported by other researchers. Xu (Xu et al., 2018) added Mg metal and Mg alloy to PLGA samples to develop scaffold materials. The effects of material osteogenesis were evaluated using ALP expression and cellular mineralization, and the Mg and Mg alloy scaffolds were concluded to outperform the control PLGA film.

These two factors could contribute to osteogenesis. On one hand, self-neutralizing ability provided a favorable environment for the osteogenic regeneration of cells. Acidic decomposition products of PLGA are known to induce inflammatory reactions (Ji et al., 2012; Washington et al., 2018). The products of Mg degradation react with the acidic byproducts of PLGA, lactic acid, and glycolic acid, leading to pH neutralization. On the other hand, Mg^{2+} ions stimulate intracellular signaling pathways that may enhance mineralization and bone regeneration. Ca^{+2} ions contribute

to osteogenic differentiation (Dvorak et al., 2004; Dvorak and Riccardi, 2004; Nakamura et al., 2010). We speculated that Mg^{2+}may act through a similar activation cascade to induce osteogenic regeneration *via* the activation of a specific transcription factor. Insulin-like growth factor 2 plays an important role in long bone growth, and its upregulation by Mg ions is indicative of the effect of Mg on bone growth (Fisher et al., 2005). Other researchers have reported that Mg^{2+} ions can upregulate Akt phosphorylation to promote ALP activity and enhance the expression of osteogenesis-related genes (Wang et al., 2017). These conclusions confirm our results.

In conclusion, PLGA with an Mg composite biodegradable material demonstrated favorable cytocompatibility and osteogenesis in MC3T3-E1 cells. Compared with PLGA with 5 wt% Mg and PLGA groups, PLGA with 10 wt% Mg possessed effective osteogenic properties and showed no toxicity to cells. Therefore, the novel composite material could provide a wide range of applications in bone defect repair and scaffold-based tissue engineering in clinical practice.

DATA AVAILABILITY STATEMENT

The raw data supporting the conclusion of this article will be made available by the authors, without undue reservation.

AUTHOR CONTRIBUTIONS

Original article preparation: XW and MS; designing the material: QW; performing *in vitro* experiments: HS; designing the experiment: GY. All authors have read and agreed on the final version of the article.

FUNDING

This research was funded by the project from Natural Science Foundation of Liaoning Province of China (No. 2019-ZD-0793).

REFERENCES

Amukarimi, S., and Mozafari, M. (2021). Biodegradable Magnesium-based Biomaterials: An Overview of Challenges and Opportunities. *MedComm* 2 (2), 123–144. doi:10.1002/mco2.59

Bolton, D. L., and Roederer, M. (2009). Flow Cytometry and the Future of Vaccine Development. *Expert Rev. Vaccin.* 8 (6), 779–789. doi:10.1586/erv.09.41

Brown, A., Zaky, S., Ray, H., and Sfeir, C. (2015). Porous Magnesium/PLGA Composite Scaffolds for Enhanced Bone Regeneration Following Tooth Extraction. *Acta Biomater.* 11, 543–553. doi:10.1016/j.actbio.2014.09.008

Chakraborty Banerjee, P., Al-Saadi, S., Choudhary, L., Harandi, S. E., and Singh, R. (2019). Magnesium Implants: Prospects and Challenges. *Materials* 12 (1), 136. doi:10.3390/ma12010136

Chen, C., Tan, J., Wu, W., Petrini, L., Zhang, L., Shi, Y., et al. (2018). Modeling and Experimental Studies of Coating Delamination of Biodegradable Magnesium Alloy Cardiovascular Stents. *ACS Biomater. Sci. Eng.* 4 (11), 3864–3873. doi:10.1021/acsbiomaterials.8b00700

Chen, Y., Yan, J., Wang, X., Yu, S., Wang, Z., Zhang, X., et al. (2014). *In Vivo* and *In Vitro* Evaluation of Effects of Mg-6Zn alloy on Apoptosis of Common Bile Duct Epithelial Cell. *Biometals* 27 (6), 1217–1230. doi:10.1007/s10534-014-9784-x

Ding, W. (2016). Opportunities and Challenges for the Biodegradable Magnesium Alloys as Next-Generation Biomaterials. *Regen. Biomater.* 3 (2), 79–86. doi:10.1093/rb/rbw003

Dvorak, M. M., and Riccardi, D. (2004). Ca2+ as an Extracellular Signal in Bone. *Cell Calcium* 35 (3), 249–255. doi:10.1016/j.ceca.2003.10.014

Dvorak, M. M., Siddiqua, A., Ward, D. T., Carter, D. H., Dallas, S. L., Nemeth, E. F., et al. (2004). Physiological Changes in Extracellular Calcium Concentration Directly Control Osteoblast Function in the Absence of Calciotropic Hormones. *Proc. Natl. Acad. Sci.* 101 (14), 5140–5145. doi:10.1073/pnas.0306141101

Farraro, K. F., Kim, K. E., Woo, S. L.-Y., Flowers, J. R., and McCullough, M. B. (2014). Revolutionizing Orthopaedic Biomaterials: The Potential of Biodegradable and Bioresorbable Magnesium-Based Materials for Functional Tissue Engineering. *J. Biomech.* 47 (9), 1979–1986. doi:10.1016/j.jbiomech.2013.12.003

Fisher, M. C., Meyer, C., Garber, G., and Dealy, C. N. (2005). Role of IGFBP2, IGF-I and IGF-II in Regulating Long Bone Growth. *Bone* 37 (6), 741–750. doi:10.1016/j.bone.2005.07.024

Fu, K., Pack, D. W., Klibanov, A. M., and Langer, R. (2000). Visual Evidence of Acidic Environment within Degrading Poly(lactic-Co-Glycolic Acid) (PLGA) Microspheres. *Pharm. Res.* 17 (1), 100–106. doi:10.1023/a:1007582911958

Gentile, P., Chiono, V., Carmagnola, I., and Hatton, P. (2014). An Overview of Poly(lactic-Co-Glycolic) Acid (PLGA)-based Biomaterials for Bone Tissue Engineering. *Ijms* 15 (3), 3640–3659. doi:10.3390/ijms15033640

Golub, E. E., Harrison, G., Taylor, A. G., Camper, S., and Shapiro, I. M. (1992). The Role of Alkaline Phosphatase in Cartilage Mineralization. *Bone Mineral.* 17 (2), 273–278. doi:10.1016/0169-6009(92)90750-8

Goth, S., Sawatari, Y., and Peleg, M. (2012). Management of Pediatric Mandible Fractures. *Management Pediatr. mandible fractures* 23 (1), 47–56. doi:10.1097/SCS.0b013e318240c8ab

Guo, M., Cao, L., Lu, P., Liu, Y., and Xu, X. (2011). Anticorrosion and Cytocompatibility Behavior of MAO/PLLA Modified Magnesium alloy WE42. *J. Mater. Sci. Mater. Med.* 22 (7), 1735–1740. doi:10.1007/s10856-011-4354-z

Hallab, N. J., Vermes, C., Messina, C., Roebuck, K. A., Glant, T. T., and Jacobs, J. J. (2002). Concentration- and Composition-dependent Effects of Metal Ions on Human MG-63 Osteoblasts. *J. Biomed. Mater. Res.* 60 (3), 420–433. doi:10.1002/jbm.10106

Hort, N., Huang, Y., Fechner, D., Störmer, M., Blawert, C., Witte, F., et al. (2010). Magnesium Alloys as Implant Materials - Principles of Property Design for Mg-RE Alloys☆. *Acta Biomater.* 6 (5), 1714–1725. doi:10.1016/j.actbio.2009.09.010

Hutmacher, D. W. (2000). Scaffolds in Tissue Engineering Bone and Cartilage. *Biomaterials* 21 (24), 2529–2543. doi:10.1016/s0142-9612(00)00121-6

Jana, A., Das, M., and Balla, V. K. (2021). *In Vitro* and *In Vivo* Degradation Assessment and Preventive Measures of Biodegradable Mg Alloys for Biomedical Applications. *J. Biomed. Mater. Res* 110, 462–487. doi:10.1002/jbm.a.37297

Ji, W., Yang, F., Seyednejad, H., Chen, Z., Hennink, W. E., Anderson, J. M., et al. (2012). Biocompatibility and Degradation Characteristics of PLGA-Based Electrospun Nanofibrous Scaffolds with Nanoapatite Incorporation. *Biomaterials* 33 (28), 6604–6614. doi:10.1016/j.biomaterials.2012.06.018

Jin, S., Zhang, Y., Wang, Q., Zhang, D., Zhang, S., and surfaces, B. B. (2013). Influence of TiN Coating on the Biocompatibility of Medical NiTi alloy. *Colloids Surf. B: Biointerfaces* 101, 343–349. doi:10.1016/j.colsurfb.2012.06.029

Johnson, I., Wang, S. M., Silken, C., and Liu, H. (2016). A Systemic Study on Key Parameters Affecting Nanocomposite Coatings on Magnesium Substrates. *Acta Biomater.* 36, 332–349. doi:10.1016/j.actbio.2016.03.026

Landi, E., Logroscino, G., Proietti, L., Tampieri, A., Sandri, M., and Sprio, S. (2008). Biomimetic Mg-Substituted Hydroxyapatite: from Synthesis to *In Vivo* Behaviour. *J. Mater. Sci. Mater. Med.* 19 (1), 239–247. doi:10.1007/s10856-006-0032-y

Li, J., Nemes, P., and Guo, J. (2018). Mapping Intermediate Degradation Products of Poly(lactic- Co -glycolic Acid) in vitroMapping Intermediate Degradation

Products of Poly(lactic-Co-Glycolic Acid) *In Vitro*. *J. Biomed. Mater. Res.* 106 (3), 1129–1137. doi:10.1002/jbm.b.33920

Liu, H., Wang, R., Chu, H. K., and Sun, D. (2015). Design and Characterization of a Conductive Nanostructured Polypyrrole-Polycaprolactone Coated Magnesium/PLGA Composite for Tissue Engineering Scaffolds. *J. Biomed. Mater. Res.* 103 (9), 2966–2973. doi:10.1002/jbm.a.35428

Maecker, H. T. (2009). Multiparameter Flow Cytometry Monitoring of T Cell Responses. *Multiparameter flow cytometry Monit. T Cel. responses* 485, 375–391. doi:10.1007/978-1-59745-170-3_25

Makadia, H. K., and Siegel, S. J. (2011). Poly Lactic-Co-Glycolic Acid (PLGA) as Biodegradable Controlled Drug Delivery Carrier. *Polymers* 3 (3), 1377–1397. doi:10.3390/polym3031377

Mardas, N., Dereka, X., Donos, N., and Dard, M. (2014). Experimental Model for Bone Regeneration in Oral and Cranio-Maxillo-Facial Surgery. *J. Invest. Surg.* 27 (1), 32–49. doi:10.3109/08941939.2013.817628

Martins, C., Sousa, F., Araújo, F., and Sarmento, B. (2018). Functionalizing PLGA and PLGA Derivatives for Drug Delivery and Tissue Regeneration Applications. *Adv. Healthc. Mater.* 7 (1), 1701035. doi:10.1002/adhm.201701035

Middleton, J. C., and Tipton, A. J. (2000). Synthetic Biodegradable Polymers as Orthopedic Devices. *Biomaterials* 21 (23), 2335–2346. doi:10.1016/s0142-9612(00)00101-0

Nakamura, S., Matsumoto, T., Sasaki, J.-I., Egusa, H., Lee, K. Y., Nakano, T., et al. (2010). Effect of Calcium Ion Concentrations on Osteogenic Differentiation and Hematopoietic Stem Cell Niche-Related Protein Expression in Osteoblasts. *Tissue Eng. A* 16 (8), 2467–2473. doi:10.1089/ten.TEA.2009.0337

Omezli, M. M., Torul, D., Polat, M. E., and Dayi, E. (2015). Biomechanical Comparison of Osteosynthesis with Poly-L-Lactic Acid and Titanium Screw in Intracapsular Condylar Fracture Fixation: An Experimental Study. *Niger. J. Clin. Pract.* 18 (5), 589–593. doi:10.4103/1119-3077.158946

Ostrowski, N. J., Lee, B., Roy, A., Ramanathan, M., and Kumta, P. N. (2013). Biodegradable Poly(lactide-Co-Glycolide) Coatings on Magnesium Alloys for Orthopedic Applications. *J. Mater. Sci. Mater. Med.* 24 (1), 85–96. doi:10.1007/s10856-012-4773-5

Phasuk, K., Haug, S. P., and America, M. S. C. O. N. (2018). Maxillofacial Prosthetics. *Oral Maxill. Surg. Clin. North America* 30 (4), 487–497. doi:10.1016/j.coms.2018.06.009

Pogorielov, M., Husak, E., Solodivnik, A., Zhdanov, S., and science, a. (2017). Magnesium-based Biodegradable Alloys: Degradation, Application, and Alloying Elements. *Interv. Med. Appl. Sci.* 9 (1), 27–38. doi:10.1556/1646.9.2017.1.04

Ren, B., Lu, J., Li, M., Zou, X., Liu, Y., Wang, C., et al. (2021). Anti-inflammatory Effect of IL-1ra-loaded Dextran/PLGA Microspheres on Porphyromonas Gingivalis Lipopolysaccharide-Stimulated Macrophages *In Vitro* and *In Vivo* in a Rat Model of Periodontitis. *Biomed. Pharmacother.* 134, 111171. doi:10.1016/j.biopha.2020.111171

Shih, C.-M., Huang, C.-Y., Liao, L.-R., Hsu, C.-P., Tsao, N.-W., Wang, H.-S., et al. (2015). Nickel Ions from a Corroded Cardiovascular Stent Induce Monocytic Cell Apoptosis: Proposed Impact on Vascular Remodeling and Mechanism. *J. Formos. Med. Assoc.* 114 (11), 1088–1096. doi:10.1016/j.jfma.2014.03.007

Staiger, M. P., Pietak, A. M., Huadmai, J., and Dias, G. (2006). Magnesium and its Alloys as Orthopedic Biomaterials: a Review. *Biomaterials* 27 (9), 1728–1734. doi:10.1016/j.biomaterials.2005.10.003

Tang, H., Li, S., Zhao, Y., Liu, C., Gu, X., and Fan, Y. (2022). A Surface-Eroding Poly(1,3-Trimethylene Carbonate) Coating for Magnesium Based Cardiovascular Stents with Stable Drug Release and Improved Corrosion Resistance. *Bioactive Mater.* 7 (6), 144–153. doi:10.1016/j.bioactmat.2021.05.045

Thrivikraman, G., Athirasala, A., Twohig, C., Boda, S. K., and Bertassoni, L. E. (2017). Biomaterials for Craniofacial Bone Regeneration. *Dental Clin. North America* 61 (4), 835–856. doi:10.1016/j.cden.2017.06.003

Vincent, M., Duval, R. E., Hartemann, P., and Engels-Deutsch, M. (2018). Contact Killing and Antimicrobial Properties of Copper. *J. Appl. Microbiol.* 124 (5), 1032–1046. doi:10.1111/jam.13681

Wang, J., Ma, X.-Y., Feng, Y.-F., Ma, Z.-S., Ma, T.-C., Zhang, Y., et al. (2017). Magnesium Ions Promote the Biological Behaviour of Rat Calvarial Osteoblasts by Activating the PI3K/Akt Signalling Pathway. *Biol. Trace Elem. Res.* 179 (2), 284–293. doi:10.1007/s12011-017-0948-8

Washington, M. A., Balmert, S. C., Fedorchak, M. V., Little, S. R., Watkins, S. C., and Meyer, T. Y. (2018). Monomer Sequence in PLGA Microparticles: Effects on Acidic Microclimates and *In Vivo* Inflammatory Response. *Acta Biomater.* 65, 259–271. doi:10.1016/j.actbio.2017.10.043

Wei, S., Ma, J.-X., Xu, L., Gu, X.-S., and Ma, X.-L. (2020). Biodegradable Materials for Bone Defect Repair. *Mil. Med Res* 7 (1), 54. doi:10.1186/s40779-020-00280-6

Wong, H. M., Yeung, K. W. K., Lam, K. O., Tam, V., Chu, P. K., Luk, K. D. K., et al. (2010). A Biodegradable Polymer-Based Coating to Control the Performance of Magnesium alloy Orthopaedic Implants. *Biomaterials* 31 (8), 2084–2096. doi:10.1016/j.biomaterials.2009.11.111

Xu, T. O., Kim, H. S., Stahl, T., and Nukavarapu, S. P. (2018). Self-neutralizing PLGA/magnesium Composites as Novel Biomaterials for Tissue Engineering. *Biomed. Mater.* 13 (3), 035013. doi:10.1088/1748-605X/aaaa29

Yoshizawa, S., Brown, A., Barchowsky, A., and Sfeir, C. (2014). Magnesium Ion Stimulation of Bone Marrow Stromal Cells Enhances Osteogenic Activity, Simulating the Effect of Magnesium alloy Degradation. *Acta Biomater.* 10 (6), 2834–2842. doi:10.1016/j.actbio.2014.02.002

Yu, W., Li, R., Long, J., Chen, P., Hou, A., Li, L., et al. (2019). Use of a Three-Dimensional Printed Polylactide-Coglycolide/tricalcium Phosphate Composite Scaffold Incorporating Magnesium Powder to Enhance Bone Defect Repair in Rabbits. *J. Orthopaedic Translation* 16 (16), 62–70. doi:10.1016/j.jot.2018.07.007

Zaritskaya, L., Shurin, M. R., Sayers, T. J., and Malyguine, A. M. (2010). New Flow Cytometric Assays for Monitoring Cell-Mediated Cytotoxicity. *Expert Rev. Vaccin.* 9 (6), 601–616. doi:10.1586/erv.10.49

Zhang, Q., Wu, W., Qian, C., Xiao, W., Zhu, H., Guo, J., et al. (2019). Advanced Biomaterials for Repairing and Reconstruction of Mandibular Defects. *Mater. Sci. Eng.* 103, 109858. doi:10.1016/j.msec.2019.109858

Zhao, C., Wu, H., Ni, J., Zhang, S., and Zhang, X. (2017). Development of PLA/Mg Composite for Orthopedic Implant: Tunable Degradation and Enhanced Mineralization. *Composites Sci. Tech.* 147, 8–15. doi:10.1016/j.compscitech.2017.04.037

Zhao, D., Zhu, T., Li, J., Cui, L., Zhang, Z., Zhuang, X., et al. (2021). Poly(lactic-co-glycolic Acid)-Based Composite Bone-Substitute Materials. *Bioactive Mater.* 6 (2), 346–360. doi:10.1016/j.bioactmat.2020.08.016

Conflict of Interest: The authors declare that the research was conducted in the absence of any commercial or financial relationships that could be construed as a potential conflict of interest.

Publisher's Note: All claims expressed in this article are solely those of the authors and do not necessarily represent those of their affiliated organizations, or those of the publisher, the editors and the reviewers. Any product that may be evaluated in this article, or claim that may be made by its manufacturer, is not guaranteed or endorsed by the publisher.

frontiers in Bioengineering and Biotechnology

REVIEW
published: 25 March 2022
doi: 10.3389/fbioe.2022.856398

Biodegradable Inks in Indirect Three-Dimensional Bioprinting for Tissue Vascularization

Yiting Ze[1,2†], Yanxi Li[1,2†], Linyang Huang[1,2], Yixin Shi[1,2], Peiran Li[1,2], Ping Gong[1,2], Jie Lin[1,2] and Yang Yao[1,2*]*

[1]State Key Laboratory of Oral Diseases, West China Hospital of Stomatology, Sichuan University, Chengdu, China, [2]National Clinical Research Center for Oral Diseases, West China Hospital of Stomatology, Sichuan University, Chengdu, China

Mature vasculature is important for the survival of bioengineered tissue constructs, both *in vivo* and *in vitro*; however, the fabrication of fully vascularized tissue constructs remains a great challenge in tissue engineering. Indirect three-dimensional (3D) bioprinting refers to a 3D printing technique that can rapidly fabricate scaffolds with controllable internal pores, cavities, and channels through the use of sacrificial molds. It has attracted much attention in recent years owing to its ability to create complex vascular network-like channels through thick tissue constructs while maintaining endothelial cell activity. Biodegradable materials play a crucial role in tissue engineering. Scaffolds made of biodegradable materials act as temporary templates, interact with cells, integrate with native tissues, and affect the results of tissue remodeling. Biodegradable ink selection, especially the choice of scaffold and sacrificial materials in indirect 3D bioprinting, has been the focus of several recent studies. The major objective of this review is to summarize the basic characteristics of biodegradable materials commonly used in indirect 3D bioprinting for vascularization, and to address recent advances in applying this technique to the vascularization of different tissues. Furthermore, the review describes how indirect 3D bioprinting creates blood vessels and vascularized tissue constructs by introducing the methodology and biodegradable ink selection. With the continuous improvement of biodegradable materials in the future, indirect 3D bioprinting will make further contributions to the development of this field.

Keywords: biodegradable ink, indirect 3D bioprinting, vascularization, scaffold, tissue engineering

OPEN ACCESS

Edited by:
Liqun Yang,
China Medical University, China

Reviewed by:
Qing Gao,
Zhejiang University, China
Yi Deng,
Sichuan University, China
Yiyan He,
Nanjing Tech University, China

****Correspondence:***
Jie Lin
84204362@qq.com
Yang Yao
yaoyang9999@126.com

[†]These authors have contributed equally to this work and share first authorship

Specialty section:
This article was submitted to Biomaterials, a section of the journal Frontiers in Bioengineering and Biotechnology

Received: *17 January 2022*
Accepted: *09 March 2022*
Published: *25 March 2022*

Citation:
Ze Y, Li Y, Huang L, Shi Y, Li P, Gong P, Lin J and Yao Y (2022) Biodegradable Inks in Indirect Three-Dimensional Bioprinting for Tissue Vascularization. Front. Bioeng. Biotechnol. 10:856398. doi: 10.3389/fbioe.2022.856398

INTRODUCTION

At present, only a few tissue-engineered products, such as skin (Ryssel et al., 2008) and cartilage (Makris et al., 2015), have achieved clinical success. For organs and tissues with more complex structure, such as the heart, liver, or spleen, there is still a long way to go (Berthiaume et al., 2011; Datta et al., 2017). An immature vascular system is one of the most important reasons for the failure of these products (Duan, 2017; Richards et al., 2017). In recent years, the rise of 3D bioprinting technology has enabled outstanding contributions to be made towards solving the problem of vasculature fabrication, thus extending the potential application of artificial tissues (Zhu et al., 2016; Alonzo et al., 2019; Hann et al., 2019). Indirect 3D bioprinting increasingly attracts research attention because of its superior capabilities with respect to vascularization (Wang Z. et al., 2019). Biodegradable materials are a crucial part of tissue engineering. They are typically designed to promote new tissue generation by serving as temporary templates and

providing physical or chemical signals for cells (Asghari et al., 2017). Biodegradable materials also have interesting applications and new challenges in indirect 3D bioprinting for vascularization. In this review, we describe the printing methods, selection of biodegradable inks, and applications of indirect 3D bioprinting for blood vessels and vascularized tissue constructs; furthermore, we point out the existing challenges and trends for future development.

INDIRECT 3D BIOPRINTING FOR TISSUE VASCULARIZATION

Vascularization Challenges in 3D Bioprinting

Vasculature is an essential part of the human body. Mature vasculature provides continuous perfusion, transporting nutrients to and removing metabolic wastes from cells, thus maintaining high cell viability and normal tissue function (Leong et al., 2013; Kim et al., 2016; Hann et al., 2019). For nonvascular tissues, the diffusion range of oxygen and nutrients is generally 100–200 μm (Carmeliet and Jain, 2000; Kaully et al., 2010). This means that, for successful *in vivo* implantation of engineered tissue constructs any larger in scale than this limit, it is necessary to ensure sufficient vasculature throughout the construct and good integration with the host vascular system (Ko et al., 2007). However, the vascularization of thick tissues has always been a major challenge and a research hotspot in tissue engineering.

3D bioprinting technology, also referred to as additive manufacturing, uses special 3D printers and bioinks containing cellular/bioactive components to fabricate scaffolds that imitate living tissues, in a layer-by-layer deposition approach with the help of computer-aided design (CAD) (Datta et al., 2017; Abdollahi et al., 2019). Compared with other tissue fabrication methods, 3D bioprinting stands out because of its convenience of customization, precise multi-dimensional control, and ability to fabricate 3D biostructures with suitable mechanical properties. In particular, its accurate control of complex and delicate structures within constructs, combined with the adoption of bioinks, make 3D bioprinting a powerful and efficient tool to address the problem of vascularization by creating a vasculogenic (Laschke and Menger, 2012; Balaji et al., 2013) (generating new blood vessels from endothelial cells or vascular progenitor cells) and angiogenic (Patel-Hett and D'Amore, 2011; Bae et al., 2012; Rouwkema and Khademhosseini, 2016) (germination or remodeling of existing vessels) environment for blood vessel formation. Most studies focus on two aspects: the fabrication of vascular grafts or vascular networks in thick constructs; however, these studies share one goal: to manufacture bionic vasculature that can work stably and continuously both *in vitro* and *in vivo*.

Although technological progress has helped the progress of vascularization in bioengineered constructs, major challenges remain (Novosel et al., 2011; Nazeer et al., 2021). The first challenge is the stable and delicate printing of microvascular networks. The diameters of capillaries, small vessels (small arteries and small veins), and small arteries with a three-layered structure are about 5–10 μm, 10–200 μm, and 30 μm, respectively; but the resolution of most 3D bioprinting is at the 100 μm level or above (Norotte et al., 2009; Hasan et al., 2014), making it difficult to print smaller diameter channels or the complex three-layered structure (adventitia, intima, and media) of blood vessels. Furthermore, the tiny hollow structure is unstable and prone to deformation or collapse owing to several factors, such as poor strength of the material, curing expansion of the bioink, or improper external extrusive force. In addition, microvascular networks should have complex multi-level branching structures. At present, the complexity of printed microvasculature hardly matches that of native vasculature (Robu et al., 2019).

The second challenge is the integration of allogeneic and autologous vascular networks. Effective integration with host circulation is the precondition of effective blood perfusion after implantation (Reis et al., 2016). Studies have shown that in implant tissue engineering, compared to the disordered vascular network formed by randomly distributed cells in culture, ordered vascular structure showed faster integration with the host and more stable perfusion, for which 3D bioprinting has the advantage (Vacanti, 2012; Baranski et al., 2013). However, the physiological blood vessel structure is so subtle that it is still difficult to use 3D bioprinting to fabricate smooth and regularly arranged microchannels at the micron level. Furthermore, most experiments are conducted *in vitro*. To date, no *in vivo* experiment has shown that, even with good integration with the host, thick tissue constructs remain viable for long or that necrosis will not occur after implantation.

Thirdly, it is difficult to ensure complex but stable blood perfusion in thick tissue constructs. Good blood perfusion is a necessary condition for engineered tissue survival *in vivo*. Currently, many strategies depend on the ingrowth of host vessels to achieve graft blood perfusion (Cheng et al., 2011; White et al., 2014; Kang et al., 2015), which is very slow (<1 mm per day) (Zhang et al., 2020), to preserve cell viability within thick tissue grafts (Sooppan et al., 2016). In order to accelerate the process, prevascularization is widely applied. Prevascularization refers to the generation of preformed microvasculature before tissue construct implantation (Laschke and Menger, 2016). It relies on seeding or encapsulating endothelial cells (ECs) in the construct *in vitro*. However, the process of cell infiltration and growth *in vitro* is uncertain, and the resultant vasculature is usually inhomogeneous (Leong et al., 2013). When implanted, immature vasculature results in insufficient blood perfusion and induces core necrosis in constructs (Asakawa et al., 2010), causing the failure of thick constructs to survive (Rouwkema et al., 2008).

Nowadays, many 3D bioprinting methods have been developed to mimic vasculature, including extrusion-, laser-based systems, electrospinning, stacking of micropatterns or modules, and cell sheet techniques (Yamamura et al., 2007; Kolesky et al., 2014; Sarker M. et al., 2018; Sarker M. D. et al., 2018). New methods are constantly being explored to solve the abovementioned problems, and indirect 3D bioprinting may cast light on vascularization in tissue engineering.

Indirect 3D Bioprinting to Address the Problem of Tissue Vascularization

Instead of directly simulating and manufacturing the target constructs, indirect 3D bioprinting fabricates a sacrificial mold

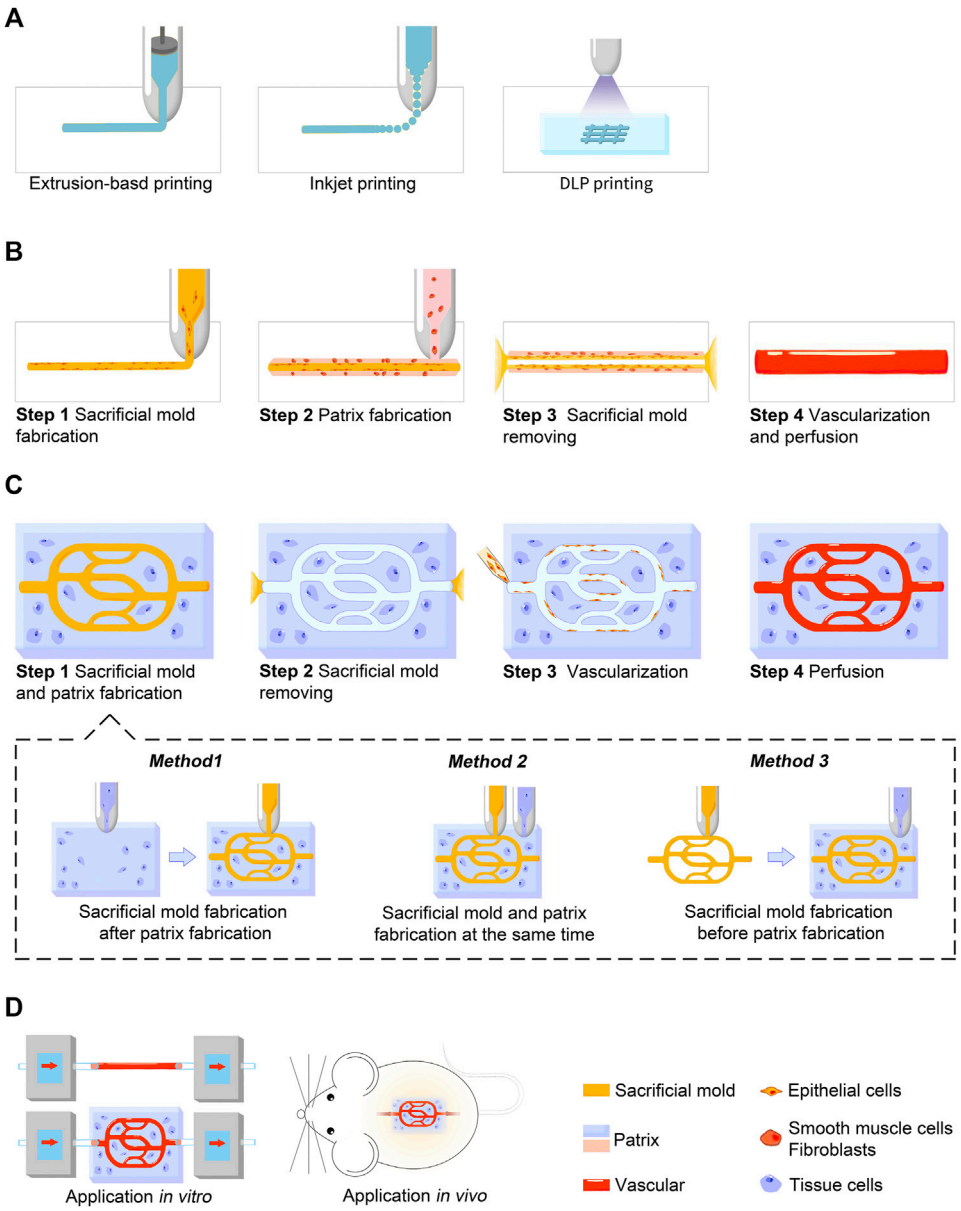

FIGURE 1 | Schematic illustration showing the indirect 3D bioprinting process for blood vessels and vascularized tissue constructs. **(A)** Three major techniques used in indirect 3D bioprinting for both sacrificial mold and patrix fabrication, including extrusion-based printing, inkjet-based printing, and DLP printing. **(B)** Process of blood vessel fabrication. **(C)** Process of vascularized tissue construct fabrication. Sacrificial mold and patrix fabrication can be further divided into three methods according to the sequence of fabrication in step 1. **(D)** Applications *in vitro* or *in vivo*. Blood vessel grafts constructed by indirect 3D bioprinting are currently used for studies *in vitro*, while vascularized tissue constructs are used for both studies *in vitro* and animal experiments *in vivo*.

or template (negative model) and fills it with a second material. After selective dissolution, the sacrificial mold or template is removed while the construct (patrix) formed by the second material is preserved (Lee et al., 2013; Van Hoorick et al., 2015). Through this approach, pores, cavities, and channels can be precisely made throughout thick constructs (Lee et al., 2008; Schumacher et al., 2010). Owing to its specific manner of printing, other names for indirect 3D printing include lost-mold technique, indirect rapid prototyping, indirect additive manufacturing, and indirect solid free-form fabrication (Chu et al., 2001; Schumacher et al., 2010; Van Hoorick et al., 2015; Houben et al., 2016; Houben et al., 2017).

Currently, indirect 3D bioprinting has made progress in both hard and soft tissue engineering systems. Some specific tissue constructs such as functional nerve guide conduits, human knee meniscal scaffolds, sized vascular grafts, can be successfully produced in laboratories as proof of concept (Schöneberg et al., 2018; Huang et al., 2021; P B et al., 2022). At the same time, with the assistance of sacrificial molds, materials that are traditionally difficult to print can be utilized to manufacture fine

structures. For example, ceramic materials play a vital role in bone tissue engineering, but its additive manufacturing is considered challenging. Chawich et al. creatively utilized a sacrificial honeycomb mold of polylactic acid (PLA), and they ultimately produced customizable stable Si-based 3D non-oxide cellular ceramic structures (El Chawich et al., 2022). Another team produced stiffness memory nanohybrid scaffolds from poly(urea-urethane) (PUU) solution which exhibits outstanding performance in long-term implantable cardiovascular devices but can not be printed directly (Wu et al., 2018). Of all the breakthroughs, the greatest concern is the potential for this technique to address problems where vascularization is a key issue.

Generally, indirect 3D bioprinting for blood vessels and vascularized tissue constructs includes two general aspects: channel fabrication and vascularization. Channel fabrication can be further divided into three steps: sacrificial mold fabrication, patrix fabrication, and sacrificial mold removal. Manufacture of the negative mold is designed to simulate the shape and extension direction of the vascular network in a solid columnar form. In patrix fabrication, the patrix is built around the sacrificial mold to form the final scaffold or construct. Afterwards, special steps are performed to remove the sacrificial mold, leaving isometric hollow channels inside the scaffold or construct. The detailed production process and precautions of each step have been described in excellent reviews (Lee and Yeong, 2016; Houben et al., 2017; Zhu et al., 2021). **Figure 1** provides a brief overview of the printing process. Here we mainly introduce the techniques frequently used and bioink selection.

The three main techniques are extrusion-based, inkjet-based, and light-assisted 3D printing (Vijayavenkataraman et al., 2018). Each technique has advantages and disadvantages, and raise different requirements for bioinks. In extrusion-based printing, the most common technique, 3D structures are built layer by layer using a nozzle to dispense continuous filament (Štumberger and Vihar, 2018; Yang et al., 2020). This technique can achieve resolutions of >100 μm, uniform cell distribution, and moderate printing speed (Placone and Engler, 2018). The technique is compatible with various materials with a viscosity range of 30 mPa s to 6×10^7 mPa s (Murphy and Atala, 2014). Furthermore, its cell-friendly printing environment allows it to be used for printing scaffolds with high cell density (Skardal et al., 2015). One promising method is coaxial printing, also referred to as coaxial extrusion. Its key features are the concentric and multi-layered nozzles that enable concentric multi-material deposition. With the use of sacrificial materials, this technique allows synchronous manufacturing of the sacrificial mold and scaffold, simplifying the production process (Kjar et al., 2021). However, for extrusion-based printing, the shear stress produced during printing is an important cause of cell death and, because the nozzle size is inversely proportional to extrusion pressure, small nozzles used to improve resolution may have a greater negative impact on cell viability (Kyle et al., 2017).

Inkjet-based printing is defined as dispensing bioink through small orifices via piezoelectric, thermal, or electrostatic actuators, and accurately positioning a very small amount of the bioink on a substrate (Calvert, 2007; Datta et al., 2017). This technique can reach high resolutions of 10–100 μm with short printing times (Poellmann et al., 2011; Gudapati et al., 2016). Different inkjet printing techniques require different material viscosities. For thermal, piezoelectric, and electrostatic inkjet printing the ink viscosity should be relatively low, because the nozzle diameter is usually small and is prone to clogging (Li et al., 2020). However, for electrohydrodynamic jet bioprinting which produces droplets through an electric field, bioink with a high viscosity of over 2000 mPa s can be printed (Workman et al., 2014). Nozzle clogging, small nozzle aperture indirectly leading to cell viability damage, and low-viscosity bioink resulting in poor shape fidelity present challenges to broadening the range of implementation (Chahal et al., 2012; Malda et al., 2013; Zhu et al., 2017).

Light-assisted printing includes digital light processing (DLP)-based and laser-based printing. DLP printing is realized by dynamically projecting an entire computer-generated optical mask into a photosensitive prepolymer solution to induce photopolymerization, while laser-based printing uses a bottom-up approach (drop-by-drop) to build constructs (Zhu et al., 2021). DLP printing is now attracting greater attention as this technique provides precise control of scaffold structures and features and high printing speed (Mandrycky et al., 2016). Nevertheless, the selection of biomaterials is limited to photosensitive polymers and additional chemical modifications are required for most biomaterials (Yue et al., 2015). Moreover, the properties of printing complex patterns directly make DLP more frequently used in direct printing. Therefore, light-assisted printing has only been used in a few cases of indirect 3D printing (Thomas et al., 2020).

Another technique called embedded extrusion bioprinting involves printing a cell-containing hydrogel in a supporting bath, which serves as a sacrificial printing environment (Rocca et al., 2018). As atypical indirect 3D bioprinting, this technique does not impose any requirements for the shape of the sacrificial mold but instead skips this step and directly prints the male mold. The advantage is that low-viscosity hydrogels can be used to construct complex draping and hollow structures with the support of the sacrificial supporting bath via free-form bioprinting, which is difficult to achieve in air. Limitations are that shape fidelity of the complex pore structure is low, resolution is currently at the millimeter level, and the removal of the sacrificial supporting bath is relatively cumbersome (Afghah et al., 2020).

Table 1 summarizes the characteristics of the common techniques covered in this review.

Vascularization Strategies

Vascularization is essential for engineered tissue grafts to achieve biological function and can be realized by seeding ECs into hollow scaffold channels (Bae et al., 2012; Massa et al., 2017). After migration, survival, proliferation, and differentiation of ECs, a monolayer of cells is ultimately formed on the surface of the channels, mimicking the physiological vessel wall. Usually, growth factors and other bioactive factors are perfused along with ECs to regulate cell behavior or promote cell differentiation

TABLE 1 | 3D bioprinting techniques for indirect 3D bioprinting covered in this review.

3D bioprinting techniques	Sacrificial mold or patrix fabrication	Supported bioink viscosity	Minimum feature resolution	Printing speed	Shape fidelity	Frequency of use	References
Extrusion	Sacrificial mold and patrix fabrication	Wide range of 30–6 × 10^7 mPa s	>100 μm	Moderate	Good	+++	Murphy and Atala, (2014) Massa et al. (2017) Yang et al. (2020) Zou et al. (2020)
Inkjet	Sacrificial mold and patrix fabrication	Low in most cases	10–100 μm	High	Poor	+++	Yeong et al. (2007) Chahal et al. (2012) Schöneberg et al. (2018) Xu et al. (2018)
Light-assisted	Sacrificial mold and patrix fabrication	Low	5–300 μm	High	Good	+	Kang and Cho, (2012) Mandrycky et al. (2016) Ji et al. (2019) Thomas et al. (2020)
Embedded extrusion	Patrix fabrication in sacrificial supporting bath	Low to medium	At millimeter level	Slow	Medium	++	Rocca et al. (2018) Štumberger and Vihar, (2018) Afghah et al. (2020) Chiesa et al. (2020)

(Auger et al., 2013). The generation of new blood vessels involves complex effects of a variety of cells, factors released by platelets, extracellular matrix, and angiogenic and anti-angiogenic factors. Vascular endothelial growth factor (VEGF) and fibroblast growth factor b (FGFb) are the most effective angiogenic growth factors and are commonly used in the making of angiogenic biomaterials (Sun et al., 2011; Matsui and Tabata, 2012). Research reports successful seeding of human umbilical vein endothelial cells (HUVECs) into microchannels after mold sacrifice, and a uniform HUVEC layer formation coating the channels. It was demonstrated that the HUVEC layer could, to some extent, act as a barrier to protect scaffold cells from harmful substances (Massa et al., 2017). However, a potential problem is that the channel diameter may affect cell inoculation. Narrow channels will become blocked by ECs, hindering perfusion, while diameters too large will require more time for cells to cover the channel surface. Studies have shown that ideal channel diameter ranges from 280 to 1,270 μm (Zhang et al., 2016).

Another elegant vascularization strategy of indirect 3D bioprinting is to encapsulate ECs in the sacrificial ink to realize synchronous distribution of ECs in the process of blood vessel (sacrificial channel) fabrication. This approach reduces the manufacturing process and can realize precise control of cell distribution (Thomas et al., 2020). Owing to direct contact with cells and bioactive factors, biocompatibility and biodegradability of materials are particularly important. Studies have demonstrated that cells show increased proliferation and proliferation in hydrogels with faster degradation rates (Patterson and Hubbell, 2010). A further study suggests that biodegradable materials can promote angiogenesis through temporarily controlled delivery of siRNAs (Nelson et al., 2014). Application of biodegradable materials may better promote vascularization.

BIODEGRADABLE INK SELECTION

Biodegradable materials are the main scaffold materials in the field of tissue engineering, which have a broad range of applications in medicine and pharmacy because of good biosafety, reducing inflammation, ability to mimic the extracellular matrix (ECM), and enzymatic degradation *in vivo* (Asghari et al., 2017). Eventually these scaffolds are replaced by host tissues (Silva et al., 2020). Biodegradable materials are generally classified into synthetic materials and natural materials. Synthetic materials such as polyglycolic acid (PGA), polycaprolactone (PCL), PLA, poly (N-isopropylacrylamide), and their copolymers have already been widely used in tissue engineering. Advantages are that the key properties of these materials as scaffolds can be artificially controlled, such as degradation rate and some specific mechanical properties, including stiffness and elasticity; however, their biosafety is comparatively poor. Natural materials, such as chitin, alginate, collagen, and gelatin, are polymers produced by biological systems. Natural materials have many advantages and disadvantages. The most prominent advantage is their similarity to host tissues, including the ability to communicate with biological systems, enzymatic degradation, metabolic compatibility, and low inflammatory response (Asghari et al., 2017). However, owing to the poor strength of natural materials, scaffolds often collapse before finishing their task. In addition, they generally show slow and inhomogeneous degradation *in vivo*, and are inconsistent with host tissue regeneration rate.

In the field of indirect 3D printing, biodegradable polymers play vital roles in fabricating vascular or vascularized tissue: 1) As scaffold materials, they allow endothelial cells and a variety of angiogenic factors to exist, as well as providing a flexible

TABLE 2 | Common biomaterial inks for indirect 3D bioprinting covered in this review.

Biomaterials	Scaffold or sacrificial material	Natural or synthetic	Biodegradable or non-degradable	Biocompatibility	Mechanical property	Combinations	Applications	References
Gelatin	Scaffold and sacrificial material	Natural	Biodegradable	Good	Poor	PVA, Pluronic, agarose, HA, xanthan-gum	Earlobe-shaped channel system, liver model	Liu et al. (2008) Benton et al. (2009) Nichol et al. (2010) O'Bryan et al. (2017) Štumberger and Vihar, (2018)
Fibrin	Scaffold material	Natural	Biodegradable	Good	Poor	Gelatin, carbohydrate glass	Arteriole/venule	Hu et al. (2018) Schöneberg et al. (2018) Duarte Campos et al. (2020)
Alginate	Scaffold and sacrificial material	Natural	Biodegradable	Good	Medium	PVA, agarose, Pluronic F127, carbohydrate glass	Human heart- and kidney-like objects	Lee and Mooney, (2012) Rocca et al. (2018) Piras and Smith, (2020)
SF	Scaffold material	Natural	Biodegradable	Good	Good	Thermoplastic, plaster	Bone and cartilage engineering	Liu et al. (2013) Bidgoli et al. (2019)
PVA	Sacrificial material	Synthetic	Biodegradable	Good	Good	Gelatin, silk, agarose, alginate, fibrin, Matrigel, PLCL, PUU	100–1750 μm diameter channels	Tocchio et al. (2015) Hernández-Córdova et al. (2016) Hu et al. (2018) Im et al. (2018) Kim et al. (2018) Charron et al. (2019) Wu et al. (2019)
HA	Sacrificial material	Synthetic	Biodegradable	Good	Poor	Gelatin	Enzymatically digestible, 360–720 μm diameter channels	Thomas et al. (2020)
Agarose fiber	Sacrificial material	Natural	Biodegradable	Good	Good	Alginate, Gelatin	100–1,000 μm diameter channels	Bertassoni et al. (2014) Massa et al. (2017) López-Marcial et al. (2018)
Carbohydrate glass	Sacrificial material	Synthetic	Non-degradable	Cytotoxic when dissolved	Good	PEG, fibrin, alginate, agarose	150–750 μm diameter channels	Khattak et al. (2005) Miller et al. (2012)
Pluronic F127	Sacrificial material	Synthetic	Non-degradable	Cytotoxic	Good	Gelatin, sodium alginate, decellularized extracellular matrix	150–3,000 μm diameter channels	Homan et al. (2016) Daly et al. (2018) Ding and Chang, (2018) Hu et al. (2018) Xu et al. (2018) Yang et al. (2020)

environment for complex angiogenesis. 2) As sacrificial materials, compared with non-degradable ones, the damage to cell activity when manufacturing or removing the sacrificial molds is much lower. 3) Since the biodegradable materials can degrade *in vivo*, the use of them as sacrificial material helps to skip the processing step of sacrificial mold removal *in vitro*, thus shortening the manufacturing time. 4) In theory, by regulating and matching the degradation rate of scaffolds and sacrificial materials, the removal of sacrificial channels and channel endothelialization can be completed *in vivo* before the scaffolds completely degrade, thus realizing the direct *in vivo* application of constructs.

In the following section, we mainly enumerate the commonly used biodegradable polymers in indirect 3D bioprinting for blood vessels and vascularized tissue constructs. **Table 2** summarizes the characteristics, combinations, and current applications of different scaffold and sacrificial materials.

Scaffold Materials

Scaffold materials, whose purpose is to simulate the ECM and provide support for tissue regeneration in the human body, should have good biosafety, biocompatibility, biodegradability, and mechanical properties that are favorable for cell growth, proliferation, and migration (Lee A. Y. et al., 2014). Ideally, they

should also be able to promote angiogenesis (Do et al., 2015; Xu et al., 2018). After crosslinking, scaffold materials need a certain degree of stiffness to maintain structural integrity during removal of sacrificial materials, and to support the flow of perfusion (Skylar-Scott et al., 2019). Controllable degradation rate consistent with the growth and repair rate of host tissue *in vivo* is also necessary (Malda et al., 2013; Serbo and Gerecht, 2013).

To date, various natural biodegradable polymers have been used for scaffold bioprinting, such as gelatin (Chen et al., 2012), fibrin (Schöneberg et al., 2018), and alginate (Jia et al., 2014); they are collectively referred to as hydrogels. They show excellent human ECM features and allow cell encapsulation (Malda et al., 2013), but they have all been deficient in some respect. Uncontrolled degradation and poor mechanical properties are the main problems, and they are also the research focus of material modification. The simplest and most used method is blending modification. In this approach, the hydrogel ratio is controlled to prevent excessive polymer concentration or dilution, which may have an adverse effect on cell behavior or mechanical properties (Malda et al., 2013; Duarte Campos et al., 2016; Zou et al., 2020).

Gelatin is one of the most widely used scaffold materials extracted from collagen, the main component of natural human ECM. Gelatin is composed of 85–92% protein, water, and mineral salts, and is highly susceptible to several proteases (Bello et al., 2020). Its excellent biocompatibility and similarity with collagen have made it the preferred material for the assembly of scaffolds. However, as a biomaterial ink, gelatin does have several drawbacks; these include low viscosity and yield stress, as well as relatively long crosslinking time, which leads to poor shape retention and structural collapse, and is the main obstacle to creating high resolution 3D pore or microchannel structures (O'Bryan et al., 2017). These disadvantages can be improved by making gelatin composites, or applying sacrificial materials to support the scaffold hydrogel before crosslinking (Moroni et al., 2018). In addition, the degradation rate of large solid gelatin *in vivo* is relatively slow (Daly et al., 2018). Large numbers of gelatin residues within thick tissues remain a challenge. Solutions may include lowering the degree of metacrylation and the macromer concentration (Nichol et al., 2010; Chen et al., 2012). Furthermore, by creating microchannels within the hydrogels to enhance host interaction, the degradation of gelatin can be enhanced (Daly et al., 2018). This is possibly because of the increased invasion by host immune cells, such as macrophages, which is vital for degrading gelatin hydrogels (Kim et al., 2014).

Gelatin-methacryloyl (GelMA) is the most commonly used material among gelatin derivatives and composites. GelMA is a photopolymerizable hydrogel made of gelatin derivatized with methacrylamide side groups (Van Den Bulcke et al., 2000). It has high biosafety compared with several gelatin-based hydrogels formed by chemical crosslinking methods, such as ones fabricated using glutaraldehyde or transglutimase derived from bacteria (Benton et al., 2009). GelMA is sensitive to matrix metalloproteinases and can be degraded by cells (Nichol et al., 2010). By adjusting the rate of polymerization and ratio of methacrylic acid, GelMA can maintain relatively good shape with adjustable mechanical properties (Benton et al., 2009). Research has shown that ECs as well as endothelial colony-forming cells can undergo active angiogenesis or vasculogenesis in GelMA hydrogels either *in vivo* or *in vitro* (Chen et al., 2012; Massa et al., 2017).

Fibrin scaffolds have a wide range of applications in tissue engineering, especially in bone tissue engineering. Fibrin is a natural biopolymer produced by thrombin cleavage of fibrinogen, and serves as a temporary scaffold for tissue healing in physiologic processes (Noori et al., 2017). It also plays an important role in specific receptor-mediated interactions with cells because of its ability to bind different types of proteins and growth factors, including FGF and VEGF that promote angiogenesis (Breen et al., 2009; Litvinov and Weisel, 2017). Fibrin hydrogel can be easily remodeled by ECs, which is favorable for fast angiogenesis. Nevertheless, similar to gelatin, fibrin rapidly degrades, and has poor mechanical stability, durability, and shape fidelity (Calderon et al., 2017). To overcome these problems, fibrin composites and mimics have been developed in 3D bioprinting. For example, by combining fibrin and gelatin, the stiffness of the hydrogel increased, and lower water loss on compression was observed (Schöneberg et al., 2018). Another attempt at a fibrin composite is called ELP-RGD, composed of ELP (elastin-like protein) hydrogel along with a cell adhesion RGD amino acid sequence derived from fibronectin. ELP hydrogel contains elastin (a kind of fibrin) -like repeat units alternating with biologically active domains (Madl et al., 2017). As a scaffold material, ELP-RGD has adjustable stiffness, is readily hydrolyzable with protease, and is able to promote matrix remodeling as well as cell proliferation (Chung et al., 2012). It has been demonstrated to be suitable for on-chip platforms with vascular-like networks (Duarte Campos et al., 2020).

Alginate is a natural polysaccharide extracted from alginic acid. The long polysaccharide chains provide it with pliability and gelling adeptness, and it undergoes hydrolytic cleavage under acidic conditions or enzymatic degradation by lyase (Pawar and Edgar, 2012; Rastogi and Kandasubramanian, 2019). Despite its mechanical instability and poor cell attachment, alginate is widely used as a hydrogel because of its low cost, good biosafety, and its ability to be rapidly but reversibly crosslinked by Ca^{2+} under mild conditions (Jia et al., 2016; Rastogi and Kandasubramanian, 2019). However, one important limitation of alginate application *in vivo* is the low degradation rate and unpredictable degradation process owing to the lack of alginate degrading enzyme in the human body (Reakasame and Boccaccini, 2018). Moreover, alginate shows relatively poor cell adhesion and infiltration (Balakrishnan et al., 2014). Measures like modification or mixing in additives, such as nanomaterials, peptides, and growth factors, are useful to regulate rheological properties, promote cell adhesion, or guide cell differentiation (Lee and Mooney, 2012; Piras and Smith, 2020). For example, by oxidative modification, more reactive sites are provided to the structure, accelerating the alginate's biodegradability (Liang et al., 2011). Ino et al. combined sodium alginate with sacrificial molds of sugar structures, and by soaking the structure in a $CaCl_2$ solution they achieved

simultaneous dissolution of the mold and formation of calcium alginate hydrogel, thus simplifying and hastening the manufacturing process (Ino et al., 2020).

Silk fibroin (SF), a silk-derived protein-based material approved by the FDA (Perrone et al., 2014), has been used to make clinical sutures for many years. In recent decades, because of new processing techniques and further understanding of its properties, SF has attracted great interest in bone and cartilage engineering (Liu et al., 2013). Compared with the abovementioned materials, native silk fibers have excellent mechanical properties including good strength and toughness (Kundu et al., 2013; M et al., 2017). Other advantages of SF include good biosafety, good biocompatibility, controllable biodegradability and bone induction, and low immunogenicity (Wenk et al., 2009; Kundu et al., 2013). The host immune system has been shown to play a significant role in the degradation of SF scaffolds. Macrophages mediate the process, suggesting that SF is also bioresorbable (Wang et al., 2008). It is worth noting that SF remains strong during degradation, which is its unique advantage in tissue engineering (Kundu et al., 2013). Studies were carried out to produce vascularized scaffolds via SF. In combination with indirect 3D bioprinting, a layered SF-bioactive glass composite scaffold with excellent compressive strength, flexibility, and 10–50 μm micropores has been fabricated (Bidgoli et al., 2019). The scaffold comprises hierarchically micro and sub-micro pores, which are important features for promoting cell migration, differentiation, bone formation, and angiogenesis (Qi et al., 2018); results showed that the scaffold enhanced cell adhesion and cell proliferation (Bidgoli et al., 2019). However, drawbacks of SF such as lack of biological activity, general poor performance under humid conditions, and the difficulty of transportation and long-term storage may limit its further application. These limitations are potential future research directions.

Other scaffold materials commonly used in indirect 3D bioprinting but that are not yet, or rarely, used for vasculature fabrication include polyethylene glycol (PEG), hyaluronic acid (HA), PLA, PCL, poly (L-lactide-co-ε-caprolactone) (PLCL), and poly(lactic-co-glycolic) acid (PLGA) (Park et al., 2014; Houben et al., 2016; Aljohani et al., 2018; Im et al., 2018). Inorganic substances are more frequently used for osteochondral tissue fabrication because of their excellent mechanical properties. Future studies on these materials can be performed in the field of indirect 3D bioprinting for tissue vascularization.

Sacrificial Materials

Ideal sacrificial materials should have good fluidity for free molding, rapid solidification to save printing time, a low expansion rate, and appropriate mechanical strength to achieve good shape fidelity. During the process of printing, there should be no adverse reactions with the scaffold material that result in deformation of the scaffold structure. If working in combination with scaffold materials containing cells or other bioactive factors, sacrificial materials should be chosen to ensure non-toxic and non-stimulatory conditions. Also, the conditions for their state transformation and removal should be mild and easy to achieve, preserving the shape and properties of the scaffold. When exposed to living cells *in vivo* or bioactive components, cytotoxicity, biocompatibility, and whether the removal conditions are inconducive are usually considered first.

Currently the commonly used sacrificial materials that come closest to meeting the conditions described earlier are carbohydrate glass (Miller et al., 2012), Pluronics (Afghah et al., 2020), and PVA (Zou et al., 2020). Carbohydrate glass and Pluronics are nonbiodegradable materials. Carbohydrate glass is a simple glass consisting of a mixture of carbohydrates, including glucose, sucrose, and dextran, and was one of the first materials applied to indirect 3D bioprinting as a sacrificial biomaterial ink (Miller et al., 2012). The synthetic glass shows sufficient mechanical stiffness to maintain its shape in air, as well as rapid dissolution to accelerate the process. Results demonstrated that it can be compatible with a variety of natural or synthetic hydrogel materials, such as agarose, alginate, fibrin, and Matrigel, adapting well to their different properties and means of crosslinking (Miller et al., 2012). Currently, vessels with diameters ranging from 150 μm to 1 mm and smooth in-plane junctions can be achieved with this sacrificial ink (Pollet et al., 2019). Pluronics are a class of amphiphilic tri-block copolymers popular in drug and clinical applications. Because they have the characteristics of solubilizer, emulsifier, and stabilizer, they are often used as excipients in pharmaceutical preparations (Jarak et al., 2020). The most frequently used Pluronic in tissue engineering is Pluronic F127, which can rapidly dissolve in aqueous media or biological fluids. Its sol-gel transition at room temperature and convenient removal attracts attention as a sacrificial ink. Channels with a diameter as small as 150 μm can now be printed with Pluronic F127 (Homan et al., 2016). However, both carbohydrate glass and Pluronic F127 show cytotoxicity when dissolved, which is one of the most prominent shortcomings (Miller et al., 2012; Deng et al., 2020). Besides, Pluronic F127 liquifies at low temperatures, making it difficult to use with some scaffold materials that require these temperatures during casting, such as collagen and matrix gelatin (Ding and Chang, 2018; Hu et al., 2018).

As mentioned above, nonbiodegradable materials usually exhibit certain cytotoxicity and their removal is relatively cumbersome. As a result, researchers have investigated biodegradable materials, which show higher biosafety and are expected to achieve direct application *in vivo*.

PVA, a commonly used biodegradable sacrificial material, has satisfactory biocompatibility and similar functions to natural tissues, including high water content, high elasticity, and low interfacial tension with biological fluids (Teodorescu et al., 2019). It shows resistance to protein absorption, which is important for bone formation (Kim et al., 2018). The ease of printability allows it to be used for repeatable fabrication of complex vascular patterns (Hu et al., 2018). In terms of mechanical properties, PVA has good strength and stiffness at 25°C (Charron et al., 2019) and fits well with different biodegradable natural polymers, such as gelatin and silk (Mohanty et al., 2016). Tocchio et al. used PVA successfully to make sacrificial templates with characteristic sizes of 100–500 μm in multi-branch structures, which helped to further simulate the complex environment of cell growth, and

showed great potential for production of large-sized vascularized scaffolds that would meet clinical needs (Tocchio et al., 2015). Compared to other sacrificial materials, the stable chemical properties, convenience of preservation, and low cost of PVA are huge advantages for its use in industrial production. However, owing to the lack of bioactive components, PVA tends to be resistant to protein absorption and cell adhesion, which limits its further application outside bone tissue engineering (Schmedlen et al., 2002). Furthermore, if PVA filaments are too large in diameter (>500 μm reported), they are likely to deform as they cannot support their own weight (Hernández-Córdova et al., 2016). More in-depth research is needed in the future.

HA-based enzymatically degradable photoink was developed by different research teams (Zhu et al., 2017; Thomas et al., 2020). HA is a linear polysaccharide. It is an essential component of the ECM and has vital effects on many cellular responses, including cellular signaling, wound repair, morphogenesis, and angiogenesis (Burdick and Prestwich, 2011). In the abovementioned two experiments, HA was chemically modified to achieve photopolymerization and mixed with gelatin to form the photoink. The hydrogels could be digested with hyaluronidase to achieve fast (within hours) and collaborative (not limited by graft size) degradation. Channels ranging from 50 to 720 μm have been successfully fabricated and achieved vascularization. However, the enzymolysis process may reduce EC activity, and because the enzyme is encapsulated in the bioink, degradation occurs at the same time as printing, which exerts a certain amount of time pressure (Zhu et al., 2017; Thomas et al., 2020).

Other research teams have also produced alternate solutions; for example, agarose was used as a sacrificial ink (Massa et al., 2017). It shows good rheological properties and printability similar to Pluronics when combined with alginate (López-Marcial et al., 2018). Currently, agarose has been shown capable of fabricating 100–1,000 μm diameter pipes and forming a smooth channel surface for cell inoculation (Massa et al., 2017). Another example is gelatin, that has been used as a sacrificial material and is removed by warming (Skylar-Scott et al., 2019). Channels over 400 μm in diameter could be printed with high fidelity. Another team used alginate and $CaCl_2$ to create ultrafine fibers with a size range of 150–200 μm, and clear, interconnected microchannel structures were observed through the hydrogel as a result (Hammer et al., 2014). It is worth mentioning that some of the removal processes of these biodegradable sacrificial materials are physical processes. The utilization of their biodegradable properties needs to be further explored, as they show great potential to facilitate simplified fabrication processes and direct *in vivo* application of tissue constructs.

Cells and Biological Factors

When 3D printing techniques print with cells, the printing ink is also referred to as bioink. It includes cells, biomaterials that serve as a cell-delivery medium, and biological factors (Groll et al., 2018). The existence of cells and biological factors require higher biosafety of the materials to maintain good bioactivity of the bioinks as discussed before. Also, to prevent cells from excessive shear forces, low viscosity fluid is required. Viscosity and rheological properties greatly influence the printability of the bioinks, and they are mainly determined by the molecular weight and concentration of polymer in solution (Schwab et al., 2020). Gels with shear-thinning properties or solutions containing hydrogel precursors are preferred. In current studies of indirect 3D bioprinting for vascular systems, HUVECs, smooth muscle cells (SMCs), and fibroblasts have been used, and the cell viability is generally over 80% with high cell density (**Table 3**). Still, more efforts should be put on developing optimized bioinks in future investigations.

PRECLINICAL AND CLINICAL APPLICATIONS OF INDIRECT 3D PRINTING FOR DIFFERENT TISSUE VASCULARIZATION AND BIODEGRADABLE INK SELECTION

Nowadays, only a few tissues with less stringent vascular structures, such as cartilage and the cornea, have achieved good clinical outcomes (Rouwkema et al., 2010; Seifu and Mequanint, 2012; Pimentel et al., 2018). Advanced techniques and suitable biomaterials are essential for the development of functional engineered tissues. Indirect 3D bioprinting and the related biodegradable inks provide new opportunities for commercial development. The process has been applied to manufacturing various tissues and has achieved corresponding results. In general, our appraisal can be divided into vascular grafts and vascularized tissue; the latter includes highly vascularized tissue, vascularized osteochondral tissue, and vascularized skin, as shown in **Table 3**.

Vascular Grafts

Most vascular regions treated during surgery are larger than 1 mm in diameter, which, theoretically, both direct and indirect 3D bioprinting can achieve. Biomaterial selection requirements for tissue-engineered vascular grafts are low immunogenicity, good mechanical properties, and similarity to native tissue characteristics (Liu et al., 2018). Compared with non-degradable polymers, biodegradable natural polymers (such as decellularized tissue scaffolds and fibrin) have relatively poor mechanical properties, but they have lower antigenicity and can better simulate natural tissue structures (Aper et al., 2016). Meanwhile, biodegradable synthetic polymers (such as PGA and PCL) can have adjustable mechanical properties and degradation rate, and they are considered the ideal biomaterials for tissue-engineered vascular grafts (Liu et al., 2018). Afghah et al. used embedded extrusion bioprinting with a composite Pluronic-nanoclay support-bath and biocompatible alginate to create a branched vascular structure with diameters of several millimeters. This vascular mold showed good mechanical properties and preservation of shape fidelity after removal from the support-bath, but its biological functions have not yet been verified (Afghah et al., 2020). While Schöneberg et al. used the indirect bioprinting technique to fabricate biofunctional multi-

TABLE 3 | Summary of indirect 3D bioprinting applications and bioink selection for different tissue vascularization covered in this review.

Category	Sub-category	Sacrificial material	Scaffold material	Cells and cell density	Cell viability	Progress	Limitations	References
Vascular grafts	Arteriole/venule	Gelatin	Fibrin and collagen/fibrin blends	HUVECs (~10^7 cells/ml); SMCs (~10^6 cells/ml); normal human dermal fibroblasts (—)	~83%/91% (1d/4d, SMCs)	*In vitro* model success	Unable to meet human transplantation standards	Schöneberg et al. (2018)
	Branched vascular structure	Pluronic-nanoclay	Alginate	—	—	*In vitro* non-cell model success	No biological function	Afghah et al. (2020)
Highly vascularized tissue	Heart-like structure	Pluronic F127	Alginate	—	—	Simplified models for conceptual validation	No good method to fabricate complex structures	Zou et al. (2020)
	Valentine-shaped heart	PVA	Alginate and agarose	HUVECs (~10^6 cells/mL); H9c2 rat myoblasts (~10^6 cells/ml)	~95%/90% (1d/14d)	A hollow structure containing a network of micro-fluid channels	Difficult to imitate the ultrastructure of capillaries; low degree of simulation	Zou et al. (2020)
	Simplified cardiac scaffolds	PVA	PUU	Primary human cardiac myocytes (~10^4 cells/scaffold)	94% (1d)	A perfusable scaffold with mechanical properties similar to cardiac tissue, and good biocompatibility with cardiac myocytes	A geometrically simplified *in vitro* scaffold mainly for material performance test	Hernández-Córdova et al. (2016)
	Cardiac spheroids	Gelatin	Collagen I and Matrigel	Cardiomyocytes with primary cardiac fibroblasts (~10^9 cells/ml in total); HUVECs (~10^7 cells/ml)	Enhanced cell viability throughout the bulk tissue compared to nonvascular tissue	A perfusable cardiac tissue that fuses and beats synchronously over a 7-day period with high cellular density	Lack of sufficient microvascular network formation; a modest contractility (~1% strain) only	Skylar-Scott et al. (2019)
	Gut-like tissue fragments	PVA	Matrigel, gelatin, and fibrin	Caco-2 intestinal epithelial cells; HUVECs (~10^7 cells/ml)	Good cell co-culture results	An *in vitro* gut model capable of sustaining cells long term	A simplified model mainly for conceptual validation	Hu et al. (2018)
	Liver tissue model	Agarose fiber	GelMA	HUVECs (~10^5 cells/ml); HepG2/C3A cells (~10^6 cells/ml)	>80% (2d)	A vascularized liver tissue model for mimicking *in vivo* conditions and testing drug diffusion and toxicity	Difficult to imitate the ultrastructure of capillaries	Massa et al. (2017)
	Liver tissue fragments	PVA and PLA	Gelatin	Liver hepatocellular carcinoma (HepG2) cells (~10^6–10^8 cells/ml)	Good HepG2 cell proliferation to a high cell density	A perfusable thick engineered construct with cellular densities of native tissues	A simplified model for conceptual validation; difficult to create channels with diameter <1 mm	Pimentel et al. (2018)
	Renal proximal tubule models	Pluronic F127	Gelatin	Proximal tubule epithelial cells (~10^7 cells/ml); glomerular microvascular epithelial cells (—)	Healthy cell phenotype was observed	A 3D vascularized proximal tubule model that can be independently addressed to investigate renal reabsorption	The reabsorptive properties may be improved by reducing the proximal tubule lumen diameter and the separation distance between the	Lin et al. (2019)

(Continued on following page)

TABLE 3 | (*Continued*) Summary of indirect 3D bioprinting applications and bioink selection for different tissue vascularization covered in this review.

Category	Sub-category	Sacrificial material	Scaffold material	Cells and cell density	Cell viability	Progress	Limitations	References
							proximal tubule and vascular conduits	
	Kidney-like structure	Pluronic F127	Alginate	—	—	Simplified models for conceptual validation	No good method to fabricate 3D highly vascularized network in thick tissue or organ	Rocca et al. (2018)
Vascularized osteochondral tissue	Cartilage tissues	Pluronic F127	GelMA	Bone marrow derived mesenchymal stem cells (~10^7 cells/ml)	Cells remained viable after 24 h	A promising approach for guiding vascularization and implant remodeling during endochondral bone repair	No obvious enhanced overall-level bone formation	Daly et al. (2018)
Vascularized skin	Finger-shaped highly elastic scaffold	PVA	PLCL	Human dermal fibroblasts (~10^6 cells/ml)	Considerable collagen and new blood vessels were observed at 4 weeks	A customized scaffold successful in animal experiments and may act as a dermis substitute	A simplified model without hierarchical structure	Im et al. (2018)
	Thermoresponsive 'stiffness memory' elastomeric nanohybrid scaffolds	PVA	PUU-POSS	3T3-J2 mouse embryonic dermal fibroblasts (~10^4 cells/scaffold)	Good ingrowth of tissue and new blood vessels were observed at 4 weeks	A unique smart elastomer scaffold that can guide the growth of myofibroblasts, collagen fibers, and blood vessels at real 3D scales	Slow ingrowth of host blood capillaries; local inflammatory response	Wu et al. (2019)

layered blood vessel models *in vitro*, which direct printing cannot yet achieve (Schöneberg et al., 2018). They used three different degradable hydrogels with three different cell types to simulate and reconstruct the adventitia (fibroblast matrix), medial layer (elastic SMC), and intima (endothelium), and successfully replicate the three-layered natural vascular channel structure with a wall thickness of up to 425 μm, and diameters of around 1 mm (**Figure 2**). These bioinks provide a friendly living environment for cells. Currently, engineered vascular grafts do not meet human transplantation standards, and most of them are used for *in vitro* experiments, such as drug prescreening or preliminary concept verification.

Highly Vascularized Tissue

Currently, most studies are in the conceptual validation phase and, to date, there are no good methods or compatible bioinks to fabricate a 3D functional, highly vascularized network in thick tissue or organ constructs, which limits the development of tissue engineering (Duan, 2017).

For highly vascularized tissue, such as liver, kidney, and heart, more precise microvessels are required, ranging from a few microns to millimeters. However, the current techniques have difficulty achieving this accuracy and resolution. Zou et al. created a valentine-shaped synthetic heart with a simplified aorta by using indirect 3D bioprinting and biodegradable alginate (Zou et al., 2020). They demonstrated no collapse of the scaffold structure and 90% cell viability. Nevertheless, the constructed microchannels are still at the level of hundreds of microns, and it remains difficult to emulate the ultrastructure of capillaries. An *in vitro* liver model (GelMA loaded with HepG2/C3A) was developed to test drug toxicity (Massa et al., 2017), and 3D human heart- and kidney-like objects, composed of dozens of alginate layers, were produced by embedded extrusion bioprinting (Rocca et al., 2018); however, these models were about 2 cm^3 in size, with very simple vascular structure, and were used only for concept validation. Lin et al. used indirect 3D bioprinting to fabricate adjacent open cavities (representing proximal renal tubules and parallel blood vessels) embedded in the permeable ECM. After endothelialization and epithelization, the selective reabsorption and vectorial transmission of solute were realized through external circulation devices, which favor the further study of tissue-engineered kidneys (Lin et al., 2019).

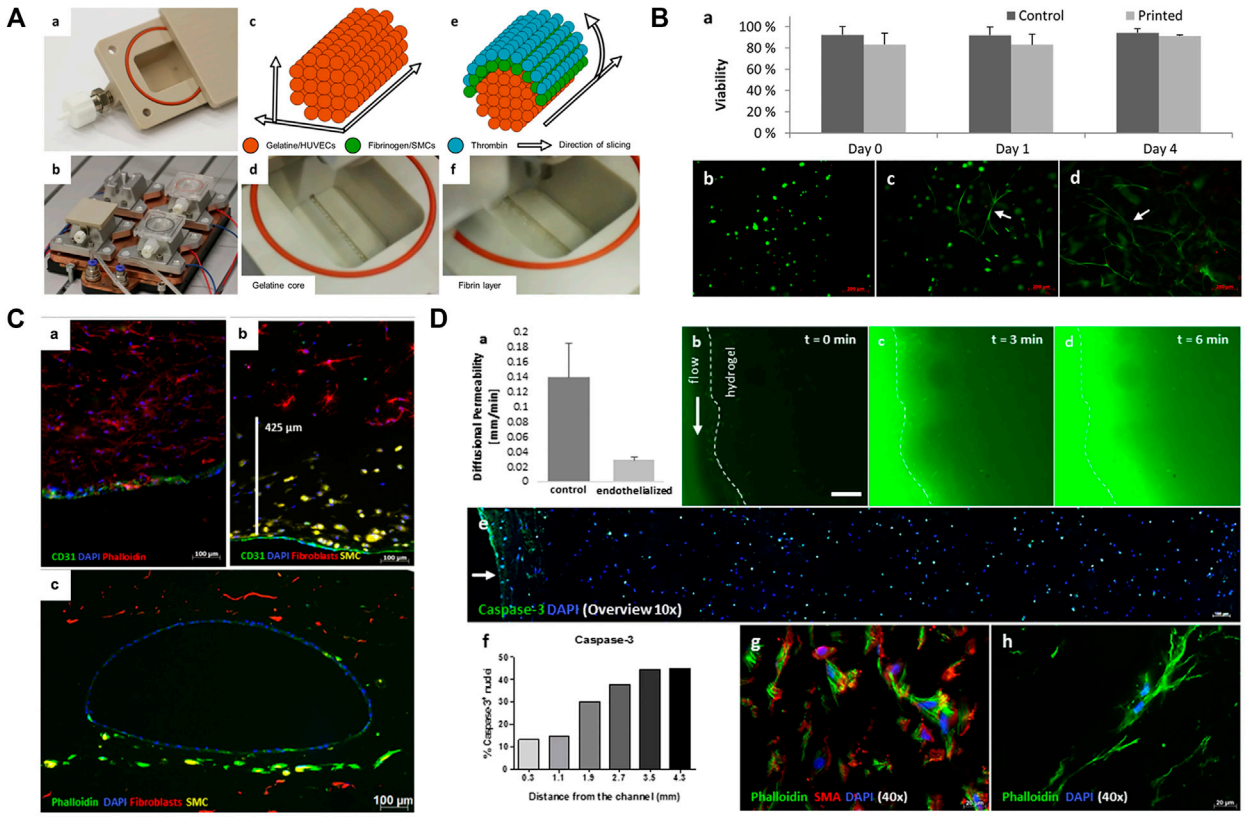

FIGURE 2 | Printing of blood vessels with multi-layered structure. **(A)** Schematic diagram showing the printing procedure in a bioreactor. The printing includes a gelatin core and a surrounding fibrin layer. **(B)** Results showed that cell viability was not affected after the printing process. **(C)** Fluorescence micrographs show the homogenous distribution and good combination of ECs, SMCs, and fibroblasts. **(D)** Permeability testing and cell viability evaluation. Adapted with permission (Schöneberg et al., 2018). Copyright 2018, Nature Publishing Group.

There are also some special needs for biomaterials. Highly vascularized tissues usually consist of large amounts of active cells, which require the biomaterials to be sufficiently friendly to cells and cell migration, growth, and proliferation, and should facilitate substance exchange (Xie et al., 2020). Usually, softer biomaterials are needed; indeed, one important requirement for cardiac scaffolds is that it should not provide resistance to muscle contraction during systole while providing mechanical support to resist the tensile stress during diastole (Hernández-Córdova et al., 2016). This requires the elastic modulus of the biomaterial to match that of the myocardial reported interval (7.9–1,200 kPa) (Courtney et al., 2006; Chan et al., 2013; Hernández-Córdova et al., 2016). Alginate, gelatin, fibrin, and collagen can be used for cardiac scaffolds (Alonzo et al., 2019). In an indirect 3D bioprinting case, PUU was developed as a scaffold material that had suitable elastic modulus. They also used PVA as sacrificial material, and finally created a cardiac scaffold containing 300–500 µm channels. The biomaterial showed good biocompatibility with cardiomyocytes (Hernández-Córdova et al., 2016). Meanwhile, to verify the feasibility of multicellular tissue printing, Skylar-Scott et al. reported an embedded indirect 3D bioprinting method to create perfusable vascular channels in ECM solution with organ building blocks (OBBs) composed of thousands of patient-specific-induced pluripotent stem cell–derived organoids, as shown in **Figure 3**. As an example, they then fabricated a cardiac tissue with physiological functions over a 7-day period with high cellular density, showing the huge prospects of indirect 3D bioprinting (Skylar-Scott et al., 2019).

Vascularized Osteochondral Tissue

The 3D printing technique is relatively mature in the field of osteochondral tissue engineering and has been used in the fabrication of long bones, mandibles, cheekbones, human finger bones, and other structures (Hollister et al., 2005; Lee et al., 2005; Wang et al., 2009). Biomaterials for osteochondral tissue engineering emphasize mechanical properties (Daly et al., 2017). For the design and production of vascularized bone tissue engineering scaffolds, pore-forming agents are usually added to form pores of specific sizes (>300 µm) to promote angiogenesis (Karageorgiou and Kaplan, 2005; Wang J.-Q. et al., 2019; Gonzalez-Fernandez et al., 2019). Uniform channels of controlled size that simulate the natural morphology of bone tissue, including Volkman's and Haversian canals for better osteogenesis, are more and more created in molds via indirect 3D bioprinting (Houben et al., 2016; Houben et al., 2017).

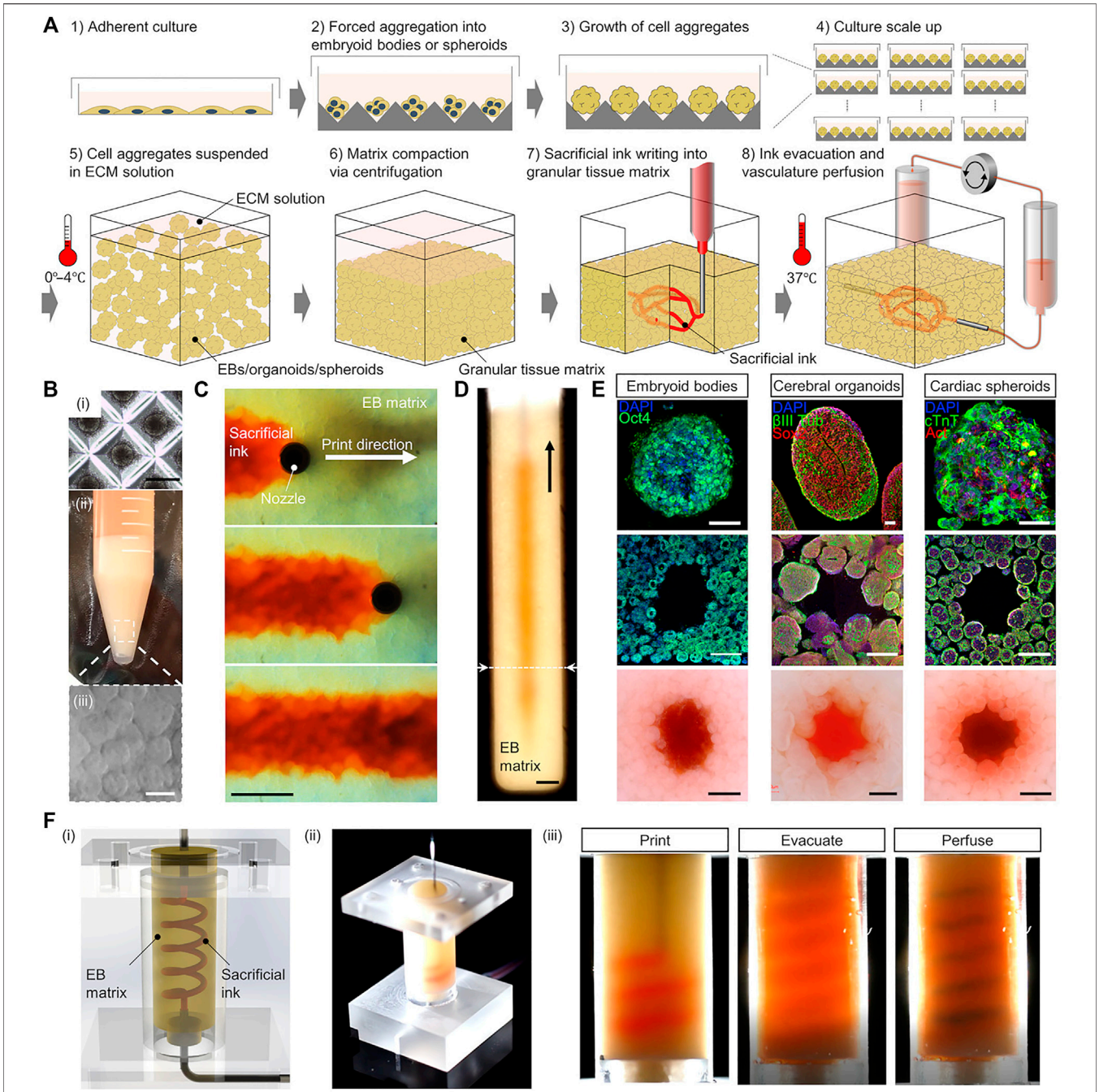

FIGURE 3 | Printing of highly vascularized tissues with high cell density. **(A)** Schematic diagram of the indirect 3D bioprinting workflow. **(B)** Organ building block (OBB) tissue matrix formation. **(C,D)** Sacrificial ink writing within an embryoid body (EB) matrix. **(E)** Examples of different OBB-based matrices. **(F)** Fabrication of a helical vascular structure in an EB matrix. Reproduced with permission (Skylar-Scott et al., 2019). Copyright 2019, American Association for the Advancement of Science (AAAS).

However, few studies have focused on the analysis of angiogenesis and new bioink development.

For endochondral bone repair, current techniques enable *in vivo* angiogenesis around cartilage models (Thompson et al., 2016), but the internal regions of the models remain nonvascular (Mesallati et al., 2015). Daly et al. constructed a microchanneled cartilage template using sacrificial Pluronic ink. After *in vivo* cultivation, they found that, compared to solid templates, channeled templates showed better vascularization, more degradation of cartilage precursor hydrogel in the core region, less ectopic bone formation, and better integration with the host tissue, which are all clinically important (Daly et al.,

2018). However, more evidence is needed to demonstrate a difference in total bone formation between the channeled and solid templates for endochondral bone repair.

Vascularized Skin

Creating man-made skin grafts for wounds and burn healing is the primary purpose of skin tissue engineering (Adams and Ramsey, 2005). Tissue-engineered skin grafts should be non-toxic, have low inflammatory response, allow water vapor transmission, and act as a barrier. They are also expected to quickly adhere to the wound surface, have controllable degradation, and promote angiogenesis (MacNeil, 2007). Biodegradable, non-toxic, non-immunogenic, and non-inflammatory biomaterials with low risk of disease transmission and easy access are ideal skin substitutes (Vig et al., 2017). To date, indirect 3D bioprinting has not been widely applied in vascularized skin tissue fabrication. Wu et al. created a thermoresponsive stiffness memory elastomer nanohybrid scaffold via indirect 3D bioprinting and found that the scaffold promoted fibroblast proliferation *in vitro* and angiogenesis *in vivo* (Wu et al., 2019). Another team found that by combining bioactive peptide hydrogels with scaffolds having finger-shaped pores created via indirect 3D bioprinting, more vessels and more collagen I and III formed in the scaffolds (Im et al., 2018). Most studies that focused on tissue design have been based on simplified skin models, while few models consider controlled porosity, biodegradable material selection, and cell distribution (Lee V. et al., 2014; Yan et al., 2018). It is important to mention that for the reconstruction of simple epidermis or thin dermis, vascularization is not necessary.

CONCLUSION

As described in this paper, tissue vascularization has always been a critical issue in tissue engineering and is key to the application and survival of engineered tissue constructs *in vivo*. Many accomplishments have demonstrated the feasibility of indirect 3D bioprinting for manufacturing blood vessels and vascularized tissue constructs, and most experiments show that indirect 3D bioprinting has advantages in channel structure design and construction. On the other hand, the selection of biodegradable inks is an important aspect of indirect 3D bioprinting for successful 3D tissue construct fabrication and *in vitro/vivo* application. Theoretically, indirect 3D bioprinting allows a wider range of materials to be used, since the use of sacrificial materials lowers the mechanical performance requirements for scaffold materials. However, this introduces new requirements for the sacrificial materials. At present, owing to the lack of satisfactory biodegradable materials, further *in vivo* applications are limited. A large number of studies are investigating advanced sacrificial/scaffold bioinks, which assists in the assembly of biodegradable, biosafe, bioactive, and more bionic structures at higher resolution. Efforts are now transitioning from theoretical verification to tissue and organ model construction. We expect that with the future continuous development of biodegradable materials, the use of indirect 3D bioprinting will continue to increase and will contribute to the field of tissue engineering.

AUTHOR CONTRIBUTIONS

JL and YY conceived and coordinated this project. YZ and YL wrote this article. LH and YS collected and summarized literatures. PL edited pictures in this paper. PG revised this paper. All authors contributed to manuscript revision, read and approved the submitted version.

FUNDING

We thank the financial support from the Sichuan University-Luzhou City Cooperaton Program (No.2021CDLZ-8), the Horizontal Project of Sichuan University (No. 21H0441), and the College Students' Innovative Entrepreneurial Training Plan Program in Sichuan University (No.20221220L).

REFERENCES

Abdollahi, S., Boktor, J., and Hibino, N. (2019). Bioprinting of Freestanding Vascular Grafts and the Regulatory Considerations for Additively Manufactured Vascular Prostheses. *Translational Res.* 211, 123–138. doi:10.1016/j.trsl.2019.05.005

Adams, D. C., and Ramsey, M. L. (2005). Grafts in Dermatologic Surgery: Review and Update on Full- and Split-Thickness Skin Grafts, Free Cartilage Grafts, and Composite Grafts. *Dermatol. Surg.* 31 (8 Pt 2), 1055–1067. doi:10.1111/j.1524-4725.2005.31831

Afghah, F., Altunbek, M., Dikyol, C., and Koc, B. (2020). Preparation and Characterization of Nanoclay-Hydrogel Composite Support-bath for Bioprinting of Complex Structures. *Sci. Rep.* 10 (1), 5257. doi:10.1038/s41598-020-61606-x

Aljohani, W., Ullah, M. W., Zhang, X., and Yang, G. (2018). Bioprinting and its Applications in Tissue Engineering and Regenerative Medicine. *Int. J. Biol. Macromolecules* 107 (Pt A), 261–275. doi:10.1016/j.ijbiomac.2017.08.171

Alonzo, M., AnilKumar, S., Roman, B., Tasnim, N., and Joddar, B. (2019). 3D Bioprinting of Cardiac Tissue and Cardiac Stem Cell Therapy. *Translational Res.* 211, 64–83. doi:10.1016/j.trsl.2019.04.004

Aper, T., Wilhelmi, M., Gebhardt, C., Hoeffler, K., Benecke, N., Hilfiker, A., et al. (2016). Novel Method for the Generation of Tissue-Engineered Vascular Grafts Based on a Highly Compacted Fibrin Matrix. *Acta Biomater.* 29, 21–32. doi:10.1016/j.actbio.2015.10.012

Asakawa, N., Shimizu, T., Tsuda, Y., Sekiya, S., Sasagawa, T., Yamato, M., et al. (2010). Pre-vascularization of *In Vitro* Three-Dimensional Tissues Created by Cell Sheet Engineering. *Biomaterials* 31 (14), 3903–3909. doi:10.1016/j.biomaterials.2010.01.105

Asghari, F., Samiei, M., Adibkia, K., Akbarzadeh, A., and Davaran, S. (2017). Biodegradable and Biocompatible Polymers for Tissue Engineering Application: a Review. *Artif. Cell Nanomedicine, Biotechnol.* 45 (2), 185–192. doi:10.3109/21691401.2016.1146731

Auger, F. A., Gibot, L., and Lacroix, D. (2013). The Pivotal Role of Vascularization in Tissue Engineering. *Annu. Rev. Biomed. Eng.* 15, 177–200. doi:10.1146/annurev-bioeng-071812-152428

Bae, H., Puranik, A. S., Gauvin, R., Edalat, F., Carrillo-Conde, B., Peppas, N. A., et al. (2012). Building Vascular Networks. *Sci. Transl. Med.* 4 (160), 160ps123. doi:10.1126/scitranslmed.3003688

Balaji, S., King, A., Crombleholme, T. M., and Keswani, S. G. (2013). The Role of Endothelial Progenitor Cells in Postnatal Vasculogenesis: Implications for Therapeutic Neovascularization and Wound Healing. *Adv. Wound Care* 2 (6), 283–295. doi:10.1089/wound.2012.0398

Balakrishnan, B., Joshi, N., Jayakrishnan, A., and Banerjee, R. (2014). Self-crosslinked Oxidized Alginate/gelatin Hydrogel as Injectable, Adhesive Biomimetic Scaffolds for Cartilage Regeneration. *Acta Biomater.* 10 (8), 3650–3663. doi:10.1016/j.actbio.2014.04.031

Baranski, J. D., Chaturvedi, R. R., Stevens, K. R., Eyckmans, J., Carvalho, B., Solorzano, R. D., et al. (2013). Geometric Control of Vascular Networks to Enhance Engineered Tissue Integration and Function. *Proc. Natl. Acad. Sci. U.S.A.* 110 (19), 7586–7591. doi:10.1073/pnas.1217796110

Bello, A. B., Kim, D., Kim, D., Park, H., and Lee, S.-H. (2020). Engineering and Functionalization of Gelatin Biomaterials: From Cell Culture to Medical Applications. *Tissue Eng. B: Rev.* 26 (2), 164–180. doi:10.1089/ten.TEB.2019.0256

Benton, J. A., DeForest, C. A., Vivekanandan, V., and Anseth, K. S. (2009). Photocrosslinking of Gelatin Macromers to Synthesize Porous Hydrogels that Promote Valvular Interstitial Cell Function. *Tissue Eng. A* 15 (11), 3221–3230. doi:10.1089/ten.TEA.2008.0545

Bertassoni, L. E., Cecconi, M., Manoharan, V., Nikkhah, M., Hjortnaes, J., Cristino, A. L., et al. (2014). Hydrogel Bioprinted Microchannel Networks for Vascularization of Tissue Engineering Constructs. *Lab. Chip* 14 (13), 2202–2211. doi:10.1039/c4lc00030g

Berthiaume, F., Maguire, T. J., and Yarmush, M. L. (2011). Tissue Engineering and Regenerative Medicine: History, Progress, and Challenges. *Annu. Rev. Chem. Biomol. Eng.* 2, 403–430. doi:10.1146/annurev-chembioeng-061010-114257

Bidgoli, M. R., Alemzadeh, I., Tamjid, E., Khafaji, M., and Vossoughi, M. (2019). Fabrication of Hierarchically Porous Silk Fibroin-Bioactive Glass Composite Scaffold via Indirect 3D Printing: Effect of Particle Size on Physico-Mechanical Properties and *In Vitro* Cellular Behavior. *Mater. Sci. Eng. C* 103, 109688. doi:10.1016/j.msec.2019.04.067

Breen, A., O'Brien, T., and Pandit, A. (2009). Fibrin as a Delivery System for Therapeutic Drugs and Biomolecules. *Tissue Eng. Part B: Rev.* 15 (2), 201–214. doi:10.1089/ten.TEB.2008.0527

Burdick, J. A., and Prestwich, G. D. (2011). Hyaluronic Acid Hydrogels for Biomedical Applications. *Adv. Mater.* 23 (12), H41–H56. doi:10.1002/adma.201003963

Calderon, G. A., Thai, P., Hsu, C. W., Grigoryan, B., Gibson, S. M., Dickinson, M. E., et al. (2017). Tubulogenesis of Co-cultured Human iPS-Derived Endothelial Cells and Human Mesenchymal Stem Cells in Fibrin and Gelatin Methacrylate Gels. *Biomater. Sci.* 5 (8), 1652–1660. doi:10.1039/c7bm00223h

Calvert, P. (2007). Printing Cells. *Science* 318 (5848), 208–209. doi:10.1126/science.1144212

Carmeliet, P., and Jain, R. K. (2000). Angiogenesis in Cancer and Other Diseases. *Nature* 407 (6801), 249–257. doi:10.1038/35025220

Chahal, D., Ahmadi, A., and Cheung, K. C. (2012). Improving Piezoelectric Cell Printing Accuracy and Reliability through Neutral Buoyancy of Suspensions. *Biotechnol. Bioeng.* 109 (11), 2932–2940. doi:10.1002/bit.24562

Chan, V., Raman, R., Cvetkovic, C., and Bashir, R. (2013). Enabling Microscale and Nanoscale Approaches for Bioengineered Cardiac Tissue. *ACS Nano* 7 (3), 1830–1837. doi:10.1021/nn401098c

Charron, P. N., Braddish, T. A., and Oldinski, R. A. (2019). PVA-gelatin Hydrogels Formed Using Combined Theta-Gel and Cryo-Gel Fabrication Techniques. *J. Mech. Behav. Biomed. Mater.* 92, 90–96. doi:10.1016/j.jmbbm.2019.01.002

Chen, Y.-C., Lin, R.-Z., Qi, H., Yang, Y., Bae, H., Melero-Martin, J. M., et al. (2012). Functional Human Vascular Network Generated in Photocrosslinkable Gelatin Methacrylate Hydrogels. *Adv. Funct. Mater.* 22 (10), 2027–2039. doi:10.1002/adfm.201101662

Cheng, G., Liao, S., Kit Wong, H., Lacorre, D. A., di Tomaso, E., Au, P., et al. (2011). Engineered Blood Vessel Networks Connect to Host Vasculature via Wrapping-And-Tapping Anastomosis. *Blood* 118 (17), 4740–4749. doi:10.1182/blood-2011-02-338426

Chiesa, I., De Maria, C., Lapomarda, A., Fortunato, G. M., Montemurro, F., Di Gesù, R., et al. (2020). Endothelial Cells Support Osteogenesis in an *In Vitro* Vascularized Bone Model Developed by 3D Bioprinting. *Biofabrication* 12 (2), 025013. doi:10.1088/1758-5090/ab6a1d

Chu, T.-M. G., Halloran, J. W., Hollister, S. J., and Feinberg, S. E. (2001). Hydroxyapatite Implants with Designed Internal Architecture. *J. Mater. Sci. Mater. Med.* 12 (6), 471–478. doi:10.1023/a:1011203226053

Chung, C., Anderson, E., Pera, R. R., Pruitt, B. L., and Heilshorn, S. C. (2012). Hydrogel Crosslinking Density Regulates Temporal Contractility of Human Embryonic Stem Cell-Derived Cardiomyocytes in 3D Cultures. *Soft Matter* 8 (39), 10141–10148. doi:10.1039/c2sm26082d

Courtney, T., Sacks, M., Stankus, J., Guan, J., and Wagner, W. (2006). Design and Analysis of Tissue Engineering Scaffolds that Mimic Soft Tissue Mechanical Anisotropy. *Biomaterials* 27 (19), 3631–3638. doi:10.1016/j.biomaterials.2006.02.024

Daly, A. C., Freeman, F. E., Gonzalez-Fernandez, T., Critchley, S. E., Nulty, J., and Kelly, D. J. (2017). 3D Bioprinting for Cartilage and Osteochondral Tissue Engineering. *Adv. Healthc. Mater.* 6 (22), 1700298. doi:10.1002/adhm.201700298

Daly, A. C., Pitacco, P., Nulty, J., Cunniffe, G. M., and Kelly, D. J. (2018). 3D Printed Microchannel Networks to Direct Vascularisation during Endochondral Bone Repair. *Biomaterials* 162, 34–46. doi:10.1016/j.biomaterials.2018.01.057

Datta, P., Ayan, B., and Ozbolat, I. T. (2017). Bioprinting for Vascular and Vascularized Tissue Biofabrication. *Acta Biomater.* 51, 1–20. doi:10.1016/j.actbio.2017.01.035

Deng, Q., Huang, S., Wen, J., Jiao, Y., Su, X., Shi, G., et al. (2020). PF-127 Hydrogel Plus Sodium Ascorbyl Phosphate Improves Wharton's Jelly Mesenchymal Stem Cell-Mediated Skin Wound Healing in Mice. *Stem Cell Res Ther* 11 (1), 143. doi:10.1186/s13287-020-01638-2

Ding, H., and Chang, R. C. (2018). Printability Study of Bioprinted Tubular Structures Using Liquid Hydrogel Precursors in a Support Bath. *Appl. Sci.* 8. doi:10.3390/app8030403

Do, A.-V., Khorsand, B., Geary, S. M., and Salem, A. K. (2015). 3D Printing of Scaffolds for Tissue Regeneration Applications. *Adv. Healthc. Mater.* 4 (12), 1742–1762. doi:10.1002/adhm.201500168

Duan, B. (2017). State-of-the-Art Review of 3D Bioprinting for Cardiovascular Tissue Engineering. *Ann. Biomed. Eng.* 45 (1), 195–209. doi:10.1007/s10439-016-1607-5

Duarte Campos, D. F., Blaeser, A., Buellesbach, K., Sen, K. S., Xun, W., Tillmann, W., et al. (2016). Bioprinting Organotypic Hydrogels with Improved Mesenchymal Stem Cell Remodeling and Mineralization Properties for Bone Tissue Engineering. *Adv. Healthc. Mater.* 5 (11), 1336–1345. doi:10.1002/adhm.201501033

Duarte Campos, D. F., Lindsay, C. D., Roth, J. G., LeSavage, B. L., Seymour, A. J., Krajina, B. A., et al. (2020). Bioprinting Cell- and Spheroid-Laden Protein-Engineered Hydrogels as Tissue-On-Chip Platforms. *Front. Bioeng. Biotechnol.* 8, 374. doi:10.3389/fbioe.2020.00374

El Chawich, G., El Hayek, J., Rouessac, V., Cot, D., Rebière, B., Habchi, R., et al. (2022). Design and Manufacturing of Si-Based Non-oxide Cellular Ceramic Structures through Indirect 3D Printing. *Materials* 15 (2), 471. doi:10.3390/ma15020471

Gonzalez-Fernandez, T., Rathan, S., Hobbs, C., Pitacco, P., Freeman, F. E., Cunniffe, G. M., et al. (2019). Pore-forming Bioinks to Enable Spatio-Temporally Defined Gene Delivery in Bioprinted Tissues. *J. Controlled Release* 301, 13–27. doi:10.1016/j.jconrel.2019.03.006

Groll, J., Burdick, J. A., Cho, D.-W., Derby, B., Gelinsky, M., Heilshorn, S. C., et al. (2018). A Definition of Bioinks and Their Distinction from Biomaterial Inks. *Biofabrication* 11 (1), 013001. doi:10.1088/1758-5090/aaec52

Gudapati, H., Dey, M., and Ozbolat, I. (2016). A Comprehensive Review on Droplet-Based Bioprinting: Past, Present and Future. *Biomaterials* 102, 20–42. doi:10.1016/j.biomaterials.2016.06.012

Hammer, J., Han, L.-H., Tong, X., and Yang, F. (2014). A Facile Method to Fabricate Hydrogels with Microchannel-like Porosity for Tissue Engineering. *Tissue Eng. C: Methods* 20 (2), 169–176. doi:10.1089/ten.TEC.2013.0176

Hann, S. Y., Cui, H., Esworthy, T., Miao, S., Zhou, X., Lee, S.-j., et al. (2019). Recent Advances in 3D Printing: Vascular Network for Tissue and Organ Regeneration. *Translational Res.* 211, 46–63. doi:10.1016/j.trsl.2019.04.002

Hasan, A., Paul, A., Vrana, N. E., Zhao, X., Memic, A., Hwang, Y.-S., et al. (2014). Microfluidic Techniques for Development of 3D Vascularized Tissue. *Biomaterials* 35 (26), 7308–7325. doi:10.1016/j.biomaterials.2014.04.091

Hernández-Córdova, R., Mathew, D. A., Balint, R., Carrillo-Escalante, H. J., Cervantes-Uc, J. M., Hidalgo-Bastida, L. A., et al. (2016). Indirect Three-dimensional Printing: A Method for Fabricating Polyurethane-urea Based Cardiac Scaffolds. *J. Biomed. Mater. Res.* 104 (8), 1912–1921. doi:10.1002/jbm.a.35721

Hollister, S., Lin, C., Saito, E., Lin, C., Schek, R., Taboas, J., et al. (2005). Engineering Craniofacial Scaffolds. *Orthod. Craniofac. Res.* 8 (3), 162–173. doi:10.1111/j.1601-6343.2005.00329.x

Homan, K. A., Kolesky, D. B., Skylar-Scott, M. A., Herrmann, J., Obuobi, H., Moisan, A., et al. (2016). Bioprinting of 3D Convoluted Renal Proximal Tubules on Perfusable Chips. *Sci. Rep.* 6, 34845. doi:10.1038/srep34845

Houben, A., Pien, N., Lu, X., Bisi, F., Van Hoorick, J., Boone, M. N., et al. (2016). Indirect Solid Freeform Fabrication of an Initiator-free Photocrosslinkable Hydrogel Precursor for the Creation of Porous Scaffolds. *Macromol. Biosci.* 16 (12), 1883–1894. doi:10.1002/mabi.201600289

Houben, A., Van Hoorick, J., Van Erps, J., Thienpont, H., Van Vlierberghe, S., and Dubruel, P. (2017). Indirect Rapid Prototyping: Opening up Unprecedented Opportunities in Scaffold Design and Applications. *Ann. Biomed. Eng.* 45 (1), 58–83. doi:10.1007/s10439-016-1610-x

Hu, M., Dailamy, A., Lei, X. Y., Parekh, U., McDonald, D., Kumar, A., et al. (2018). Facile Engineering of Long-Term Culturable *Ex Vivo* Vascularized Tissues Using Biologically Derived Matrices. *Adv. Healthc. Mater.* 7 (23), 1800845. doi:10.1002/adhm.201800845

Huang, Y., Wu, W., Liu, H., Chen, Y., Li, B., Gou, Z., et al. (2021). 3D Printing of Functional Nerve Guide Conduits. *Burns Trauma* 9, tkab011. doi:10.1093/burnst/tkab011

Im, H., Kim, S. H., Kim, S. H., and Jung, Y. (2018). Skin Regeneration with a Scaffold of Predefined Shape and Bioactive Peptide Hydrogels. *Tissue Eng. Part A* 24 (19-20), 1518–1530. doi:10.1089/ten.TEA.2017.0489

Ino, K., Fukuda, M. T., Hiramoto, K., Taira, N., Nashimoto, Y., and Shiku, H. (2020). Fabrication of Three-Dimensional Calcium Alginate Hydrogels Using Sacrificial Templates of Sugar. *J. Biosci. Bioeng.* 130 (5), 539–544. doi:10.1016/j.jbiosc.2020.06.014

Jarak, I., Varela, C. L., Tavares da Silva, E., Roleira, F. F. M., Veiga, F., and Figueiras, A. (2020). Pluronic-based Nanovehicles: Recent Advances in Anticancer Therapeutic Applications. *Eur. J. Med. Chem.* 206, 112526. doi:10.1016/j.ejmech.2020.112526

Ji, S., Almeida, E., and Guvendiren, M. (2019). 3D Bioprinting of Complex Channels within Cell-Laden Hydrogels. *Acta Biomater.* 95, 214–224. doi:10.1016/j.actbio.2019.02.038

Jia, J., Richards, D. J., Pollard, S., Tan, Y., Rodriguez, J., Visconti, R. P., et al. (2014). Engineering Alginate as Bioink for Bioprinting. *Acta Biomater.* 10 (10), 4323–4331. doi:10.1016/j.actbio.2014.06.034

Jia, W., Gungor-Ozkerim, P. S., Zhang, Y. S., Yue, K., Zhu, K., Liu, W., et al. (2016). Direct 3D Bioprinting of Perfusable Vascular Constructs Using a Blend Bioink. *Biomaterials* 106, 58–68. doi:10.1016/j.biomaterials.2016.07.038

Kang, H.-W., and Cho, D.-W. (2012). Development of an Indirect Stereolithography Technology for Scaffold Fabrication with a Wide Range of Biomaterial Selectivity. *Tissue Eng. Part C: Methods* 18 (9), 719–729. doi:10.1089/ten.tec.2011.0621

Kang, Y., Mochizuki, N., Khademhosseini, A., Fukuda, J., and Yang, Y. (2015). Engineering a Vascularized Collagen-β-Tricalcium Phosphate Graft Using an Electrochemical Approach. *Acta Biomater.* 11, 449–458. doi:10.1016/j.actbio.2014.09.035

Karageorgiou, V., and Kaplan, D. (2005). Porosity of 3D Biomaterial Scaffolds and Osteogenesis. *Biomaterials* 26 (27), 5474–5491. doi:10.1016/j.biomaterials.2005.02.002

Kaully, T., Kaufman-Francis, K., Lesman, A., and Levenberg, S. (2010). Vascularization: The Conduit to Viable Engineered Tissues. *Tissue Eng. Part. B Rev.* 15 (2), 159–169. doi:10.1089/ten.teb.2008.0193

Khattak, S. F., Bhatia, S. R., and Roberts, S. C. (2005). Pluronic F127 as a Cell Encapsulation Material: Utilization of Membrane-Stabilizing Agents. *Tissue Eng.* 11 (5-6), 974–983. doi:10.1089/ten.2005.11.974

Kim, H., Yang, G. H., Choi, C. H., Cho, Y. S., and Kim, G. (2018). Gelatin/PVA Scaffolds Fabricated Using a 3D-Printing Process Employed with a Low-Temperature Plate for Hard Tissue Regeneration: Fabrication and Characterizations. *Int. J. Biol. Macromolecules* 120 (Pt A), 119–127. doi:10.1016/j.ijbiomac.2018.07.159

Kim, J. J., Hou, L., and Huang, N. F. (2016). Vascularization of Three-Dimensional Engineered Tissues for Regenerative Medicine Applications. *Acta Biomater.* 41, 17–26. doi:10.1016/j.actbio.2016.06.001

Kim, Y.-H., Furuya, H., and Tabata, Y. (2014). Enhancement of Bone Regeneration by Dual Release of a Macrophage Recruitment Agent and Platelet-Rich Plasma from Gelatin Hydrogels. *Biomaterials* 35 (1), 214–224. doi:10.1016/j.biomaterials.2013.09.103

Kjar, A., McFarland, B., Mecham, K., Harward, N., and Huang, Y. (2021). Engineering of Tissue Constructs Using Coaxial Bioprinting. *Bioactive Mater.* 6 (2), 460–471. doi:10.1016/j.bioactmat.2020.08.020

Ko, H., Milthorpe, B. K., Milthorpe, B., and McFarland, C. (2007). Engineering Thick Tissues - the Vascularisation Problem. *eCM* 14, 1–19. doi:10.22203/ecm.v014a01

Kolesky, D. B., Truby, R. L., Gladman, A. S., Busbee, T. A., Homan, K. A., and Lewis, J. A. (2014). 3D Bioprinting of Vascularized, Heterogeneous Cell-Laden Tissue Constructs. *Adv. Mater.* 26 (19), 3124–3130. doi:10.1002/adma.201305506

Kundu, B., Rajkhowa, R., Kundu, S. C., and Wang, X. (2013). Silk Fibroin Biomaterials for Tissue Regenerations. *Adv. Drug Deliv. Rev.* 65 (4), 457–470. doi:10.1016/j.addr.2012.09.043

Kyle, S., Jessop, Z. M., Al-Sabah, A., and Whitaker, I. S. (2017). 'Printability' of Candidate Biomaterials for Extrusion Based 3D Printing: State-Of-The-Art. *Adv. Healthc. Mater.* 6 (16), 1700264. doi:10.1002/adhm.201700264

Laschke, M. W., and Menger, M. D. (2016). Prevascularization in Tissue Engineering: Current Concepts and Future Directions. *Biotechnol. Adv.* 34 (2), 112–121. doi:10.1016/j.biotechadv.2015.12.004

Laschke, M. W., and Menger, M. D. (2012). Vascularization in Tissue Engineering: Angiogenesis versus Inosculation. *Eur. Surg. Res.* 48 (2), 85–92. doi:10.1159/000336876

Lee, A. Y., Mahler, N., Best, C., Lee, Y.-U., and Breuer, C. K. (2014a). Regenerative Implants for Cardiovascular Tissue Engineering. *Translational Res.* 163 (4), 321–341. doi:10.1016/j.trsl.2014.01.014

Lee, J.-Y., Choi, B., Wu, B., and Lee, M. (2013). Customized Biomimetic Scaffolds Created by Indirect Three-Dimensional Printing for Tissue Engineering. *Biofabrication* 5 (4), 045003. doi:10.1088/1758-5082/5/4/045003

Lee, J. M., and Yeong, W. Y. (2016). Design and Printing Strategies in 3D Bioprinting of Cell-Hydrogels: A Review. *Adv. Healthc. Mater.* 5 (22), 2856–2865. doi:10.1002/adhm.201600435

Lee, K. Y., and Mooney, D. J. (2012). Alginate: Properties and Biomedical Applications. *Prog. Polym. Sci.* 37 (1), 106–126. doi:10.1016/j.progpolymsci.2011.06.003

Lee, M., Dunn, J. C. Y., and Wu, B. M. (2005). Scaffold Fabrication by Indirect Three-Dimensional Printing. *Biomaterials* 26 (20), 4281–4289. doi:10.1016/j.biomaterials.2004.10.040

Lee, M., Wu, B. M., and Dunn, J. C. Y. (2008). Effect of Scaffold Architecture and Pore Size on Smooth Muscle Cell Growth. *J. Biomed. Mater. Res.* 87A (4), 1010–1016. doi:10.1002/jbm.a.31816

Lee, V., Singh, G., Trasatti, J. P., Bjornsson, C., Xu, X., Tran, T. N., et al. (2014b). Design and Fabrication of Human Skin by Three-Dimensional Bioprinting. *Tissue Eng. Part C: Methods* 20 (6), 473–484. doi:10.1089/ten.TEC.2013.0335

Leong, M. F., Toh, J. K. C., Du, C., Narayanan, K., Lu, H. F., Lim, T. C., et al. (2013). Patterned Prevascularised Tissue Constructs by Assembly of Polyelectrolyte Hydrogel Fibres. *Nat. Commun.* 4. doi:10.1038/ncomms3353

Li, X., Liu, B., Pei, B., Chen, J., Zhou, D., Peng, J., et al. (2020). Inkjet Bioprinting of Biomaterials. *Chem. Rev.* 120 (19), 10793–10833. doi:10.1021/acs.chemrev.0c00008

Liang, Y., Liu, W., Han, B., Yang, C., Ma, Q., Song, F., et al. (2011). An *In Situ* Formed Biodegradable Hydrogel for Reconstruction of the Corneal Endothelium. *Colloids Surf. B: Biointerfaces* 82 (1), 1–7. doi:10.1016/j.colsurfb.2010.07.043

Lin, N. Y. C., Homan, K. A., Robinson, S. S., Kolesky, D. B., Duarte, N., Moisan, A., et al. (2019). Renal Reabsorption in 3D Vascularized Proximal Tubule Models. *Proc. Natl. Acad. Sci. U.S.A.* 116 (12), 5399–5404. doi:10.1073/pnas.1815208116

Litvinov, R. I., and Weisel, J. W. (2017). Fibrin Mechanical Properties and Their Structural Origins. *Matrix Biol.* 60-61, 110–123. doi:10.1016/j.matbio.2016.08.003

Liu, C. Z., Xia, Z. D., Han, Z. W., Hulley, P. A., Triffitt, J. T., and Czernuszka, J. T. (2008). Novel 3D Collagen Scaffolds Fabricated by Indirect Printing Technique for Tissue Engineering. *J. Biomed. Mater. Res.* 85B (2), 519–528. doi:10.1002/jbm.b.30975

Liu, M. J. J., Chou, S. M., Chua, C. K., Tay, B. C. M., and Ng, B. K. (2013). The Development of Silk Fibroin Scaffolds Using an Indirect Rapid Prototyping Approach: Morphological Analysis and Cell Growth Monitoring by Spectral-Domain Optical Coherence Tomography. *Med. Eng. Phys.* 35 (2), 253–262. doi:10.1016/j.medengphy.2011.09.029

Liu, R. H., Ong, C. S., Fukunishi, T., Ong, K., and Hibino, N. (2018). Review of Vascular Graft Studies in Large Animal Models. *Tissue Eng. Part B: Rev.* 24 (2), 133–143. doi:10.1089/ten.TEB.2017.0350

López-Marcial, G. R., Zeng, A. Y., Osuna, C., Dennis, J., García, J. M., and O'Connell, G. D. (2018). Agarose-Based Hydrogels as Suitable Bioprinting Materials for Tissue Engineering. *ACS Biomater. Sci. Eng.* 4 (10), 3610–3616. doi:10.1021/acsbiomaterials.8b00903

M, J. C., Reardon, P. J., Konwarh, R., Knowles, J. C., and Mandal, B. B. (2017). Mimicking Hierarchical Complexity of the Osteochondral Interface Using Electrospun Silk-Bioactive Glass Composites. *ACS Appl. Mater. Inter.* 9 (9), 8000–8013. doi:10.1021/acsami.6b16590

MacNeil, S. (2007). Progress and Opportunities for Tissue-Engineered Skin. *Nature* 445 (7130), 874–880. doi:10.1038/nature05664

Madl, C. M., LeSavage, B. L., Dewi, R. E., Dinh, C. B., Stowers, R. S., Khariton, M., et al. (2017). Maintenance of Neural Progenitor Cell Stemness in 3D Hydrogels Requires Matrix Remodelling. *Nat. Mater* 16 (12), 1233–1242. doi:10.1038/nmat5020

Makris, E. A., Gomoll, A. H., Malizos, K. N., Hu, J. C., and Athanasiou, K. A. (2015). Repair and Tissue Engineering Techniques for Articular Cartilage. *Nat. Rev. Rheumatol.* 11 (1), 21–34. doi:10.1038/nrrheum.2014.157

Malda, J., Visser, J., Melchels, F. P., Jüngst, T., Hennink, W. E., Dhert, W. J. A., et al. (2013). 25th Anniversary Article: Engineering Hydrogels for Biofabrication. *Adv. Mater.* 25 (36), 5011–5028. doi:10.1002/adma.201302042

Mandrycky, C., Wang, Z., Kim, K., and Kim, D.-H. (2016). 3D Bioprinting for Engineering Complex Tissues. *Biotechnol. Adv.* 34 (4), 422–434. doi:10.1016/j.biotechadv.2015.12.011

Massa, S., Sakr, M. A., Seo, J., Bandaru, P., Arneri, A., Bersini, S., et al. (2017). Bioprinted 3D Vascularized Tissue Model for Drug Toxicity Analysis. *Biomicrofluidics* 11 (4), 044109. doi:10.1063/1.4994708

Matsui, M., and Tabata, Y. (2012). Enhanced Angiogenesis by Multiple Release of Platelet-Rich Plasma Contents and Basic Fibroblast Growth Factor from Gelatin Hydrogels. *Acta Biomater.* 8 (5), 1792–1801. doi:10.1016/j.actbio.2012.01.016

Mesallati, T., Sheehy, E. J., Sheehy, E., Vinardell, T., Buckley, C., and Kelly, D. (2015). Tissue Engineering Scaled-Up, Anatomically Shaped Osteochondral Constructs for Joint Resurfacing. *eCM* 30, 163–186. ; discussion 185-166. doi:10.22203/ecm.v030a12

Miller, J. S., Stevens, K. R., Yang, M. T., Baker, B. M., Nguyen, D.-H. T., Cohen, D. M., et al. (2012). Rapid Casting of Patterned Vascular Networks for Perfusable Engineered Three-Dimensional Tissues. *Nat. Mater* 11 (9), 768–774. doi:10.1038/nmat3357

Mohanty, S., Sanger, K., Heiskanen, A., Trifol, J., Szabo, P., Dufva, M., et al. (2016). Fabrication of Scalable Tissue Engineering Scaffolds with Dual-Pore Microarchitecture by Combining 3D Printing and Particle Leaching. *Mater. Sci. Eng. C* 61, 180–189. doi:10.1016/j.msec.2015.12.032

Moroni, L., Boland, T., Burdick, J. A., De Maria, C., Derby, B., Forgacs, G., et al. (2018). Biofabrication: A Guide to Technology and Terminology. *Trends Biotechnol.* 36 (4), 384–402. doi:10.1016/j.tibtech.2017.10.015

Murphy, S. V., and Atala, A. (2014). 3D Bioprinting of Tissues and Organs. *Nat. Biotechnol.* 32 (8), 773–785. doi:10.1038/nbt.2958

Nazeer, M. A., Karaoglu, I. C., Ozer, O., Albayrak, C., and Kizilel, S. (2021). Neovascularization of Engineered Tissues for Clinical Translation: Where We Are, where We Should Be? *APL Bioeng.* 5 (2), 021503. doi:10.1063/5.0044027

Nelson, C. E., Kim, A. J., Adolph, E. J., Gupta, M. K., Yu, F., Hocking, K. M., et al. (2014). Tunable Delivery of siRNA from a Biodegradable Scaffold to Promote Angiogenesis *In Vivo*. *Adv. Mater.* 26 (4), 607506–607614. doi:10.1002/adma.201303520

Nichol, J. W., Koshy, S. T., Bae, H., Hwang, C. M., Yamanlar, S., and Khademhosseini, A. (2010). Cell-laden Microengineered Gelatin Methacrylate Hydrogels. *Biomaterials* 31 (21), 5536–5544. doi:10.1016/j.biomaterials.2010.03.064

Noori, A., Ashrafi, S. J., Vaez-Ghaemi, R., Hatamian-Zaremi, A., and Webster, T. J. (2017). A Review of Fibrin and Fibrin Composites for Bone Tissue Engineering. *Ijn* 12, 4937–4961. doi:10.2147/ijn.S124671

Norotte, C., Marga, F. S., Niklason, L. E., and Forgacs, G. (2009). Scaffold-free Vascular Tissue Engineering Using Bioprinting. *Biomaterials* 30 (30), 5910–5917. doi:10.1016/j.biomaterials.2009.06.034

Novosel, E. C., Kleinhans, C., and Kluger, P. J. (2011). Vascularization Is the Key challenge in Tissue Engineering. *Adv. Drug Deliv. Rev.* 63 (4-5), 300–311. doi:10.1016/j.addr.2011.03.004

O'Bryan, C. S., Bhattacharjee, T., Niemi, S. R., Balachandar, S., Baldwin, N., Ellison, S. T., et al. (2017). Three-dimensional Printing with Sacrificial Materials for Soft Matter Manufacturing. *MRS Bull.* 42 (8), 571–577. doi:10.1557/mrs.2017.167

P B, S., S, G., J, P., Muthusamy, S., R, N., Krishnakumar, G. S., et al. (2022). Tricomposite Gelatin-Carboxymethylcellulose-Alginate Bioink for Direct and Indirect 3D Printing of Human Knee Meniscal Scaffold. *Int. J. Biol. Macromolecules* 195, 179–189. doi:10.1016/j.ijbiomac.2021.11.184

Park, J. H., Jung, J. W., Kang, H.-W., and Cho, D.-W. (2014). Indirect Three-Dimensional Printing of Synthetic Polymer Scaffold Based on thermal Molding Process. *Biofabrication* 6 (2), 025003. doi:10.1088/1758-5082/6/2/025003

Patel-Hett, S., and DAmore, P. A. (2011). Signal Transduction in Vasculogenesis and Developmental Angiogenesis. *Int. J. Dev. Biol.* 55 (4-5), 353–363. doi:10.1387/ijdb.103213sp

Patterson, J., and Hubbell, J. A. (2010). Enhanced Proteolytic Degradation of Molecularly Engineered PEG Hydrogels in Response to MMP-1 and MMP-2. *Biomaterials* 31 (30), 7836–7845. doi:10.1016/j.biomaterials.2010.06.061

Pawar, S. N., and Edgar, K. J. (2012). Alginate Derivatization: a Review of Chemistry, Properties and Applications. *Biomaterials* 33 (11), 3279–3305. doi:10.1016/j.biomaterials.2012.01.007

Perrone, G. S., Leisk, G. G., Lo, T. J., Moreau, J. E., Haas, D. S., Papenburg, B. J., et al. (2014). The Use of Silk-Based Devices for Fracture Fixation. *Nat. Commun.* 5, 3385. doi:10.1038/ncomms4385

Pimentel C., R., Ko, S. K., Caviglia, C., Wolff, A., Emnéus, J., Keller, S. S., et al. (2018). Three-dimensional Fabrication of Thick and Densely Populated Soft Constructs with Complex and Actively Perfused Channel Network. *Acta Biomater.* 65, 174–184. doi:10.1016/j.actbio.2017.10.047

Piras, C. C., and Smith, D. K. (2020). Multicomponent Polysaccharide Alginate-Based Bioinks. *J. Mater. Chem. B* 8 (36), 8171–8188. doi:10.1039/d0tb01005g

Placone, J. K., and Engler, A. J. (2018). Recent Advances in Extrusion-Based 3D Printing for Biomedical Applications. *Adv. Healthc. Mater.* 7 (8), 1701161. doi:10.1002/adhm.201701161

Poellmann, M. J., Barton, K. L., Mishra, S., and Johnson, A. J. W. (2011). Patterned Hydrogel Substrates for Cell Culture with Electrohydrodynamic Jet Printing. *Macromol. Biosci.* 11 (9), 1164–1168. doi:10.1002/mabi.201100004

Pollet, A. M. A. O., Homburg, E. F. G. A., Cardinaels, R., and den Toonder, J. M. J. (2019). 3D Sugar Printing of Networks Mimicking the Vasculature. *Micromachines* 11 (1), 43. doi:10.3390/mi11010043

Qi, X., Wang, H., Zhang, Y., Pang, L., Xiao, W., Jia, W., et al. (2018). Mesoporous Bioactive Glass-Coated 3D Printed Borosilicate Bioactive Glass Scaffolds for Improving Repair of Bone Defects. *Int. J. Biol. Sci.* 14 (4), 471–484. doi:10.7150/ijbs.23872

Rastogi, P., and Kandasubramanian, B. (2019). Review of Alginate-Based Hydrogel Bioprinting for Application in Tissue Engineering. *Biofabrication* 11 (4), 042001. doi:10.1088/1758-5090/ab331e

Reakasame, S., and Boccaccini, A. R. (2018). Oxidized Alginate-Based Hydrogels for Tissue Engineering Applications: A Review. *Biomacromolecules* 19 (1), 3–21. doi:10.1021/acs.biomac.7b01331

Reis, L. A., Chiu, L. L. Y., Feric, N., Fu, L., and Radisic, M. (2016). Biomaterials in Myocardial Tissue Engineering. *J. Tissue Eng. Regen. Med.* 10 (1), 11–28. doi:10.1002/term.1944

Richards, D., Jia, J., Yost, M., Markwald, R., and Mei, Y. (2017). 3D Bioprinting for Vascularized Tissue Fabrication. *Ann. Biomed. Eng.* 45 (1), 132–147. doi:10.1007/s10439-016-1653-z

Robu, A., Mironov, V., and Neagu, A. (2019). Using Sacrificial Cell Spheroids for the Bioprinting of Perfusable 3D Tissue and Organ Constructs: A Computational Study. *Comput. Math. Methods Med.* 2019, 1–9. doi:10.1155/2019/7853586

Rocca, M., Fragasso, A., Liu, W., Heinrich, M. A., and Zhang, Y. S. (2018). Embedded Multimaterial Extrusion Bioprinting. *SLAS TECHNOLOGY: Translating Life Sci. Innovation* 23 (2), 154–163. doi:10.1177/2472630317742071

Rouwkema, J., and Khademhosseini, A. (2016). Vascularization and Angiogenesis in Tissue Engineering: Beyond Creating Static Networks. *Trends Biotechnol.* 34 (9), 733–745. doi:10.1016/j.tibtech.2016.03.002

Rouwkema, J., Koopman, B. F. J. M., Blitterswijk, C. A. V., Dhert, W. J. A., and Malda, J. (2009). Supply of Nutrients to Cells in Engineered Tissues. *Biotechnol. Genet. Eng. Rev.* 26, 163–178. doi:10.5661/bger-26-163

Rouwkema, J., Rivron, N. C., and van Blitterswijk, C. A. (2008). Vascularization in Tissue Engineering. *Trends Biotechnol.* 26 (8), 434–441. doi:10.1016/j.tibtech.2008.04.009

Ryssel, H., Gazyakan, E., Germann, G., and Öhlbauer, M. (2008). The Use of MatriDerm in Early Excision and Simultaneous Autologous Skin Grafting in burns-A Pilot Study. *Burns* 34 (1), 93–97. doi:10.1016/j.burns.2007.01.018

Sarker, M. D., Naghieh, S., Sharma, N. K., and Chen, X. (2018b). 3D Biofabrication of Vascular Networks for Tissue Regeneration: A Report on Recent Advances. *J. Pharm. Anal.* 8 (5), 277–296. doi:10.1016/j.jpha.2018.08.005

Sarker, M., Izadifar, M., Schreyer, D., and Chen, X. (2018a). Influence of Ionic Crosslinkers (Ca2+/Ba2+/Zn2+) on the Mechanical and Biological Properties of 3D Bioplotted Hydrogel Scaffolds. *J. Biomater. Sci. Polym. Edition* 29 (10), 1126–1154. doi:10.1080/09205063.2018.1433420

Schmedlen, R. H., Masters, K. S., and West, J. L. (2002). Photocrosslinkable Polyvinyl Alcohol Hydrogels that Can Be Modified with Cell Adhesion Peptides for Use in Tissue Engineering. *Biomaterials* 23 (22), 4325–4332. doi:10.1016/s0142-9612(02)00177-1

Schöneberg, J., De Lorenzi, F., Theek, B., Blaeser, A., Rommel, D., Kuehne, A. J. C., et al. (2018). Engineering Biofunctional *In Vitro* Vessel Models Using a Multilayer Bioprinting Technique. *Sci. Rep.* 8 (1), 10430. doi:10.1038/s41598-018-28715-0

Schumacher, M., Uhl, F., Detsch, R., Deisinger, U., and Ziegler, G. (2010). Static and Dynamic Cultivation of Bone Marrow Stromal Cells on Biphasic Calcium Phosphate Scaffolds Derived from an Indirect Rapid Prototyping Technique. *J. Mater. Sci. Mater. Med.* 21 (11), 3039–3048. doi:10.1007/s10856-010-4153-y

Schwab, A., Levato, R., D'Este, M., Piluso, S., Eglin, D., and Malda, J. (2020). Printability and Shape Fidelity of Bioinks in 3D Bioprinting. *Chem. Rev.* 120 (19), 11028–11055. doi:10.1021/acs.chemrev.0c00084

Seifu, D. G., and Mequanint, K. (2012). Fabrication of Vascular Tissue Engineering Scaffolds with Enhanced Oxygen Diffusivity and Cell Infiltration. *j biomat tissue engng* 2 (4), 280–291. doi:10.1166/jbt.2012.1061

Serbo, J. V., and Gerecht, S. (2013). Vascular Tissue Engineering: Biodegradable Scaffold Platforms to Promote Angiogenesis. *Stem Cell Res Ther* 4 (1). doi:10.1186/scrt156

Silva, M., Ferreira, F. N., Alves, N. M., and Paiva, M. C. (2020). Biodegradable Polymer Nanocomposites for Ligament/tendon Tissue Engineering. *J. Nanobiotechnol* 18 (1), 23. doi:10.1186/s12951-019-0556-1

Skardal, A., Devarasetty, M., Kang, H.-W., Mead, I., Bishop, C., Shupe, T., et al. (2015). A Hydrogel Bioink Toolkit for Mimicking Native Tissue Biochemical and Mechanical Properties in Bioprinted Tissue Constructs. *Acta Biomater.* 25, 24–34. doi:10.1016/j.actbio.2015.07.030

Skylar-Scott, M. A., Uzel, S. G. M., Nam, L. L., Ahrens, J. H., Truby, R. L., Damaraju, S., et al. (2019). Biomanufacturing of Organ-specific Tissues with High Cellular Density and Embedded Vascular Channels. *Sci. Adv.* 5 (9), eaaw2459. doi:10.1126/sciadv.aaw2459

Sooppan, R., Paulsen, S. J., Han, J., Ta, A. H., Dinh, P., Gaffey, A. C., et al. (2016). *In Vivo* Anastomosis and Perfusion of a Three-Dimensionally-Printed Construct Containing Microchannel Networks. *Tissue Eng. Part C: Methods* 22 (1), 1–7. doi:10.1089/ten.TEC.2015.0239

Štumberger, G., and Vihar, B. (2018). Freeform Perfusable Microfluidics Embedded in Hydrogel Matrices. *Materials* 11 (12), 2529. doi:10.3390/ma11122529

Sun, G., Shen, Y.-I., Kusuma, S., Fox-Talbot, K., Steenbergen, C. J., and Gerecht, S. (2011). Functional Neovascularization of Biodegradable Dextran Hydrogels with Multiple Angiogenic Growth Factors. *Biomaterials* 32 (1), 95–106. doi:10.1016/j.biomaterials.2010.08.091

Teodorescu, M., Bercea, M., and Morariu, S. (2019). Biomaterials of PVA and PVP in Medical and Pharmaceutical Applications: Perspectives and Challenges. *Biotechnol. Adv.* 37 (1), 109–131. doi:10.1016/j.biotechadv.2018.11.008

Thomas, A., Orellano, I., Lam, T., Noichl, B., Geiger, M.-A., Amler, A.-K., et al. (2020). Vascular Bioprinting with Enzymatically Degradable Bioinks via Multi-Material Projection-Based Stereolithography. *Acta Biomater.* 117, 121–132. doi:10.1016/j.actbio.2020.09.033

Thompson, E. M., Matsiko, A., Kelly, D. J., Gleeson, J. P., and O'Brien, F. J. (2016). An Endochondral Ossification-Based Approach to Bone Repair: Chondrogenically Primed Mesenchymal Stem Cell-Laden Scaffolds Support Greater Repair of Critical-Sized Cranial Defects Than Osteogenically Stimulated Constructs *In Vivo*. *Tissue Eng. Part A* 22 (5-6), 556–567. doi:10.1089/ten.TEA.2015.0457

Tocchio, A., Tamplenizza, M., Martello, F., Gerges, I., Rossi, E., Argentiere, S., et al. (2015). Versatile Fabrication of Vascularizable Scaffolds for Large Tissue Engineering in Bioreactor. *Biomaterials* 45, 124–131. doi:10.1016/j.biomaterials.2014.12.031

Vacanti, J. P. (2012). Tissue Engineering and the Road to Whole Organs. *Br. J. Surg.* 99 (4), 451–453. doi:10.1002/bjs.7819

Van Den Bulcke, A. I., Bogdanov, B., De Rooze, N., Schacht, E. H., Cornelissen, M., and Berghmans, H. (2000). Structural and Rheological Properties of Methacrylamide Modified Gelatin Hydrogels. *Biomacromolecules* 1 (1), 31–38. doi:10.1021/bm990017d

Van Hoorick, J., Declercq, H., De Muynck, A., Houben, A., Van Hoorebeke, L., Cornelissen, R., et al. (2015). Indirect Additive Manufacturing as an Elegant Tool for the Production of Self-Supporting Low Density Gelatin Scaffolds. *J. Mater. Sci. Mater. Med.* 26 (10), 247. doi:10.1007/s10856-015-5566-4

Vig, K., Chaudhari, A., Tripathi, S., Dixit, S., Sahu, R., Pillai, S., et al. (2017). Advances in Skin Regeneration Using Tissue Engineering. *Ijms* 18 (4), 789. doi:10.3390/ijms18040789

Vijayavenkataraman, S., Yan, W.-C., Lu, W. F., Wang, C.-H., and Fuh, J. Y. H. (2018). 3D Bioprinting of Tissues and Organs for Regenerative Medicine. *Adv. Drug Deliv. Rev.* 132, 296–332. doi:10.1016/j.addr.2018.07.004

Wang, J.-Q., Jiang, B.-J., Guo, W.-J., and Zhao, Y.-M. (2019a). Indirect 3D Printing Technology for the Fabrication of Customised β-TCP/chitosan Scaffold with the Shape of Rabbit Radial Head-An *In Vitro* Study. *J. Orthop. Surg. Res.* 14 (1), 102. doi:10.1186/s13018-019-1136-7

Wang, P., Hu, J., and Ma, P. X. (2009). The Engineering of Patient-specific, Anatomically Shaped, Digits. *Biomaterials* 30 (14), 2735–2740. doi:10.1016/j.biomaterials.2009.01.037

Wang, Y., Rudym, D. D., Walsh, A., Abrahamsen, L., Kim, H.-J., Kim, H. S., et al. (2008). *In Vivo* degradation of Three-Dimensional Silk Fibroin Scaffolds. *Biomaterials* 29 (24-25), 3415–3428. doi:10.1016/j.biomaterials.2008.05.002

Wang, Z., Mithieux, S. M., and Weiss, A. S. (2019b). Fabrication Techniques for Vascular and Vascularized Tissue Engineering. *Adv. Healthc. Mater.* 8 (19), 1900742. doi:10.1002/adhm.201900742

Wenk, E., Meinel, A. J., Wildy, S., Merkle, H. P., and Meinel, L. (2009). Microporous Silk Fibroin Scaffolds Embedding PLGA Microparticles for Controlled Growth Factor Delivery in Tissue Engineering. *Biomaterials* 30 (13), 2571–2581. doi:10.1016/j.biomaterials.2008.12.073

White, S. M., Pittman, C. R., Hingorani, R., Arora, R., Esipova, T. V., Vinogradov, S. A., et al. (2014). Implanted Cell-Dense Prevascularized Tissues Develop Functional Vasculature that Supports Reoxygenation after Thrombosis. *Tissue Eng. Part A* 20 (17-18), 2316–2328. doi:10.1089/ten.TEA.2013.0311

Workman, V. L., Tezera, L. B., Elkington, P. T., and Jayasinghe, S. N. (2014). Controlled Generation of Microspheres Incorporating Extracellular Matrix Fibrils for Three-Dimensional Cell Culture. *Adv. Funct. Mater.* 24 (18), 2648–2657. doi:10.1002/adfm.201303891

Wu, L., Magaz, A., Maughan, E., Oliver, N., Darbyshire, A., Loizidou, M., et al. (2019). Cellular Responses to Thermoresponsive Stiffness Memory Elastomer Nanohybrid Scaffolds by 3D-TIPS. *Acta Biomater.* 85, 157–171. doi:10.1016/j.actbio.2018.12.019

Wu, L., Virdee, J., Maughan, E., Darbyshire, A., Jell, G., Loizidou, M., et al. (2018). Stiffness Memory Nanohybrid Scaffolds Generated by Indirect 3D Printing for Biologically Responsive Soft Implants. *Acta Biomater.* 80, 188–202. doi:10.1016/j.actbio.2018.09.016

Xie, R., Zheng, W., Guan, L., Ai, Y., and Liang, Q. (2020). Engineering of Hydrogel Materials with Perfusable Microchannels for Building Vascularized Tissues. *Small* 16 (15), 1902838. doi:10.1002/smll.201902838

Xu, Y., Hu, Y., Liu, C., Yao, H., Liu, B., and Mi, S. (2018). A Novel Strategy for Creating Tissue-Engineered Biomimetic Blood Vessels Using 3D Bioprinting Technology. *Materials* 11 (9), 1581. doi:10.3390/ma11091581

Yamamura, N., Sudo, R., Ikeda, M., and Tanishita, K. (2007). Effects of the Mechanical Properties of Collagen Gel on the *In Vitro* Formation of Microvessel Networks by Endothelial Cells. *Tissue Eng.* 13 (7), 1443–1453. doi:10.1089/ten.2006.0333

Yan, W.-C., Davoodi, P., Vijayavenkataraman, S., Tian, Y., Ng, W. C., Fuh, J. Y. H., et al. (2018). 3D Bioprinting of Skin Tissue: From Pre-processing to Final Product Evaluation. *Adv. Drug Deliv. Rev.* 132, 270–295. doi:10.1016/j.addr.2018.07.016

Yang, S., Tang, H., Feng, C., Shi, J., and Yang, J. (2020). The Research on Multi-Material 3D Vascularized Network Integrated Printing Technology. *Micromachines* 11 (3), 237. doi:10.3390/mi11030237

Yeong, W.-Y., Chua, C.-K., Leong, K.-F., Chandrasekaran, M., and Lee, M.-W. (2007). Comparison of Drying Methods in the Fabrication of Collagen Scaffold via Indirect Rapid Prototyping. *J. Biomed. Mater. Res.* 82B (1), 260–266. doi:10.1002/jbm.b.30729

Yue, K., Trujillo-de Santiago, G., Alvarez, M. M., Tamayol, A., Annabi, N., and Khademhosseini, A. (2015). Synthesis, Properties, and Biomedical Applications of Gelatin Methacryloyl (GelMA) Hydrogels. *Biomaterials* 73, 254–271. doi:10.1016/j.biomaterials.2015.08.045

Zhang, G., Varkey, M., Wang, Z., Xie, B., Hou, R., and Atala, A. (2020). ECM Concentration and Cell-mediated Traction Forces Play a Role in Vascular Network Assembly in 3D Bioprinted Tissue. *Biotechnol. Bioeng.* 117 (4), 1148–1158. doi:10.1002/bit.27250

Zhang, W., Zhang, Y. S., Bakht, S. M., Aleman, J., Shin, S. R., Yue, K., et al. (2016). Elastomeric Free-form Blood Vessels for Interconnecting Organs on Chip Systems. *Lab. Chip* 16 (9), 1579–1586. doi:10.1039/c6lc00001k

Zhu, J., Wang, Y., Zhong, L., Pan, F., and Wang, J. (2021). Advances in Tissue Engineering of Vasculature through Three-dimensional Bioprinting. *Dev. Dyn.* 250 (12), 1717–1738. doi:10.1002/dvdy.385

Zhu, W., Ma, X., Gou, M., Mei, D., Zhang, K., and Chen, S. (2016). 3D Printing of Functional Biomaterials for Tissue Engineering. *Curr. Opin. Biotechnol.* 40, 103–112. doi:10.1016/j.copbio.2016.03.014

Zhu, W., Qu, X., Zhu, J., Ma, X., Patel, S., Liu, J., et al. (2017). Direct 3D Bioprinting of Prevascularized Tissue Constructs with Complex Microarchitecture. *Biomaterials* 124, 106–115. doi:10.1016/j.biomaterials.2017.01.042

Zou, Q., Grottkau, B. E., He, Z., Shu, L., Yang, L., Ma, M., et al. (2020). Biofabrication of valentine-shaped Heart with a Composite Hydrogel and Sacrificial Material. *Mater. Sci. Eng. C* 108, 110205. doi:10.1016/j.msec.2019.110205

Conflict of Interest: The authors declare that the research was conducted in the absence of any commercial or financial relationships that could be construed as a potential conflict of interest.

The reviewer YD declared a shared affiliation, with no collaboration, with all of the authors to the handling editor at the time of the review.

Publisher's Note: All claims expressed in this article are solely those of the authors and do not necessarily represent those of their affiliated organizations, or those of the publisher, the editors, and the reviewers. Any product that may be evaluated in this article, or claim that may be made by its manufacturer, is not guaranteed or endorsed by the publisher.

frontiers | Frontiers in Bioengineering and Biotechnology

REVIEW
published: 01 April 2022
doi: 10.3389/fbioe.2022.859927

Hydrogel Encapsulation: Taking the Therapy of Mesenchymal Stem Cells and Their Derived Secretome to the Next Level

Yuling Huang[1], *Xin Li*[2]* *and Lina Yang*[1]*

[1]Departments of Geriatrics, First Affiliated Hospital of China Medical University, Shenyang, China, [2]Departments of Infectious Disease, First Affiliated Hospital of China Medical University, Shenyang, China

Biomaterials have long been the focus of research and hydrogels are representatives thereof. Hydrogels have attracted much attention in the medical sciences, especially as a candidate drug-carrier. Mesenchymal stem cells (MSC) and MSC-derived secretome are a promising therapeutic method, owing to the intrinsic therapeutic properties thereof. The low cell retention and poor survival rate of MSCs make further research difficult, which is a problem that hydrogel encapsulation largely solved. In this review, safety and feasibility of hydrogel-encapsulated MSCs, the improvement of the survival, retention, and targeting, and the enhancement of their therapeutic effect by hydrogels were studied. The status of the hydrogel-encapsulated MSC secretome was also discussed.

Keywords: hydrogel, extracellular vesicles, biomaterials, secretome, mesenchymal stem cells

OPEN ACCESS

Edited by:
Jianshe Hu,
Northeastern University, China

Reviewed by:
Chun Pan,
Southeast University, China
Yang Chen,
University of Texas MD Anderson Cancer Center, United States

***Correspondence:**
Xin Li
xuanfeng7890@163.com
Lina Yang
yanglina1984@163.com

Specialty section:
This article was submitted to Biomaterials, a section of the journal Frontiers in Bioengineering and Biotechnology

Received: *22 January 2022*
Accepted: *03 March 2022*
Published: *01 April 2022*

Citation:
Huang Y, Li X and Yang L (2022) Hydrogel Encapsulation: Taking the Therapy of Mesenchymal Stem Cells and Their Derived Secretome to the Next Level. Front. Bioeng. Biotechnol. 10:859927. doi: 10.3389/fbioe.2022.859927

1 INTRODUCTION

The study of biomaterials has been advancing rapidly in recent years. On the one hand, biomaterials can fill and repair tissue defects directly as accessible grafts, for example, calcium phosphate materials have been studied widely in the treatment of bone defects (Humbert et al., 2019). On the other hand, biomaterials enhance the effects of other therapies by various methods, such as drug delivery, targeted injury, and controlled release. Of those biomaterials, hydrogels have attracted attention in drug-delivery investigations due to their outstanding biocompatibility, degradability, and processability. There are various preparation methods for hydrogels, including covalent bonding, photopolymerization, thermo-gelation hydrogels, cryo-gelation, and other non-covalent bonding (Huang et al., 2017a). According to the origin of the gel precursor molecules, hydrogels can be divided into natural and synthetic hydrogels: the former hydrogels demonstrate better biocompatibility; while the latter has better stability (Salinas and Anseth, 2009). Additionally, based on application purpose, strong machinability enables hydrogels to be formed into different shapes and sizes, such as fibers, microbeads, or nanoparticles (Pishavar et al., 2021).

MSCs, multipotential stem cells, are derived from various tissues, including bone marrow (BM-MSCs), adipose (AD-MSCs), umbilical cord (UC-MSCs), peripheral blood, etc. According to "Minimal criteria that define multipotent mesenchymal stromal cells," MSCs adhere to plastics under standard culture conditions; CD105, CD73 and CD90 are specific surface markers; through *in vitro* induction, MSCs can differentiate into bone, adipose, and cartilage (Dominici et al., 2006). Early studies also generally suggested that differentiation is the main mechanism of MSC therapy (Lange et al., 2005). With further exploration, secretomes such as soluble trophic factors and extracellular vesicles (EVs) play a more important role in the treatment of MSCs. The MSC

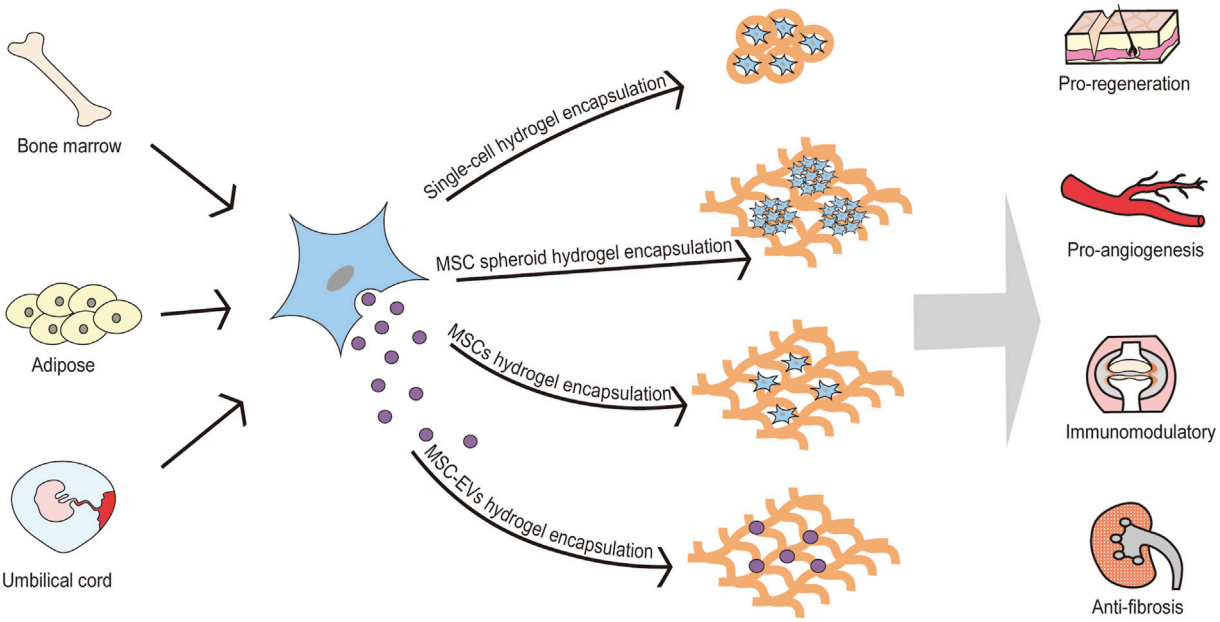

FIGURE 1 | Hydrogel encapsulation may bring the treatment of MSCs and their secretome to the next level. MSCs are derived from various tissues, including bone marrow, adipose, umbilical cord, peripheral blood, etc. MSCs can be encapsulated by hydrogel in various formation (single-cell hydrogel encapsulation, MSC spheroid hydrogel encapsulation, and MSCs hydrogel encapsulation). Also, MSC-EVs can be encapsulated by hydrogel for pro-regenerative, pro-angiogenic, immunomodulation and anti-fibrotic effects. MSC: mesenchymal stem cell; MSC-EVs: mesenchymal stem cell-derived extracellular vesicles.

secretome includes soluble trophic factors (secreting growth factors, chemokines, cytokines, etc.) and EVs. The sac-like structures formed by EVs can encapsulate specific factors (DNA, RNA, protein, and amino acids metabolites) secreted by mother cells to transmit information in a stable manner *in vivo* and vitro (Kalluri and LeBleu, 2020). Numerous preclinical studies confirmed the benefits of MSCs and their secreted factors. For example, UC-MSC administration improved the outcomes of patients with severe COVID-19 pneumonia without any infusion reaction (Guo et al., 2020). Mesenchymal stem cell-derived extracellular vesicles (MSC-EVs) attenuated renal inflammation and fibrosis in pigs with metabolic syndrome and renal artery stenosis (Eirin et al., 2017).

Infusion of MSCs and their derived secretome, as an emerging therapeutic modality, which can be proregenerate, proangiogenisis, immunomodulate, anti-inflammatory, anti-fibrotic, etc. has been recognized by experts in many diseases. Clinically, MSCs have been approved for the treatment of Crohn's complicated intestinal fistula and graft-versus-host disease. However, the non-targeted distribution of MSCs and their derived secretomes, low tissue retention, and high metabolic rate greatly limit their applications. Hydrogel encapsulation can solve the above problems and provide a new drug route for MSCs. More interestingly, incorporation of various bioactive factors can improve directional delivery and promote specific behavior of MSCs. Therefore, hydrogel encapsulation may bring the treatment of MSCs and their secretome to the next level (**Figure 1**). The manuscript will be generally introduced from two aspects: hydrogels encapsulate MSC and hydrogels encapsulate MSC secretome: the former includes premise, mechanism, and advance of hydrogels-encapsulated MSCs; the latter is composed according to the classification and components of MSC secretome.

2 HYDROGELS ENCAPSULATE MESENCHYMAL STEM CELLS

Biomaterials combined with MSCs were initially mainly used for tissue regeneration, especially bone regeneration. Researchers found that the addition of MSCs can significantly promote regeneration compared with the filling of defective bone tissue with biomaterials (De Kok et al., 2003). Later, the same researchers proposed that injecting the hydrogel could help stimulate bone marrow to produce stem cells to grow new cartilage in cartilage repair surgery (Huang et al., 2010). Subsequently, hydrogels have been widely recognized as a high water-absorbing and high water-holding material to load medicines in drug delivery applications. It is noteworthy that the focus of the present research is to encapsulate MSCs with hydrogels to achieve targeted delivery, increase the retention at the injury site, and enhance the function of MSCs. This is different from the addition of MSCs when the biomaterial fills the defective tissue. A wide variety of hydrogels are used to encapsulate MSCs. The main natural polymer hydrogels are comprised of alginic acid (Ho et al., 2016), hyaluronic acid (Liu et al., 2019), chitosan (Boido et al., 2019) and collagen (Huang et al., 2017b), etc. Synthetic hydrophilic polymers include polyethylene glycol (PEG) (Sylvester et al., 2021) and acrylic

acid (Qiu et al., 2011). In addition, based on a single hydrogel, mixing other hydrogels and incorporating some bioactive factors can guide MSCs to exert more specific functions. Hydrogel-encapsulated MSCs are widely used, and existing studies involve various tissues and organs: bone, cartilage, heart, kidney, skin, spinal cord, etc.

2.1 Safety and Feasibility of Hydrogels-Encapsulated Mesenchymal Stem Cells

The safety and feasibility of hydrogel-encapsulated MSCs are the prerequisites for the clinical translation of this therapy. On the one hand, whether MSCs can successfully perform their therapeutic functions in hydrogels is very important. Wu et al. found that self-assembled supramolecular hydrogel-encapsulated MSCs could maintain cell morphology and viability, which demonstrate the biocompatibility and non-cytotoxicity of the hydrogels (Wu et al., 2008). In the chitosan-based hydrogel developed by Boido et al., the viability and paracrine activity of MSCs were not affected by the hydrogel, and the encapsulated MSCs could release MSC vesicles and maintain their antioxidant function (Boido et al., 2019). Papa et al. found that MSCs in arginine-glycine-aspartate (RGD) -extracellular matrix hydrogel scaffolds could maintain cellular structure *in situ* and gradually release CCL2 chemokine, which can promote functional recovery from spinal cord injury (SCI) (Papa et al., 2018). The study of Bussche et al. showed that the microencapsulation of MSCs did not interfere with the release of bioactive factors (Bussche et al., 2015). Furthermore, co-gelation of acellular vascular matrix and collagen enhanced the survival and paracrine effects of MSCs in the injured kidney (Huang et al., 2017b). However, some studies pointed out that the 3D microenvironment hinders the trans-differentiation of MSCs and the production of secreted factors in the onerous microenvironment of myocardial infarction (MI) (Sylvester et al., 2021).

On the other hand, the biocompatibility of hydrogels as allografts is worth investigating. Yuan et al. studied and compared the changes in immunological properties associated with different scaffolds and found that MSC-hydrogel structures caused rather low proliferation of allogeneic lymphocytes, especially when prepared from higher concentrations of collagen in the hydrogel (Yuan et al., 2011). Also, attenuating innate immune responses could be achieved by modifying hydrogels. Ghanta et al. used immune-evasive and small-molecule-modified alginate encapsulation to enable MSCs to persist and localize on the heart, and then to improve cardiac function after acute MI (Ghanta et al., 2020). Similarly, Alvarado-Velez et al. engineered an agarose hydrogel that releases Fas ligand, a protein that induces apoptosis in cytotoxic $CD8^+$ T cells, to increase MSC survival rate of allogeneic transplantation near the injury site (Alvarado-Velez et al., 2021). Moreover, in the clinical study of He et al., intramyocardial injection of UC-MSC-loaded collagen hydrogel showed no serious adverse reactions, proving that the use of collagen hydrogel for cell delivery is safe and feasible (He et al., 2020).

2.2 Hydrogel Encapsulation Improves Mesenchymal Stem Cells Survival, Retention, and Targeting

2.2.1 Improving Mesenchymal Stem Cells Survival

Before encapsulation, several conditions affected the viability of MSCs. Chen et al. proposed hydrogel-induced BM-MSCs under conditions of cell density ($<2 \times 10^7$ cells/mL), DMSO concentration (<0.5%), and needle gauge (25G or 27G). The survival rate could be maintained above 82% (Chen et al., 2017). Osama et al. proposed a different view: MSCs injected with a 30G needle showed significantly better viability when the hydrogel was in the pre- and post-gel state (Osama et al., 2018). Additionally, the different kinds of hydrogel encapsulation can play different effects. For example, single-cell hydrogel-encapsulated MSCs could interact with the cell-matrix via the activation of ERK/MAPK signaling cascade, thereby increasing cell viability (Karoubi et al., 2009). Isolated MSCs/secretome hydrogel encapsulation is applied in most experiments. Compared with isolated MSCs, MSC spheroids exhibit higher therapeutic potential in various aspects, improving cell survival, anti-inflammatory and angiogenic potential (Ho et al., 2016).

Adding some chemicals or bioactive factors to the hydrogel also promoted the viability of MSCs (**Table 1**). Cellulose nanocrystal-enhanced collagen-based nanocomposite hydrogels protected cells during injection (Zhang et al., 2020a). In the hypoxic environment of MI, graphene oxide added to alginate composite microgels protected MSCs from the harsh hypoxic environment (Choe et al., 2019). Compared to chemical modification, bioactive factors appeared to have better biocompatibility. Superoxide dismutase also protected MSCs encapsulated in hydrogels from superoxide attack (Li et al., 2009). The platelet-rich plasma gel provided a favorable survival environment for MSCs, and the optimal platelet concentration was 1×10^6 platelets/μl (Jalowiec et al., 2016). Fibrin hydrogels that were loaded with platelet-derived growth factor BB doubled the survival rate of MSC spheroids, indicating that platelet-derived growth factor BB could serve as a biochemical cue to promote the survival of MSC spheroids *in vivo* (Zhao et al., 2020). Heparan sulfate mimetic addition to hydrogels restored extracellular matrix network and enhanced growth factor bioactivity, increasing cell engraftment and cell survival (Moussa et al., 2019). In addition, miR-21 was retained in collagen hydrogels, targeted to activate downstream therapeutic cytokines, and significantly enhanced the anti-apoptotic capacity of MSCs (Zhang et al., 2017).

2.2.2 Improving Mesenchymal Stem Cells Retention, and Targeting

Obviously, hydrogel encapsulation can improve MSC retention, which is closely related with different kinds of hydrogel. The degradation rate of the hydrogel was found to determine the cell delivery, retention, and controlled release to a certain extent (Qiu et al., 2011). In a femoral defect model, Hoffman et al. controlled longitudinal localization of MSCs on the surface of allografts by altering hydrogel degradation kinetics (Hoffman et al., 2014).

TABLE 1 | Some chemicals or bioactive factors in hydrogel promoting the viability of MSCs.

Factor	Type of hydrogels	MSC origin	Characteristic	Efficacy	References
Cellulose Nanocrystal	Collagen-Based Nanocomposite Hydrogel	BM-MSCs	fast shear thinning, self-healing and improved elastic modulus	high cell viability after extrusion *in vitro*, improved implant integrity and higher cell retention	Zhang et al. (2020a)
Reduced graphene oxide	Reduced graphene oxide	UC-MSCs	Anti-oxidant activity	higher cell viability and cardiac maturation	Choe et al. (2019)
ROS	Collagen biocomposite	BM-MSCs	Anti-oxidant activity	suppressed superoxide penetration into the hydrogel and cell membrane and stimulating MSC growth	Li et al. (2009)
Platelet-rich plasma	chitosan, batroxobin, thrombin, calcium chloride, or a combination of the latter two	BM-MSCs	promoting growth factor and inflammatory proteins release	the highest cell viability and DNA content found in PRP-gels with 1×10^6 platelets/mL	Jalowiec et al. (2016)
PDGF-BB	Aptamer-functionalized fibrin hydrogel	MSC spheroids	Inhibiting the apoptosis and promoting the proliferation	promoted the survival of MSC spheroids	Zhao et al. (2020)
Heparan sulfate mimetics	Si-HPMC hydrogel	AD-MSCs	Restore the extracellular matrix network and enhance the biological activity of growth factors	increased cell engraftment and cell survival, and improved the therapeutic benefit	Moussa et al. (2019)
miR-21	Collagen hydrogel	AD-MSCs	interfering the expressions of apoptotic related proteins	protect MSCs from ROS-induced cellular dysfunction	Zhang et al. (2017)

Adding some chemicals or bioactive factors to the hydrogel also promoted the viability of MSCs. Compared to chemical modification, bioactive factors appeared to have better biocompatibility. MSC: mesenchymal stem cell; ROS: reactive oxygen species; BM-MSCs: MSCs derived from bone marrow; UC-MSCs: MSCs derived from umbilical cord; AD-MSCs: MSCs derived from adipose.

Hydrogel encapsulation can improve efficient distribution and targeting of MSCs. The current research mainly achieves target of MSC through direct contact. For example, covering the surface of injured skin can limit the local spread of MSCs (Zhou et al., 2019a). Intramyocardial injection of MSC-loaded collagen hydrogel can improve distribution of MSCs in heart (He et al., 2020). Also, modifying hydrogel is a feasible method, but the research has not applied in hydrogel encapsulation. For example, by the coating of lipid-conjugated heparin, AD-MSCs without hydrogel encapsulation can target the damaged liver with enhanced delivery and longer retention (Hwang et al., 2019).

2.3 Hydrogel Encapsulation Guide Mesenchymal Stem Cells to Perform Specific Functions Using Tailored Biochemical and Biophysical Cues

MSCs have the properties of tissue repair ability and immune regulation ability. Hydrogel encapsulation enhances the therapeutic capacity of MSCs by increasing survival, retention, and targeting. The therapeutic efficacy of hydrogel-loaded MSCs has been demonstrated in many diseases, for example, the function of gel-encapsulated MSCs has been continuously explored in bone and cartilage regeneration, wound repair, MI, and other studies.

2.3.1 Tissue Repair

Angiogenesis plays an irreplaceable role in the process of tissue repair. Glycine-histidine-lysine-modified alginate hydrogels could upregulate the ability of MSCs to secrete pro-angiogenic factors (Jose et al., 2014). Intramuscular injection of MSCs within a PEGylated fibrin gel matrix was found to promote the formation of mature blood vessels in a model of hind limb ischemia (Ricles et al., 2016). Also, a novel hydrogel composed of pooled human platelet lysates could localize ischemic tissue to promote angiogenesis (Robinson et al., 2016).

MI is a common ischemic disease. Gao et al. used BG/γ-PGA/CS hydrogel to activate the interaction between MSCs and cell matrix, resulting in decreased apoptosis and enhanced angiogenesis, improved cardiac function, and attenuated cardiac remodeling (Gao et al., 2020). In addition, epicardial placement of MSCs-loaded POx hydrogels also improved neovascularization in rats with MI (You et al., 2021).

In wound repair, the pro-angiogenic effect of MSCs is crucial. Pharmacological pre-treatment of MSCs with the natural potent antioxidant was reported to increase the amount of pro-angiogenic cytokines and the speed of wound closure (Touani et al., 2021). The pore size of the hydrogel scaffolds can also act as a regulator of the paracrine effects of MSC angiogenesis, with medium-pore-size scaffolds having the highest paracrine effects of angiogenic cytokines (Qazi et al., 2019). MSC spheroids are currently being studied more, and compared with isolated MSCs, MSC spheroids exhibit higher therapeutic potential in various aspects, improving cell survival, anti-inflammatory and angiogenic potential (Ho et al., 2016). Especially in the promotion of wound healing, multiple studies showed that hydrogel-encapsulated MSC spheroids have faster wound closure and more obvious angiogenesis (Murphy et al., 2017; Yang et al., 2020a). For contaminated wounds, adding antibiotics such as minocycline (Guerra et al., 2017) or FMZC to the base hydrogel encapsulating MSCs was able to reduce bacterial bioburden and promote wound repair (Rafie and Meshkini, 2021).

2.3.2 Immunomodulatory and Anti-Fibrotic

In myocardial ischemia/reperfusion injury, MSCs encapsulated in a hydrogel carrier mediate the conversion of AMP to adenosine

by CD73, exerting a powerful anti-inflammatory effect (Shin et al., 2020). In osteoarthritis, Gómez-Aristizábal et al. found that hyaluronic acid binding to MSCs has an additive effect on MSC-mediated immune modulation (Gómez-Aristizábal et al., 2016). Sodium alginate microencapsulation could also modulate MSC paracrine function and enhance the therapeutic effect of MSCs in OA (McKinney et al., 2021). In injured vocal cords, MSCs + hyaluronic acid hydrogel exerted an equivalent inhibitory effect on inflammation *in vivo* (Hertegård et al., 2019). In colonic radiation-induced injury, MSCs in silylated hydroxypropylmethylcellulose hydrogel were capable of secreting trophic factors and responded to the inflammatory milieu (Moussa et al., 2017). In addition to immune regulation, anti-fibrosis is also an important function of MSCs. Gelatin-microcryogel-loaded MSCs protected 5/6 nephrectomized kidneys through anti-inflammatory and anti-fibrotic effects (Geng et al., 2019). In a radiation therapy-induced esophageal fibrosis model, Kim et al. used catechol-functionalized hyaluronic acid hydrogel-encapsulated MSC spheroids to improve esophageal injury (Kim et al., 2021).

TABLE 2 | Hydrogel-encapsulated MSC secretome in treating diseases.

Type of hydrogel	MSC origin	Type of secretome	Administration	Mechanism	Application	References
Hyaluronic acid hydrogel	BMMSCs	Non-specific	Intrauterine administration	Restored endometrial morphology and function	Asherman's Syndrome	Liu et al. (2019)
Composed of COLI and LMWHA or COLI and PEG	ADMSCs	Non-specific	*In vitro* study	Counteract 6-OHDA toxicity with upregulation of the antioxidant enzyme sirtuin 3	Parkinson's disease	Chierchia et al. (2020)
GelMA PEGDA hybrid hydrogels	BMMSCs	Conditioned media	*In vitro* study	Promoted proliferative and migratory activities of hyperglycemic fibroblasts	Diabetic or chronic wounds	Sears et al. (2021)
Collagen hydrogel	ADMSCs	Non-specific	*In vitro* study	Increased proliferation of skin-origin cells and improved angiogenic properties of endothelial cells	Chronic wounds	Kraskiewicz et al. (2021)
Chitosan/collagen/β-glycerophosphate thermosensitive hydrogel	UCMSCs	Conditioned media	Covering the wounds	Limited the area of inflammation, enhanced reepithelialization, promoted the formation of granulation tissue, and attenuated the formation of fibrotic and hypertrophic scar tissue	Burn wounds	Zhou et al. (2019a)
Self-assembling peptide nanofiber hydrogel	BMMSCs	EVs	Renal capsule injection	Reduced tubular cell apoptosis, pro-inflammatory cytokine expression, and macrophage infiltration	Renal ischemia-reperfusion injury	Zhou et al. (2019b)
RGD hydrogel	hP-MSCs	EVs	kidney cortex injection	Facilitated MSC derived let-7a-5p-containing-EVs, improved reparative potential against AKI	AKI	Zhang et al. (2020b)
PEG hydrogel	ES-MSCs	EVs	Systemic administration	Improved the anti-fibrosis, anti-inflammation, anti-apoptosis and regenerative effects of EVs	Chronic liver fibrosis	Mardpour et al. (2019)
Chitosan hydrogel	hP-MSCs	EVs	Subcutaneous injection	Delayed the skin aging processes by ameliorating the function of aging DFLs	Aging skin	Zhao et al. (2021)
GelMA hydrogel	BMMSCs	EVs	Sprayed onto the surface of the heart	Alleviated apoptosis and promote angiomyogenesis	MI	Tang et al. (2021)
Pluronic F127 hydrogel	UCMSCs	Exosomes	Covering the wounds	Enhanced regeneration of granulation tissue and upregulated expression of VEGF and TGFβ-1	Chronic wounds	Yang et al. (2020b)
Peptide-modified adhesive hydrogel	hP-MSCs	Exosomes	Intravenous injection	Elicited significant nerve recovery and urinary tissue preservation by effectively mitigating inflammation and oxidation	Spinal cord injury	Li et al. (2020)
Chitosan hydrogel	hP-MSCs	Exosomes	Intramuscular injection	Improved survival and angiogenesis of endothelial cells and accelerated the recovery of ischemic hindlimbs	Hindlimb ischemia	Zhang et al. (2018)
Diels–Alder crosslinked hyaluronic acid/PEG hydrogel	IMSCs	sEVs	Intraarticular injection	Improved the bioavailability and therapeutic efficacy of MSC-sEVs for OA improvement	Osteoarthritis	Yang et al. (2021)
Sodium alginate hydrogel	BMMSCs	sEVs	Intramyocardial injection	Promoted angiogenesis, reduced cardiac apoptosis and fibrosis, enhanced scar thickness, and eventually improved cardiac function	MI	Lv et al. (2019)

Multiple experiments have shown that hydrogels can continuously release MSC secretome, and effectively exert pro-regenerative, pro-angiogenic, and anti-fibrotic effects. MSC: mesenchymal stem cell; BM-MSCs: MSCs derived from bone marrow; UC-MSCs: MSCs derived from umbilical cord; AD-MSCs: MSCs derived from adipose; hP-MSCs: MSCs derived from human placenta; IMSCs: induced MSCs; COLI: collagen type I; LMWHA: low molecular weight hyaluronic acid; RGD: arginine-glycine-aspartate; PEG: polyethylene glycol; MI: myocardial infarction.

3 HYDROGELS ENCAPSULATE MESENCHYMAL STEM CELLS SECRETOME

According to the current study, MSCs mainly exert their therapeutic effects through paracrine. Compared with MSCs, MSC secretome has more advantages: 1. Cell-free treatment reduces the requirement for MSCs, resulting in a large amount of storage and transportation logistics; 2. MSC secretome shows a smaller risk of embolism; 3. MSC secretome avoids the potential of MSC tumorigenicity. Therefore, hydrogel-encapsulated MSC secretome in treating diseases is also a key research topic (**Table 2**).

Just like MSCs, multiple experiments have shown that hydrogels can continuously release MSC secretome, and effectively exert pro-regenerative, pro-angiogenic, and anti-fibrotic effects. Achieving sustained release is one of the important reasons for the recognition of hydrogels. In a rat model of Asherman syndrome, Liu et al. loaded a cross-linked hyaluronic acid gel with MSC secretome to create a sustained release system that repaired endometrial damage and enabled viable pregnancy (Liu et al., 2019). Hydrogels composed of bovine collagen type I (COLI) and low molecular weight hyaluronic acid (LMWHA) or COLI and PEG could control the release of active AD-MSC secretome, counteracting 6-OHDA toxicity while upregulating antioxidant enzymes Sirtuin 3 (SIRT3) in a neurodegeneration-related experimental setting (Chierchia et al., 2020). Liguori et al. proposed that trophic factors have different release kinetics and hydrogelation by a study of bioactive decellularized cardiac extracellular matrix-based hydrogels to release MSC secretome-derived trophic factors in a sustained manner, which is related to the initial concentration of conditioned medium (CM) in the gel (Liguori et al., 2021).

Pro-regeneration is the main function of the MSC secretome, and encapsulation with hydrogels significantly enhances the therapeutic effect, especially in skin lesions. In diabetic wounds mimicking fibroblasts cultured in a high-glucose environment, cell-free hydrogel dressings loaded with MSC-CM were shown to improve cell proliferation and migration through controlled release of bioactive factors (Sears et al., 2021). Pro-regenerative and pro-angiogenic can promote rapid skin repair. Kraskiewicz et al. demonstrated that collagen hydrogel maintained the therapeutic effect of AD-MSC secretome and improved chronic wound healing through proliferation of skin-derived cells and increased angiogenesis of endothelial cells (Kraskiewicz et al., 2021). Similarly, MSC-CM/hydrogel limited inflammatory development, promoted re-epithelialization and granulation tissue formation, and attenuated fibrotic and hypertrophic scar tissue formation outside the wound in third-degree burns in mice (Zhou et al., 2019a).

3.1 Hydrogels Encapsulate Mesenchymal Stem Cells-Extracellular vesicles

Hydrogel encapsulation can help to achieve spatio-temporal control of MSC-EVs activity *in vivo*, thereby increasing the therapeutic efficiency of EVs in various disease studies. In mice with renal ischemia-reperfusion injury, EVs released from matrix metalloproteinase-2-sensitive self-assembled peptide (KMP2) hydrogels demonstrated similar structures and bioactivities to fresh, isolated EVs, indicating that the hydrogels can effectively preserve biological function of EVs. The experimental results also proved that KMP2-EVs better promote endothelial cell proliferation and angiogenesis, and subsequently reduce renal chronic renal fibrosis, compared to KMP2 or EVs alone (Zhou et al., 2019b). *In vivo* tracking of labeled EVs showed that RGD peptide hydrogel increased EV retention and stability and promoted the efficacy of MSC-derived let-7a-5p-containing EVs in the treatment of AKI models (Zhang et al., 2020b). PEG hydrogels were found to sustain the release of EVs for up to 1 month in a rat model of chronic liver fibrosis (Mardpour et al., 2019). In the study of skin aging treatment, after subcutaneous injection treatment, CS hydrogel also prolonged the release of EVs and significantly increased the retention of EVs *in vivo*, delaying the skin-aging process (Zhao et al., 2021). In addition, hydrogel encapsulation also provides a new method of delivery of EVs compared to traditional arterial, intravenous, or intramuscular injection. For example, EVs were physically encapsulated in a GelMA hydrogel network covering the surface of the heart, and this local delivery could significantly improve retention (Tang et al., 2021).

3.2 Hydrogels Encapsulate Mesenchymal Stem Cells-Derived Exosomes

According to the diameter of the vesicles, EVs can be further divided into micro-vesicles (200–1,000 nm), exosomes (30–150 nm) and apoptotic bodies (800–5,000 nm). This subset of exosomes has been recognized as a new candidate for cell-free therapy of various diseases. Like MSC-EVs, the hydrogel enhanced the retention and stability of MSC-Exos *in vivo*. Yang et al. discovered that the thermosensitive PF-127 hydrogel delivered UC-MSC-exos, enhanced the regenerative capacity of exosomes, and promoted diabetes compared with UC-MSC-exos, UC-MSC-exos, PF-127-only, or control treatments (Yang et al., 2020b). Li et al. grafted MSC-Exos immobilized in peptide-modified adhesive hydrogels. The efficient retention and sustained release of MSC-Exos could attenuate inflammation and oxidation resulting in significant neurological recovery and urinary tissue protection, thereby effectively treating SCI (Li et al., 2020). In mice with hind limb ischemia, Gaussia luciferase imaging verified that CS hydrogels significantly increased the stability of proteins and microRNAs in MSC-Exos, and further enhanced MSC-Exos endothelial protection and pro-angiogenic capacity (Zhang et al., 2018).

3.3 Hydrogels Encapsulate Mesenchymal Stem Cells-Small Extracellular Vesicles

It is difficult to purify already pure exosome subsets further so people usually purify vesicles with a diameter of less than 200 nm, so people refer to them as small extracellular vesicles (sEVs). Yang

et al. suggested that intra-articular injection of Diels-Alder cross-linked hyaluronic acid/PEG hydrogels achieved sustained release of MSC-sEVs through degradation control, enhancing the efficacy of MSC-sEVs in improving OA (Yang et al., 2021). In a model of MI, the addition of alginate hydrogels to MSC-sEVs significantly increased their retention in the heart, decreased cardiomyocyte apoptosis, and increased scar thickness and angiogenesis compared with sEV-only treatment (Lv et al., 2019).

4 CONCLUSION AND FUTURE PERSPECTIVES

In conclusion, the clinical translation of hydrogel encapsulation into MSCs and their secretome is a novel step to a very promising technology. Biomaterials are now a research hotspot, garnering more attention among researchers in the medical sciences. As a representative, hydrogel is summarized in this paper as a carrier to encapsulate MSCs and the related literature on their secretome is reviewed. At present, although there are many preclinical studies on hydrogel-encapsulated MSCs, the research is not deep enough, and clinical research therein remains sparse. There are still many gaps in the understanding of targeting of MSCs *in vivo*. The current research on hydrogel encapsulation tends towards cell-free therapy, and the MSC secretome may be the future development direction. However, MSCs still play an irreplaceable role in treatment of utilizing MSC differentiation. The texture of the gel is soft, and most of them are currently suitable for soft tissue, which limits the application on hard tissue to a certain extent. For the delivery of hard tissue MSCs and their secretome, more materials need to be explored to supplement. The composition of most gel carriers with obvious functions is relatively complex, and it may be possible to undertake further study in the future to achieve a simpler composition with stronger functions.

AUTHOR CONTRIBUTIONS

XL and LY contributed to the conception of this manuscript. XL, YH, and LY drafted and revised the manuscript. All authors read and approved the final manuscript.

FUNDING

We are grateful to the National Natural Science Foundation of China (Grant No. 81970663) and the Natural Science Foundation of Liaoning Province (Grant No. 2019-BS-277).

REFERENCES

Alvarado-Velez, M., Enam, S. F., Mehta, N., Lyon, J. G., LaPlaca, M. C., and Bellamkonda, R. V. (2021). Immuno-suppressive Hydrogels Enhance Allogeneic MSC Survival after Transplantation in the Injured Brain. *Biomaterials* 266, 120419. doi:10.1016/j.biomaterials.2020.120419

Boido, M., Ghibaudi, M., Gentile, P., Favaro, E., Fusaro, R., and Tonda-Turo, C. (2019). Chitosan-based Hydrogel to Support the Paracrine Activity of Mesenchymal Stem Cells in Spinal Cord Injury Treatment. *Sci. Rep.* 9 (1), 6402. doi:10.1038/s41598-019-42848-w

Bussche, L., Harman, R. M., Syracuse, B. A., Plante, E. L., Lu, Y. C., Curtis, T. M., et al. (2015). Microencapsulated Equine Mesenchymal Stromal Cells Promote Cutaneous Wound Healing *In Vitro*. *Stem Cel Res Ther* 6 (1), 66. doi:10.1186/s13287-015-0037-x

Chen, X., Foote, A. G., and Thibeault, S. L. (2017). Cell Density, Dimethylsulfoxide Concentration and Needle Gauge Affect Hydrogel-Induced Bone Marrow Mesenchymal Stromal Cell Viability. *Cytotherapy* 19 (12), 1522–1528. doi:10.1016/j.jcyt.2017.08.016

Chierchia, A., Chirico, N., Boeri, L., Raimondi, I., Riva, G. A., Raimondi, M. T., et al. (202055712017). Secretome Released from Hydrogel-Embedded Adipose Mesenchymal Stem Cells Protects against the Parkinson's Disease Related Toxin 6-hydroxydopamine. *Eur. J. Pharm. Biopharm.* 121, 113–120. doi:10.1016/j.ejpb.2017.09.014

Choe, G., Kim, S. W., Park, J., Park, J., Kim, S., Kim, Y. S., et al. (2019). Anti-oxidant Activity Reinforced Reduced Graphene Oxide/alginate Microgels: Mesenchymal Stem Cell Encapsulation and Regeneration of Infarcted Hearts. *Biomaterials* 225, 119513. doi:10.1016/j.biomaterials.2019.119513

De Kok, I. J., Peter, S. J., Archambault, M., van den Bos, C., Kadiyala, S., Aukhil, L., et al. (2003). Investigation of Allogeneic Mesenchyrnal Stem Cell-Based Alveolar Bone Formation: Preliminary Findings. *Clin. Oral Implants Res.* 14 (4), 481–489. doi:10.1034/j.1600-0501.2003.110770.x

Dominici, M., Le Blanc, K., Mueller, I., Slaper-Cortenbach, I., Marini, F., Krause, D., et al. (2006). Minimal Criteria for Defining Multipotent Mesenchymal Stromal Cells. The International Society for Cellular Therapy Position Statement. *CYTOTHERAPY* 8 (4), 315–317. doi:10.1080/14653240600855905

Eirin, A., Zhu, X. Y., Puranik, A. S., Tang, H., McGurren, K. A., van Wijnen, A. J., et al. (2017). Mesenchymal Stem Cell-Derived Extracellular Vesicles Attenuate Kidney Inflammation. *Kidney Int.* 92 (1), 114–124. doi:10.1016/j.kint.2016.12.023

Gao, L., Yi, M., Xing, M., Li, H., Zhou, Y., Xu, Q., et al. (2020). *In Situ* activated Mesenchymal Stem Cells (MSCs) by Bioactive Hydrogels for Myocardial Infarction Treatment. *J. Mater. Chem. B.* 8 (34), 7713–7722. doi:10.1039/d0tb01320j

Geng, X., Hong, Q., Chi, K., Wang, S., Cai, G., and Wu, D. (2019). Mesenchymal Stem Cells Loaded with Gelatin Microcryogels Attenuate Renal Fibrosis. *Biomed. Res. Int.* 2019, 6749326. doi:10.1155/2019/6749326

Ghanta, R. K., Aghlara-Fotovat, S., Pugazenthi, A., Ryan, C. T., Singh, V. P., Mathison, M., et al. (2020). Immune-modulatory Alginate Protects Mesenchymal Stem Cells for Sustained Delivery of Reparative Factors to Ischemic Myocardium. *Biomater. Sci.* 8 (18), 5061–5070. doi:10.1039/d0bm00855a

Gómez-Aristizábal, A., Kim, K. P., and Viswanathan, S. (2016). A Systematic Study of the Effect of Different Molecular Weights of Hyaluronic Acid on Mesenchymal Stromal Cell-Mediated Immunomodulation. *PLoS One* 11 (1), e0147868. doi:10.1371/journal.pone.0147868

Guerra, A. D., Rose, W. E., Hematti, P., and Kao, W. J. (2017). Minocycline Enhances the Mesenchymal Stromal/stem Cell Pro-healing Phenotype in Triple Antimicrobial-Loaded Hydrogels. *Acta Biomater.* 51, 184–196. doi:10.1016/j.actbio.2017.01.021

Guo, Z., Chen, Y., Luo, X., He, X., Zhang, Y., and Wang, J. (2020). Administration of Umbilical Cord Mesenchymal Stem Cells in Patients with Severe COVID-19 Pneumonia. *Crit. Care* 24 (1), 420. doi:10.1186/s13054-020-03142-8

He, X., Wang, Q., Zhao, Y., Zhang, H., Wang, B., Pan, J., et al. (2020). Effect of Intramyocardial Grafting Collagen Scaffold with Mesenchymal Stromal Cells in Patients with Chronic Ischemic Heart Disease. *JAMA Netw. Open* 3 (9), e2016236. doi:10.1001/jamanetworkopen.2020.16236

Hertegård, S., Nagubothu, S. R., Malmström, E., Ström, C. E., Tolf, A., Davies, L. C., et al. (2019). Hyaluronan Hydrogels for the Local Delivery of Mesenchymal Stromal Cells to the Injured Vocal Fold. *Stem Cell Development* 28 (17), 1177–1190. doi:10.1089/scd.2019.0102

Ho, S. S., Murphy, K. C., Binder, B. Y. K., Vissers, C. B., and Leach, J. K. (2016). Increased Survival and Function of Mesenchymal Stem Cell Spheroids

Entrapped in Instructive Alginate Hydrogels. *Stem Cell Transl Med* 5 (6), 773–781. doi:10.5966/sctm.2015-0211

Hoffman, M. D., Van Hove, A. H., and Benoit, D. S. (2014). Degradable Hydrogels for Spatiotemporal Control of Mesenchymal Stem Cells Localized at Decellularized Bone Allografts. *Acta Biomater.* 10 (8), 3431–3441. doi:10.1016/j.actbio.2014.04.012

Huang, A., Farrell, M. J., Farrell, M., Kim, M., and Mauck, R. (2010). Long-term Dynamic Loading Improves the Mechanical Properties of Chondrogenic Mesenchymal Stem Cell-Laden Hydrogel. *eCM* 19, 72–85. doi:10.22203/ecm.v019a08

Huang, Q., Zou, Y., Arno, M. C., Chen, S., Wang, T., Gao, J., et al. (2017). Hydrogel Scaffolds for Differentiation of Adipose-Derived Stem Cells. *Chem. Soc. Rev.* 46 (20), 6255–6275. doi:10.1039/c6cs00052e

Huang, S., Li, Y., Wang, X., Ma, X., and Zhang, X. (2017). Injectable Co-gels of Collagen and Decellularized Vascular Matrix Improve MSC-Based Therapy for Acute Kidney Injury. *J. Biomater. Sci. Polym. Edition* 28 (18), 2186–2195. doi:10.1080/09205063.2017.1388556

Humbert, P., Brennan, M. Á., Davison, N., Rosset, P., Trichet, V., Blanchard, F., et al. (2019). Immune Modulation by Transplanted Calcium Phosphate Biomaterials and Human Mesenchymal Stromal Cells in Bone Regeneration. *Front. Immunol.* 10, 663. doi:10.3389/fimmu.2019.00663

Hwang, Y., Kim, J. C., and Tae, G. (2019). Significantly Enhanced Recovery of Acute Liver Failure by Liver Targeted Delivery of Stem Cells via Heparin Functionalization. *Biomaterials* 209, 67–78. doi:10.1016/j.biomaterials.2019.04.019

Jalowiec, J. M., D'Este, M., Bara, J. J., Denom, J., Menzel, U., Alini, M., et al. (2016). AnIn VitroInvestigation of Platelet-Rich Plasma-Gel as a Cell and Growth Factor Delivery Vehicle for Tissue Engineering. *Tissue Eng. C: Methods* 22 (1), 49–58. doi:10.1089/ten.tec.2015.0223

Jose, S., Hughbanks, M. L., Binder, B. Y., Ingavle, G. C., and Leach, J. K. (2014). Enhanced Trophic Factor Secretion by Mesenchymal Stem/stromal Cells with Glycine-Histidine-Lysine (GHK)-modified Alginate Hydrogels. *Acta Biomater.* 10 (5), 1955–1964. doi:10.1016/j.actbio.2014.01.020

Kalluri, R., and LeBleu, V. S. (2020). The Biology, Function, and Biomedical Applications of Exosomes. *SCIENCE* 367 (6478), 640–+. doi:10.1126/science.aau6977

Karoubi, G., Ormiston, M. L., Stewart, D. J., and Courtman, D. W. (2009). Single-cell Hydrogel Encapsulation for Enhanced Survival of Human Marrow Stromal Cells. *Biomaterials* 30 (29), 5445–5455. doi:10.1016/j.biomaterials.2009.06.035

Kim, I. G., Cho, H., Shin, J., Cho, J. H., Cho, S.-W., and Chung, E.-J. (2021). Regeneration of Irradiation-Damaged Esophagus by Local Delivery of Mesenchymal Stem-Cell Spheroids Encapsulated in a Hyaluronic-Acid-Based Hydrogel. *Biomater. Sci.* 9 (6), 2197–2208. doi:10.1039/d0bm01655a

Kraskiewicz, H., Hinc, P., Krawczenko, A., Bielawska-Pohl, A., Paprocka, M., Witkowska, D., et al. (2021). HATMSC Secreted Factors in the Hydrogel as a Potential Treatment for Chronic Wounds-In Vitro Study. *Int. J. Mol. Sci.* 22 (22), 12241. doi:10.3390/ijms222212241

Lange, C., Tögel, F., Ittrich, H., Clayton, F., Nolte-Ernsting, C., Zander, A. R., et al. (2005). Administered Mesenchymal Stem Cells Enhance Recovery from Ischemia/reperfusion-Induced Acute Renal Failure in Rats. *Kidney Int.* 68 (4), 1613–1617. doi:10.1111/j.1523-1755.2005.00573.x

Li, L., Zhang, Y., Mu, J., Chen, J., Zhang, C., Cao, H., et al. (2020). Transplantation of Human Mesenchymal Stem-Cell-Derived Exosomes Immobilized in an Adhesive Hydrogel for Effective Treatment of Spinal Cord Injury. *Nano Lett.* 20 (6), 4298–4305. doi:10.1021/acs.nanolett.0c00929

Li, Z., Wang, F., Roy, S., Sen, C. K., and Guan, J. (2009). Injectable, Highly Flexible, and Thermosensitive Hydrogels Capable of Delivering Superoxide Dismutase. *Biomacromolecules* 10 (12), 3306–3316. doi:10.1021/bm900900e

Liguori, T. T. A., Liguori, G. R., van Dongen, J. A., Moreira, L. F. P., and Harmsen, M. C. (2021). Bioactive Decellularized Cardiac Extracellular Matrix-Based Hydrogel as a Sustained-Release Platform for Human Adipose Tissue-Derived Stromal Cell-Secreted Factors. *Biomed. Mater.* 16 (2), 025022. doi:10.1088/1748-605X/abcff9

Liu, F., Hu, S., Yang, H., Li, Z., Huang, K., Su, T., et al. (2019). Hyaluronic Acid Hydrogel Integrated with Mesenchymal Stem Cell-Secretome to Treat Endometrial Injury in a Rat Model of Asherman's Syndrome. *Adv. Healthc. Mater.* 8 (14), e1900411. doi:10.1002/adhm.201900411

Lv, K., Li, Q., Zhang, L., Wang, Y., Zhong, Z., Zhao, J., et al. (2019). Incorporation of Small Extracellular Vesicles in Sodium Alginate Hydrogel as a Novel Therapeutic Strategy for Myocardial Infarction. *Theranostics* 9 (24), 7403–7416. doi:10.7150/thno.32637

Mardpour, S., Ghanian, M. H., Sadeghi-Abandansari, H., Mardpour, S., Nazari, A., Shekari, F., et al. (2019). Hydrogel-Mediated Sustained Systemic Delivery of Mesenchymal Stem Cell-Derived Extracellular Vesicles Improves Hepatic Regeneration in Chronic Liver Failure. *ACS Appl. Mater. Inter.* 11 (41), 37421–37433. doi:10.1021/acsami.9b10126

McKinney, J. M., Pucha, K. A., Doan, T. N., Wang, L., Weinstock, L. D., Tignor, B. T., et al. (2021). Sodium Alginate Microencapsulation of Human Mesenchymal Stromal Cells Modulates Paracrine Signaling Response and Enhances Efficacy for Treatment of Established Osteoarthritis. *Acta Biomater.* S1742-7061 (21), 00848–855. doi:10.1016/j.actbio.2021.12.034

Moussa, L., Pattappa, G., Doix, B., Benselama, S. L., Demarquay, C., Benderitter, M., et al. (2017). A Biomaterial-Assisted Mesenchymal Stromal Cell Therapy Alleviates Colonic Radiation-Induced Damage. *Biomaterials* 115, 40–52. doi:10.1016/j.biomaterials.2016.11.017

Moussa, L., Demarquay, C., Réthoré, G., Benadjaoud, M. A., Siñeriz, F., Pattapa, G., et al. (2019). Heparan Sulfate Mimetics: A New Way to Optimize Therapeutic Effects of Hydrogel-Embedded Mesenchymal Stromal Cells in Colonic Radiation-Induced Damage. *Sci. Rep.* 9 (1), 164. doi:10.1038/s41598-018-36631-6

Murphy, K. C., Whitehead, J., Zhou, D., Ho, S. S., and Leach, J. K. (2017). Engineering Fibrin Hydrogels to Promote the Wound Healing Potential of Mesenchymal Stem Cell Spheroids. *Acta Biomater.* 64, 176–186. doi:10.1016/j.actbio.2017.10.007

Osama, I., Gorenkova, N., McKittrick, C. M., Wongpinyochit, T., Goudie, A., Seib, F. P., et al. (2018). *In Vitro* studies on Space-Conforming Self-Assembling Silk Hydrogels as a Mesenchymal Stem Cell-Support Matrix Suitable for Minimally Invasive Brain Application. *Sci. Rep.* 8 (1), 13655. doi:10.1038/s41598-018-31905-5

Papa, S., Vismara, I., Mariani, A., Barilani, M., Rimondo, S., De Paola, M., et al. (2018). Mesenchymal Stem Cells Encapsulated into Biomimetic Hydrogel Scaffold Gradually Release CCL2 Chemokine *In Situ* Preserving Cytoarchitecture and Promoting Functional Recovery in Spinal Cord Injury. *J. Control. Release* 278, 49–56. doi:10.1016/j.jconrel.2018.03.034

Pishavar, E., Luo, H., Naserifar, M., Hashemi, M., Toosi, S., Atala, A., et al. (2021). Advanced Hydrogels as Exosome Delivery Systems for Osteogenic Differentiation of MSCs: Application in Bone Regeneration. *Int. J. Mol. Sci.* 22 (12), 6203. doi:10.3390/ijms22126203

Qazi, T. H., Tytgat, L., Dubruel, P., Duda, G. N., Van Vlierberghe, S., and Geissler, S. (2019). Extrusion Printed Scaffolds with Varying Pore Size as Modulators of MSC Angiogenic Paracrine Effects. *ACS Biomater. Sci. Eng.* 5 (10), 5348–5358. doi:10.1021/acsbiomaterials.9b00843

Qiu, Y., Lim, J. J., Scott, L., Jr., Adams, R. C., Bui, H. T., and Temenoff, J. S. (2011). PEG-based Hydrogels with Tunable Degradation Characteristics to Control Delivery of Marrow Stromal Cells for Tendon Overuse Injuries. *Acta Biomater.* 7 (3), 959–966. doi:10.1016/j.actbio.2010.11.002

Rafie, M., and Meshkini, A. (2021). Tailoring the Proliferation of Fibroblast Cells by Multiresponsive and Thermosensitive Stem Cells Composite F127 Hydrogel Containing Folic acid.MgO:ZnO/chitosan Hybrid Microparticles for Skin Regeneration. *Eur. J. Pharm. Sci.* 167, 106031. doi:10.1016/j.ejps.2021.106031

Ricles, L. M., Hsieh, P. L., Dana, N., Rybalko, V., Kraynak, C., Farrar, R. P., et al. (2016). Therapeutic Assessment of Mesenchymal Stem Cells Delivered within a PEGylated Fibrin Gel Following an Ischemic Injury. *Biomaterials* 102, 9–19. doi:10.1016/j.biomaterials.2016.06.011

Robinson, S. T., Douglas, A. M., Chadid, T., Kuo, K., Rajabalan, A., Li, H., et al. (2016). A Novel Platelet Lysate Hydrogel for Endothelial Cell and Mesenchymal Stem Cell-Directed Neovascularization. *Acta Biomater.* 36, 86–98. doi:10.1016/j.actbio.2016.03.002

Salinas, C. N., and Anseth, K. S. (2009). Mesenchymal Stem Cells for Craniofacial Tissue Regeneration: Designing Hydrogel Delivery Vehicles. *J. Dent Res.* 88 (8), 681–692. doi:10.1177/0022034509341553

Sears, V., Danaoui, Y., and Ghosh, G. (2021). Impact of Mesenchymal Stem Cell-Secretome-Loaded Hydrogel on Proliferative and Migratory Activities of Hyperglycemic Fibroblasts. *Mater. Today Commun.* 27, 102285. doi:10.1016/j.mtcomm.2021.102285

Shin, E. Y., Wang, L., Zemskova, M., Deppen, J., Xu, K., Strobel, F., et al. (202055012018). Adenosine Production by Biomaterial-Supported Mesenchymal Stromal Cells Reduces the Innate Inflammatory Response in Myocardial Ischemia/Reperfusion Injury. *J. Am. Heart Assoc.* 7 (2), e006949. doi:10.1161/JAHA.117.006949

Sylvester, C. B., Pugazenthi, A., Grande-Allen, K. J., and Ghanta, R. K. (2021). Cell-Laden Bioactive Poly(ethylene Glycol) Hydrogels for Studying Mesenchymal Stem Cell Behavior in Myocardial Infarct-Stiffness Microenvironments. *Cardiovasc. Eng. Tech.* 12 (2), 183–199. doi:10.1007/s13239-020-00515-6

Tang, J., Cui, X., Zhang, Z., Xu, Y., Guo, J., Soliman, B. G., et al. (2021). Injection-Free Delivery of MSC-Derived Extracellular Vesicles for Myocardial Infarction Therapeutics. *Adv. Healthc. Mater.* 2021, e2100312. doi:10.1002/adhm.202100312

Touani, F. K., Borie, M., Azzi, F., Trudel, D., Noiseux, N., Der Sarkissian, S., et al. (2021). Pharmacological Preconditioning Improves the Viability and Proangiogenic Paracrine Function of Hydrogel-Encapsulated Mesenchymal Stromal Cells. *Stem Cell Int.* 2021, 6663467. doi:10.1155/2021/6663467

Wu, D. Q., Wang, T., Lu, B., Xu, X. D., Cheng, S. X., Jiang, X. J., et al. (2008). Fabrication of Supramolecular Hydrogels for Drug Delivery and Stem Cell Encapsulation. *Langmuir* 24 (18), 10306–10312. doi:10.1021/la8006876

Yang, J., Chen, Z., Pan, D., Li, H., and Shen, J. (2020). Umbilical Cord-Derived Mesenchymal Stem Cell-Derived Exosomes Combined Pluronic F127 Hydrogel Promote Chronic Diabetic Wound Healing and Complete Skin Regeneration. *Ijn* 15, 5911–5926. doi:10.2147/ijn.s249129

Yang, M., He, S., Su, Z., Yang, Z., Liang, X., and Wu, Y. (2020). Thermosensitive Injectable Chitosan/Collagen/β-Glycerophosphate Composite Hydrogels for Enhancing Wound Healing by Encapsulating Mesenchymal Stem Cell Spheroids. *ACS Omega* 5 (33), 21015–21023. doi:10.1021/acsomega.0c02580

Yang, Y., Zhu, Z., Gao, R., Yuan, J., Zhang, J., Li, H., et al. (2021). Controlled Release of MSC-Derived Small Extracellular Vesicles by an Injectable Diels-Alder Crosslinked Hyaluronic Acid/PEG Hydrogel for Osteoarthritis Improvement. *Acta Biomater.* 128, 163–174. doi:10.1016/j.actbio.2021.04.003

You, Y., Kobayashi, K., Colak, B., Luo, P., Cozens, E., Fields, L., et al. (2021). Engineered Cell-Degradable Poly(2-Alkyl-2-Oxazoline) Hydrogel for Epicardial Placement of Mesenchymal Stem Cells for Myocardial Repair. *Biomaterials* 269, 120356. doi:10.1016/j.biomaterials.2020.120356

Yuan, T., Li, K., Guo, L., Fan, H., and Zhang, X. (2011). Modulation of Immunological Properties of Allogeneic Mesenchymal Stem Cells by Collagen Scaffolds in Cartilage Tissue Engineering. *J. Biomed. Mater. Res. A.* 98 (3), 332–341. doi:10.1002/jbm.a.33121

Zhang, C., Shang, Y., Chen, X., Midgley, A. C., Wang, Z., Zhu, D., et al. (2020). Supramolecular Nanofibers Containing Arginine-Glycine-Aspartate (RGD) Peptides Boost Therapeutic Efficacy of Extracellular Vesicles in Kidney Repair. *ACS Nano* 14 (9), 12133–12147. doi:10.1021/acsnano.0c05681

Zhang, K., Zhao, X., Chen, X., Wei, Y., Du, W., Wang, Y., et al. (2018). Enhanced Therapeutic Effects of Mesenchymal Stem Cell-Derived Exosomes with an Injectable Hydrogel for Hindlimb Ischemia Treatment. *ACS Appl. Mater. Inter.* 10 (36), 30081–30091. doi:10.1021/acsami.8b08449

Zhang, S., Huang, D., Lin, H., Xiao, Y., and Zhang, X. (2020). Cellulose Nanocrystal Reinforced Collagen-Based Nanocomposite Hydrogel with Self-Healing and Stress-Relaxation Properties for Cell Delivery. *Biomacromolecules* 21 (6), 2400–2408. doi:10.1021/acs.biomac.0c00345

Zhang, X., Sun, Y., Liu, J., Yi, Z., Gao, F., Liu, Q., et al. (2017). *In Situ* forming Hydrogels with Long-Lasting miR-21 Enhances the Therapeutic Potential of MSC by Sustaining Stimulation of Target Gene. *J. Biomater. Sci. Polym. Edition* 28 (15), 1639–1650. doi:10.1080/09205063.2017.1341675

Zhao, N., Coyne, J., Abune, L., Shi, P., Lian, X. L., Zhang, G., et al. (2020). Exogenous Signaling Molecules Released from Aptamer-Functionalized Hydrogels Promote the Survival of Mesenchymal Stem Cell Spheroids. *ACS Appl. Mater. Inter.* 12 (22), 24599–24610. doi:10.1021/acsami.0c05681

Zhao, X., Liu, Y., Jia, P., Cheng, H., Wang, C., Chen, S., et al. (2021). Chitosan Hydrogel-Loaded MSC-Derived Extracellular Vesicles Promote Skin Rejuvenation by Ameliorating the Senescence of Dermal Fibroblasts. *Stem Cel Res. Ther.* 12 (1), 196. doi:10.21203/rs.3.rs-118943/v1

Zhou, P., Li, X., Zhang, B., Shi, Q., Li, D., and Ju, X. (2019). A Human Umbilical Cord Mesenchymal Stem Cell-Conditioned Medium/Chitosan/Collagen/β-Glycerophosphate Thermosensitive Hydrogel Promotes Burn Injury Healing in Mice. *Biomed. Res. Int.* 2019, 5768285. doi:10.1155/2019/5768285

Zhou, Y., Liu, S., Zhao, M., Wang, C., Li, L., Yuan, Y., et al. (2019). Injectable Extracellular Vesicle-Released Self-Assembling Peptide Nanofiber Hydrogel as an Enhanced Cell-free Therapy for Tissue Regeneration. *J. Control. Release* 316, 93–104. doi:10.1016/j.jconrel.2019.11.003

Conflict of Interest: The authors declare that the research was conducted in the absence of any commercial or financial relationships that could be construed as a potential conflict of interest.

Publisher's Note: All claims expressed in this article are solely those of the authors and do not necessarily represent those of their affiliated organizations, or those of the publisher, the editors and the reviewers. Any product that may be evaluated in this article, or claim that may be made by its manufacturer, is not guaranteed or endorsed by the publisher.

frontiers | Frontiers in Bioengineering and Biotechnology

ORIGINAL RESEARCH
published: 08 April 2022
doi: 10.3389/fbioe.2022.864041

Efficacy Evaluation of Ciprofloxacin-Loaded Poly (Trimethylene Carbonate) Implants in the Treatment of Chronic Osteomyelitis

Yixiu Liu[1,2]*, *A. Liang*[1,2], *Xu Li*[1,2], *Zhihe Ma*[3] *and Dan Zhang*[4]*

[1]Department of Orthopaedics, The Central Hospital Affiliated to Shenyang Medical College, Shenyang, China, [2]Shenyang Clinical Research Center for Hand and Foot, Shenyang, China, [3]The First People's Hospital of Shenyang, Shenyang, China, [4]Liaoning Provincial Key Laboratory of Oral Diseases, School and Hospital of Stomatology, China Medical University, Shenyang, China

In this study, poly (trimethylene carbonate) (PTMC) with excellent biocompatibility was synthesized via ring-opening of TMC to prepare the Ciprofloxacin-loaded PTMC implants, and antibacterial effects *in vitro* or *in vivo* of the resulting implants were investigated to evaluate the potential for treating chronic osteomyelitis. The *in vitro* results showed the Ciprofloxacin-loaded PTMC implants could sustain release ciprofloxacin at a release amount of about 90 μg/d for 28 days and possessed excellent antibacterial effect, as evidenced by the smaller size of the antibacterial ring of 32.6 ± 0.64 mm and the biofilm inhibition of 60% after 28 days of release. The *in vivo* results showed that after 28 days of treatment, the body weight and the white blood cell counts of chronic-osteomyelitis-model rats in the treatment group reached 381.6 ± 16.8 g and (7.86 ± 0.91) $\times 10^9$/L, respectively, returning to normal rapidly compared with the control and blank group, indicating the remarkable antibacterial effect of the Ciprofloxacin-loaded PTMC implants. X-ray images and HE staining results also confirmed that most of the proximal and middle parts of the tibia returned to typical structures and new and trabecular bone had been formed for the rats in the treatment group, and no inflammatory cells were found as compared to the control and blank groups, after 28 days of treatment. The significant lower number of colonies of (9.92 ± 1.56) × 10 CFU/g in the treatment group also suggests that the Ciprofloxacin-loaded PTMC implants achieve a practical antibacterial effect through a local application.

Keywords: poly(trimethylene carbonate), ciprofloxacin, chronic osteomyelitis, antibacterial activity, efficacy evaluation

OPEN ACCESS

Edited by:
Jianshe Hu,
Northeastern University, China

Reviewed by:
Zhangpei Chen,
Northeastern University, China
Yong Sun,
Sichuan University, China

***Correspondence:**
Yixiu Liu
liuyixiu123123@163.com
Dan Zhang
zdcmu888@outlook.com

Specialty section:
This article was submitted to Biomaterials, a section of the journal Frontiers in Bioengineering and Biotechnology

Received: *28 January 2022*
Accepted: *24 March 2022*
Published: *08 April 2022*

Citation:
Liu Y, Liang A, Li X, Ma Z and Zhang D (2022) Efficacy Evaluation of Ciprofloxacin-Loaded Poly (Trimethylene Carbonate) Implants in the Treatment of Chronic Osteomyelitis. Front. Bioeng. Biotechnol. 10:864041. doi: 10.3389/fbioe.2022.864041

INTRODUCTION

Osteomyelitis is inflammation of the bones caused by infectious microorganisms. Chronic osteomyelitis is difficult to cure and easy to relapse, bringing significant psychological and economic burden to patients (Barakat et al., 2019). Due to the severe damage to the local blood supply of the lesion, it is difficult for the blood to carry antibiotics to the infected area by oral or intravenous antibiotics, and the effective bactericidal concentration cannot be reached, which makes

the infection remain and the recurrence rate is high. Toxic and side effects damage vital organs of the body, and the emergence of drug resistance quickly occurs after repeated administration of large doses (Fantoni et al., 2019).

With the development of medical and health technology, slow-release carriers loaded with antibiotics are gradually applied to treat osteomyelitis. Compared with traditional treatment methods, the sustained-release carrier has the characteristics of releasable antibiotics and absorbability. Based on controlling infection, it avoids secondary surgery to remove, and there is no need to wait for infection control before performing secondary surgery. At present, the carriers of antibiotic sustained-release systems can be mainly divided into two categories: non-biodegradable and biodegradable (Liu et al., 2021; Wassif et al., 2021). The non-biodegradable carrier is polymethylmethacrylate (polymethylmethacrylate, PMMA) (van Vugt et al., 2019; Patel et al., 2021). It is the first carrier to treat chronic osteomyelitis. With further experimental and clinical research development, PMMA gradually affects clinical application due to its non-degradable properties and the need to remove after infection control (van Vugt et al., 2019). Biodegradable carriers mainly include calcium sulfate, polylactic acid, PLGA, etc. (Cheng et al., 2018; Nabipour et al., 2018; Andreacchio et al., 2019; Zhao et al., 2020; e Silva et al., 2021). Among them, the long-term sustained-release effect of the drug delivery system based on PLA and PLGA is ideal, and it is more suitable for treating chronic osteomyelitis [(Nabipour et al., 2018; e Silva et al., 2021; Cheng et al., 2018)]. However, the characteristic of PLA or PLGA to produce acidic degradation products during the degradation process is unavoidable (Zaaba and Jaafar, 2020; Jin et al., 2021; Ko et al., 2021), which can easily have side effects on drug activity or cause the pH of the application site to decrease, inducing sterile inflammation affects the therapeutic effect. Therefore, selecting carrier materials for biodegradable drug delivery systems is crucial for treating chronic osteomyelitis. Poly (trimethylene carbonate) (PTMC) is a polymer with excellent biocompatibility and good degradation properties, which has great potential in the fields of drug sustained release and tissue engineering (Dienel et al., 2019; Mohajeri et al., 2020; Weisgrab et al., 2020; Brossier et al., 2021). More importantly, Yang et al. show that PTMC does not generate acidic degradation products during the degradation process (Yang et al., 2014; Yang et al., 2015; Yang et al., 2016; Hou et al., 2017; Hou et al., 2019; Cai et al., 2021; Hou et al., 2021) and is an ideal carrier material for biodegradable long-acting sustained-release implants (Yang et al., 2012; Yang et al., 2013).

Ciprofloxacin has been demonstrated to be effective against a broad spectrum of bacteria associated with osteomyelitis and is an effective drug for treating osteomyelitis (Lin et al., 2019). In this study, ciprofloxacin hydrochloride, a commonly used drug for treating osteomyelitis, was used as a drug model, and PTMC was used as a drug carrier to construct a biodegradable long-term drug delivery system. The release and antibacterial properties of the Ciprofloxacin-loaded PTMC implants were investigated *in vitro*. Furthermore, a rat model of chronic osteomyelitis was established to investigate the *in vivo* antibacterial effect of PTMC implants, with the aim to verify the feasibility of PTMC implants loaded with Ciprofloxacin in the treatment of chronic osteomyelitis.

MATERIALS AND METHODS

Materials

Trimethylene carbonate (TMC) was purchased from Daigang Co., Ltd. (Jinan, Shandong, China). $Sn(Oct)_2$ (95%) was purchased from Sigma-Aldrich and used as received. Ciprofloxacin HCl was purchased from Dalian Meilun Biotechnology Co., Ltd.; Staphylococcus aureus was purchased from Shanghai Benoy Biotechnology Co., Ltd.; SPF Wistar rats were purchased from Liaoning Changsheng Biotechnology Co., Ltd. Cell Counting Kit-8 was purchased from Shanghai Aladdin Biochemical Technology Co., Ltd.

Synthesis of PTMC

PTMC was synthesized via the ring-opening polymerization (ROP) of TMC using $Sn(Oct)_2$ (1/5000 eq) as a catalyst, according to the reference (Hou et al., 2021). Briefly, the TMC monomer and the catalyst were accurately weighed and placed in an ampoule. The ampoules were purged with dry nitrogen and then heat-sealed under vacuum. Then the ampoule was immersed into an oil bath at a preset temperature of 130 ± 2°C for 24 h. After the reaction, the ampoules were cooled to room temperature and smashed to obtain the polymer. The crude oligomers were purified using ice-methanol and dried under vacuum at 37°C to constant weight.

The Biocompatibility of PTMC

The extracts of PTMC were used for the *in vitro* cell proliferation and cytotoxicity tests. PTMC samples were immersed in an α-DMEM medium with 10% fetal bovine serum for 72 h at 37°C in a humidified atmosphere of 5% CO_2. The immersion ratio was 0.1 g/ml according to ISO 10993 Part 12. α-DMEM medium with 10% fetal bovine serum is also immersed in the same volume for 72 h under the same conditions. The extracts and α-DMEM medium were filtrated and collected.

The cytotoxic effects and proliferation ability of the PTMC to MC3T3-E1 cells were evaluated using the CCK8 assay. MC3T3-E1 cells were seeded in 96-well culture plates at a 1.5 × 104 cells/ml density. 100μL extracts were added in each well of the PTMC group, 100 μL α-DMEM medium was added in each control group well. After incubation for 24, 48 and 72 h, respectively, the PTMC group and the control group were rinsed with phosphate buffer solution (PBS) for one time. Then the PTMC group and control groups were then observed under a fluorescence microscope (Nikon, Japan). The cytotoxicity evaluation was conducted by 10% (v/v) concentration of CCK-8 reagent. The spectrophotometric absorbance was measured at 450 nm using a microplate reader (Infinite M200, Tecan, Austria). Relative growth rate (RGR) was also used to evaluate the biocompatibility of PTMC. The formula for calculating RGR was RGR = ODe/ODc × 100%. ODe is the average OD value of the experimental groups. ODc is the average OD value of the control group. The cell toxicity grade (CTG) is obtained

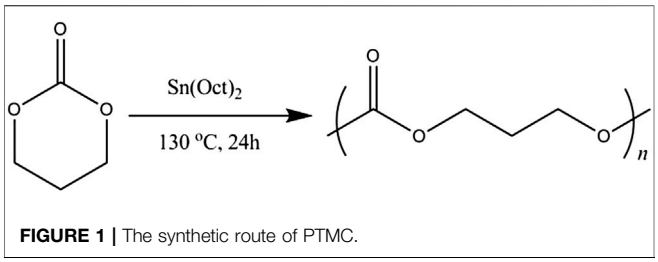

FIGURE 1 | The synthetic route of PTMC.

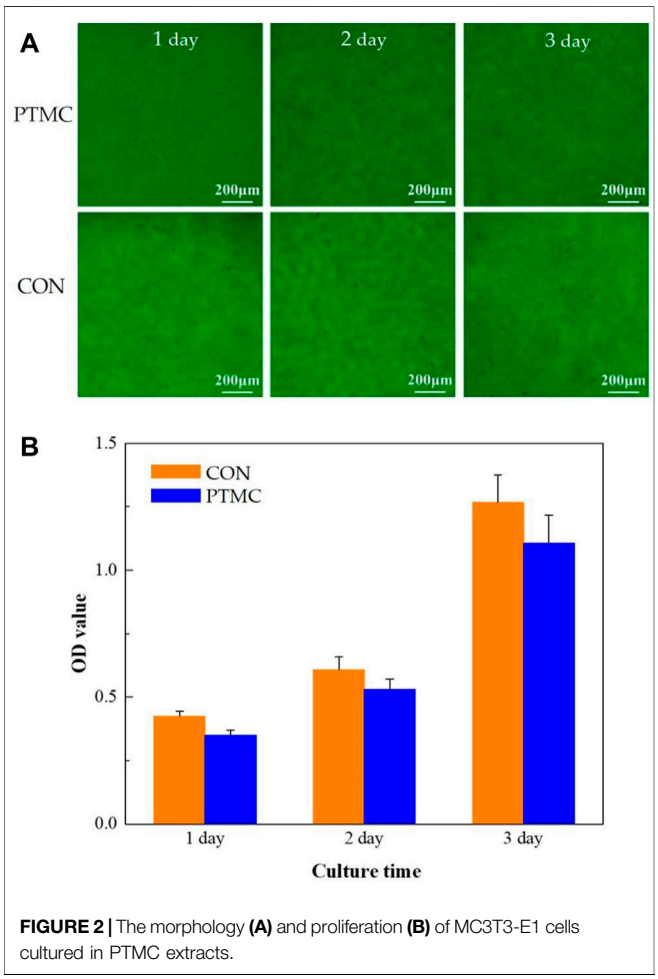

FIGURE 2 | The morphology **(A)** and proliferation **(B)** of MC3T3-E1 cells cultured in PTMC extracts.

according to the standard United States Pharmacopeia. A material is considered non-toxic when the sample has an RGR value greater than 80 and a CTG rating of 0 or one according to the standard.

Preparation and *in vitro* Release of Ciprofloxacin-Loaded PTMC Implants

Precisely weigh 5 g of PTMC, dissolve it in chloroform, and add 0.5 g of ciprofloxacin hydrochloride in a weight ratio of 1:10 of drug and carrier. The mixture was vortexed and poured into a PTFE dish. After the chloroform had evaporated entirely, the films were peeled off and dried to constant weight. Then the film was cut into small pieces and extruded into cylindrical implants (od = 1.5 mm, length = 2 cm) with a hot-melt extruder at 180 °C. After manufacture, the implants were packed in sealed bags and then irradiated with 25 kGy of 60Co for sterilization.

The PTMC implants loaded with Ciprofloxacin HCL were immersed in a glass container filled with 10 ml of PBS solution (pH = 7.4) and shaken at a frequency of 65 times/min in a constant temperature air bath at (37 ± 1) °C. The PBS solutions were changed every 24 h. Then, the replaced PBS solution was filtered through a 0.22 μm nylon membrane filter, and 2 μL of the filtrate was injected into the UHPLC system, using a mixture of 0.025 mol/L phosphoric acid solution (pH = 3.0 ± 0.1)-acetonitrile (75: 25) as mobile phase, at a flow rate of 0.1 ml/min to measure Ciprofloxacin concentration in each sample at 277 nm. The procedure was performed in triplicate for each time point, and the results were expressed as mean ± standard deviation.

TABLE 1 | The relative growth rates (RGR) and cell toxicity grade (CTG).

Time (h)	RGR	CTG
24	82.48% ± 0.04	1
48	87.24% ± 0.05	1
72	87.47% ± 0.09	1

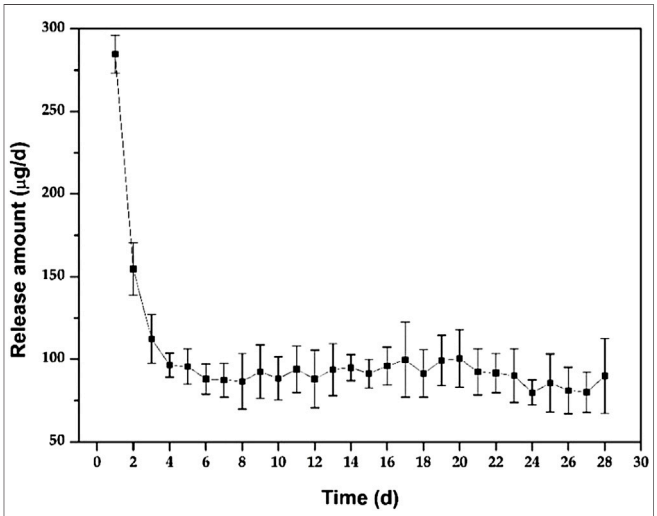

FIGURE 3 | *In vitro* release of the Ciprofloxacin-loaded PTMC implants in PBS solution.

Antibacterial Activity *in vitro* of Ciprofloxacin-Loaded PTMC Implants

The activated Staphylococcus aureus was appropriately diluted with PBS solution to obtain a 10^6 CFU/ml bacteria solution. 0.1 ml of Staphylococcus aureus bacterial solution was pipetted

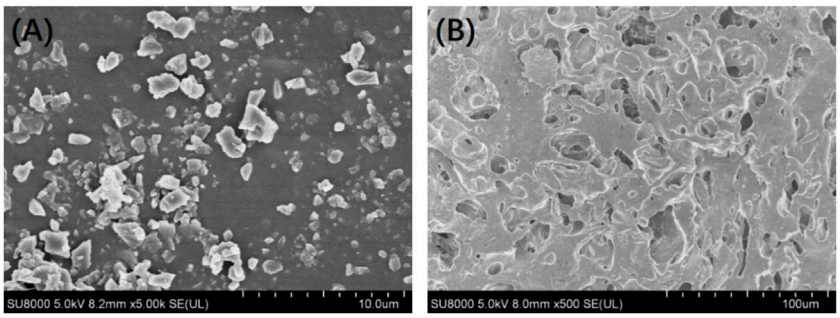

FIGURE 4 | Surface morphology of the ciprofloxacin-loaded PTMC implants before **(A)** and after **(B)** release in PBS solution.

and evenly inoculated into a nutrient agar Petri dish. Holes were punched on the nutrient agar plate in the dish, and 0.2 ml of PTMC implants release solution from days 1, 7, 14 and 28 were added. Then, the dish was incubated at 37°C for 24 h. Then, the diameter of the bacteriostatic zones was measured accurately. The procedure was performed in triplicate, and the results were expressed as mean ± standard deviation. Staphylococcus aureus was also incubated in the 25 mg/ml leaching solution of the blank PTMC implants.

After 1, 7, 14 and 28 days of the PTMC implants release, 90 μL of the release solution was taken into a 96-well plate, added with 10 μL of TSB solution containing S. aureus (approximately 1×10^6 CFU/μL) and incubated at 37°C for 24 h. Then the medium was removed, and each well was washed with 100 μL of PBS for three times, stained with 100 μL of 1% (w/v) crystal violet in water for 15 min, and then rinsed with demineralized water. 100 μL of ethanol/acetone (80:20) was added to each well to dissolve the crystal violet, and the absorbance of the crystal violet solution was measured at a wavelength of 575 nm. The absorbance (A_1) of crystal violet solution is proportional to the biofilm amount grown in each well, and the biofilm inhibition was calculated according to the following equation:

$$\text{biofilm inhibition} = \frac{A - A_1}{A} \times 100\%$$

where A was the absorbance of the crystal violet solution for the PTMC implants without Ciprofloxacin.

Establishment and Treatment of Chronic Osteomyelitis Model

The chronic osteomyelitis model was established on Wistar rats according to Karau et al. (Karau et al., 2013), and the Animal Ethics Committee of The Central Hospital Affiliated to Shenyang Medical College approved all the surgical procedures. Twenty-four rats were weighed and anaesthetized by intraperitoneal injection of sodium pentobarbital (50 mg/kg). The proximal 1/3 of the tibia of rats was exposed by the skin incision of 1.5 cm made under the right knee along the medial anterior tibial condyle. Then the bone marrow cavity of the tibia was exposed using an electric drill with a diameter of 1.5 mm, rinsed with saline, injected with 50 μL of morrhuate sodium injection, and 50 μL sterile saline of Staphylococcus aureus was injected. After that, the bone marrow cavity was closed with bone wax and sutured. After surgery, the rats were caged and allowed to move freely and eat regularly. Four weeks later, six rats were sacrificed, and the formation of chronic osteomyelitis was confirmed by X-ray (Xie et al., 2019) and HE staining (Musher and Arasaratnam, 2021).

Eighteen model rats of chronic osteomyelitis were randomly divided into a treatment group, a control group, and a blank group, with six rats in each group. The model rats were anaesthetized by intraperitoneal injection of sodium pentobarbital (50 mg/kg). Then the bone marrow cavity was exposed and opened again through the original incision with a 1.5 mm diameter electric drill for debridement to remove necrotic, sclerotic, and infected tissues, and then repeatedly flushed with 2% hydrogen peroxide and saline. The treatment group was given a 2 cm Ciprofloxacin-loaded PTMC implant, the control group was assigned a 2 cm PTMC implant without Ciprofloxacin, and the blank group has received no treatment. Afterwards, the marrow cavity was closed with bone wax and sutured. The body weight and the white blood cell (WBC) counts of rats in the three groups were observed on the 0, 7, 14, 21, and 28 days after the treatment. After 28 days of treatment, all the rats were sacrificed, and the right tibia specimen was taken. Three for HE staining and three for X-ray analysis and then pulverized into powder. 1 g of bone powder was accurately weighed and added into 1 ml of physiological saline to make a suspension. After tenfold serial dilution with saline, 0.1 ml of the diluted sample was inoculated onto blood agar plates and incubated at 37°C for 48 h to count the number of bacterial colonies. All tests were carried out in triplicate and under aseptic conditions.

RESULTS AND DISCUSSION

Synthesis of PTMC

PTMC was synthesized by bulk ring-opening copolymerization of trimethylene carbonate monomer in the presence of $SnOct_2$ as a catalyst at 130°C, as illustrated in **Figure 1**. The structure of PTMC was determined by 1H NMR [(δ, ppm from TMS in CDCl3): 2.02

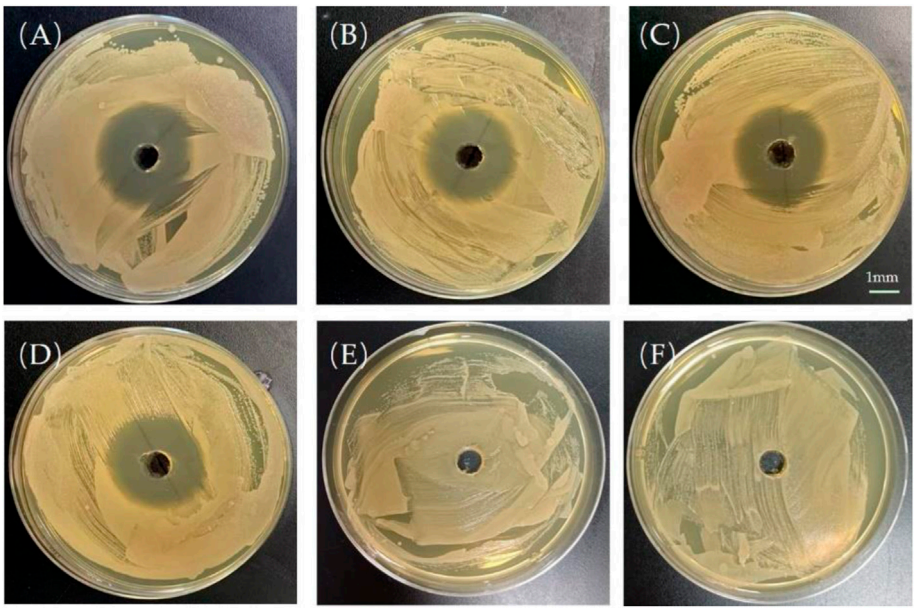

FIGURE 5 | Bacteriostatic rings produced by the release solution of the ciprofloxacin-loaded PTMC implants at day 1 **(A)**, day 7 **(B)**, day 14 **(C)**, day 28 **(D)**; Bacteriostatic rings produced by the leaching solution of blank PTMC at day 1 **(E)** and day 7 **(F)**. The scale bar is 1 mm.

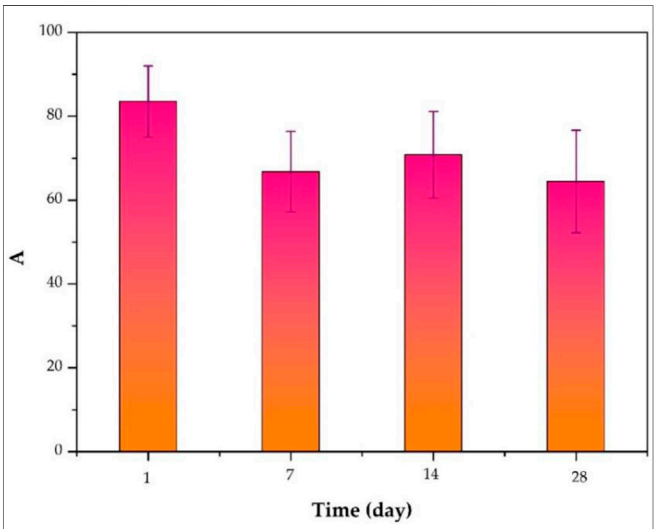

FIGURE 6 | Inhibition of S. aureus biofilm formation by the release solution of the ciprofloxacin-loaded PTMC implants at day 1, day 7, day 14, and day 28.

(-CH_2--C***H***$_2$--CH_2-) and 4.14 (-OC***H***$_2$--CH_2-)]. The molecular weight and polydispersity of PTMC were determined using GPC, showing a polydispersity of 1.07 and a molecular weight of 3.29 × 10^5 g/mol. The intrinsic viscosity of the resulting PTMC was 6.54 dl/g. The thermal properties of the PTMC were determined using DSC and TGA. The TGA thermogram of PTMC showed that the polymer began to degrade at 267.0 °C, and the DSC studies showed that the PTMC polymer was amorphous with only one glass transition temperature of -13.9 °C. The water contact angle results show that the obtained PTMC was hydrophobic with a static water contact angle of 87.25 ± 0.92°.

The Biocompatibility of PTMC

In this study, the biocompatibility of PTMC was investigated using cell proliferation and cytotoxicity tests. The MC3T3-E1 cells cultured in the well with PTMC for 24, 48 and 72 h are shown in **Figure 2A**. The results show that cells grew well in solutions containing PTMC extracts. Compared with the control group, there are no significant differences in the number and morphology of cells in the PTMC group. **Figure 2B** shows the optical densities of MC3T3-E1 cells in PTMC extracts measured by the CCK8 test. It could be seen that the optical density (OD) values of all the groups increased gradually with increasing cultivation time.

The relative growth rates (RGR) of MC3T3-E1 cells in PTMC extracts are shown in **Table 1**. From 24 to 72 h of incubation, the average RGR value was greater than 80%, and all the experimental groups showed grade 1. The cell proliferation assay results showed no significant difference between the groups, indicating that PTMC has excellent biocompatibility and would not be deleterious to cell viability. The result was similar to that of Papenburg's report (Papenburg et al., 2009), which also revealed the high cell attachment and proliferation of PTMC.

In vitro Release of Ciprofloxacin-Loaded PTMC Implants

Figure 3 shows the *in vitro* release behaviour of the Ciprofloxacin-loaded PTMC implants. The relatively high

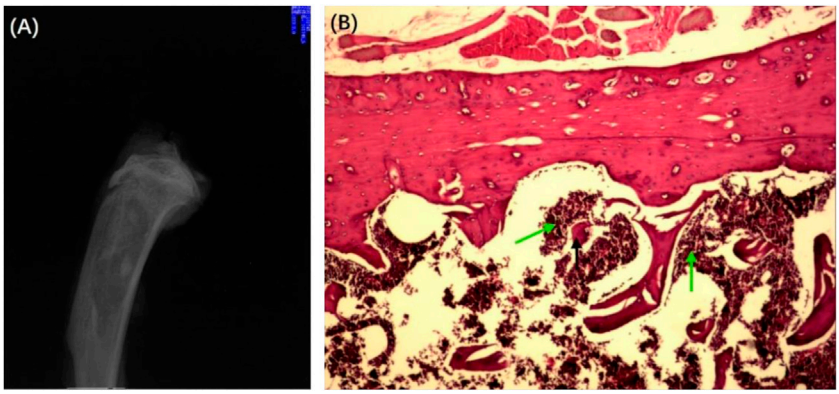

FIGURE 7 | X-ray **(A)** and HE-stained section **(B)** of the chronic osteomyelitis model. Black arrows: deadbone; green arrows: inflammatory cells.

release rate indicates a "burst release" occurred in the early stage of the *in vitro* release. Apparently, the average release amount was 284.7 ± 11.6 μg/d at day 1. It was attributed to the preferential release of Ciprofloxacin enriched on the surface of PTMC implants, as evidenced by the holes displayed on the SEM of the implant surface (**Figure 4**). As shown in **Figure 4**, ciprofloxacin particles were distributed on the surface of PTMC implants before release, while the holes rather than particles were seen after release.

After the "burst release", the release of PTMC implants decreased gradually to 96.4 ± 7.2 μg/d at day 4, and then the release tended to be gentle, with an average release amount of 89.9 ± 12.6 μg/d on day 28. The result indicates that the Ciprofloxacin concentration released from PTMC implants exceeded the minimum inhibitory concentration of Ciprofloxacin (0.4 μg/ml) and was sufficient for osteomyelitis treatment (Mirzaie et al., 2020). The "burst release" in the early stage of *in vitro* release helps to quickly inhibit inflammation, while the sustained and stable release of ciprofloxacin hydrochloride in the later stage helps to control inflammation and consolidate the anti-inflammatory effect effectively. Hence, the synergistic effect of early "burst release" and late stable, sustained release of PTMC implants is ideal for treating chronic osteomyelitis.

Furthermore, the release behaviour of PTMC implants was similar to that of poly (d, L-lactide-co-glycolide-co-ε-caprolactone) (PLGC) reported in our previous work (Liu et al., 2020). However, unlike PLGC, there is no second "burst release" caused by autocatalytic degradation of the acidic degradation products was observed for PTMC implants, resulting in much more stability of the PTMC implants and much more controllable to the release of ciprofloxacin HCL.

Antibacterial Effect *in vitro* of Ciprofloxacin-Loaded PTMC Implants

For a more direct measurement of the antimicrobial efficacy of PTMC implants *in vitro*, a semi-quantitative evaluation of the

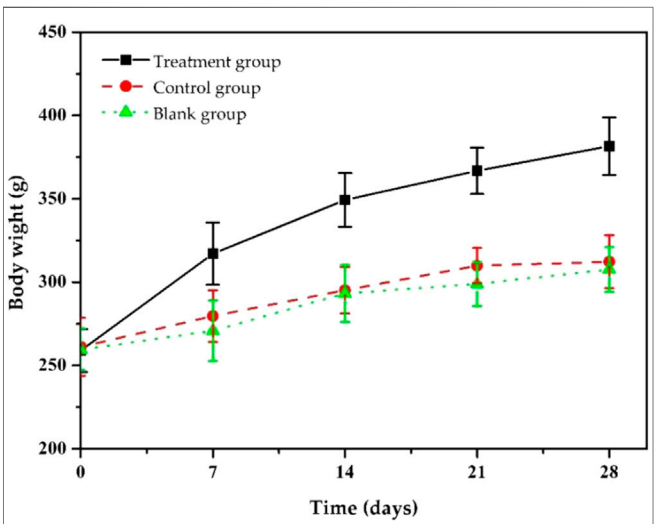

FIGURE 8 | Changes in body weights of chronic osteomyelitis model rats during treatment.

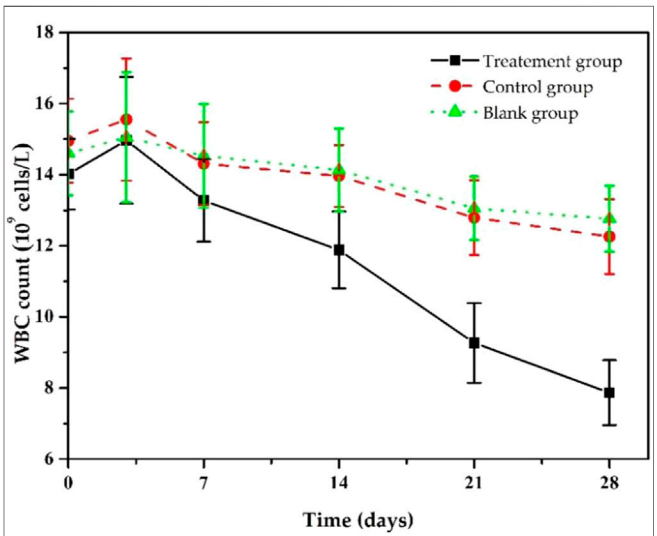

FIGURE 9 | Changes in white blood cell counts s of chronic osteomyelitis model rats during treatment.

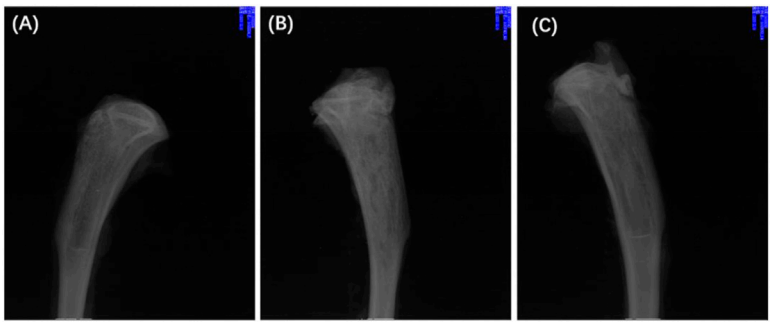

FIGURE 10 | X-rays of chronic-osteomyelitis-mode. treatment group **(A)**, control group **(B)** and blank group **(C)** after 28 days of treatments.

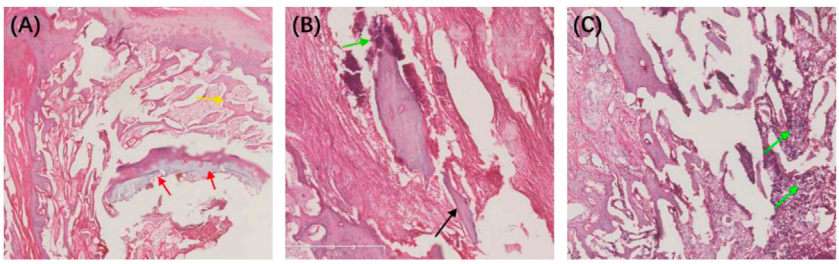

FIGURE 11 | HE-stained sections of the chronic-osteomyelitis-mode. Treatment group **(A)**, control group **(B)** and blank group **(C)** after 28 days of treatments. Red arrow, new bone; yellow arrow, trabecular bone; black arrow, dead bone; green arrow, inflammatory cells.

TABLE 2 | Counts of bacterial content in each group of bone tissue after 28 days of treatment.

No	Treatment Group	Control Group	Blank Group
1	8.2×10^{1}	6.3×10^{5}	6.6×10^{5}
2	8.8×10^{1}	$6,6\times10^{5}$	6.2×10^{5}
3	10.0×10^{1}	6.2×10^{5}	6.9×10^{5}
4	9.6×10^{1}	6.3×10^{5}	6.4×10^{5}
5	10.2×10^{1}	6.5×10^{5}	6.9×10^{5}
6	12.7×10^{1}	6.9×10^{5}	7.2×10^{5}
Average	$(9.92 \pm 1.56)\times10^{1}$	$(6.37 \pm 0.31)\times10^{5}$	$(6.70 \pm 0.38)\times10^{5}$

antibacterial effect was performed by measuring the diameter of the antibacterial ring (**Figure 5**). The presence of the bacteriostatic ring indicates that Ciprofloxacin was biologically active in PTMC implants. As shown in **Figure 3**, the size of the antibacterial ring was 38.7 ± 0.52 mm for the release solution after 1 day of release of PTMC implants. The antibacterial ring sizes of the released solutions after 7, 14 and 28 days of release were 30.6 ± 3.21 mm, 33.3 ± 1.52 mm, and 32.6 ± 0.64 mm, respectively. The results confirm that Ciprofloxacin-loaded PTMC implants could inhibit the growth of S. aureus for up to 28 days. No bacteriostatic rings were presented for the blank PTMC group, indicating that PTMC has no antibacterial effect.

The inhibition of S. aureus biofilm formation by the release solution of the ciprofloxacin-loaded PTMC implants at day 1, day 7, day 14, and day 28 (d) is presented in **Figure 6**, and the inhibition was 83.50 ± 8.52%, 66.77 ± 9.65%, 70.81 ± 10.34%, 64.44 ± 12.26%, respectively. The inhibition efficiency was proportional to the release concentration of ciprofloxacin. The higher the release concentration of ciprofloxacin (**Figure 3**), the higher inhibition efficiency (**Figure 6**), and the larger the diameter of the bacteriostatic zone (**Figure 5**). The results confirmed that after 28 days, the ciprofloxacin-loaded PTMC implants could still inhibit Staphylococcus aureus biofilm formation by more than 60%, indicating that the delivery system has an excellent antibacterial effect.

Establishment and Treatment of Chronic Osteomyelitis Model Rats

To honestly evaluate the antibacterial effect *in vivo*, the Wistar rat model of chronic osteomyelitis was first established in Wistar rats. The successful establishment of chronic osteomyelitis was confirmed by X-ray imaging (**Figure 7A**). As shown in **Figure 7A**, the tibia of all rats showed apparent signs of osteomyelitis, such as marked reduction of bone density, thinning or even disappearance of trabecular bone, damage of cortical bone, and formation of sequestrum. Other signs such as a widening of the proximal medullary cavity and periosteal reactions were also observed in **Figure 7A**. The successful establishment of chronic osteomyelitis was also confirmed by HE observation (**Figure 7B**). As shown in **Figure 7B**, many inflammatory cells, mainly plasma cells and lymphocytes, were seen in the microcavity lesions, and sequestrum formation and fibrous tissue proliferation were seen in HE sections, indicating the formation of osteomyelitis.

After the formation of osteomyelitis, the rat model was treated as follows according to the group, the treatment group was given a Ciprofloxacin-loaded PTMC implant, the control group was assigned a PTMC implant without Ciprofloxacin, and the blank group has received no treatment. Observation of physical signs showed that the mobility of the treatment group was significantly better than that of the other two groups. Seven days after implantation of PTMC implants, the swelling of the surgical site of the rats in the treatment group disappeared, and the walking was more flexible than before. Fourteen days after implantation, the wound at the surgical site of the rats was healed entirely, and the gait returned to normal.

During the treatment, we assessed the body weight changes of the model rats (**Figure 8**). As shown in **Figure 8**, after 7 days of treatment, the bodyweight of the rats in the treatment group gradually increased, and after 14 days, the bodyweight of the rats returned to normal and reached the preoperative value. After 28 days of treatment, their body weight increased to 381.6 ± 16.8 g. The weight gain in the treatment group was thought to be due to increased appetite led by reduced inflammation. Rats in the control and blank groups gained to 312.3 ± 15.9 g and 307.6 ± 13.5 g, respectively, lower than that of the treatment group because they did not significantly reduce inflammation due to insufficient antibiotic treatment. The body weight changes in each group indicate that our ciprofloxacin-loaded PTMC implants had a significant antibacterial effect.

At the same time, we also monitored the changes in the rats' white blood cell (WBC) counts in each group during the treatment (**Figure 9**). Before implantation, WBC counts of the rats in the treatment group was $(14.01 \pm 0.99)\times10^9$/L, significantly higher than the standard value, resulting from chronic bacterial inflammation. Due to postoperative stress response, it further increased to $(14.96 \pm 1.65)\times10^9$/L after 3 days of implantation, then it decreased slowly and returned to an average value of about $(7.86 \pm 0.91) \times10^9$/L after 28 days. The trends in WBC counts in the control and the blank group were similar, but the downward trend was much slower, and WBC counts were $(12.56 \pm 1.05) \times10^9$/L and $(12.76\times\pm0.93) \times10^9$/L, respectively, at day 28, higher than that of treatment group. The statistical results showed that after 28 days of treatment, the WBC changes between the treatment group and the other groups were statistically significant ($p < 0.05$), while there was no significant difference between the blank and control groups ($p > 0.05$). These results indicate that Ciprofloxacin-loaded PTMC implants have significant antibacterial efficacy.

Twenty-eight days after treatment, the X-ray imaging of the model rats in each group was determined (**Figure 10**). The radiographic results show that most of the proximal and middle parts of the tibia in the treatment group returned to typical structures, and no bone destruction and periosteal reaction were found (**Figure 10A**), while the signs as mentioned above of osteomyelitis were still found in the control group, and blank group (**Figures 10B, C**). The results confirmed the effective antibacterial activity of the Ciprofloxacin-loaded PTMC implants *in vivo*.

We also performed HE staining analysis on the tibia tissue of the model rats in each group after treatment. The results showed that the new and trabecular bone in the treatment group had been formed, and no inflammatory cells were found (**Figure 11A**). However, the dead bone and inflammatory cells were clearly visible in the control and blank groups (**Figures 11B, C**). These results directly indicate that the Ciprofloxacin-loaded PTMC implants can eliminate bacterial infections.

Finally, we evaluated the therapeutic efficacy of the Ciprofloxacin-loaded PTMC implants in treating chronic osteomyelitis using a microbiological test, and the results were expressed as bacterial colonies per Gram of bone tissue (**Table 2**). The results showed that the number of colonies in the treatment group was $(9.92 \pm 1.56)\times10^1$ CFU/g, while that in the control and blank groups were $(6.37 \pm 0.31)\times10^5$ and $(6.70 \pm 0.38)\times10^5$, respectively. Obviously, the number of colonies in the treatment group was significantly lower than in the other groups. The statistical results showed that the difference between the treatment group and the other groups was statistically significant ($p < 0.05$), while the difference between the control group and the blank group was not statistically significant ($p > 0.05$). These results suggest that the Ciprofloxacin-loaded PTMC implants achieve a practical antibacterial effect through a local application.

$$(\mathrm{CFU/g}, \mathrm{x} \pm \mathrm{s}, \mathrm{n} = 3)$$

CONCLUSION

To overcome the disadvantages of non-degradable PMMA and acidic degradation products of PLGA in the existing local treatment methods for osteomyelitis, PTMC was synthesized as the carrier to fabricate a ciprofloxacin-loaded PTMC implant in this study to develop a new strategy for the treatment of chronic osteomyelitis. The antibacterial effect and the therapeutic effect of the resulting system on chronic osteomyelitis were investigated.

In vitro, drug release results and antibacterial effects such as antibacterial rings and biofilms inhibition suggest that ciprofloxacin-loaded PTMC implants can sustainably release Ciprofloxacin HCL at sufficient concentrations and maintain antibacterial effects for 28 days. *In vivo*, treatment of chronic osteomyelitis model rats showed the considerable antibacterial effect of the ciprofloxacin-loaded PTMC implants, as evidenced by the gradual return of rat body weight and WBC counts to pre-implantation levels. X-ray imaging, HE staining, and lower bacterial colonies per Gram of bone tissue also confirmed the unique antimicrobial effect of ciprofloxacin-loaded PTMC implants. Through *in vitro* and *in vivo* antibacterial results, this study confirmed the great potential of the ciprofloxacin-loaded PTMC implants in treating chronic osteomyelitis.

DATA AVAILABILITY STATEMENT

The raw data supporting the conclusion of this article will be made available by the authors, without undue reservation.

ETHICS STATEMENT

The animal study was reviewed and approved by the Animal Ethics Committee of The Central Hospital Affiliated to Shenyang Medical College.

AUTHOR CONTRIBUTIONS

YL and XL performed the experiments; YL prepared the original manuscript, ZM collected and analyzed the data; YL and DZ conceived and designed the experiments; AL reviewed and edited the draft. All authors listed have made substantial contribution to the manuscript, which is acknowledged and confirmed by themselves. All authors have read and agreed on the final version of the manuscript.

FUNDING

This work was supported by the Shenyang Science and Technology Bureau (No. 21-173-9-29) and Liaoning Science and Technology Program (No. 2021-MS-185).

REFERENCES

Andreacchio, A., Alberghina, F., Paonessa, M., Cravino, M., De Rosa, V., and Canavese, F. (2019). Tobramycin-impregnated Calcium Sulfate Pellets for the Treatment of Chronic Osteomyelitis in Children and Adolescents. *J. Pediatr. Orthopaedics B* 28 (3), 189–195. doi:10.1097/bpb.0000000000000517

Barakat, A., Schilling, W. H., Sharma, S., Guryel, E., and Freeman, R. (2019). Chronic Osteomyelitis: a Review on Current Concepts and Trends in Treatment. *Orthopaedics and Trauma* 33 (3), 181–187. doi:10.1016/j.mporth.2019.03.005

Brossier, T., Volpi, G., Vasquez-Villegas, J., Petitjean, N., Guillaume, O., Lapinte, V., et al. (2021). Photoprintable Gelatin-Graft-Poly(trimethylene Carbonate) by Stereolithography for Tissue Engineering Applications. *Biomacromolecules* 22 (9), 3873–3883. doi:10.1021/acs.biomac.1c00687

Cai, G., Hou, Z., Li, P., Sun, W., Guo, J., Yang, L., et al. (2021). More Precise Control of the *In Vitro* Enzymatic Degradation via Ternary Self-Blending of High/medium/low Molecular Weight Poly (Trimethylene Carbonate). *Front. Mater.* 8, 367. doi:10.3389/fmats.2021.733535

Cheng, T., Qu, H., Zhang, G., and Zhang, X. (2018). Osteogenic and Antibacterial Properties of Vancomycin-Laden Mesoporous Bioglass/PLGA Composite Scaffolds for Bone Regeneration in Infected Bone Defects. *Artif. Cell Nanomed Biotechnol* 46 (8), 1935–1947. doi:10.1080/21691401.2017.1396997

Dienel, K. E. G., van Bochove, B., and Seppälä, J. V. (2019). Additive Manufacturing of Bioactive Poly(trimethylene Carbonate)/β-Tricalcium Phosphate Composites for Bone Regeneration. *Biomacromolecules* 21 (2), 366–375. doi:10.1021/acs.biomac.9b01272

e Silva, G. L. G., de Bustamante, M. S. S., dos Santos Matos, A. P., Santos-Oliveria, R., Kenechukwu, F. C., Ricci-Junior, E., et al. (2021). Nanofibers in the Treatment of Osteomyelitis and Bone Regeneration. *J. Drug Deliv. Sci. Tech.* 67, 102999. doi:10.1016/j.jddst.2021.102999

Fantoni, M., Taccari, F., and Giovannenze, F. (2019). Systemic Antibiotic Treatment of Chronic Osteomyelitis in Adults. *Eur. Rev. Med. Pharmacol. Sci.* 23 (2 Suppl. l), 258–270. doi:10.26355/eurrev_201904_17500

Hou, Z., Chen, S., Li, Z., Chen, Z., Hu, J., Guo, J., et al. (2021). Controllable Degradation of Poly (Trimethylene Carbonate) via Self-Blending with Different Molecular Weights. *Polym. Degrad. Stab.* 189, 109596. doi:10.1016/j.polymdegradstab.2021.109596

Hou, Z., Hu, J., Li, J., Zhang, W., Li, M., Guo, J., et al. (2017). The *In Vitro* Enzymatic Degradation of Cross-Linked Poly(trimethylene Carbonate) Networks. *Polymers* 9 (11), 605. doi:10.3390/polym9110605

Hou, Z., Zhang, W., Guo, J., Chen, Z., Hu, J., and Yang, L. (2019). The *In Vitro* Enzymatic Degradation of Poly(trimethylene Carbonate-Co-2, 2′-dimethyltrimethylene Carbonate). *Eur. Polym. J.* 112, 51–59. doi:10.1016/j.eurpolymj.2018.12.027

Jin, S., Xia, X., Huang, J., Yuan, C., Zuo, Y., Li, Y., et al. (2021). Recent Advances in PLGA-Based Biomaterials for Bone Tissue Regeneration. *Acta Biomater.* 127, 56–79. doi:10.1016/j.actbio.2021.03.067

Karau, M. J., Schmidt-Malan, S. M., Greenwood-Quaintance, K. E., Mandrekar, J., Cai, J., Pierce, W. M., et al. (2013). Treatment of Methicillin-Resistant *Staphylococcus aureus* Experimental Osteomyelitis with Bone-Targeted Vancomycin. *SpringerPlus* 2 (1), 329. doi:10.1186/2193-1801-2-329

Ko, K.-W., Choi, B., Kang, E. Y., Shin, S.-W., Baek, S.-W., and Han, D. K. (2021). The Antagonistic Effect of Magnesium Hydroxide Particles on Vascular Endothelial Activation Induced by Acidic PLGA Degradation Products. *Biomater. Sci.* 9 (3), 892–907. doi:10.1039/d0bm01656j

Lin, L., Shao, J., Ma, J., Zou, Q., Li, J., Zuo, Y., et al. (2019). Development of Ciprofloxacin and Nano-Hydroxyapatite Dual-Loaded Polyurethane Scaffolds for Simultaneous Treatment of Bone Defects and Osteomyelitis. *Mater. Lett.* 253, 86–89. doi:10.1016/j.matlet.2019.06.028

Liu, F., Cui, Y., and Liu, H. (2021). Advantages and Problems of Local Antibiotic Delivery System in the Treatment of Osteomyelitis. *Chin. J. Tissue Eng. Res.* 25 (4), 614. doi:10.3969/j.issn.2095-4344.2332

Liu, Y., Bai, X., and A, L. (2020). *In Vitro* and *In Vivo* Evaluation of a Ciprofloxacin Delivery System Based on poly(DLLA-co-GA-co-CL) for Treatment of Chronic Osteomyelitis. *J. Appl. Biomater. Funct. Mater.* 18, 2280800020975727–13. doi:10.1177/2280800020975727

Mirzaie, A., Peirovi, N., Akbarzadeh, I., Moghtaderi, M., Heidari, F., Yeganeh, F. E., et al. (2020). Preparation and Optimization of Ciprofloxacin Encapsulated Niosomes: A New Approach for Enhanced Antibacterial Activity, Biofilm Inhibition and Reduced Antibiotic Resistance in Ciprofloxacin-Resistant Methicillin-Resistance *Staphylococcus aureus*. *Bioorg. Chem.* 103, 104231. doi:10.1016/j.bioorg.2020.104231

Mohajeri, S., Chen, F., de Prinse, M., Phung, T., Burke-Kleinman, J., Maurice, D. H., et al. (2020). Liquid Degradable Poly(trimethylene-Carbonate-Co-5-Hydroxy-Trimethylene Carbonate): An Injectable Drug Delivery Vehicle for Acid-Sensitive Drugs. *Mol. Pharmaceutics* 17 (4), 1363–1376. doi:10.1021/acs.molpharmaceut.0c00064

Musher, D. M., and Arasaratnam, R. J. (2021). *Contributions of Animal Studies to the Understanding of Infectious Diseases*. Clinical Infectious Diseases. ciab844. doi:10.1093/cid/ciab844

Nabipour, Z., Nourbakhsh, M. S., and Baniasadi, M. (2018). Evaluation of Ibuprofen Release from Gelatin/hydroxyapatite/polylactic Acid Nanocomposites. *Iranian J. Pharm. Sci.* 14 (1), 75–84. doi:10.22034/IJPS.2018.32051

Papenburg, B. J., Schüller-Ravoo, S., Bolhuis-Versteeg, L. A. M., Hartsuiker, L., Grijpma, D. W., Feijen, J., et al. (2009). Designing Porosity and Topography of Poly(1,3-Trimethylene Carbonate) Scaffolds. *Acta Biomater.* 5 (9), 3281–3294. doi:10.1016/j.actbio.2009.05.017

Patel, K. H., Bhat, S. N., and H, M. (2021). Outcome Analysis of Antibiotic-Loaded Poly Methyl Methacrylate (PMMA) Beads in Musculoskeletal Infections. *J. Taibah Univ. Med. Sci.* 16 (2), 177–183. doi:10.1016/j.jtumed.2020.10.015

van Vugt, T. A. G., Arts, J. J., and Geurts, J. A. P. (2019). Antibiotic-loaded Polymethylmethacrylate Beads and Spacers in Treatment of Orthopedic Infections and the Role of Biofilm Formation. *Front. Microbiol.* 10, 1626. doi:10.3389/fmicb.2019.01626

Wassif, R. K., Elkayal, M., Shamma, R. N., and Elkheshen, S. A. (2021). Recent Advances in the Local Antibiotics Delivery Systems for Management of Osteomyelitis. *Drug Deliv.* 28 (1), 2392–2414. doi:10.1080/10717544.2021.1998246

Weisgrab, G., Guillaume, O., Guo, Z., Heimel, P., Slezak, P., Poot, A., et al. (2020). 3D Printing of Large-Scale and Highly Porous Biodegradable Tissue

Engineering Scaffolds from Poly(trimethylene-Carbonate) Using Two-Photon-Polymerization. *Biofabrication* 12 (4), 045036. doi:10.1088/1758-5090/abb539

Xie, K., Zhou, Z., Guo, Y., Wang, L., Li, G., Zhao, S., et al. (2019). Long-Term Prevention of Bacterial Infection and Enhanced Osteoinductivity of a Hybrid Coating with Selective Silver Toxicity. *Adv. Healthc. Mater.* 8 (5), 1801465. doi:10.1002/adhm.201801465

Yang, L.-Q., He, B., Meng, S., Zhang, J.-Z., Li, M., Guo, J., et al. (2013). Biodegradable Cross-Linked Poly(trimethylene Carbonate) Networks for Implant Applications: Synthesis and Properties. *Polymer* 54 (11), 2668–2675. doi:10.1016/j.polymer.2013.03.059

Yang, L.-Q., Yang, D., Guan, Y.-M., Li, J.-X., and Li, M. (2012). Random Copolymers Based on Trimethylene Carbonate and ε-caprolactone for Implant Applications: Synthesis and Properties. *J. Appl. Polym. Sci.* 124 (5), 3714–3720. doi:10.1002/app.35355

Yang, L., Li, J., Li, M., and Gu, Z. (2016). The *In Vitro* and *In Vivo* Degradation of Cross-Linked Poly(trimethylene Carbonate)-Based Networks. *Polymers* 8 (4), 151. doi:10.3390/polym8040151

Yang, L., Li, J., Meng, S., Jin, Y., Zhang, J., Li, M., et al. (2014). The *In Vitro* and *In Vivo* Degradation Behavior of Poly (Trimethylene Carbonate-Co-ε-Caprolactone) Implants. *Polymer* 55 (20), 5111–5124. doi:10.1016/j.polymer.2014.08.027

Yang, L., Li, J., Zhang, W., Jin, Y., Zhang, J., Liu, Y., et al. (2015). The Degradation of Poly(trimethylene Carbonate) Implants: The Role of Molecular Weight and Enzymes. *Polym. Degrad. Stab.* 122, 77–87. doi:10.1016/j.polymdegradstab.2015.10.016

Zaaba, N. F., and Jaafar, M. (2020). A Review on Degradation Mechanisms of Polylactic Acid: Hydrolytic, Photodegradative, Microbial, and Enzymatic Degradation. *Polym. Eng. Sci.* 60 (9), 2061–2075. doi:10.1002/pen.25511

Zhao, Z., Wang, G., Zhang, Y., Luo, W., Liu, S., Liu, Y., et al. (2020). The Effect of Calcium Sulfate/calcium Phosphate Composite for the Treatment of Chronic Osteomyelitis Compared with Calcium Sulfate. *Ann. Palliat. Med.* 9, 944. doi:10.21037/apm.2020.03.23

Conflict of Interest: The authors declare that the research was conducted in the absence of any commercial or financial relationships that could be construed as a potential conflict of interest.

Publisher's Note: All claims expressed in this article are solely those of the authors and do not necessarily represent those of their affiliated organizations, or those of the publisher, the editors and the reviewers. Any product that may be evaluated in this article, or claim that may be made by its manufacturer, is not guaranteed or endorsed by the publisher.

frontiers | Frontiers in Bioengineering and Biotechnology

ORIGINAL RESEARCH
published: 23 May 2022
doi: 10.3389/fbioe.2022.868719

Integration of Bioglass Into PHBV-Constructed Tissue-Engineered Cartilages to Improve Chondrogenic Properties of Cartilage Progenitor Cells

Ke Xue[1,2†], Shuqi Zhang[3†], Jin Ge[4], Qiang Wang[5], Lin Qi[6] and Kai Liu[1]**

[1]Department of Plastic and Reconstructive Surgery, Shanghai 9th People's Hospital, Shanghai Jiao Tong University School of Medicine, Shanghai, China, [2]Department of Burn and Plastic Surgery, Hainan Western Central Hospital, Hainan, China, [3]Chongqing Key Laboratory of Oral Diseases and Biomedical Sciences, Chongqing Municipal Key Laboratory of Oral Biomedical Engineering of Higher Education, Stomatological Hospital of Chongqing Medical University, Chongqing, China, [4]Shanghai Key Laboratory of Stomatology and Shanghai Research Institute of Stomatology, Department of Oral Surgery, Shanghai Ninth People's Hospital, College of Stomatology, Shanghai Jiao Tong University School of Medicine, Shanghai, China, [5]Liaoning Provincial Key Laboratory of Oral Diseases, School and Hospital of Stomatology, China Medical University, Shenyang, China, [6]Department of Radiology, Huadong Hospital Affiliated to Fudan University, Shanghai, China

OPEN ACCESS

Edited by:
Hasan Uludag,
University of Alberta, Canada

Reviewed by:
Yong Sun,
Sichuan University, China
Hongwei Wu,
Zhejiang University, China

***Correspondence:**
Lin Qi
qilin86521@163.com
Kai Liu
drkailiu@163.com

†These authors have contributed equally to this work

Specialty section:
This article was submitted to Biomaterials, a section of the journal Frontiers in Bioengineering and Biotechnology

Received: 03 February 2022
Accepted: 30 March 2022
Published: 23 May 2022

Citation:
Xue K, Zhang S, Ge J, Wang Q, Qi L and Liu K (2022) Integration of Bioglass Into PHBV-Constructed Tissue-Engineered Cartilages to Improve Chondrogenic Properties of Cartilage Progenitor Cells. Front. Bioeng. Biotechnol. 10:868719. doi: 10.3389/fbioe.2022.868719

Background: The Poly (3-hydroxybutyrate-co-3-hydroxyvalerate) (PHBV) scaffold has proven to be a promising three-dimensional (3D) biodegradable and bioactive scaffold for the growth and proliferation of cartilage progenitor cells (CPCs). The addition of Bioglass into PHBV was reported to increase the bioactivity and mechanical properties of the bioactive materials.

Methods: In the current study, the influence of the addition of Bioglass into PHBV 3D porous scaffolds on the characteristics of CPC-based tissue-engineered cartilages *in vivo* were compared. CPCs were seeded into 3D macroporous PHBV scaffolds and PHBV/10% Bioglass scaffolds. The CPC–scaffold constructs underwent 6 weeks *in vitro* chondrogenic induction culture and were then transplanted *in vivo* for another 6 weeks to evaluate the difference between the CPC–PHBV construct and CPC–PHBV/10% Bioglass construct *in vivo*.

Results: Compared with the pure PHBV scaffold, the PHBV/10% Bioglass scaffold has better hydrophilicity and a higher percentage of adhered cells. The CPC–PHBV/10% Bioglass construct produced much more cartilage-like tissues with higher cartilage-relative gene expression and cartilage matrix protein production and better biomechanical performance than the CPC–PHBV construct.

Conclusion: The addition of Bioglass into 3D PHBV macroporous scaffolds improves the characteristics of CPC-based tissue-engineered cartilages *in vivo*.

Keywords: cartilage progenitor cells, PHBV, Bioglass, hydrophilicity, cartilage engineering

INTRODUCTION

Cartilage defects caused by trauma, tumors, and degenerative diseases are becoming increasingly popular, which resulted in significant morbidity and pain over time. Cartilage regenerative medicine and cartilage tissue engineering provide a new and more effective treatment option for the repair of cartilage deficiencies (Hacken et al., 2020). Seeding isolated chondrocytes, mesenchymal stem cells, or cartilage progenitor cells on three-dimensional (3D) biodegradable scaffolds to produce tissue-engineered cartilages is a promising method in cartilage tissue engineering and cartilage regenerative medicine (Kwon et al., 2019).

Autologous chondrocytes is the first option of seeding cells. Vacanti et al. reported the regeneration of nasoseptal cartilage replacements constructed by biodegradable polymers and chondrocytes (Puelacher et al., 1994). Kyoung-Ho Yoon et al. reported that autologous costal chondrocyte implantations can be used as a promising treatment option for repairing articular cartilage defects with good structural regeneration and clinical outcomes and with stable results at midterm follow-up (Yoon et al., 2020). Ning Ma et al. used the tissue-engineered cartilage constructed by autologous chondrocytes and allogeneic, acellular cartilage matrices to repair the cartilage defects (Ma et al., 2017). However, cartilage tissue engineering needed a large number of cells, while chondrocyte expansion *in vitro* led to aging and loss of the chondrocyte phenotype (Thompson et al., 2017).

Bone marrow-derived stem cells (BMSCs) were considered to be promising seeding cells due to their multipotent differentiation ability toward osteogenesis, adipogenesis, and chondrogenesis and high proliferation ability (Fu et al., 2019). Liu et al. reported that BMSC combined with the PRP scaffold differentiated into cartilage tissues and may be a promising therapeutic option for the repair of cartilage defects (Liu et al., 2019). Xue et al. indicated that acellular cartilage sheets could efficiently repair articular cartilage defects by promoting endogenous chondrogenesis *in situ* or inducing chondrogenic differentiation of BMSCs (Xue et al., 2018a). However, it is reported that BMSCs underwent "dedifferentiation" and "phenotypic loss" during *in vitro* expansion and the chondrogenic differentiation process (Vinardell et al., 2012).

In our previous studies, we found that cartilage progenitor cells (CPCs) could be promising alternative cell sources in cartilage tissue engineering and regenerative medicine, and the CPC–poly (3-hydroxybutyrate-co-3-hydroxyvalerate) (PHBV) constructs could form ivory-whitish cartilage-like tissues, with typical cartilage structures (Xue et al., 2019). However, PHBV has weak surface hydrophilic properties, which led to a low number of adhered cells.

Bioglass is a bioactive inorganic material consisting of CaO, Na_2O, SiO_2, and P_2O_5 in certain proportions. 45S5 is the original component of Bioglass (Islam et al., 2022). It has been reported that the addition of 45S5 Bioglass into PHBV can increase the hydrophilicity of the biomaterials. Therefore, PHBV and PHBV/10% Bioglass (45S5) 3D biomaterial scaffolds were prepared in this study, CPCs were combined with two different scaffolds and incubated *in vitro* for 6 weeks, and then subcutaneous transplantation was performed for another 6 weeks. The cell adhesion, production of the extracellular matrix, size, structure, and functional and biomechanical characteristics of the regenerated cartilage were determined to analyze the influence of the addition of 10%Bioglass into the PHBV scaffold on the function and structure of the neocartilage.

MATERIALS AND METHODS

All animal experimental procedures and operation in the current research have been approved by the Ethics Committee of Shanghai 9th People's Hospital, Shanghai Jiao Tong University School of Medicine (SH9H-2021-A416-SB).

Preparation of PHBV and PHBV/10% Bioglass Composite Scaffolds

PHBV (Mw = 300,000), consisting of 3 mol% 3-hydroxyvalerate units, was purchased from Tianan Biologic Material Co., Ltd. (Ninbo, China). A solvent casting/particulate leaching method was used to produce PHBV and PHBV/10%Bioglass bioactive composite scaffolds as reported previously (Aboudzadeh et al., 2021). Briefly, the dissolution of 1 g of PHBV powder into 10 ml of chloroform produced a concentration of 10% (w/v), and then Bioglass powder (0.125 g) was dissolved into the mixture to obtain the PHBV/10%Bioglass composite scaffolds. After the sodium chloride (NaCl) particles were mixed into the above solution as porogens, the mixture was transferred to a Teflon mold (inner diameter 80 mm, height 2 mm). The samples were air-dried for 24 h to remove the solvent and then were vacuum-dried for 48 h at 60°C to evaporate any remaining water-insoluble solvent.

The NaCl (porogens) in the dried scaffold was leached out by immersing in deionized water and then was vacuum-dried to produce porous 3D bioactive scaffolds. The scaffolds were prepared in the shape of a cylinder (5 mm side diameter, 2 mm thick) in the current research.

Property of the PHBV and PHBV/10% Bioglass Scaffolds

Optical microscopy and scanning electron microscopy (SEM) were used to evaluate the difference between the two kinds of scaffolds. ImageJ software was used to analyze/process the SEM images of the scaffolds to obtain the porosity and pore size distribution data. The mass of the scaffolds and dimensions were measured to analyze the porosity ratio of the 3D porous bioactive scaffolds as previously described (El-Shanshory et al., 2022). The compressive strength of the 3D bioactive scaffolds was determined according to the force–displacement curve with a Shimadzu AG mechanical tester (Wright et al., 2022) (Shimadzu Co., Japan).

Hydrophilicity, Water Absorption, and Cell Adhesion Determination

The water contact angles of the nonporous PHBV and PHBV/10% Bioglass composite cuboids were evaluated to determine the

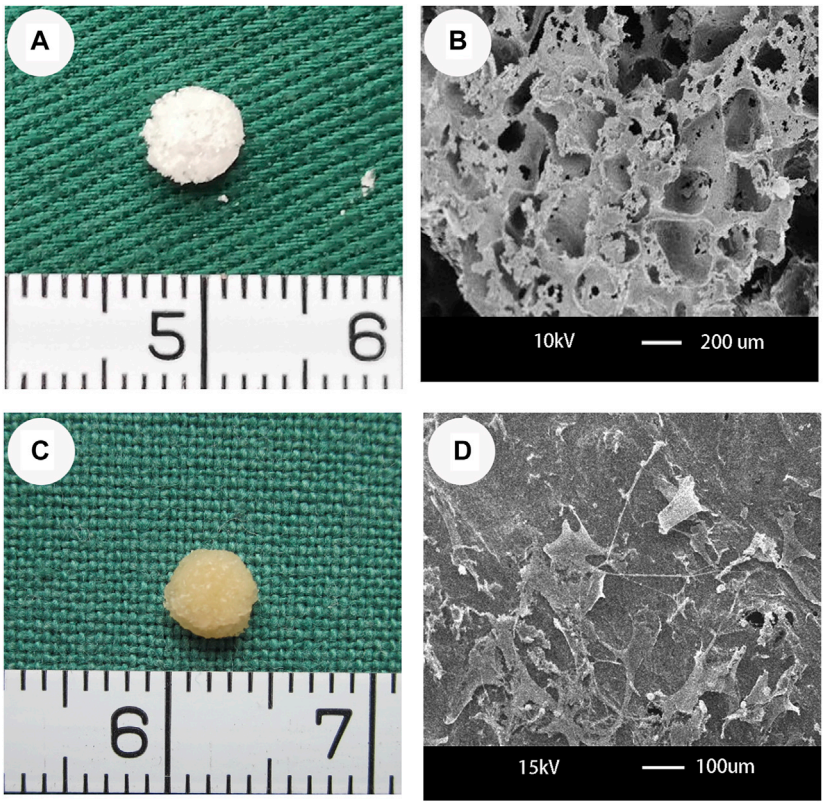

FIGURE 1 | Optical microscopy and SEM of PHBV/10%Bioglass scaffolds and the CPC–PHBV/10%Bioglass construct. **(A)** The PHBV/10%Bioglass scaffolds exhibited a cylindrical shape (5 mm diameter and 2 mm thickness), with a lot of pores on the surface of the composite scaffolds. **(B)** PHBV/10%Bioglass composite porous 3D scaffolds had a macroporous structure with interconnected open pores of 30–300 μm in diameter. **(C)** Gross view of *in vitro* CPC–scaffold constructs after 6 weeks of *in vitro* culture. These engineered tissues roughly maintained their original cylindrical shape and size and exhibited an ivory-whitish appearance. **(D)** SEM view of CPCs-PHBV/10%Bioglass constructs after 6 weeks of *in vitro* culture, exhibiting abundant extracellular matrix production and good compatibility of the CPCs with the composite scaffold.

hydrophilicity of the two kinds of scaffold composites. The sessile drop technique was used to evaluate the water contact angles at 25°C using a contact angle measuring instrument (SZ10-JC2000A, Shanghai, China) (Yang et al., 2020).

The water absorption of the two kinds of 3D scaffolds was tested according to the protocol described previously (Tan et al., 2022). The weights of completely dried PHBV and PHBV/10% Bioglass bioactive scaffolds were measured (W dry), and then they were immersed in deionized water to achieve water absorption equilibration for 4 h at 25 °C. Then, the weight of hydrated 3D scaffolds was measured (W wet), and the water absorptivity was determined according to the formula

$$\text{ratio}\ (\%) = (\text{Wwet} - \text{Wdry})/\text{Wdry} \times 100\%.$$

The percentage of adhered cells was determined by 3-(4,5-dimethylthiazol-2-yl)-2,5-diphenyltetrazonium bromide (MTT)-based colorimetric assay as previously described (Xue et al., 2019). Briefly, the CPCs at passage 2 were harvested and seeded onto the sterilized PHBV and PHBV/10%Bioglass composite substrates and then cultured in a CO_2 incubator for 4 h. Then, 1 ml of fresh low-glucose Dulbecco's modified Eagle's medium (DMEM) was dropped into each well, and the MTT method was used to measure the number of living cells.

Cell Harvesting and Construction of Tissue-Engineered Cartilages

The differential adhesion to the fibronectin method was used to obtain CPCs from chondrocytes. The harvested articular cartilage mass was cut into (1–2) mm^2 fragments and then washed with sterile chloromycetin and phosphate-buffered saline (PBS) thrice. The minced cartilage fragments were digested in a solution of collagenase II (0.2% w/v) in high-glucose DMEM, then were filtered with a 200 μm filter to remove undigested tissues, and then were subjected to cell suspension. 5,000 cells/ml were plated onto 100 mm dishes (prior treated with 10 μg/ml fibronectin for 24 h) at 37°C for 20 min in a Thermo Scientific™ CO_2 incubator. The nonadherent cells were removed after 20 min and washed with PBS twice, and then 10 ml of low-glucose DMEM with 10% fetal bovine serum (FBS) was dropped into each dish. The remaining cells were incubated for 7–10 days until the cell confluence reached 80%. Then, the cells were subcultured at a density of 3×10^4 cells/cm^2.

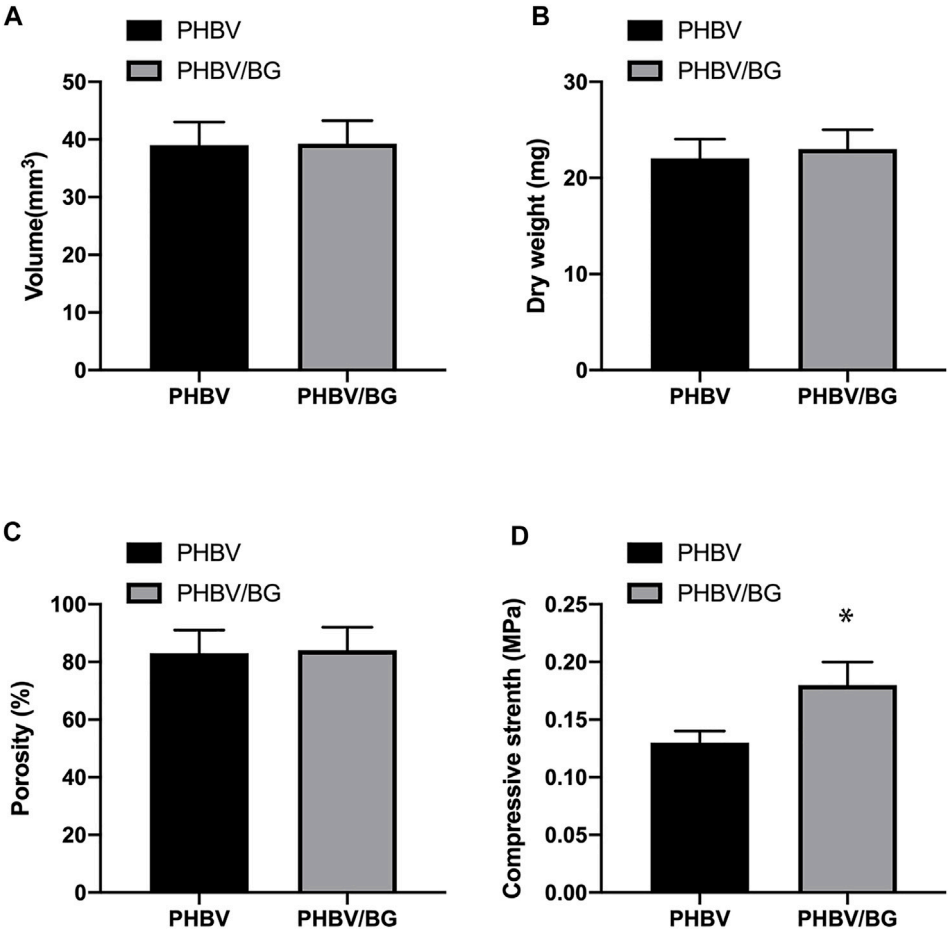

FIGURE 2 | Characterization of PHBV and PHBV/10%Bioglass 3D porous scaffolds. The PHBV and PHBV/10%Bioglass 3D porous scaffolds exhibited the same volume **(A)** and dry weight **(B)** and the same porosity **(C)** ($p > 0.05$). The compressive modulus **(D)** of the CPC–PHBV/10%Bioglass constructs was greater than that of CPC–PHBV constructs ($p < 0.05$).

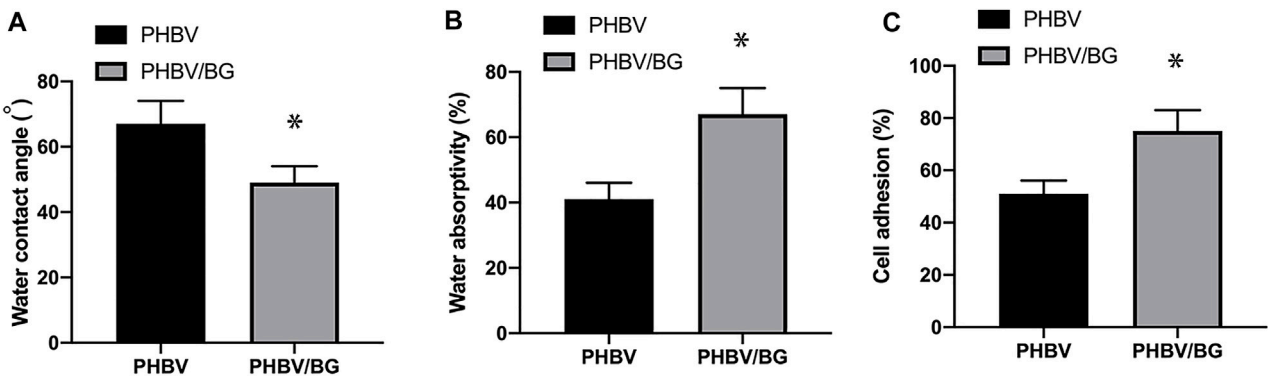

FIGURE 3 | Contact angle, water absorptivity, and cell adhesion of the scaffolds. **(A)** The water contact angles of the PHBV/Bioglass composite scaffolds were significantly lower than that of the pure PHBV scaffold, indicating that there was a significant increase in surface hydrophilicity with the addition of Bioglass into PHBV ($p < 0.05$). **(B)** The water absorptivity of the PHBV/Bioglass composite scaffolds was obviously greater than that of pure PHBV ($p < 0.05$). **(C)** The percentage of adhered cells increased significantly with the addition of Bioglass ($p < 0.05$).

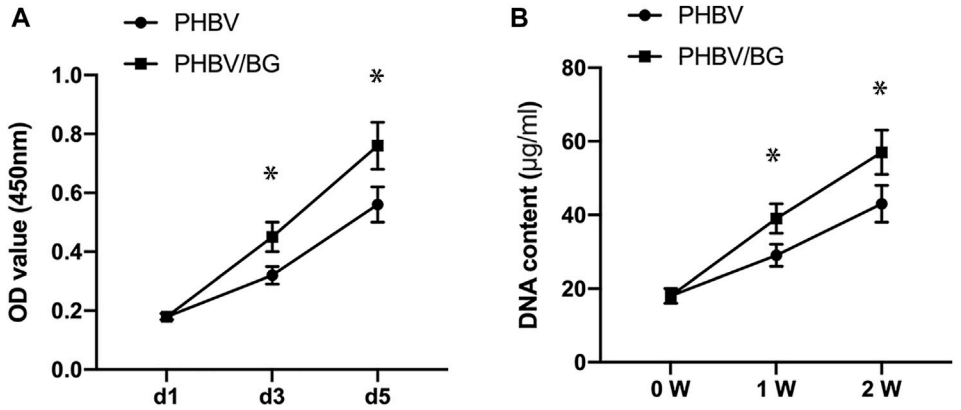

FIGURE 4 | Cell Proliferation. There was an obvious difference in the cellular proliferation between the CPC–PHBV construct and CPC–PHBV/10%Bioglass construct ($p < 0.05$) **(A)**. The DNA content of the CPC–PHBV/10%Bioglass construct is higher than that of the CPC–PHBV construct ($p < 0.05$) **(B)**.

The cylindrical PHBV scaffold and PHBV/10%Bioglass scaffold were sterilized and placed in the center of six-well polystyrene culture plates. 30 μl (5×10^7 cell/ml) of the CPC suspension at passage 2 was seeded onto the 3D bioactive scaffold and inoculated at 37°C for 4 h. This allowed adequate attachment of the CPCs onto the 3D bioactive scaffolds. Then, 5 ml of low-glucose DMEM with 10% FBS was dropped into each well after 4 h, and the culture medium was refreshed every 2 or 3 days. The athymic C57BL/6 nude mice were anesthetized intraperitoneally with sodium pentobarbital (60 mg/kg); then the cell-scaffold constructs after 6-week *in vitro* culture were transplanted into the subcutaneous tissue of the back of the mice for another 6 weeks, and then the specimens were harvested.

Cell Proliferation

The DNA content of the samples was tested to determine the number of CPCs on the scaffolds after being *in vitro* cultured for 1 week and 2 weeks (Luo et al., 2021). The cell proliferation on the scaffolds was assessed via the MTT assay, and the CPCs were incubated for 1 day, 3 days, and 5 days and then tested with the MTT method.

Chondrogenic Induction *in Vitro*

After 3 days of incubation in low-glucose DMEM composed of 10% FBS, the regular culture medium was refreshed with a chondrogenic induction medium containing high-glucose DMEM containing 10% FBS supplemented with 50 ng/ml insulin-like growth factor 1 (IGF-1, Peprotech, Rocky Hill, NJ), 10 ng/ml transforming growth factor β1 (TGF-β1, Peprotech, Rocky Hill, NJ), and 40 ng/ml dexamethasone (Sigma, St. Louis, MO). The culture medium change was performed every 3 days.

Characterization of *in Vivo* Tissue-Engineered Cartilages

Gross Evaluation of *in Vivo* Tissue-Engineered Cartilages

After 6 weeks of subcutaneous implantation, the thickness and diameter of the cell–scaffold construct were measured using a vernier caliper, and the volume of the cell–scaffold construct was determined using a volumenometer.

Quantitative Evaluation of *in Vivo* Tissue-Engineered Cartilages

The wet weight, total collagen content (Guedes et al., 2022), and glycosaminoglycan (GAG) content (Nunes et al., 2021) of the specimen after 6 weeks of subcutaneous transplantation were determined using the protocol previously reported. The biomechanical testing was tested using a biomechanical analyzer according to the previous protocol, and the force–displacement curve was used to calculate the compression strength of the cell-scaffold construct (Wright et al., 2022).

Histological Evaluation

The specimen after subcutaneous implantation for 6 weeks was immersed in 10% neutral buffered formalin, washed with PBS, dehydrated, embedded in paraffin, cut into slices of a 5 μm thickness, and stained with hematoxylin and eosin. 5 μm slices were immunostained with a type II collagen antibody as previously described (Lv et al., 2020).

RT-PCR Analysis

Total RNA was extracted from the specimen, and cDNA was harvested by reverse transcription (RT) using previous protocols (Xue et al., 2018b). Real-time quantitative polymerase chain reaction (RT-PCR) was used to analyze the cartilage-specific gene expression: type II collagen (COL II) a1 (Sense 5′-TGC TGCTGACGCTGCTC-3′, Antisense 5′-GTTCTCCTTTCCTGT CCCTTTG-3′), SOX-9 (Sense 5′-GGCTCGGACACAGAGAAC AC-3′, Antisense 5′-GTGCGGCTTATTCTTGCTCG-3′), and aggrecan (Sense 5′-GGGGAATCTTCTGGCATTAA-3′, Antisense 5′-CGTTGGAGCCTGGGTT-3′). The β-actin (Sense 5′-ACATCAAGGAGAAGCTCTGCTACG-3′, Antisense 5′-GAGGGGCGATGATCTTGATCTTCA-3′) mRNA level was used as an internal control.

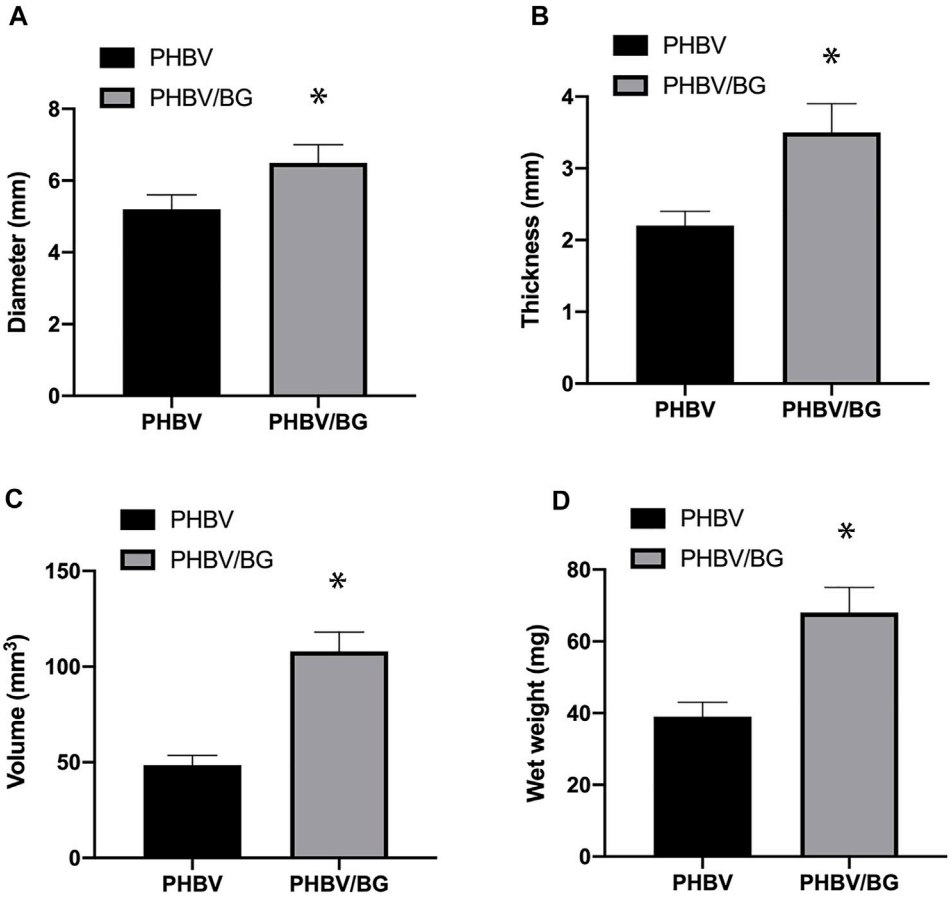

FIGURE 5 | Gross analysis of *in vivo* engineered tissue cartilages. The diameter **(A)**, thickness **(B)**, volume **(C)**, and wet weight **(D)** of the CPC–PHBV/10%Bioglass construct were higher than those of the CPC–PHBV construct *in vivo* ($p < 0.05$).

Statistical Analysis

All harvested data were expressed as the means ± standard deviation ($n = 6$). The data differences between the PHBV and PHBV/10%Bioglass bioactive scaffolds were evaluated by Student's t-test. A p-value less than 0.05 was considered to be statistically significant.

RESULTS

Optical Microscopy and SEM of PHBV/10% Bioglass Scaffolds and the CPCs–PHBV/10%Bioglass Construct

The PHBV/10%Bioglass scaffolds exhibited a cylindrical porous scaffold shape (**Figure 1A**). PHBV/10%Bioglass composite scaffolds show a three-dimensionally interconnected macroporous structure with the pore diameter distribution varying from 30 to 300 μm (**Figure 1B**). A gross view of *in vitro* CPC–scaffold constructs after culture for 6 weeks shows that these engineered tissues maintained their original sizes roughly and exhibited a yellowish appearance (**Figure 1C**). The SEM view of cell–PHBV/Bioglass constructs after 6 weeks of *in vitro* culture shows that the CPCs adhered to the scaffold pore walls and distributed throughout the scaffold pores homogeneously, showed an extended morphology, and exhibited abundant extracellular matrix production and good compatibility of the CPCs with the PHBV/10%Bioglass (**Figure 1D**).

Properties of PHBV and PHBV/10%Bioglass Bioactive Scaffolds

The PHBV and PHBV/10%Bioglass 3D scaffolds had similar porosities ($p > 0.05$), and the size of interconnected open pores varied from 30 to 300 μm (shown by SEM analysis). The compressive modulus of the PHBV scaffolds was 0.13 ± 0.01 MPa, while the compressive modulus of the PHBV/10% Bioglass scaffolds was 0.18 ± 0.02 MPa ($p < 0.05$) (**Figure 2**).

Contact Angle, Water Absorptivity, and Cell Adhesion of the PHBV and PHBV/10% Bioglass Scaffolds

The water contact angle of the PHBV/10%Bioglass is (49 ± 5.1°), while the water contact angle of pure PHBV composites is (67 ±

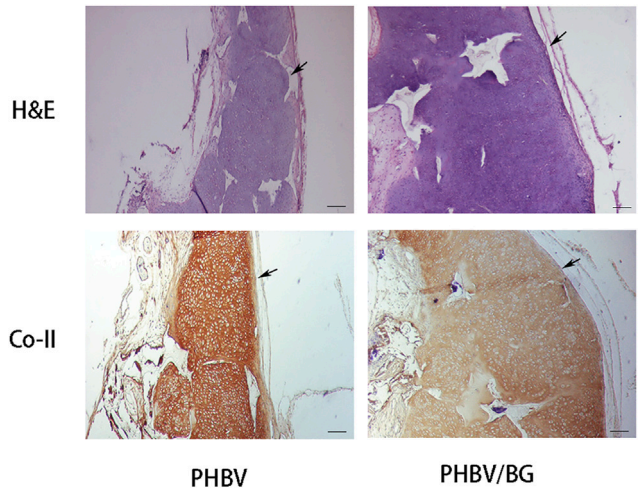

FIGURE 6 | Histological and immunohistological analysis of *in vivo* engineered constructs. There is an obvious difference in the thickness between the CPC–PHBV/10%Bioglass construct and CPC–PHBV construct ($p < 0.05$). The CPC–PHBV/10%Bioglass construct produced much more cartilage-like tissues than the CPC–PHBV construct. Scale bar = 100 μm.

7.2°) ($p < 0.05$) (**Figures 3A,B**). The water absorptivity of the PHBV/10%Bioglass is (72 ± 8.1%), while the water absorptivity of pure PHBV composites is (57 ± 6.2%) ($p < 0.05$) (**Figure 3B**). The percentage of adhered cells of the PHBV/10%Bioglass is (75 ± 7.6%), while the percentage of adhered cells of pure PHBV composites is (51 ± 5.2%) ($p < 0.05$) (**Figure 3C**).

Cell Proliferation

There was an obvious difference in the cellular proliferation of CPC–PHBV constructs and that of CPC–PHBV/10%Bioglass constructs ($p < 0.05$). The DNA content of CPC–PHBV/10% Bioglass constructs is higher than that of CPC–PHBV constructs ($p < 0.05$) (**Figure 4**).

Analysis of *in Vivo* Tissue-Engineered Cartilages on PHBV and PHBV/10% Bioglass Scaffolds

Gross Analysis of *in Vivo* Tissue-Engineered Cartilages

After subcutaneous transplantation for 6 weeks, the CPC–PHBV constructs and CPC–PHBV/10%Bioglass constructs kept their original cylinder shape and size basically and demonstrated a white cartilage-like appearance. The thickness, diameter, volume, and wet weight of CPC–PHBV/10%Bioglass constructs were more than that of CPC–PHBV constructs ($p < 0.05$) (**Figure 5**).

Histological and Immunohistochemical Evaluation

The cartilage-like tissue was produced in both CPC–PHBV constructs and CPC–PHBV/10%Bioglass constructs, with mature cartilage lacuna structure formation and obvious positive type II collagen expression (**Figure 6**). The histological and immunohistochemical analyses show that the tested specimen produced more cartilage extracellular matrices and created much more cartilage-like tissues in the CPC–PHBV/10%Bioglass constructs than that in CPC–PHBV constructs.

Collagen Content, GAG Content, and Compression Strength

The collagen content of CPC–PHBV/10%Bioglass constructs was 8.1 ± 1.1 mg/g, while the collagen of CPC–PHBV constructs was 13.6 ± 1.45 mg/g ($p < 0.05$). The GAG content of CPC–PHBV/10%Bioglass constructs was 2.3 ± 0.32 mg/g, while the GAG content of CPC–PHBV constructs was 3.6 ± 0.45 mg/g ($p < 0.05$). The compression modulus of CPC–PHBV/10%Bioglass constructs was 11.5 ± 01.7 MPa, while the compression modulus of CPC–PHBV constructs was 18.3 ± 2.2 MPa ($p < 0.05$) (**Figure 7**).

RT-PCR Analysis

PCR analysis exhibited that aggrecan, collagen II, and SOX-9 of CPC–PHBV/10%Bioglass constructs were all significantly highly expressed compared to CPC–PHBV constructs ($p < 0.05$), indicating that the addition of Bioglass into PHBV may enhance the chondrogenic differentiation of CPCs (**Figure 8**).

DISCUSSION

Seed cells, biodegradable scaffolds, and the environment are three key elements in tissue engineering (Antunes et al., 2020). The seed cells on the biomaterial scaffolds should maintain their mature and stable chondrogenic phenotype and produce rich extracellular matrices, which can replace the biodegradable scaffolds eventually and determine the fate of tissue-engineered cartilages (Francis et al., 2018). Due to "dedifferentiation" and "phenotypic loss" during *in vitro* expansion and the chondrogenic differentiation process, bone marrow-derived stem cells (BMSCs) and chondrocytes were not the ideal seeding cells (Shi et al., 2017; Ripmeester et al., 2018). CPCs harvested from cartilage tissues present chondrogenic characteristics and good proliferation ability, thus becoming novel promising seeding cells (Xue et al., 2019).

Due to its appropriate biodegradability and biocompatibility, PHBV has been shown to be a biodegradable biomaterial scaffold used in cartilage tissue engineering and regenerative medicine (Rodrigues et al., 2021). In our previous research, the feasibility of combining CPCs with PHBV to construct tissue-engineered tissues was explored, and we found that the tissue-engineered cartilage on PHBV scaffolds had an insufficient thickness and inadequate biomechanical strength due to the surface hydrophobicity of the scaffold (Xue et al., 2019).

The hydrophilicity is a critical element influencing cell attachment, growth and proliferation, biocompatibility, fast cell adhesion and growth, and physical–chemical resistance (Wang et al., 2022). Hydrophilicity of the material surface can influence cell attachment and cell shape, which can also dictate proliferation and differentiation of cells on the material surface or in the materials (Kunrath et al., 2020). Marcel F Kunrath et al. proposed that the application of plasma-treated surfaces resulted in the most hydrophilic

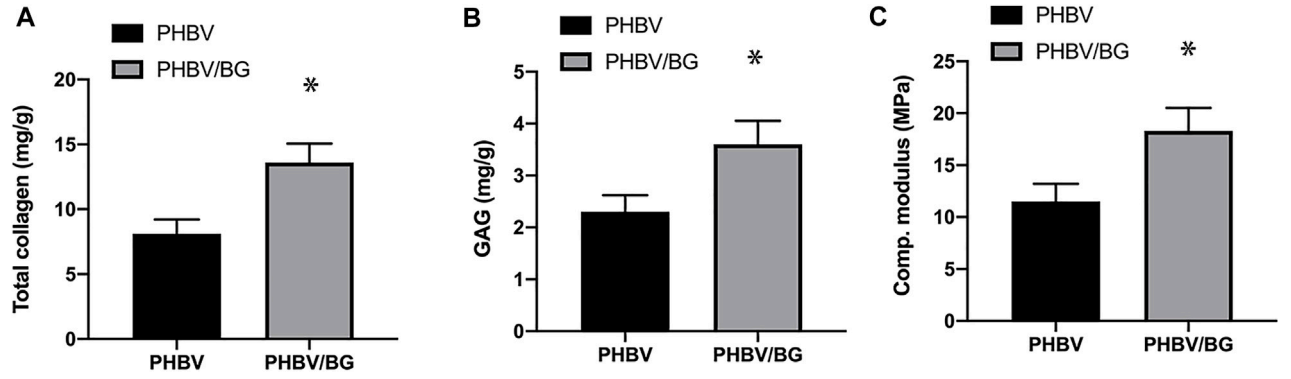

FIGURE 7 | Collagen content, GAG content, and compression modulus. There is a significant difference in terms of collagen **(A)** and GAG **(B)** contents and the compression modulus **(C)** between the CPC–PHBV construct and CPC–PHBV/10%Bioglass construct ($p < 0.05$).

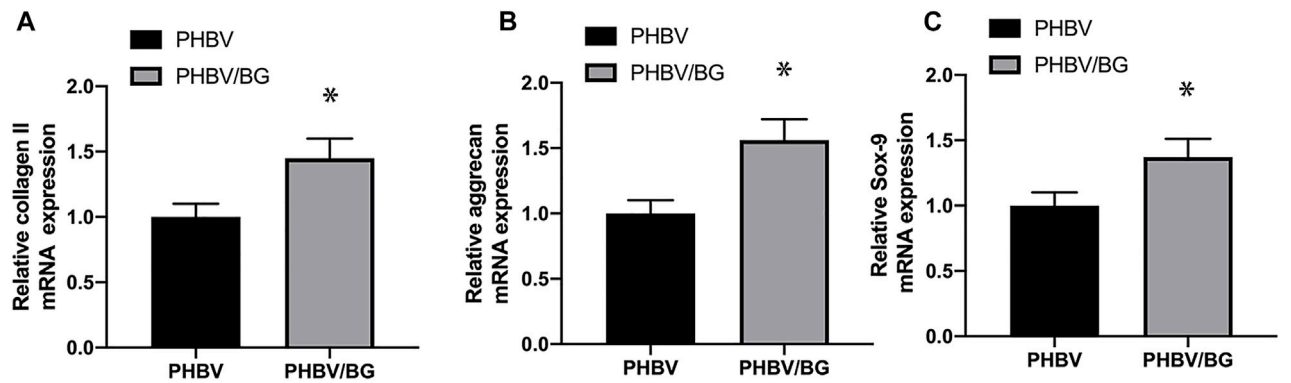

FIGURE 8 | Chondrogenic differentiation of the CPC–PHBV construct and CPC–PHBV/10%Bioglass construct. RT-PCR analysis reveals the stronger expression of COL II **(A)**, aggrecan **(B)**, and the SOX-9 gene of the CPC–PHBV/10%Bioglass construct than the CPC–PHBV construct ($p < 0.05$).

specimen (Kunrath et al., 2020). Some studies have proposed the application of nonthermal atmospheric pressure plasma, and ultraviolet treatments change negatively charged hydrophobic (bioinert) surfaces into positively charged hydrophilic (bioactive) surfaces, improving osteoblastic cell adhesion, albumin adsorption, and cytoskeleton development (Choi et al., 2016). Similarly, UV light has been used to increase hydrophilicity (Ogawa, 2014).

The addition of hydrophilic inorganic substances into hydrophobic materials (PHBV) has been found to be a feasible approach to increase the hydrophilicity of PHBV (Li et al., 2005). Therefore, we investigated the addition of 45S5 Bioglass into PHBV to increase the hydrophilic property of the PHBV scaffold. 45S5 Bioglass is a bioactive glass with remarkable biodegradability and biocompatibility, composed of 24.5 wt% Na_2O, 45 wt% SiO_2, 6 wt% P_2O_5, and 24.5 wt% CaO (Rizwan et al., 2017). Compared with the pure PHBV 3D porous scaffolds, the addition of 45S5 Bioglass into PHBV has been proven to have better biodegradation, bioactivity, and mechanical properties (Li et al., 2005). Therefore, 10% Bioglass was added into PHBV scaffolds to prepare PHBV/10%Bioglass porous composite scaffolds in current studies.

The water contact angle values are an important measure of the hydrophilicity/hydrophobicity that gives information on the surface properties and wettability of the material surface (Huhtamäki et al., 2018). The superhydrophilic materials (a contact angle less than 10°) will be superhydrophilic with good self-cleaning ability and higher wettability. Similarly, if the contact angle is greater than 150°, the materials will repel water and reduce the water absorption (Yorseng et al., 2020). The water contact angle of PHBV/10%Bioglass composites decreased with the addition of Bioglass. Compared with pure PHBV composites, the water contact angle of the PHBV/10% Bioglass decreased significantly, indicating faster liquid spread over the material surface and better wettability and suggesting that PHBV/10%Bioglass is a more hydrophilic composite biomaterial scaffold. The water absorptivity increased with the addition of Bioglass into PHBV, which indicated that the addition of Bioglass resulted in better wettability and water absorptivity. In addition, the addition of Bioglass did not decrease porosity, the dry weight, the volume, and the structure of the scaffold. The hydrophilicity may increase due to the Bioglass addition, leading to improved cell-adhesion ability. The histological and

immunohistochemical staining of the *in vivo* tissue-engineered tissue shows that the CPC–PHBV/10%Bioglass constructs producedmuch more cartilage-like tissues than CPC–PHBV after 6 weeks of subcutaneous implantation.

The compression modulus analysis suggested that tissue-engineered cartilages constructed by PHBV/10%Bioglass scaffolds had better biomechanical properties. On one hand, the addition of Bioglass into PHBV enhanced the mechanical strength of the composite scaffold; the compressive modulus of the PHBV/10%Bioglass composite scaffolds was significantly greater than that of PHBV scaffolds as the PHBV/10%Bioglass composite scaffolds and pure PHBV scaffolds had the same size, volume, and porosity. This indicated that the addition of the Bioglass increased the compressive properties of the 3D composite porous scaffolds significantly. On the other hand, the improved hydrophilicity led to improved cell-adhesion ability. The much more cartilage-like tissues produced by the CPC-PHBV/10%Bioglass construct may be due to increased cell-adhesion ability, leading to the increased compressive strength of the tissue-engineered cartilage.

The extracellular matrix content (GAG and total collagen) determined the mechanical properties of the tissue-engineered cartilage. It was found in our study that the GAG content and the total collagen content of the CPC–PHBV/10%Bioglass construct were significantly greater than those of the CPC–PHBV construct, which also resulted in the increased mechanical strength. In addition, the result of PCR analysis suggested that the addition of Bioglass into PHBV may enhance the chondrogenic differentiation of CPCs.

CONCLUSION

The addition of Bioglass into PHBV improved the properties of CPC-based tissue-engineered cartilages *in vivo*, which provide an effective approach for the preparation of 3D porous biodegradable scaffolds with improved bioactivity and mechanical properties for cartilage tissue engineering and cartilage regeneration.

DATA AVAILABILITY STATEMENT

The original contributions presented in the study are included in the article/Supplementary Material, further inquiries can be directed to the corresponding authors.

ETHICS STATEMENT

The animal study was reviewed and approved by the Ethics Committee of the Shanghai Jiao Tong University School of Medicine.

AUTHOR CONTRIBUTIONS

Conceptualization, KX and KL; methodology, LQ; software, JG; validation, KX and JG; formal analysis, LQ; investigation, KX and SZ; resources, KL; data curation, KX; writing—original draft preparation, KX; writing—review and editing, KL; visualization, SZ; supervision, KL and QW; project administration, KL and QW; funding acquisition, KX. All authors have read and agreed to the published version of the manuscript.

FUNDING

This work was supported by Hainan Province natural Science Foundation of China (822CXTD537) and the National Natural Science Foundation of China (81801929).

REFERENCES

Aboudzadeh, N., Khavandi, A., Javadpour, J., Shokrgozar, M. A., and Imani, M. (2021). Effect of Dioxane and N-Methyl-2-Pyrrolidone as a Solvent on Biocompatibility and Degradation Performance of PLGA/nHA Scaffolds. *ibj* 25 (6), 408–416. doi:10.52547/ibj.25.6.408

Antunes, A., Popelka, A., Aljarod, O., Hassan, M. K., Kasak, P., and Luyt, A. S. (2020). Accelerated Weathering Effects on Poly(3-Hydroxybutyrate-Co-3-Hydroxyvalerate) (PHBV) and PHBV/TiO2 Nanocomposites. *Polymers (Basel)* 12 (8), 1743. doi:10.3390/polym12081743

Choi, S.-H., Jeong, W.-S., Cha, J.-Y., Lee, J.-H., Yu, H.-S., Choi, E.-H., et al. (2016). Time-dependent Effects of Ultraviolet and Nonthermal Atmospheric Pressure Plasma on the Biological Activity of Titanium. *Sci. Rep.* 6, 33421. doi:10.1038/srep33421

El-Shanshory, A. A., Agwa, M. M., Abd-Elhamid, A. I., Soliman, H. M. A., Mo, X., and Kenawy, E. R. (2022). Metronidazole Topically Immobilized Electrospun Nanofibrous Scaffold: Novel Secondary Intention Wound Healing Accelerator. *Polymers (Basel)* 14 (3), 454. doi:10.3390/polym14030454

Francis, S. L., Di Bella, C., Wallace, G. G., and Choong, P. F. M. (2018). Cartilage Tissue Engineering Using Stem Cells and Bioprinting Technology-Barriers to Clinical Translation. *Front. Surg.* 5, 70. doi:10.3389/fsurg.2018.00070

Fu, X., Liu, G., Halim, A., Ju, Y., Luo, Q., and Song, A. G. (2019). Mesenchymal Stem Cell Migration and Tissue Repair. *Cells* 8 (8), 784. doi:10.3390/cells8080784

Guedes, P. L. R., Carvalho, C. P. F., Carbonel, A. A. F., Simoes, M. J., Icimoto, M. Y., Aguiar, J. A. K., et al. (2022). Chondroitin Sulfate Protects the Liver in an Experimental Model of Extra-hepatic Cholestasis Induced by Common Bile Duct Ligation. *Molecules* 27 (3), 654. doi:10.3390/molecules27030654

Hacken, B. A., LaPrade, M. D., Stuart, M. J., Saris, D. B. F., and Krych, A. J. (2020). Small Cartilage Defect Management. *J. Knee Surg.* 33 (12), 1180–1186. doi:10.1055/s-0040-1716359

Huhtamäki, T., Tian, X., Korhonen, J. T., and Ras, R. H. A. (2018). Surface-wetting Characterization Using Contact-Angle Measurements. *Nat. Protoc.* 13 (7), 1521–1538. doi:10.1038/s41596-018-0003-z

Islam, M. T., Nuzulia, N. A., Macri-Pellizzeri, L., Nigar, F., Sari, Y. W., and Ahmed, I. (2022). Evolution of Silicate Bioglass Particles as Porous Microspheres with a View towards Orthobiologics. *J. Biomater. Appl.* 36 (8), 1427–1443. doi:10.1177/08853282211059294

Kunrath, M. F., Vargas, A. L. M., Sesterheim, P., Teixeira, E. R., and Hubler, R. (2020). Extension of Hydrophilicity Stability by Reactive Plasma Treatment and Wet Storage on TiO 2 Nanotube Surfaces for Biomedical Implant Applications. *J. R. Soc. Interf.* 17 (170), 20200650. doi:10.1098/rsif.2020.0650

Kwon, H., Brown, W. E., Lee, C. A., Wang, D., Paschos, N., Hu, J. C., et al. (2019). Surgical and Tissue Engineering Strategies for Articular Cartilage and

Meniscus Repair. *Nat. Rev. Rheumatol.* 15 (9), 550–570. doi:10.1038/s41584-019-0255-1

Li, H., Du, R., and Chang, J. (2005). Fabrication, Characterization, and *In Vitro* Degradation of Composite Scaffolds Based on PHBV and Bioactive Glass. *J. Biomater. Appl.* 20 (2), 137–155. doi:10.1177/0885328205049472

Liu, F., Xu, H., and Huang, H. (2019). A Novel Kartogenin-Platelet-Rich Plasma Gel Enhances Chondrogenesis of Bone Marrow Mesenchymal Stem Cells *In Vitro* and Promotes Wounded Meniscus Healing *In Vivo*. *Stem Cel Res Ther* 10 (1), 201. doi:10.1186/s13287-019-1314-x

Luo, L., Foster, N. C., Man, K. L., Brunet, M., Hoey, D. A., Cox, S. C., et al. (2021). Hydrostatic Pressure Promotes Chondrogenic Differentiation and Microvesicle Release from Human Embryonic and Bone Marrow Stem Cells. *Biotechnol. J.* 1, e2100401. doi:10.1002/biot.202100401

Lv, X., Sun, C., Hu, B., Chen, S., Wang, Z., Wu, Q., et al. (2020). Simultaneous Recruitment of Stem Cells and Chondrocytes Induced by a Functionalized Self-Assembling Peptide Hydrogel Improves Endogenous Cartilage Regeneration. *Front. Cel Dev. Biol.* 8, 864. doi:10.3389/fcell.2020.00864

Ma, N., Wang, H., Xu, X., Wan, Y., Liu, Y., Wang, M., et al. (2017). Autologous-cell-derived, Tissue-Engineered Cartilage for Repairing Articular Cartilage Lesions in the Knee: Study Protocol for a Randomized Controlled Trial. *Trials* 18 (1), 519. doi:10.1186/s13063-017-2251-6

Nunes, R. d. M., Girão, V. C. C., Cunha, P. L. R., Feitosa, J. P. A., Pinto, A. C. M. D., and Rocha, F. A. C. (2021). Decreased Sulfate Content and Zeta Potential Distinguish Glycosaminoglycans of the Extracellular Matrix of Osteoarthritis Cartilage. *Front. Med.* 8, 612370. doi:10.3389/fmed.2021.612370

Ogawa, T. (2014). Ultraviolet Photofunctionalization of Titanium Implants. *Int. J. Oral Maxillofac. Implants* 29 (1), e95–e102. doi:10.11607/jomi.te47

Puelacher, W. C., Mooney, D., Langer, R., Upton, J., Vacanti, J. P., and Vacanti, C. A. (1994). Design of Nasoseptal Cartilage Replacements Synthesized from Biodegradable Polymers and Chondrocytes. *Biomaterials* 15 (10), 774–778. doi:10.1016/0142-9612(94)90031-0

Ripmeester, E. G. J., Timur, U. T., Caron, M. M. J., and Welting, T. J. M. (2018). Recent Insights into the Contribution of the Changing Hypertrophic Chondrocyte Phenotype in the Development and Progression of Osteoarthritis. *Front. Bioeng. Biotechnol.* 6, 18. doi:10.3389/fbioe.2018.00018

Rizwan, M., Hamdi, M., and Basirun, W. J. (2017). Bioglass 45S5-Based Composites for Bone Tissue Engineering and Functional Applications. *J. Biomed. Mater. Res.* 105 (11), 3197–3223. doi:10.1002/jbm.a.36156

Rodrigues, A. A., Batista, N. A., Malmonge, S. M., Casarin, S. A., Agnelli, J. A. M., Santos, A. R., Jr., et al. (2021). Osteogenic Differentiation of Rat Bone Mesenchymal Stem Cells Cultured on Poly (Hydroxybutyrate-co-hydroxyvalerate), Poly (ε-Caprolactone) Scaffolds. *J. Mater. Sci. Mater. Med.* 32 (11), 138. doi:10.1007/s10856-021-06615-6

Shi, Q., Qian, Z., Liu, D., Sun, J., Xu, J., and Guo, X. (2017). Maintaining the Phenotype Stability of Chondrocytes Derived from MSCs by C-type Natriuretic Peptide. *Front. Physiol.* 8, 143. doi:10.3389/fphys.2017.00143

Tan, Y., Chen, D., Wang, Y., Wang, W., Xu, L., Liu, R., et al. (2022). Limbal Bio-Engineered Tissue Employing 3D Nanofiber-Aerogel Scaffold to Facilitate LSCs Growth and Migration. *Macromol Biosci.* 1, e2100441. doi:10.1002/mabi.202100441

Thompson, C., Plant, J. C., Plant, J., Wann, A., Bishop, C., Novak, P., et al. (2017). Chondrocyte Expansion Is Associated with Loss of Primary Cilia and Disrupted Hedgehog Signalling. *eCM* 34, 128–141. doi:10.22203/ecm.v034a09

Vinardell, T., Sheehy, E. J., Buckley, C. T., and Kelly, D. J. (2012). A Comparison of the Functionality and *In Vivo* Phenotypic Stability of Cartilaginous Tissues Engineered from Different Stem Cell Sources. *Tissue Eng. Part. A.* 18 (11-12), 1161–1170. doi:10.1089/ten.TEA.2011.0544

Wang, C., Lin, B., and Qiu, Y. (2022). Enhanced Hydrophilicity and Anticoagulation of Polysulfone Materials Modified via Dihydroxypropyl, Sulfonic Groups and Chitosan. *Colloids Surf. B: Biointerfaces* 210, 112243. doi:10.1016/j.colsurfb.2021.112243

Wright, D. J., DeSanto, D. J., McGarry, M. H., Lee, T. Q., and Scolaro, J. A. (2022). Nail Diameter Significantly Impacts Stability in Combined Plate-Nail Constructs Used for Fixation of Supracondylar Distal Femur Fractures. *OTA Int.* 5 (1), e174. doi:10.1097/OI9.0000000000000174

Xue, J., He, A., Zhu, Y., Liu, Y., Li, D., Yin, Z., et al. (2018). Repair of Articular Cartilage Defects with Acellular Cartilage Sheets in a Swine Model. *Biomed. Mater.* 13 (2), 025016. doi:10.1088/1748-605x/aa99a4

Xue, K., Zhang, X., Gao, Z., Xia, W., Qi, L., and Liu, K. (2019). Cartilage Progenitor Cells Combined with PHBV in Cartilage Tissue Engineering. *J. Transl Med.* 17 (1), 104. doi:10.1186/s12967-019-1855-x

Xue, V. W., Ng, S. S. M., Leung, W. W., Ma, B. B. Y., Cho, W. C. S., Au, T. C. C., et al. (2018). The Effect of Centrifugal Force in Quantification of Colorectal Cancer-Related mRNA in Plasma Using Targeted Sequencing. *Front. Genet.* 9, 165. doi:10.3389/fgene.2018.00165

Yang, J., Gu, C., Chen, W., Yuan, Y., Wang, T., and Sun, J. (2020). Experimental Study of the Wettability Characteristic of Thermally Treated Shale. *ACS Omega* 5 (40), 25891–25898. doi:10.1021/acsomega.0c03258

Yoon, K.-H., Park, J.-Y., Lee, J.-Y., Lee, E., Lee, J., and Kim, S.-G. (2020). Costal Chondrocyte-Derived Pellet-type Autologous Chondrocyte Implantation for Treatment of Articular Cartilage Defect. *Am. J. Sports Med.* 48 (5), 1236–1245. doi:10.1177/0363546520905565

Yorseng, K., Mavinkere Rangappa, S., Parameswaranpillai, J., and Siengchin, S. (2020). Influence of Accelerated Weathering on the Mechanical, Fracture Morphology, Thermal Stability, Contact Angle, and Water Absorption Properties of Natural Fiber Fabric-Based Epoxy Hybrid Composites. *Polymers (Basel)* 12 (10), 2254. doi:10.3390/polym12102254

Conflict of Interest: The authors declare that the research was conducted in the absence of any commercial or financial relationships that could be construed as a potential conflict of interest.

Publisher's Note: All claims expressed in this article are solely those of the authors and do not necessarily represent those of their affiliated organizations or those of the publisher, the editors, and the reviewers. Any product that may be evaluated in this article or claim that may be made by its manufacturer is not guaranteed or endorsed by the publisher.

Advantages of publishing in Frontiers

OPEN ACCESS
Articles are free to read for greatest visibility and readership

FAST PUBLICATION
Around 90 days from submission to decision

HIGH QUALITY PEER-REVIEW
Rigorous, collaborative, and constructive peer-review

TRANSPARENT PEER-REVIEW
Editors and reviewers acknowledged by name on published articles

Frontiers
Avenue du Tribunal-Fédéral 34
1005 Lausanne | Switzerland

Visit us: www.frontiersin.org
Contact us: frontiersin.org/about/contact

REPRODUCIBILITY OF RESEARCH
Support open data and methods to enhance research reproducibility

DIGITAL PUBLISHING
Articles designed for optimal readership across devices

FOLLOW US
@frontiersin

IMPACT METRICS
Advanced article metrics track visibility across digital media

EXTENSIVE PROMOTION
Marketing and promotion of impactful research

LOOP RESEARCH NETWORK
Our network increases your article's readership